



UNIVERSITY OF NAIROBI

**FACULTY OF SCIENCE & TECHNOLOGY
DEPARTMENT OF CHEMISTRY**

**ANAEROBIC DECOMPOSITION AND VOLTAGE
PRODUCED BY SELECTED PESTICIDES USING MICROBIAL
FUEL CELL TECHNOLOGY**

BY

AJULIU PATRICK KINYUA

REG.NO. I80/52551/2018

**Thesis Submitted in Partial fulfillment for the Degree of Doctor of Philosophy in
Chemistry of the University of Nairobi**

JUNE 2023

DECLARATION

I hereby declare that this Thesis is my original work and has never been submitted elsewhere for award of any degree in this or any other university. Where other people's work or my own work has been used, this has properly been acknowledged and referenced in accordance with the University of Nairobi's requirements.

AJULIU PATRICK KINYUA

Signature

Date

REG. NO.: I80 /52551/2018

18th June 2023

Department of Chemistry



University

of Nairobi

We confirm that this thesis has been submitted with our knowledge as university supervisors

Signature

Date

Dr. Mbui D.



18th June 2023

Department of Chemistry

University of Nairobi

P.O Box 30197-00100

Nairobi Kenya

Signature

Date

Dr. Kithure J. G.



19th June 2023

Department of Chemistry

University of Nairobi

P.O Box 30197-00100

Nairobi Kenya

Prof. Wandiga Shem

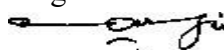
Signature

Date

Department of Chemistry

P.O. BOX 30197

University of Nairobi



22nd June 2023

DEDICATION

To my lovely wife Mary Muthoni Kinyua and to our wonderful children Kelvin, Kennedy and Lilian, who gave me all the support and inspiration I needed during the study.

ACKNOWLEDGMENT

Always thank the Almighty God for His constant love during this research work. I wish to acknowledge Prof. Shem O. Wandiga, Dr. Mbuyi Damaris, and Dr. Kithure Joyce of the Department of Chemistry who showed unwavering guidance and direction.

I'd like to thank the Pesticide Laboratory personnel for allowing me to utilize their GC-MS for sample analysis, especially Dr. Enock Osoro, who assisted with the GC-MS analysis.

All the personnel at the University of Nairobi Department of Chemistry, as well as my fellow students, for providing moral support and company in the laboratory during the research. Dr. James Kamau Mbugua provided research methodology updates, assistance in modeling and simulation techniques which I truly appreciate. I am grateful to late Prof. Kamau for encouraging me to follow this path.

Finally, I appreciate my beloved wife Mary for her patience and financial support, as well as my children Kelvin, Kennedy, and Lilian for their help and understanding throughout the research.

PUBLISHED PAPERS

1. J.K, M., A, K., D.N, M., J.L, K., S.O, W., & A.G, W. (2022). Microbial Fuel Cell Bio-Remediation of Lambda Cyhalothrin, Malathion and Chlorpyrifos on Loam Soil Inoculated with Bio-Slurry. *American Journal of Environment and Climate*,1(1): 34–41.
2. **Kinyua A.**, Mbugua J. K, Mbui D. N, Kithure J., Michira I, Wandiga S. O. (2022). Bio-Remediation of Lambda Cyhalothrin, Malathion and Chlorpyrifos Using Microbial Fuel Cells. *International Journal of Scientific Research in Chemistry (IJSRCH)*. 7(2):22-32
3. **Kinyua A**, Mbugua J.K, Waswa A.G, Mbui D.N, Kithure J, Michira I and Wandiga S.O. (2022). Bio-Remediation of Lambda Cyhalothrin, Malathion and Chlorpyrifos Using Anaerobic Digestion Bio-Slurry Microbes. *Medicon Agriculture & Environmental Sciences*. 2(5): 03-12
4. **Kinyua A.**, Mbugua J. K, Mbui D. N, Kithure J., Michira I, Wandiga S.O.(2022). Voltage Recovery from Pesticides Doped Tomatoes, Cabbages and Loam Soil Inoculated with Rumen Waste: Microbial Fuel Cells. *International Journal of Scientific Research in Science, Engineering and Technology (IJSRSET)*. 9(2):172-180.
5. **Kinyua A. P**, Mbugua J. K, Imwene K. O, Mbui D. N, Kithure J.G. N, Wandiga S.O. Michira I. (2021). Current and voltage data logging from microbial fuel cells using *Arduino* based sensors. *International Robotics & Automation Journal*.7 (3):90–93.
6. Imwene K. O, Mbui D. N, Mbugua J.K, **Kinyua A. P**, Kairigo P. K, Onyatta J. O. (2021). Kinetic Modelling of Microbial Fuel Cell Voltage Data from Market Fruit Wastes in Nairobi, Kenya. *International Journal of Scientific Research in Chemistry (IJSRCH)*. 6(5): 25-37.
7. Imwene K.O, Mbui D., **Kinyua A.P**, Mbugua J.K, Ahenda S., Onyatta J.O. (2021) Biotransformation of Biodegraded Organic Waste from a Batch Mode Microbial Fuel Cell to Organic Fertilizer. *J Bioremediat Biodegrad* 12:011.

ABSTRACT

In this study, combined anaerobic and aerobic conditions were employed inside an air cathode double-chamber MFC, in an attempt to bio-remediate lambda-cyhalothrin, chlorpyrifos, and malathion in loam soil, tomato and cabbage surfaces.

Conventional procedures were used to determine the proximate qualities of the tomato and cabbage. The colony-forming units were calculated using the conventional plate method. Optimization of variables (external resistance, microbe level, pesticide concentration, proximal matters, and operation pH) was performed as the current and voltage were monitored on an automated Arduino-based voltage and current sensor and a digital voltmeter. Pesticide concentrations were assessed by employing a GC-MS after QUECHERS extraction. The degradation levels were fitted into first, second, and third order decay equations and the collected information was modeled, simulated, then fitted applying linear, Gaussian, Boltzmann, as well as Lorentz models.

The outcome demonstrated that the matrices' energy levels ranged from 292.37 Kcal/100g in tomatoes to 303.96 Kcal/100g in cabbage. The carbon content in tomatoes and cabbage were 47.13% and 47.45%, respectively, the bacterial count was observed to be $1.31 \pm 0.05 \times 10^6$ cfu/g in tomato, $1.01 \pm 0.03 \times 10^5$ cfu/g in cabbage, $3.01 \pm 0.02 \times 10^9$ cfu/g in loam soil, and $3.15 \pm 0.01 \times 10^{10}$ cfu/ml in rumen fluid. The average potential difference and current in rumen fluid were 0.290 ± 0.057 V and 0.027 ± 0.008 mA, respectively. For chlorpyrifos, lambda-cyhalothrin, malathion, and pesticide mix, the produced potential difference varied between 0.227 and 0.551 V, 0.217 and 0.565 V, and 0.190 and 0.533 V respectively. Due to the strong microbial population feasting on the substrate, significant microbe concentration (1:2) was detected together with a high potential difference of 0.568 V and current (0.231 mA).

Non-linear regression models showed closely fitting ranging from 0.9387 to 0.9997 coefficients. Therefore, the MFC system was able to both generate substantial electrical energy and degrade harmful pesticides in the environment. We recommend that mechanism of remediation be pursued by simultaneous monitoring on the GC-MS.

Keywords: *Bio-remediation, Current, Modeling, Pesticides, Voltage.*

TABLE OF CONTENTS

DECLARATION	ii
DEDICATION	iii
ACKNOWLEDGMENT	iv
PUBLISHED PAPERS	v
ABSTRACT	vi
TABLE OF CONTENTS	vii
LIST OF ABBREVIATIONS AND SYMBOLS	xx
LIST OF APPENDICES	xxii
CHAPTER ONE	1
INTRODUCTION	1
1.1 Background information of the study	1
1.1.1 Importation of Pesticides in Kenya	3
1.1.2 Pesticide usage in Kenya	4
1.1.3 Pesticide use in vegetable farming	4
1.2 Microbial Fuel cells (MFC)	5
1.2.1 Potential difference and current measurement in MFC	7
1.2.2 Hardware Description-Arduino Mega	8
1.2.3 Soil Microbial Fuel Cell (SMFC)	11
1.3 Statement of the Problem	12
1.4 General Objectives	13
1.4.1 Specific Objectives	14
1.5 Justification	14
CHAPTER TWO	15
LITERATURE REVIEW	15
2.1 Fate of Pesticides in the Environment	15
2.2 Pesticide Degradation	17
2.2.1 Bio-remediation Kinetics	18
2.2.2 Photo-degradation	19
2.2.3 Microbial degradation	20
2.2.4 Bacterial Bioremediation	21

2.2.5 Bio-electrochemical Bioremediation	23
2.2.6 Pesticide Bio-remediation via Microbial Fuel Cells	23
2.2.7 Microbial Degradation of Organophosphate Pesticides	25
2.2.7.1 Chlorpyrifos	25
2.2.7.2 Malathion	27
2.2.7.3 Lambda Cyhalothrin	29
2.3 Bioremediation of pesticides using MFC	31
2.4 Summary of Gaps in Knowledge	37
CHAPTER THREE	38
3.1 MATERIALS AND METHODS	38
3.2 Materials and Reagents	38
3.3 Sampling Area	39
3.4 Assessment of microbes	40
3.4.1 Preparation of MacKonkey Agar	40
3.4.2 Preparation of Blood Agar	41
3.5 Bacteria Total Count	41
3.6 Loam soil analysis	41
3.7 Assessment of tomato and cabbage waste	43
3.7.1 Analysis for pesticide concentration	43
3.7.2 Macro and micronutrient and heavy metals analysis	44
3.8 Proximate analysis	44
3.8.1 Moisture Content Analysis (M)	44
3.8.2 Determination of Ash	45
3.8.3 Crude Protein Assessment	46
3.8.4 Determination of crude fat	47
3.8.5 Determination of crude fiber	47
3.8.6 Nitrogen free Extract (NFE)	48
3.8.7 Energy calculation	48
3.9 Microbial Fuel Cells Construction	48
3.9.1 Salt bridge	49
3.9.2 Electrode preparation	50

3.9.3 Circuit Assembly	51
3.10 Control experiments	51
3.11 Voltage and current measurements	54
3.11.1 Multimeter voltage and current measuring method	54
3.12 Data collection and observation.....	59
3.13 Pesticide solutions	59
3.13.1 Preparation of Standard Stock Solution	59
3.13.2 Preparation of working Stock Solution	60
3.13.3 Investigation of the potential of cabbages, tomato, loam soil and rumen wastes	60
3.13.4 Microbial Fuel Cell Parameter Optimization	60
3.13.4.1 Analyzing the impact of microbe concentration	61
3.13.4.2 The impact of pH on the production of electricity	61
3.13.4.3 Investigation of the effect of External Resistance	61
3.13.4.4 Investigation of the effect of concentration of pesticides	62
3.14 Bioremediation studies	62
3.15 Fitting, modeling and simulation of degradation data	63
3.15.1 Microbial Growth Simulation	63
3.15.2 Microbial Fuel Cells Kinetic Study	65
3.15.2.1 Linear kinetic model	65
3.15.2.2 Gaussian Kinetic Model	65
3.16 Bio-remediation Decay Kinetics	66
CHAPTER FOUR	68
4.1 RESULTS AND DISCUSSION	68
4.2 The food Wastage situation in Kenya	68
4.3 Cabbage and tomato analysis	69
4.3.2 Proximate analysis	70
4.3.3 Elemental composition of the samples	72
4.3.4 Inoculum analysis	74
4.3.5 Features of loam soil	76
4.4 Microbial Fuel Cells	78
4.4.1 The voltage and current of the MFC	78
4.4.2 Voltage and Current Measurements	78

4.5 Control Experiment	81
4.5.1 Pesticide Voltage study	84
4.5.2 Voltage from Bioremediation studies	85
4.6 Optimization of Microbial Fuel Cell Parameters	88
4.6.1 Examining the impact of the concentration of microbes.	88
4.6.2 Impact of pH on electricity generation	91
4.6.3 Study of the effect of External Resistance	96
4.6.4 Examining the impact of pesticide concentration	98
4.7 Bioremediation Studies	102
4.7.1 Concentration studies	102
4.7.2 Bio-remediation on different matrices	105
4.8 Discussion on Degradation Data	119
4.9 Modeling kinetics of voltage	121
4.9.1 Anode respiration Kinetic parameter estimation	121
4.9.1.1 Bacterial development	122
4.9.1.2 Substrate self-inhibitory effect	125
4.9.1.3 Severe inhibitor concentration	127
4.9.2 Modeling, simulating, and fitting decaying data	129
4.9.2.1 Linear plots	131
4.9.3 Bio-remediation Decay orders	136
CHAPTER FIVE	158
CONCLUSION AND RECOMMENDATIONS	158
5.1 CONCLUSION	158
5.2 Recommendations	159
5.3 Recommendations for further works	159
REFERENCES	161
APPENDICES	182

LIST OF FIGURES

LIST OF TABLES	xviii
Figure 1:1 Pesticides usage per area of cropland (Source: FAOSTAT, 2021).	2
Figure 1.2: Pesticides usage from year 1990 to year 2016 (Source: FAOSTAT, 2021)	2
Figure 1.4: Structural formula for (a) Chlorpyrifos (b) Malathion ((c) lambda cyhalothrin	4
Figure 1.5:(a) A twin-chambered MFC and (b) a mono-chambered MFC (Chaturvedi and Verma, 2016)	7
Figure 1.6: Set-up of a dual chamber MFC with a multi-meter	8
Figure 1.7:Arduino Mega Board (Kumar <i>et al.</i> , 2015).	9
Figure 1.8: (a) A voltage Sensor Module (b) Internal Circuit of voltage sensor (Webb and Møller-Holst, 2018)	9
Figure 1.9: An ASC712 Current Sensor Module (Webb and Møller-Holst, 2001)	10
Figure 1.10: Pesticide on the surface of the soil as well as tomato waste	13
Figure 2.1:A Representation of movement of pesticide residue in the environment, (Marek Biziuk, <i>et al</i> 2016)	16
Figure 2.2: Pesticides Dissipation pathways (Kinyua <i>et al.</i> , 2016).	19
Figure 2.3:Organophosphate pesticide biodegradation products (Sighn and Walker, 2006)	25
Figure 2.4: Chlorpyrifos microbial breakdown mechanism (Singh and Walker, 2006).	27
Figure 2.5: A proposed malathion breakdown by bacterial <i>Ochrobactrum</i> sp. (Verma <i>et al.</i> , 2021).	29
Figure 2.6: A suggested lambda cyhalothrin degradation mechanism (Chen <i>et al.</i> ,	

2015)	31
Figure 2.7: A typical bacterial growth curve (Yates, G. T., & Smotzer, 2007)	34
Figure 3.1: (a) Dagoretti slaughter house (b) Thigio area where loam soil, tomato and cabbage were sampled	40
Figure 3.2: plastic containers representing the anodic and cathodic chambers.	49
Figure 3.3: The wicks used to construct the salt bridge.	50
Figure 3.4: A representation of the graphite rods and copper wire that were used	50
Figure 3.5: A multi-meter equipped twin cell (MFC)	51
Figure 3.6: Microbial fuel cell control experiment setup with rumen in the anodic chamber	52
Figure 3.7: Microbial fuel cell control experiment setup with cabbage in the anodic chamber	52
Figure 3.8: microbial fuel cell control experiment setup with tomato in the anodic chamber	53
Figure 3.9: Microbial fuel cell control experiment setup with Loam soil in the anodic chamber	53
Figure 3.10: A multimeter displayed voltage reading	54
Figure 3.11: A block diagram for connecting potential difference and current sensors to the Arduino board.	56
Figure 3.12: Diagram showing connections between the Arduino boards, sensors and LCD connections.	57
Figure 3.13: Arduino potential difference and current MFC monitoring gadget	58
Figure 4.1: (a) Image of tomatoes that had been sprayed (b) sorted as waste/	

unsuitable for use (c) tomatoes being sorted.	69
Figure 4.2: GC-MS chromatogram for mixed tomato and cabbage samples	70
Figure 4.3: The cultured and isolated bacteria from Rumen fluid	75
Figure 4.4: The cultured and isolated bacteria from cow dung	76
Figure 4.5: Plot of multi-meter voltage and current interpretations from tomato and rumen	79
Figure 4.6: A plot of multimeter and Arduino sensor-based voltage and current readings from tomato samples.	80
Figure 4.7: A plot of voltage and current from rumen on the Arduino-Uno and the multi-meter.	81
Figure 4.8: Daily voltage readings from tomato, cabbage, loam soil, and rumen samples.	82
Figure 4.9: Daily voltage generated from tomato, cabbage, loam soil, and rumen waste	83
Figure 4.10: Daily voltage readings from pesticide doped un-inoculated samples.	84
Figure 4.11: Daily voltage generated from the three samples loaded with pesticide	85
Figure 4.12: The daily voltage produced by loam soil doped with the pesticide mixture chlorpyrifos, lambda cyhalothrin, and malathion.	86
Figure 4.13: A plot of daily voltage readings for the pesticide mixture, malathion, and tomato waste that has been injected with CLM.	87
Figure 4.14: A plot of daily voltage readings for the pesticide mixture, individual pesticides for cabbage waste.	88
Figure 4.15: Daily voltage readings for various tomato: inoculum ratios	89
Figure 4.16: Shows the voltage produced by various cabbage-to-inoculum ratios.	89

Figure 4.17: Daily Voltage produced by various loam soil inoculation ratios	90
Figure 4.18: Daily pH changes per substrate waste.	91
Figure 4.19: Voltage produced by rumen fluid doped with pesticides at various pH levels	92
Figure 4.20: Voltage produced from doped tomato at different pH levels	93
Figure 4.21: Voltage produced from doped cabbage at different pH	94
Figure 4.22: Voltage produced by doped loam soil at various pH levels	94
Figure 4.23: Plot showing the voltage produced across different external resistors by rumen fluid containing chlorpyrifos.	96
Figure 4.24: Voltage generated from lambda cyhalothrin-doped rumen fluid across different external resistors	97
Figure 4.25: Voltage generated from malathion doped rumen across various external resistors	97
Figure 4.26: Voltage produced by pesticide-contaminated tomato waste	99
Figure 4.27: the voltage produced by pesticide-doped cabbage.	100
Figure 4.28: Voltage produced by rumen fluid containing varying pesticide combination	101
Figure 4.29: Voltage produced by pesticide-infused loam soil	102
Figure 4.30: A GC-MS chromatogram for standard pesticides.	103
Figure 4.31: Malathion calibration curve	104
Figure 4.32: Lambda cyhalothrin calibration curve	104
Figure 4.33: Chlorpyrifos calibration curve	105
Figure 4.34: Daily voltage produced for cabbage treated with a pesticide mixture,	

malathion, and chlorpyrifos	106
Figure 4.35: The levels of pesticide degradation in rumen fluid.	107
Figure 4.36: A 3D plot of the rumen fluid's chlorpyrifos concentration, voltage, and retention time.	108
Figure 4.37: A 3D plot of the concentration, voltage, and retention time of lambda-cyhalothrin in rumen fluid	108
Figure 4.38: 3-D plot of Malathion concentration, voltage, and retention time in rumen fluid.	109
Figure 4.39: Pesticide mixture, chlorpyrifos, lambda cyhalothrin, and daily voltage-generated tomato	110
Figure 4.40: The degradation levels from pesticide-treated tomato fruits.....	110
Figure 4.41: Displays a 3D plot of the concentration, voltage, and retention time of chlorpyrifos in tomato.	111
Figure 4.42: shows the concentration, voltage, and retention time of lambda-cyhalothrin in a tomato in a 3D plot	111
Figure 4.43: shows the concentration, voltage, and retention time of malathion in a tomato in a 3D plot.	112
Figure 4.44: A daily voltage-generated of pesticide mixture -doped cabbage	113
Figure 4.45: Pesticide-infused cabbage daily voltage and degradation levels	114
Figure 4.46: shows a 3D plot of the voltage, retention time, and Chlorpyrifos concentration in cabbage.	114
Figure 4.47: shows a 3D plot of the concentration, voltage, and retention time of lambda-cyhalothrin in cabbage	115
Figure 4.48: Malathion concentration, voltage, and retention time in cabbage are	

depicted in a 3D plot	115
Figure 4.49: A pesticide mixture, chlorpyrifos, lambda cyhalothrin, and daily voltage-generated cabbage.....	116
Figure 4.50: Pesticide-infused loam soil daily voltage and degradation levels	117
Figure 4.51: A 3D plot of the concentration, voltage, and retention time of chlorpyrifos in a loam soil.	117
Figure 4.52: A 3D plot of the concentration, voltage, and retention time of lambda-cyhalothrin in loam soil.	118
Figure 4.53: A 3D plot of concentration, voltage, and retention time for malathion-doped loam soil.	118
Figure 4.54: The general Chlorpyrifos breakdown mechanism (Singh, 2009; Singh & Walker, 2006; Reddy et al., 2013).	119
The proposed degradation pathway for malathion is illustrated in figure 4.55 below.	120
Figure 4.55: Malathion (2-(dimethoxyphosphinothioylthio) decomposition pathway (Mulla et al. 1981)	120
Figure 4.56: Lambda cyhalothrin degradation pathway. (Zining Ci <i>et al.</i> 1980)	121
Figure 4.57: Voltage produced by rumen, tomatoes, cabbages, and loam soil solutions doped with pesticides.	130
Figure 4.58: Linear plot of voltage against time in days.	131
Figure 4.59: Modeling of voltage bio-remediation of pesticide mix in loam soil	133
Figure 4.60: Modeling of voltage bio-remediation of pesticide mix in tomato.....	133

Figure 4.61: Modeling of voltage bio-remediation of pesticide mix in cabbage.....	134
Figure 4.62: Modeling of voltage bio-remediation of pesticide mix in rumen fluid.	135
Figure 4.63:Fitted plots of chlorpyrifos degradation curves in loam soil.	137
Figure 4.64 :Fitted plots of lambda-cyhalothrin decay curve in loam soil	139
Figure 4.65: Fitted plots of malathion degradation curves in loam soil	140
Figure 4.66: Fitted plots of chlorpyrifos degradation curves in rumen fluid.....	142
Figure 4.67: Fitted plots of the lambda-cyhalothrin decay curves in rumen fluid	143
Figure 4.68: Fitted plots of malathion decay curves in rumen fluid	145
Figure 4.69: Fitted plots of chlorpyrifos decay curves in tomato	146
Figure 4.70:Fitted plots of decay curves in tomato	148
Figure 4.71: Fitted plots of decay curves in tomato	149
Figure 4.72:Close-fitting subversions of chlorpyrifos decay curves in cabbage	151
Figure 4.73:Fitted plots of decay curves in cabbage	153
Figure 4.74 Fitted plots of malathion degradation curves in cabbage	155

LIST OF TABLES

Table 2.1: Some microbes previously employed in bio-remediation of pesticides	32
Table 4.1: Analyzed fresh weight on fruit and vegetable wastes	71
Table 4.2: Proximate analyzed dry weight of fruit and vegetable waste	71
Table 4.3: The ultimate composition of fruit and vegetable waste.....	72
Table 4.4: The physical characteristics of different market wastes	73
Table 4.5: Total microbial count from dung and rumen fluid samples	74
Table 4.6: Characteristics of the loam soil used.	77
Table 4.7: Maximum growth rate, growth yield coefficient, and half-saturation coefficient	123
Table 4.8: Self-inhibitory effect coefficient for all the samples	126
Table 4.9: Critical inhibitor concentration coefficient for all the samples	128
Table 4.10: Table of linear plot equation and regression values.....	129
Table 4.11: Arithmetical study data for chlorpyrifos decay curves in loam soil	138
Table 4.12: Statistical analysis data for lambda-cyhalothrin decay curves in loam soil	139
Table 4.13: Statistics on the decay curves of malathion in loam soil	141
Table 4.14: Statistical data for the rumen fluid's chlorpyrifos decay curves.	142
Table 4.15: Statistical study of lambda-cyhalothrin decay curves in rumen fluid	144
Table 4.16: Arithmetic study data for malathion decay curves in rumen fluid	145
Table 4.17: Statistical analysis data for chlorpyrifos decay curves in tomato.....	147
Table 4.18: Statistical analysis data for lambda-cyhalothrin decay curves in tomato	148
Table 4.19: Statistical analysis data for malathion decay curves in tomato	150

Table 4.20: Statistical analysis data for chlorpyrifos decay curves in cabbage..... 152

Table 4.21: Statistical data for lambda-cyhalothrin decay curves in cabbage 154

Table 4.22: Statistical data analysis for malathion decay curves in cabbage 156

LIST OF ABBREVIATIONS AND SYMBOLS

BES.....	Bio electrochemical system
CFU.....	Colony forming unit
CO ₂	Carbon (iv) Oxide
COD.....	Chemical Oxygen Demand
DDT.....	Dichlorodiphenyltrichloroethane
DDD.....	Dichlorodiphenyldichloroethane
EAB.....	Electro active bacteria
GC-MS	Gas chromatography-Mass Spectrometry
GMO.....	Genetically modified Organisms
GTZ.....	German Technical Cooperation Agent
HCB.....	Hexachlorobenzene
HPLC	High pressure liquid chromatography
LOQ.....	Limit of Quantitation
MERC	Microbial Electro-remediating Cell
MBR.....	Membrane Bio Reactor
MCPA	2-Methyl-4-Chlorophenoxyacetic acid
MFC	Microbial Fuel Cell
OPP	Organo-phosphate pesticide
PAHs.....	Polyaromatic hydrocarbons

PH.....Power of Hydrogen
PCBP..... Pest control products board
PCP.....Pentachlorophenol
QSART.....Quantitative structure activity relationship
RMSE..... Root means square error
RSS..... Residue sum squares
SMFC.....Soil microbial fuel cell

UNITS OF MEASUREMENT

- g grams
- kΩ..... kilo ohms
- m² meters square
- mA milli-amperes
- ml milliliter
- mv..... milli-volts
- ppm..... parts per million
- μWmicro watts
- V.....Volt

LIST OF APPENDICES

APPENDICES	182
Appendix 1: Arduino Based Voltage and Current MFC Code	182
Appendix 2: Malathion calibration curve	182
Appendix 3 :Lambda Cyhalothrin Calibration Curve	184
Appendix 4:Calibration of Chlorpyrifos	184
Appendix 5: Pesticide Recovered after Spiking the Substrates	185
Appendix 6:Tetramethrin (C ₁₉ H ₂₅ NO ₄) Curve	186
Appendix 7:Statistical parameters for Modeling of voltage bio-remediation of pesticide mix in loam soil	187
Appendix 8:Statistical parameters for Modeling of voltage bio-remediation of pesticide mix on Tomato	187
Appendix 9: Statistical parameters for Modeling of voltage bio-remediation of pesticide mix on Cabbage	189
Appendix 10: Statistical parameters for Modeling of voltage bio-remediation of pesticide mix in Rumen Fluid	190

CHAPTER ONE

INTRODUCTION

1.1 Background information of the study

The agriculture sector in Kenya remains the one of the most important and distinct primary sectors that continues to play the vital role in Kenya's economy accounting for 30% of the country's Gross Domestic Product (GDP). The sector employs over 40% of the total population and slightly above 70% of the rural population. (CBK Agriculture survey July 2022). Despite the availability of food increasing alongside the growing human population over the last 30 years, over 800 million East African people are suffering from lack of proper nutrition. This problem is not only the inadequate distribution but also insufficient food production and financial inability to purchase food of reasonable quantities and quality to satisfy their needs (FAO, 1993a). Approximately 4.4 million people are projected to be facing high levels of serious food insecurity that is integrated food security phase classification (IPC) Phase 3 or above. Overall, 3.1 million people (roughly 21 percentage of the population analyzed by IGAD Climate Prediction and Applications Centre (ICPAC) are likely to be in Crisis IPC Phase 3 About 1.2 million people (8 percentage) is in Emergency (IPC Phase 4). In Kenya food security is worsening every other day. The most current analysis done in July 2022 to September 2022 indicate that, 3.5 million people (24% of the population of Arid and Semi-Arid Land) are facing a very serious food insecurity levels – IPC Phase 3 and above. About 2.7 million people are in IPC Phase 3 (Crisis) and nearly a population of 785,000 are in IPC Phase 4 (Emergency).

In an endeavor to redeem the situation of food crisis, farming using modern technology has been applied. For example, pesticides have been applied in the farming sector to eradicate crop diseases and prevent pests from crop attack. The pesticide sprays used and the ruminant pesticide extend into unintended targets in the environment, for example into water sources, soil and even into the air causing environmental pollution. According to reports, millions of tons of pesticides were used between 1990

and 2018, primarily in Asia and America (Tudi *et al.*, 2021). Below Figure 1.1, shows the average pesticide usage. It increased from 1.55 kg per hectare in 1990 to 2.63 kg per hectare in 2018. Pesticide usage by type is illustrated in figure 1.2 below.

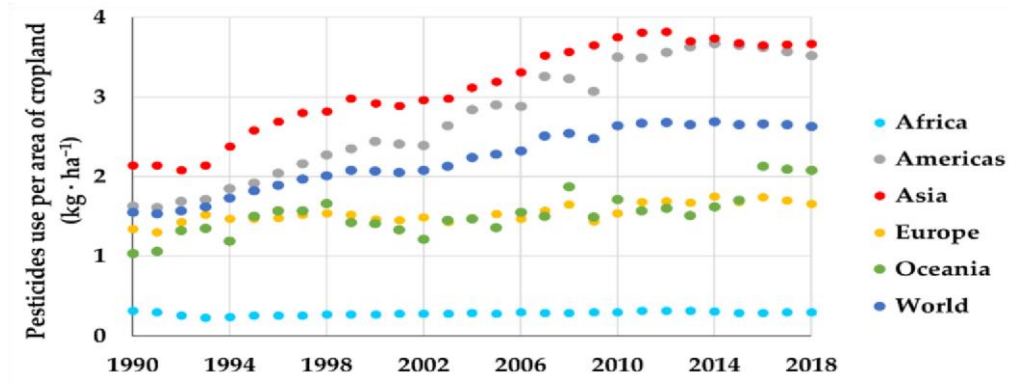


Figure 1:1 Pesticides usage per area of cropland (Source: FAOSTAT, 2021).

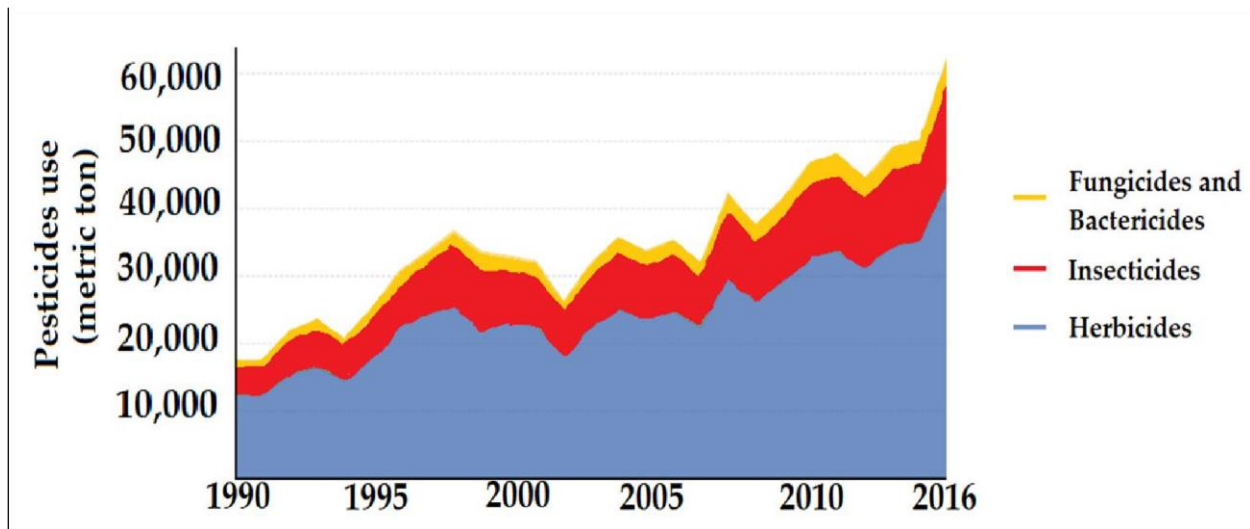


Figure 1.1: Pesticides usage from year 1990 to year 2016 (Source: FAOSTAT, 2021)

1.1.1 Importation of Pesticides in Kenya

Kenya is mostly an agricultural nation, hence there is a significant demand for pesticides, a factor that means that the domestic market's demand and that for export to its neighbors is expanding. Approximately 12,983 metric tons of pesticides were shipped into Kenya in 2011 and 2012 costing

Ksh10.7 billion (PCPB, 2012). In figure 1.3, the main kinds of pest management goods imported from the years 2003/2004 to 2011/2012 are depicted in tonnes.

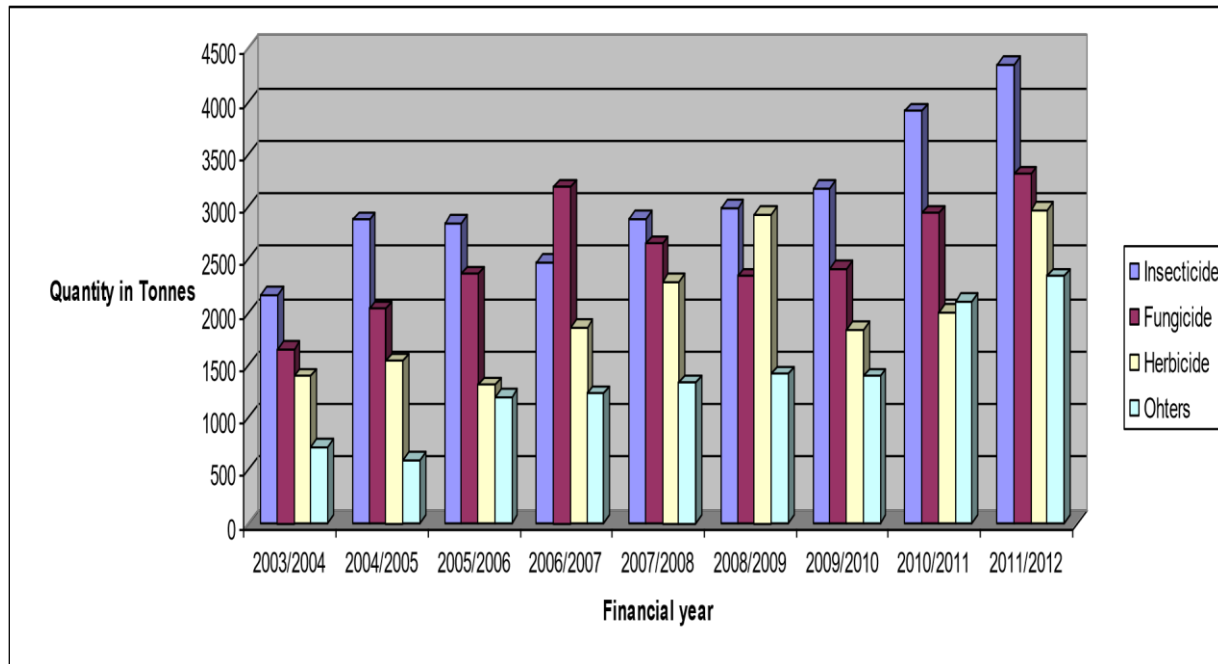


Figure1.2: Amounts of pesticides shipped entering Kenya between 2003/04 and 2011/2012 (Source: PCPB, 2012).

In Kenya, companies that manufacture pesticide components make up the majority of the pesticide sector. There are more than eleven companies in the Kenya that produce and market different pesticide products (PCBP, 2008). Herbicides, miticides, plant growth regulators, as well as insect repellents are some of the pesticides manufactured and sold in Kenya (PCBP, 2008).

1.1.2 Pesticide usage in Kenya

With just an 87 percent increase in import capacity and an 88 percent increase in import expenses, Kenya's dependence on pesticides has been increasing (PCBP, 2008). Climate (especially temperature and rainfall), type of soil including vegetation cover, biological action, illuminance, farming practices,

and the pesticide's mechanism of delivery into a particular environmental compartment are some of the factors that have an impact on pesticide contamination (PCBP, 2012).

1.1.3 Pesticide use in vegetable farming

In "container gardens," pesticides like lambda cyhalothrin, malathion, and chlorpyrifos are frequently employed (Mbugua *et al.*, 2015). A pesticide and all-purpose, non-systemic fungicide, malathion is an organophosphate, and the pyrethroid, lambda cyhalothrin, are found in a various form, for example, can be in powder form, pellets, liquid, tiny capsules, and ear tags (Ecobichon, 2001; Sarkar *et al.*, 2021). Chlorpyrifos, on the other hand, is a wood preservative, insecticide, fungicide, and herbicide and is an organo-chlorine pesticide (WHO, 2007). Figure 1.4 (a), (b) and (c) shows the structural formula of chlorpyrifos, Malathion and lambda cyhalothrin respectively.

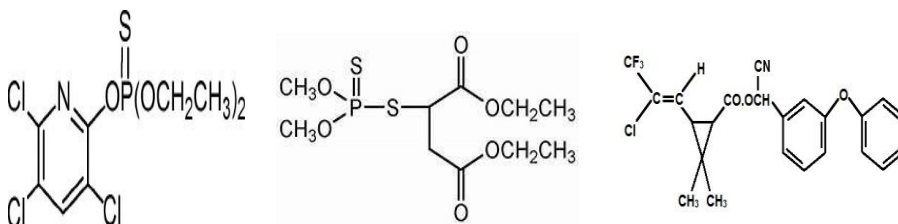


Figure 1.3: Structural formula for (a) Chlorpyrifos (b) Malathion (c) lambda cyhalothrin

When pesticides are released into the environment, they often undergo degradation. Pesticide degradation is the decomposition or rather the complex parent pesticide molecule breaks down into simpler byproducts, some of which may be non-toxic while others may still be harmful (WHO, 2007). Pesticides are broken down into the environment by a variety of processes, including photo degradation and hydrolysis. There have been reports that fungi and bacteria help in pesticide degradation to a good extent (Vargas, 1975). Biological approaches have drawn a lot of interest in the treatment of pesticides in soil/water systems because of their ecologically benign character (Helbling, 2015). Since pesticides are used to enhance and improve agricultural production; they significantly contribute to food security.

However, a significant amount of the pesticide is left in the environment, creating a huge health threat. Studies by Lorenz (2009) have shown that such contaminants are resistant to biodegradation and contaminate soils, groundwater, and surface water. Pesticides bio-accumulate in the ecosystem, exposing the environment and people to various dangers for example to diseases like cancer. Additionally, pesticides are deposited in the bodies of the flora and fauna. For example, fish containing significant amounts of mercury, chlorpyrifos, and other substances have been discovered (Bloom 1992).

To reduce the use of pesticides, many countries have enacted regulations, for example the European Union's Regulation (EC) 1107/2009 (Regulation (EC, 2009) as well as the Stockholm Convention (Stockholm Convention, 2021).

Pesticides can be rendered less hazardous by decomposing them into less harmful entities, through a variety of processes, for example photo degradation, catalytic degradation, and anaerobic degradation. However, some of these can produce potentially dangerous byproducts (Fenner et al., 2013). Therefore, it is essential to develop new techniques that may be more efficient in the degradation process. One of these technologies is the microbial fuel cells, MFC.

1.2 Microbial Fuel cells (MFC)

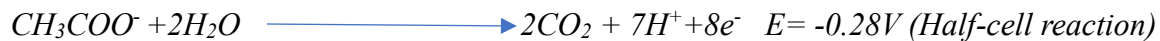
Fuel cells are voltaic or electrochemical cells that can generate electricity as a result of reactions between an oxidant such as oxygen and a fuel. MFCs are classified into two main categories, namely, mono (single) and dual (two) chambers. Single chambered MFCs feature a single compartment for the cathode and anode whereas the two chambered MFC has separate cathodic and anodic compartments.

Uninterrupted electricity production by fuel cells lasts for some time until the cells exhaust

the reacting substances. Benefits of fuel cells include: few or no contaminants, no noise adulteration, and no air adulteration. Depending on the fuel, oxidant, electrolyte, as well as temperature of operation, there are various types of fuel cells e.g., polymer electrolyte membrane fuel cell, alkaline fuel cell, direct methanol fuel cell etc. (Marcella *et al*, 2007).

Microbes use recurrent reactions to oxidize natural and inorganic mixes into adenosine triphosphate (ATP), which is subsequently used to produce energy in microbial fuel cells (MFCs) (Torres *et al*, .2009). In the Microbial fuel cells, a cationic film is positioned in between the anode and the cathode. The anodic cell is home to the degradation agents that use glucose (decomposing molecules) as an electron source. Protons and electrons are simultaneously produced by the metabolites, and the exchange of electrons happens on the anode's surface. Afterwards, protons are oxidized to form water, as electrons are moved from anode to cathode via an electrical circuit. Free oxygen is frequently used as an electron acceptor (Rabaey *et al*. 2004). Figure 1.5 below shows the dual compartments and single chambered MFC. The Chemical equations to demonstrate anodic and cathodic reaction where acetate is used as the substrate in the anode chamber.

Anodic chamber reaction,



Cathodic chamber reaction,



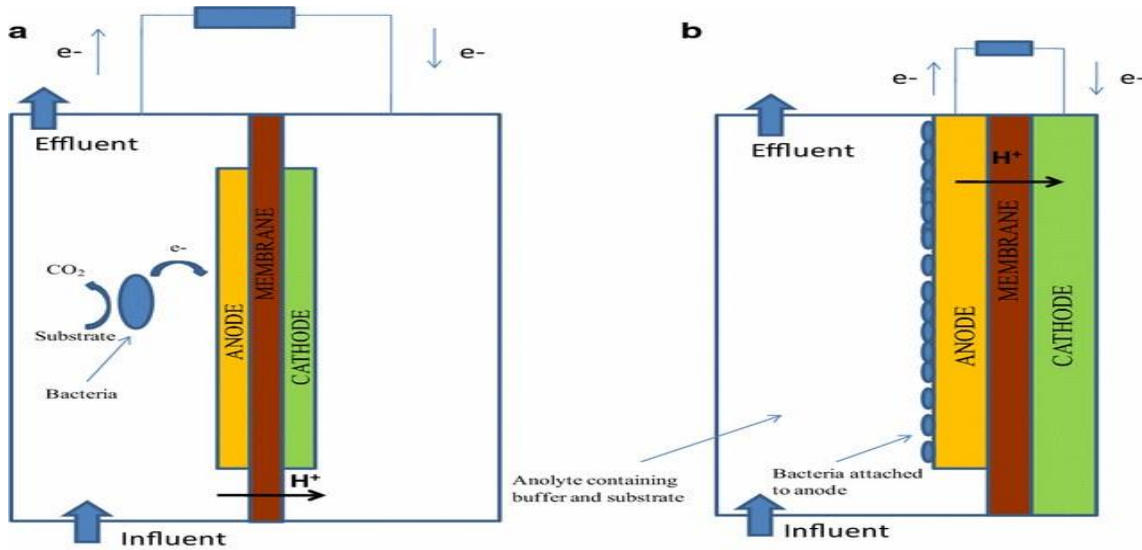
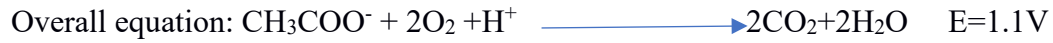


Figure 1.4:(a) A twin-chambered MFC and (b) a mono-chambered MFC (Chaturvedi and Verma, 2016)

1.2.1 Potential difference and current measurement in MFC

Microbial fuel cells produce energy by utilizing microbes' ability to decompose substrates. The potential difference and rate of flow of electricity (currents) produced can be quantified using multimeters or Arduino based sensors.

1.2.1.1 Potential difference and current measurements with a Multi meter.

An illustration of a double (dual) chamber MFC coupled with a multi meter is shown in figure 1.6. In this setup, the transferred electrons—rate of flow of electrons and potential difference—are displayed on the multimeters and are monitored using the volt/ohm meter measurement method (Kamau *et al.*, 2018a). This method is relatively straightforward, but has the disadvantages of taking a relatively long time and not being consistent (Kinyua *et al.*, 2021).

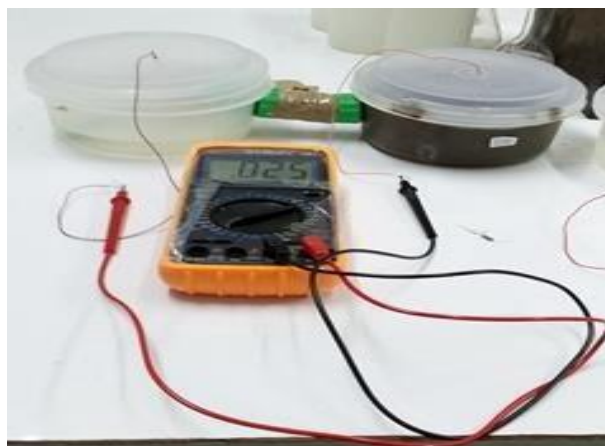


Figure 1.5: Set-up of a dual chamber MFC with a multi-meter

1.2.1.2 Measurements of current and voltage using Arduino-based sensors.

To measure DC voltage, there would be a need for a resistor of 100 k Ω connected between ground and analogue pin 0. Then connect the 1m resistor to analogue pin 0 and the other side of this resistor to the voltage you would like to test. The code is uploaded to the Arduino and the voltage displayed at the serial monitor immediately the connections are switched on. With these resistor values up to 50 V can be measured. The code to the Arduino is uploaded and serial monitor is opened, thereafter the voltage is displayed.

1.2.2 Hardware Description-Arduino Mega

According to Kumar *et al.* (2015) and Blum (2013), the Arduino Mega/UNO is a microcontroller board built on the ATmega1280 with a 10-bit analog to digital converter (ADC) resolution. The Arduino board's various components were detailed by Webb and Meller-Holst in 2001. The components in the Arduino's boards are shown in figure 1.7 below.

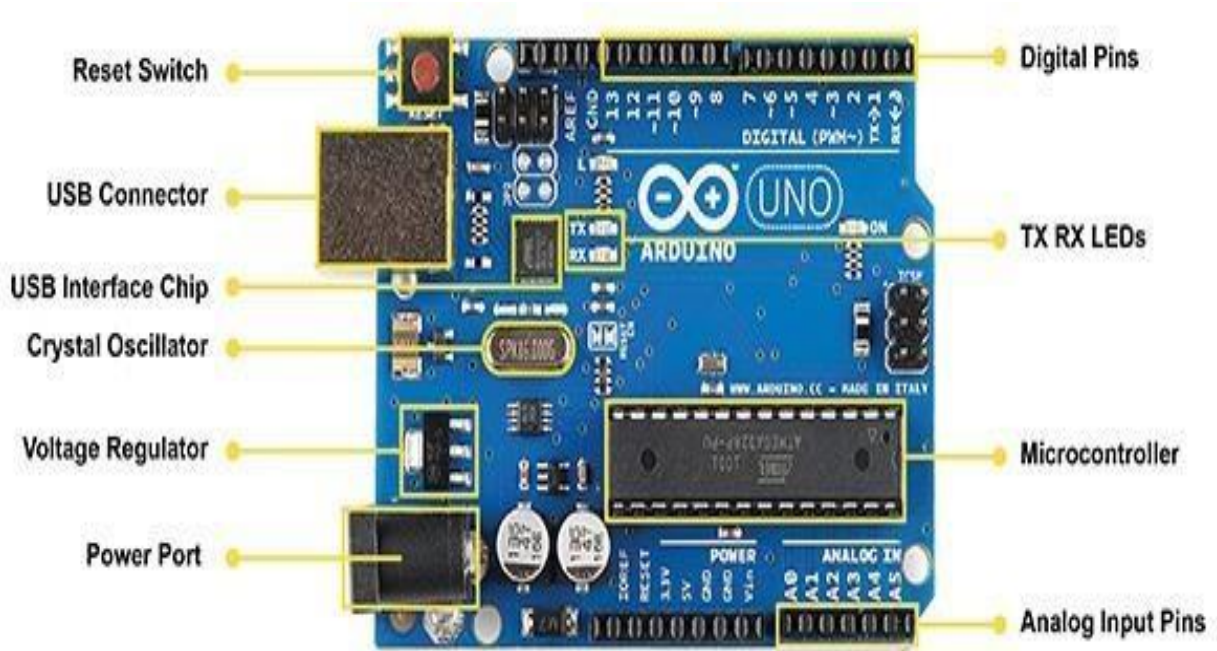
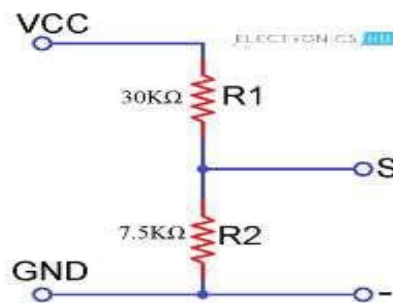
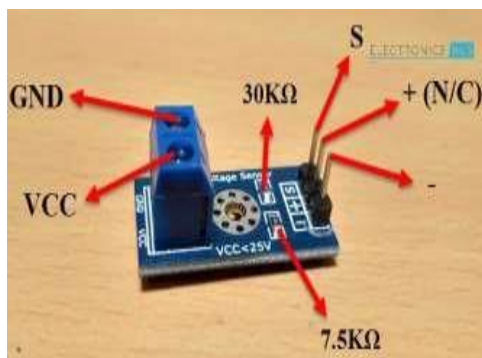


Figure 1.6: Arduino Mega Board (Kumar *et al.*, 2015).

1.2.2.1 Potential difference sensor

A potential difference sensor connected to the Arduino board has the ability to gauge any system's external potential difference. It must have a potential difference of at least 5V (Mulder *et al.*, 2008).

The pins of the potential difference sensor module are displayed in figure 1.8 below.



Figure

Figure 1.8: (a) A voltage Sensor Module (b) Internal Circuit of voltage sensor (Webb and Møller-

Holst, 2018)

Where:

- i) VCC: Positive terminal
- ii) -: GND of Arduino
- iii) S:
- iv) +: Not connected (N/C)
- v) -: GND: Negative terminal
- vi) R1/R2: Resistors
- vii) Switch

1.2.2.2 Current sensor module

A device called a current sensor on the Arduino board (IC) can be used to accurately determine both AC and DC currents. The IC has an inbuilt Hall Effect device, and the device is reliant on the Hall Effect. An analog potential difference is produced by the ACS712 Current Sensor (Webb and MillerHolst, 2001) in proportion to DC or AC currents depending on the parameter being measured.

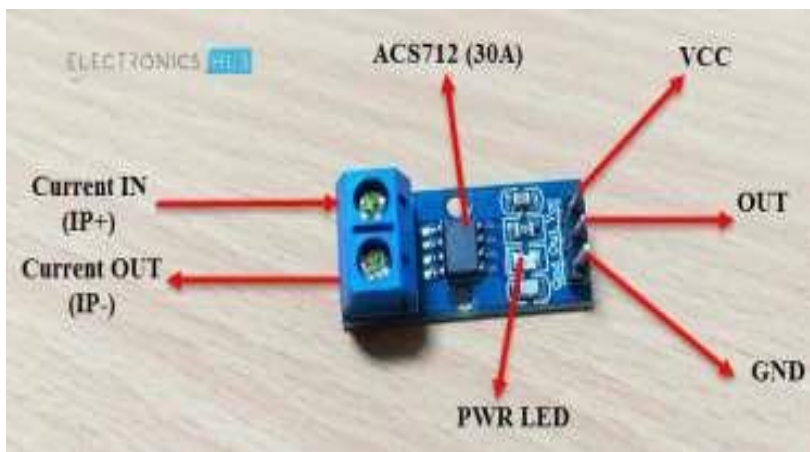


Figure 1.9: An ASC712 Current Sensor Module (Webb and Møller-Holst, 2001)

- i) VCC: Positive terminal (0-25V)
- ii) -: GND of Arduino
- iii) -: GND of Arduino
- iv) +: Not connected (N/C)
- v) OUT: Analog Input of Arduino

The potential difference and current sensor are usually connected to the Arduino board, and then a code script is created in the Arduino integrated development environment (IDE) prior to being uploaded through a USB cable to the board (Mbugua, 2021 *et al*).

1.2.3 Soil Microbial Fuel Cell (SMFC)

A bio-catalytic device known as the soil microbial fuel cell (SMFC) uses soil-based microbes as catalysts. These microbes are known as exo-electrogenic bacteria and oxidize organic substrates to liberate electrons. According to Wolińska (2014), soil microbial fuel cell has a low-bioenergy potential, and the amount of soil bioelectricity they produce is usually small. It is unclear how these soil-based microbes relate to the SMFC conditions.

Engelwaran *et al* (2019) pointed out that SMFC are usually optimized to enhance and sustain the bioelectricity generation of SMFCs by adding glucose, nutritious broth, and exo-electrogenic bacteria. The kind of conductors connected to the electrolyte, soil moisture intake, and separation between positively and negatively charged electrodes are usually examined as factors in SMFC operation. The soil properties, for example, organic composition, pH and microbial community influence the performance of the SMFCs. Zhi *et al.* (2014) isolated three different types of phyla including *Proteobacteria*, *Firmicutes* and *Acidobacteria* from wastewater and sediments. SMFCs are very appropriate in bio-remediation because pollutant toxicity and soil microbe's activities can be monitored by the electrical signals generated in the MFCs, for example, quantity of electrons, peak voltage and start-up time (Jiang Y.B. *et al* 2016). Also, the use of MFCs leads to elimination of soil pollutants such as oil, phenol and petrol. Lastly, the MFCs operation mitigates methane emissions from anthropogenic soil and dregs. MFCs do not require energy input, instead, it generates small amount of electrical power. Hence, MFCs are considered as a source of appropriate and sustainable technology (Jiang, *et al.*, 2016).

1.3 Statement of the Problem

In order to manage pests, pesticides are extensively employed in both agricultural and public health. Unfortunately, not all pesticides are deployed to their optimal capacity, and the extra compounds end up in drinking water, skins of fruits, vegetables, and the ecosystem. Because of their widespread use, pesticides are released into the atmosphere, in groundwater resources, in soil, in sediment, and on the land. Majority of pesticides are difficult to remove and have been shown to be naturally malignant, even in low quantities.

The cleanup of organic pollutants has been attempted using a variety of conventional methods, including light decomposition, Fenton degradation, ozonation, adsorption, as well as cremation. Unfortunately, these physiochemical techniques are expensive and unfavorable to the ecosystem since dangerous toxic substances are generated as byproducts. The microbial fuel cells method corrects these issues because it is inexpensive to implement, produces no harmful by-products and produces green energy.

Due to the global population increase as well as food shortages, pesticides' chemical materials, and chemical agents have been used, causing environmental degradation (Mirsal, 2008). These pollutants are usually ingested into human body especially by eating unwashed fruits. Figure 1.9, for instance, depicts contaminated tomatoes and soils after the harvest.



Figure 1.10: Pesticide on the surface of the soil as well as tomato waste

Soil contamination leads to pollution of ground waters and killing of soil microbes. For example, in figure 1.9, low weed growth is observed, suggesting deteriorating soil conditions due to high pesticide contamination. Soil microbial fuel cell technology is an appropriate technique employed to enhance soil pollutant bio-remediation which is one of the goals in this study. Bioremediation is cheaper than other methods because, besides decomposition of the pesticides, it has the advantage of generating green and renewable energy essential for house lighting and low voltage appliances. Therefore, pesticides together with the substrate using the MFC technology could be a viable way of solving the power menace in Kenya.

1.4 General Objectives

The main goal of this research is to evaluate the potential of microbial fuel cell technology for the anaerobic-aerobic decomposition of chlorpyrifos, malathion, and lambda cyhalothrin on loam soil, cabbage wastes, tomato and rumen waste.

1.4.1 Specific Objectives

This study focuses on the following specific goals:

- i) To assess the amount of electricity generated in a MFC by various pesticides on various substrates
- ii) To determine optimal conditions for degradation of the pesticides on the substrates
- iii) To evaluate modeling, mineralization data from biodegradation of the pesticides on various substrates.
- iv) To evaluate mineralization data from biodegradation of the pesticides on various substrates.

1.5 Justification

Numerous farm products are sprayed with pesticides in order to manage pests and diseases. Between one and 2.5 million tonnes of active pesticide chemicals are used yearly worldwide. Herbicides alone make a mark up of around 47% of pesticides administered currently, followed by insecticides (35%), fungicides (11%), and miscellaneous pesticides (7%) (WHO, 2007). Most of these pesticides when they are administered end up in non-targeted surfaces. Routt Reigart J· (2009) , Indicated that toxicity of pesticides varies from one pesticide to another. Usually, high toxicity is represented by LD50 and less than 500 mg/Kg, LD50 500mg to 1000mg/Kg indicates moderate toxicity whereas LD50 1000mg/Kg to 2000mg/Kg represents low toxicity. Pesticide degradation refers to the phenomenon whereby a pesticide is converted into a benign or malignant material that is either ecologically friendly or incompatible with the place where it was administered. The disadvantages of traditional pesticide degradation processes such as biodegradation, catalytic photo degradation, and hydrolysis is that they have a high implementation cost and have lengthy processing times. In addition to using a significant amount of energy, incinerating waste produces air pollution. Breakdown of pesticides using microorganisms on the other hand, is relatively safe, since benign by products are generated, inexpensive, and can also lead to production of energy. There hasn't been any known study on how microorganisms assist in the breakdown of pesticides in Kenya. Consequently, the focus of this study is on the bioremediation of chlorpyrifos , malathion and lambda-cyhalothrin on loam soil .

CHAPTER TWO

LITERATURE REVIEW

2.1 Fate of Pesticides in the Environment

Pesticides are chemical or biological substances that are used to eradicate and/or control pests. These chemicals that can be found in forms of biological agents and chemical substances are used to kill pests (Gilden, 2010), control weeds, and prevent disease. They can change into complicated metabolites in the soil (Vicente and Yolanda, 2004). Depending on the pests they are intended to control, they are classified as herbicides, insecticides, fungicides, etc. Pyrethroids are insecticides that are made from plant extracts (Raffa and Chiampo, 2021).

When experimental synthesis was developed in the 1930s, pesticide application underwent a revolution. Sulfur and arsenic, for instance, were applied to protect crops. After World War II, herbicides such as 2-methyl-4-chlorophenoxyacetic acid (MCPA) and 2,4-dichlorophenoxyacetic acid (2,4-D) were used instead of pesticides. Other pesticides that were used include dichlorodiphenyltrichloroethane (DDT), aldrin, and dieldrin (Raffa and Chiampo, 2021)

The path taken by a pesticide after it has been sprayed or administered to its surroundings is gets into the air, underground water and the soil. Only about 1.1% of the pesticide actually kills the pest (Mbugua, 2015), while the rest of the pesticide is deposited in non-intended zones. For example, after pesticide is sprayed to the plants, some sprays particles get into the surrounding air through drift, volatilization. Other pesticide particles get into the soil through adsorption, while other pesticide molecules get into the ground water through leaching, run off and surface flow as depicted in figure 2.1 below. Exposure to human beings can occur by ingestion of contaminated water or goods, by inhalation and by direct occupational, agricultural, and residential use. The toxins enter the body via the skin, the gastrointestinal tract, the respiratory system, and the eyes (Kim *et al.*, 2017).

Electrical properties and molecular structure, in addition to quantity and contact timeframes, are crucial factors in determining a pesticide's toxicity (Hamadache *et al.*, 2016; Heard *et al.*, 2017).

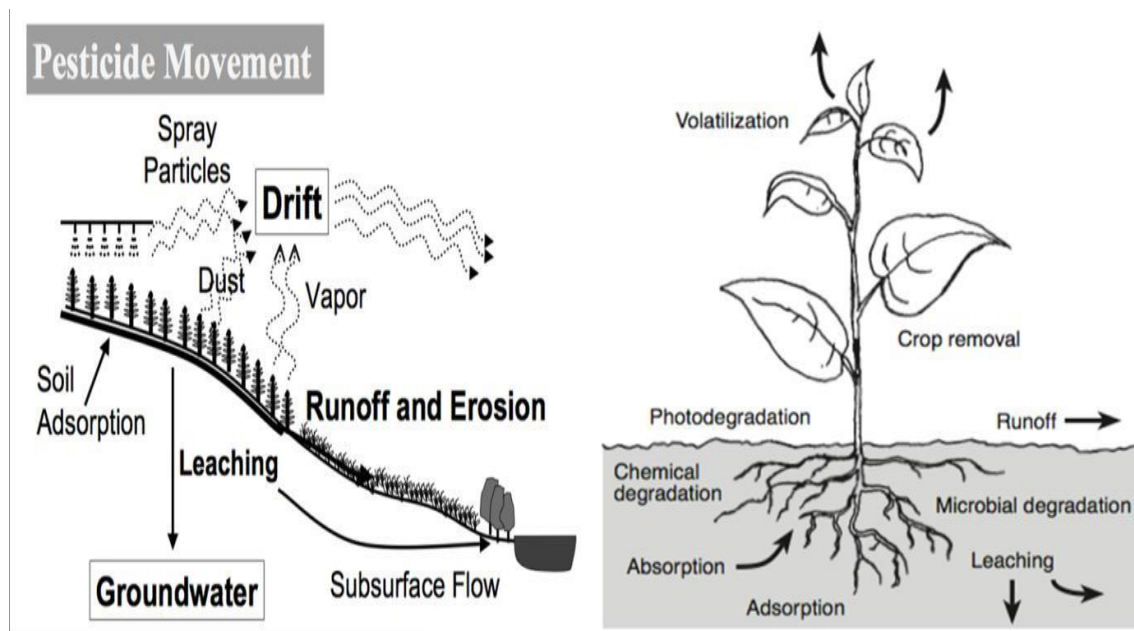


Figure 2.1: A Representation of movement of pesticide residue in the environment, (Marek Biziuk, *et al* 2016)

2.2 Pesticide Degradation

It is crucial to remove all lingering remnants from pesticides from the environment. Decontamination procedures ought to be easy to implement and safe for the environment. A wide variety of microorganisms, most notably bacteria (Doolotkeldieva *et al.*, 2018) and fungi (Erguven, 2018), break down pesticides into simpler molecules like carbon dioxide (CO₂), water (H₂O), oxides, and mineral salts that are used as carbon, mineral, and energy sources. This is usually referred to as pesticide degradation. To speed up degradation reactions, enzymes play a crucial role (Senko *et al.*, 2017).

Some degradation processes include bioremediation, photo degradation and microbial degradation processes. Bioremediation is a technology that is being used by people to utilize microbes to detoxify contaminants in the soil and generally in environmental organic matter cleanup. Photo degradation is

the chemical decomposition of pesticides in the sunshine. The pace of degradation is affected by the amount of sun as well as how long it is exposed to the sun.

Microbial degradation is a natural process, where the degradation of toxic chemicals or chemicals foreign to the organism's life (xenobiotic factors) is a strategy for the organisms' own survival.

The main difference between bioremediation and biodegradation is biodegradation is a natural process that occurs in the environment while bioremediation is an engineered technology used by human beings to clean the environment. The similarity between the two processes is that both are governed mainly by the microorganisms. Bioremediation process stands out clearly as the most effective way to manage and reclaim polluted water and soil.

2.2.1 Bio-remediation Kinetics

Determining whether or not contaminants from pesticides are pervasive in the ecosystem relies heavily on how quickly pesticides breakdown. The rate at which these substances are degraded depends on a number of environmental conditions, e.g., temperature, P_H , amount of oxygen, the irradiation of light and the amount of organic matter in a given volume of solvent. Kinetic studies can use the kinetics of mineralization to learn how organic pollutants break down (Dyson *et al.*, 2002). Inorganic chemicals including carbon dioxide, chloride ions, sulphate ions, nitrate ions, and PO_4^{3-} are monitored to evaluate mineralization activity. Total organic carbon (TOC) analysis is the gold standard for spotting mineralization.

Some research efforts have focused on elucidating the kinetics of pesticide breakdown as a means of gauging pesticide stability in the environment. To determine the byproducts of catalytic degradation of triazophos with a titanium dioxide catalyst, Penuela and Barcelo published a report in 1998. In their report, they intimated that, after being subjected to TiO_2 , triazophos absorbs light then degrades in 4.5

hours. Irradiation with TiO₂ for 60 minutes eradicated 2, 3, 6-trichlorobenzoic acid entirely (Prevot & Pramauro, 1999). This chemical disintegrated at a much faster pace at a pH value of 3, but rates lowered at lower pH values.

Blanco *et al.* (1996) studied kinetics of pesticide breakdown in water samples using ultra violet (UV) light and realized that pollutants began to degrade after more than five hours of irradiation.

Several authors have focused their attention on calculating the kinetics of pesticide breakdown as a means of gauging pesticide persistence in the environment.

Rates of disintegration of the five pesticides tested by Soliman (2012) were found to differ with molecular structure, exposure duration, as well as UV-ray wavelength. With respect to the five pesticides tested, methomyl was the one most affected by ultraviolet light. After being exposed to Ultra Violet light for an hour, the levels of ES-Fenvalerate 11.30%, pirimicarb 14.80%, imidacloprid 29.03%, buprofenzin 31.83%, and methomyl 39.0%. Pesticide residue photo degradation was found to be influenced by temperature, pesticide molecular structure, light intensity, and period of exposing it when incandescent and fluorescent tubes were exposed to spinach leaf surfaces for varied time intervals (Mbugua *et al.*, 2022).

2.2.2 Photo-degradation

The phrase "photo-degradation" refers to the chemical decomposition of pesticides when exposed to solar energy. The pace of degradation is affected by the amount of sunlight as well as the duration of exposure to sunlight. Pesticides absorbed or adsorbed onto the sediment and the one applied to the leaf surfaces must be irradiated to measure the rates of photo degradation. The ecological dispersal routes of a pesticide molecule are shown in Figure 2.2.

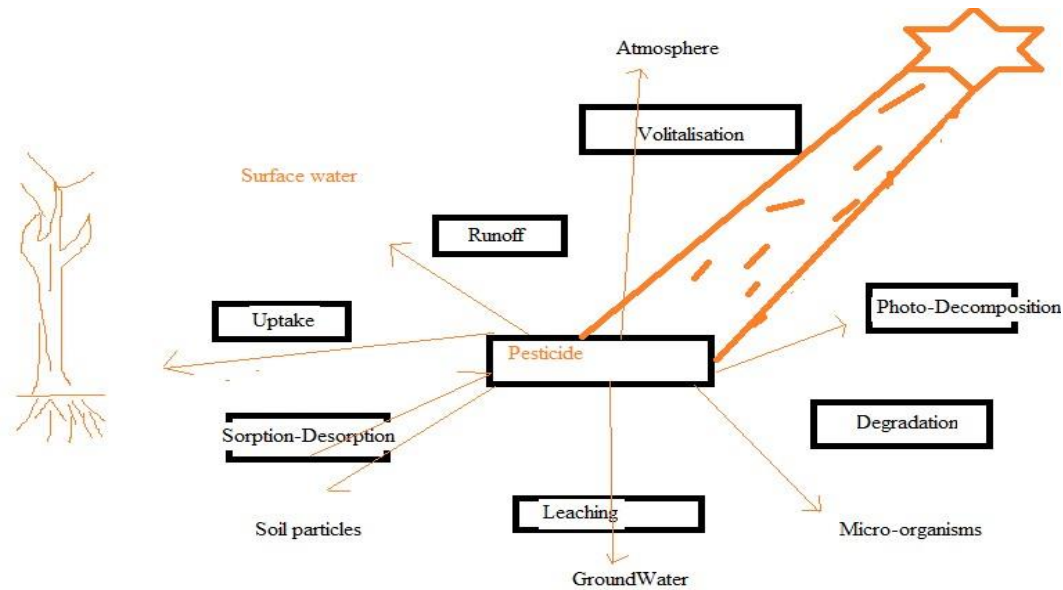


Figure 2.2: Pesticides Dissipation pathways (Kinyua *et al.*, 2016).

2.2.3 Microbial degradation

Microorganisms (bacteria and fungi) are able to derive energy from pesticides if no other sources of carbon and nitrogen are accessible. Molecular insecticides can bind to each other, to other chemical substances or to soil particles fairly well. Microorganisms on the other hand are able to take up and degrade pesticides. Biological pesticide degradation technologies are cheap and effective for a number of organic contaminants (Das and Dash, 2014). Ideally, pesticides should degrade into less reactive substances such as CO₂, water, and minerals (Konradsen *et al.*, 2003). Partial degradation of pesticides could lead to toxic transitional molecules if bacteria don't use them as a food or energy source (residues may have biological activity). A booster that enhances microbial activity may hasten the breakdown of pesticides. Soil microorganisms and parasites use a variety of metabolic pathways, some of which work in tandem with one another to degrade such stubborn toxins. Soil microorganisms including bacteria have been linked to the decomposition of the chloro-aromatic fungicide such as Pentachlorophenol, according to a developed impediment technique (Zhai *et al.*, 2012).

Two main divisions of bio-remediation are in-situ and ex-situ microbial bio-remediation systems. The in-situ procedures treat pollutants right where they are produced, ex-situ techniques remove them off polluted sites and transport them to a central treatment facility. Ex-situ treatment has been deemed ineffective by several specialists owing to its multiple drawbacks for example large quantities of soil or water cannot be decontaminated; soil excavation is costly and may lead to pollution of clean sites (Azubuike et al., 2016).

Another category of bioremediation is in the *invivo* and *invitro* category. Microorganisms which aid in the remediation of toxins *in vitro* might not be competent to accomplish this task *invivo* (Head *et al.*, 2003; Barupal *et al.*, 2019a, b), and their cost-effectiveness varies by region. Further study of the mechanisms of action and the proliferation of microbes in polluted environments is required for a fuller comprehension of these issues (Lovley, 2003).

2.2.4 Bacterial Bioremediation

Microorganisms, either aerobic or anaerobic, are used in bacterial disintegration to decompose environmental contaminants. In bio-stimulation, bacteria in the soil are enriched selectively; in bioaugmentation, additional bacteria are introduced; and in bio-accumulation, contaminants find a home within the cells themselves (Srivastava *et al.*, 2014). Through continuous interactions with other species as well as their surroundings, bacteria are able to acquire carbon nutrients and energy necessary for growth (Srivastava *et al.*, 2014).

Carbon availability is a fundamental determinant of bacterial development, which in turn reduces the rates of the breakdown of pollutants (El-Bestawy *et al.*, 2014). As per Liebig's Law of the Minimum, the declining substrate requirements of individual microbes are the primary limiting force.

Consequently, locating and delivering the scarce resource(s) can boost bioremediation effectiveness (Benyahia and Embaby, 2016). The toxin being catabolized by a heterotrophic microorganism ought to be both carbon (C) and energy sources

According to Mota *et al.* (2016), cyanobacteria, which is an autotrophic bacterium, bio-degrades non-carbon contaminants such as metals, and *Thiobacillus sp.*, a chemolithoautotrophic bacteria, has the capacity to decompose heavy metals in the environment to form a metal-leachate (Lloyd, 2000). . Therefore, carbon is a significant determinant of bacterial development that in turn lowers the rates of pollutant disintegration (El-Bestawy *et al.*, 2014). By Liebig's Law of the Minimum's reckoning, the decreased substrates per microbe need are a primary major bottleneck. In this way, locating and giving the scarce resource(s) can boost bio-remediation effectiveness (Benyahia and Embaby, 2016), and a catabolized pollutant in the case of a hetero-trophic organisms ought to be a source of both energy and carbon.

Considerable success has been found where microorganisms which are genetically modified have been utilized in bioremediation. Utilization of modified organisms in bio-remediation is beneficial in certain ways, unleashing lab-created germs into the wild has some undesirable consequences (Peixoto *et al.*, 2011; Huang *et al.*, 2015). Given reducing conditions, microorganisms perform reductive de-chlorination of Dichlorodiphenyltrichloroethane (DDT), the first step in making Dichlorodiphenyldichloroethane (DDD). Reductive de-chlorination necessitates the transfer of electrons, the discharge of a chloride ion (Cl⁻), and the formation of R radical (alkyl group) (Aislabie *et al.*, 1997).

Multiple bacteria have demonstrated the ability to dechlorinate DDT via a reductive pathway (Aislabie *et al.*, 1997; El-Bestawy *et al.*, 2014). A good example is coliform bacteria isolated from rat intestines were shown by Mendel *et al.* (1996) to be capable of reductively dechlorinating DDT to DDD. Other creatures rely on oxidative catabolism. Nadeau *et al.* (2013) looked into whether or not

Alcaligenes eutrophus bacteria could break down DDT (1994) and found that during the initial stage, 2, 3-dihydrodiol-DDT (two hydroxyl-DDT) is formed via oxidation of the phenyl ring at ortho and meta positions close to the phenyl ring (Nadeau *et al.*, 1994). *Shewanella putrefaciens* employs a similar reductive dichlorination process to break down DDT (Jin *et al.*, 2015). *S. putrefaciens* is a member of the *Shewanella* genus and an exo-electrogenic species that can be cultured in bio electrochemical systems (Pandit *et al.*, 2014) and then implanted into contaminated soils, where it could potentially hasten the breakdown of DDT. Catabolizing microbes can utilize organic pollutants as both a carbon and energy source. Aerobic bacteria which feed solely on trichloroethene (TCE) convert this common groundwater pollution into harmless byproducts (Schmidt *et al.*, 2014).

2.2.5 Bio-electrochemical Bioremediation

Diverse Bio-electrochemical systems (BESs) have used bioremediation in both regulated studies in laboratory and in trials for limited field. Occasionally, BESs could be preferable to conventional bioremediation methods. For example, when conventional bioremediation is compared to use of Iron (III)-only, it was found to be slow and ineffective.

MFCs demonstrated promising results in decomposing polyaromatic hydrocarbons (PAHs) in water sediments, (Yin *et al.*, 2009). After 240 days, the MFC containing ferric hydroxide was 99.47% effective in removing phenanthrene and 94.79% effective at removing pyrene (Yan *et al.*, 2012). Naphthalene, acenaphthene, and phenanthrene are just a few of the PAHs that might be degraded by MFCs as they produce energy (Quince *et al.*, 2009). Cultivation of bio-remediation microbes can be hard compared to introducing them to the environment.

2.2.6 Pesticide Bio-remediation via Microbial Fuel Cells

Today use of micro-organisms that exist naturally for environmental clean-up (bioremediation) has grown in popularity, despite the fact that its implementation has been constrained by the bacteria's

extremely low effectiveness as well as poor controllability (Cao *et al.*, 2017; Mandal and Das, 2018). To give just one scenario, the pesticide such as hexachlorobenzene (HCB) is extremely harmful to both environment and human beings. To get rid of hexachlorobenzene in soil, people have turned to MFCs. The effectiveness of hexachlorobenzene degradation and power generation in soilMFC was analyzed by Cao *et al.* in 2015, and found that when they compared it to various removal systems, such as the soil mfc system, the open circuit control system, and the no addition anaerobic sludge blank system, the HCB removal efficiencies were 71.15%, 52.49 %, and 38.92 %, respectively. The maximum power density measured was 77.5 mW m^{-2} with an external resistance of 1000 Ohms. Soil MFC degraded HCB through the reductive de-chlorination route when the soil was aerobically depleted of oxygen. More electrons were produced when anode-promoted electrogenic bacteria were present, which in turn could increase the efficiency with which HCB was removed from soil MFC (Mandal and Das, 2018).

For better pollutant biological degradation, microbial electro-remediating cells, a bio-electrochemical technique which seeks to alleviate electron acceptor limitation and boost metabolic oxidation, can be employed (Rodrigo Quejigo *et al.*, 2016). Research conducted by Rodrigo *et al.* (2016) found that using Microbial Electro-remediating Cell (MERC) principles stimulated soil bacteria to break down ^{14}C isoproturon to $^{14}\text{CO}_2$ at a 100% efficiency rate. Using an electrode positive potential (+600 mV against Ag/AgCl) boosted mineralization 20 times compared to the electrode-free control (Rodrigo *et al.*, 2016). Borrello *et al.*, (2021) examined the use of MFCs to purify soil loaded with DDE by applying numerous trial setups (such as compost addition as well as open/closed circuit) to find ways to improve MFC effectiveness in favor of DDE eradication. Two months later, they found that MFCs performance fostered considerable DDE eradication (69 percent). After introduction of compost, microbial activity increased and MFC functionality significantly improved for quite a longer duration of time. In a separate investigation, using MERC principles in various combinations to promote soil microbes, the

herbicide 14C-atrazine (ATR) was entirely and readily biodegradable to CO₂ in soils. According to the research, 20 times more ATR mineralization occurred when electrodes were used at a positive potential (+600 mV vs Ag/AgCl). An ecotoxicological analysis of the soil following the bio-electro venting treatment also showed a 20-day efficient clean-up. Such environmentally benign innovations have great potential, as shown by the impact of electrodes on soil bioremediation where electron generating bacteria are adsorbed. (Domnguez-Garay *et al.*, 2018).

2.2.7 Microbial Degradation of Organophosphate Pesticides

Organophosphates are frequently combined with 2 organic compounds, a side chain of cyanide and thiocyanate, or phenoxy moieties (Balali-Mood and Abdollahi, 2014). The transformation of organophosphate pesticides generally follows the scheme shown in figure 2.3.

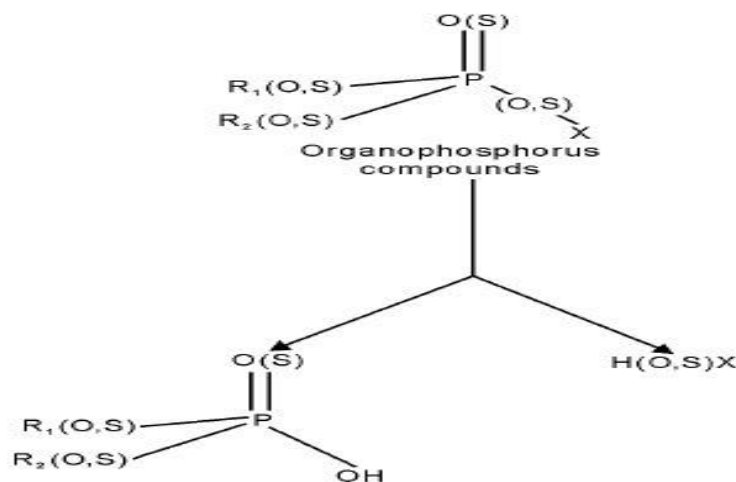


Figure 2.3: Organophosphate pesticide biodegradation products (Sighn and Walker, 2006)

2.2.7.1 Chlorpyrifos

Chlorpyrifos is extensively used in the management of agricultural insect pests. It is extensively employed in the United States of America where over 11 million pounds of organophosphate pesticides (chlorpyrifos) was the most widely used pesticide in 2007 (Grube *et al.*, 2011). This substance controls a wide range of residential, foliar crop, and soil pests as well as mosquitoes (both larvae and adults), flies, and other pests. Regarding the destiny of chlorpyrifos in the ecosystem, substantial studies have

been carried out (Kim and Ahn, 2009). In the deterioration of soil, both microbial activity and chemical hydrolysis are involved. The $\frac{1}{2}$ life of chlorpyrifos in soil is approximately 38 days but for the same pesticide, the hydrolysis (in water) $\frac{1}{2}$ life is 2118 days (Kegley *et al.*, 2014). Chlorpyrifos is degraded by bacteria isolated from a variety of matrices, comprising industrial wastewater, activated sludge, arable soil, as well as effluents (Li *et al.*, 2007, 2008; Kim and Ahn, 2009; Chishti *et al.*, 2013). In agricultural soils and polluted wastewaters throughout the globe, *Pseudomonas nitroreducens*, *Pseudomonas putida*, *Pseudomonas aeruginosa*, *Pseudomonas stutzeri*, and *Pseudomonas uorescence* have all been reported to be particularly effective at biodegrading chlorpyrifos (Latifi *et al.*, 2012; Sasikala *et al.*, 2012). At a concentration of 200 mg/mL, the *Bacillus aryabhatai* that Pailan *et al.* (2015) recovered from agricultural soil in West Bengal, India, effectively broke down both chlorpyrifos and parathion. It was discovered that *Stenotrophomonas sp.*, prevalent in China's contaminated effluent, was able to break down 63 percent of chlorpyrifos in 24 hours at a starting level of 50 mg/mL.

The specific mechanism for the oxidation of chlorpyrifos as well as its various transitional molecules is shown in Figure 2.4. According to Huang *et al.* (2000), who looked into the breakdown of chlorpyrifos in chicken and cow wastewaters, chlorpyrifos was consumed by aerobic microbial activity in animal-derived lagoon wastewaters. Singh *et al.*'s (2003), in their study on the biodegradation of chlorpyrifos at pH levels ranging from 4.7 to 8.4 in the UK and Australia realized that soil microbes were responsible for the pesticide's decomposition. A bacterial population that used chlorpyrifos as a carbon source was discovered in an Australian soil, and the enhanced ability to decompose chlorpyrifos was later transported to soils in the United Kingdom (Singh *et al.*, 2003).

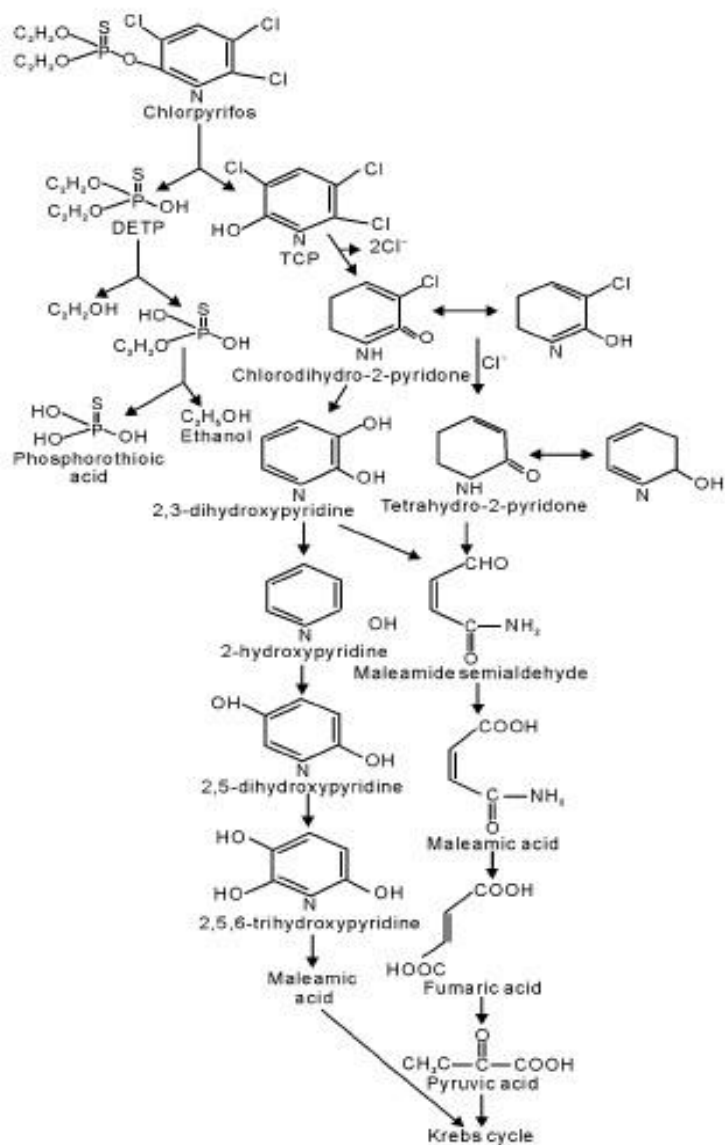


Figure 2.4: Chlorpyrifos microbial breakdown mechanism (Singh and Walker, 2006).

2.2.7.2 Malathion

Malathion is an organophosphorus pesticide (OPP) called diethyl-2-dimethoxyphosphonothiol-sulfalbutane-dioate used to eradicate thrips, bagworms, woolly aphids, boxelder bugs, lace bugs, four-lined leaf bugs, leafhoppers, red spider mites, Japanese beetles, and red spider mite eggs (Wallace 2010). From 1980 till 2012, the chemical Malathion became one of the most widely used pesticides in the market. This pesticide is primarily produced in China and India, and from 2012 to 2017, it ranked

as the second commonly used pesticide in India (Kumar *et al.* 2019). Malathion continues to be used for pest control throughout many third-world countries as well as developing nations even though numerous governments, notably India, explicitly outlawed its usage and substituted it with non-toxic insecticides (Loha *et al.*, 2018). Its accumulation and longevity in the environment are well known owing to the widespread usage of it in farming techniques (Jallow *et al.* 2017; Galani *et al.* 2018) ; Ramadan *et al.* 2020). Malathion remnants have been found in a number of farm products, particularly vegetables and fruit crops, providing severe health concerns to non-target groups, including people. Malathion was originally categorized by the US EPA in 2006 as a pesticide with class III toxicity, but subsequent carcinogenicity evidence on human populations led to its reclassification as a pesticide with class IIA toxicity (Chiu *et al.* 2018).

The most common negative health consequences of malathion include neurotoxicity (acetylcholinesterase inhibition), immunologic diseases, reproductive disorders, cytotoxicity, hyperglycemia, genotoxicity, vertebrate adrenal gland malfunction, and teratogenic disorders. This dangerous contaminant should therefore be removed from polluted ecosystems as much as it is possible. Bioremediation has been found to be the most effective means as well as longest efficient method for malathion clean up from the environment. Malathion can be effectively biodegraded by a variety of bacterial and fungal species, but no effective psychrophilic or psychrotolerant microbial species have been reported yet (Kumar *et al.* 2019). The first studies to attempt to degrade malathion was conducted by Yirui *et al* (2009) where they used *Ochrobactrium* ssp bacteria for its effective attempts to degrade Phthalates, polyaromatic hydrocarbons, heavy metals and numerous varieties of pesticides such as fungicide and herbicides (Zhang *et al.* 2006; Zhao *et al.* 2012), (Shi *et al.* 2011; Hadi *et al.* 2013), (Pandey *et al.* 2013; Ghosal *et al.* 2016). Figure 2.5 below demonstrates the proposed malathion breaks down into its components.

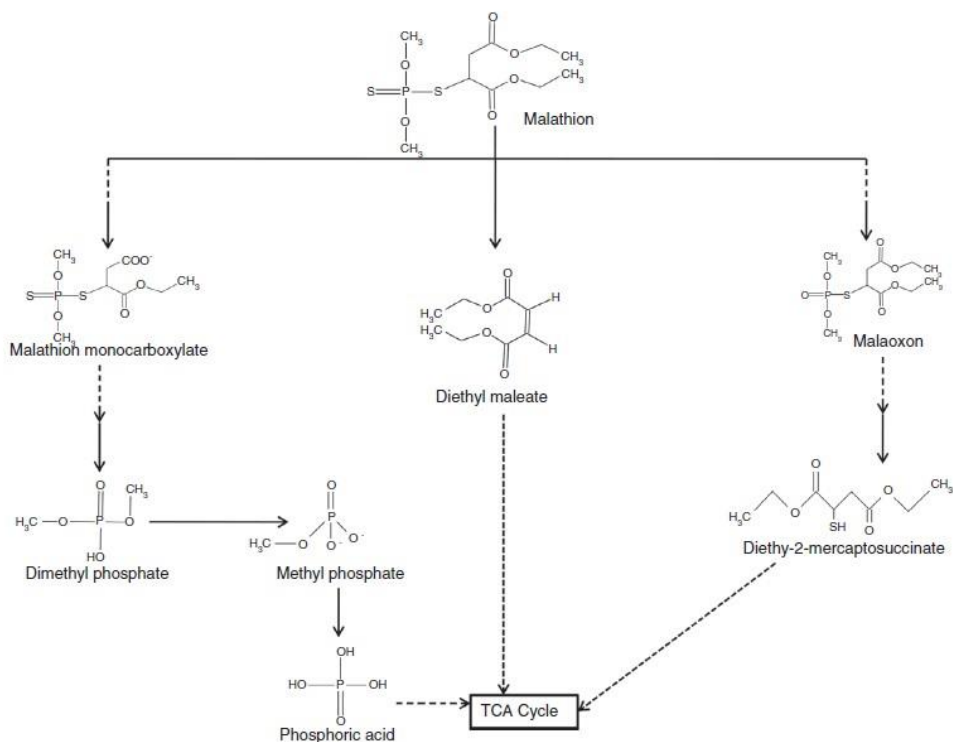


Figure 2.5: A proposed malathion breakdown by bacterial *Ochrobactrum* sp. (Verma *et al.*, 2021).

Figure 2.5 displays all molecules recognized in figure 2.5 above have been identified and determined by the Gas Chromatography-Mass Spectrometry (GC-MS) analysis. The broken lines and arrows indicate that there may be numerous steps in the degradation pathway before the metabolites join the tricarboxylic acid (TCA) cycle. These metabolites were not identified in figure 2.5. The metabolite(s) that might have been produced following malathion decomposition and have been previously documented but were not observed by Verma et al. (2021) as in figure 2.5, is shown using a combination of broken and solid lines/arrows.

2.2.7.3 Lambda Cyhalothrin

Lambda Cyhalothrin is the commonest pyrethroid used in houses, healthcare, horticulture, forestry, public health, as well as construction sites (Spurlock & Lee, 2008). Common environmental toxins like cyhalothrin

endanger non-target animals like human beings. Many conventional methods have been tried to detoxify organic pollutants, for example photo-decomposition, Fenton degradation, ozonation, adsorption, and cremation (Arora *et al.*, 2012; Yang *et al.*, 2011). Unfortunately, these physicochemical procedures are expensive and hostile to the ecosystem since they produce potentially toxic substances as by-products (Arora *et al.*, 2014a; Arora *et al.*, 2014b). Biodegradation has lately become a viable and appropriate option for minimizing contamination, due to its affordability and advantages for being environmentally friendly (Wang, S. & He, 2013; Singh, 2009). Pyrethroids biodegrading strains, namely *Serratia* sp. JCN13 (Zhang *et al.*, 2010) and *Brevibacterium aureum* (Chen *et al.*, 2013), have been employed to decompose cyhalothrin together with the three genes *Estp*, *pytH*, and *PytZ* encoding pyrethroid-hydrolyzing as shown in figure 2.6 below.

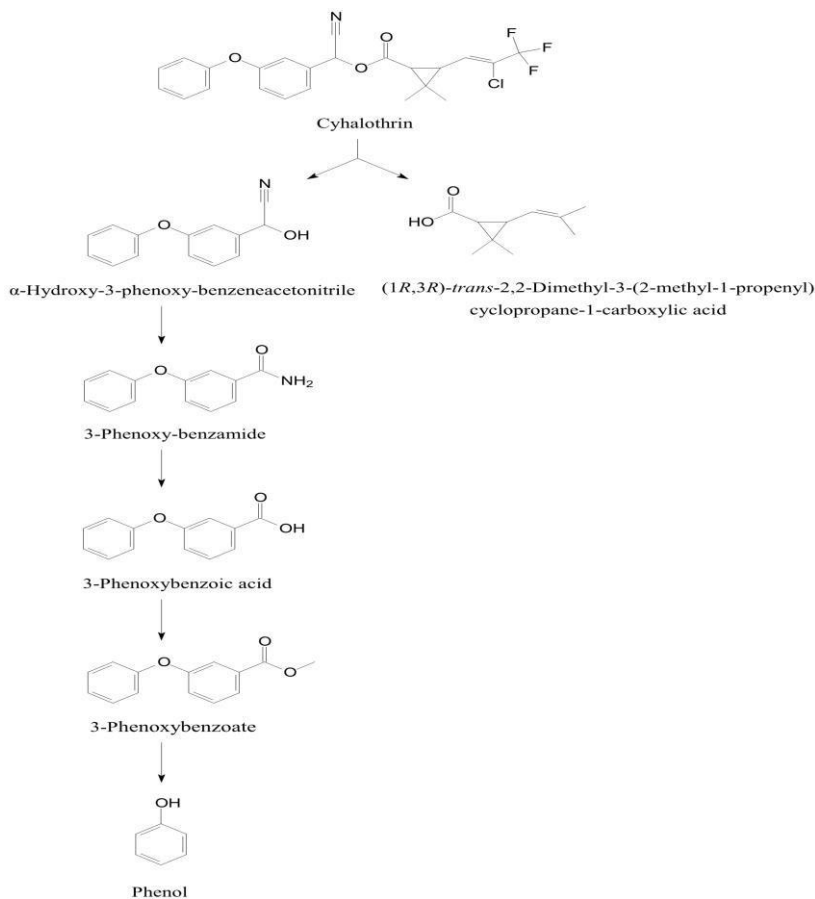


Figure 2.6: A suggested lambda cyhalothrin degradation mechanism (Chen *et al.*, 2015)

2.3 Bioremediation of pesticides using MFC

Numerous bacterial, yeast, and fungal species have been employed to remediate pesticides from surfaces. To show the scientific community's emphasis on bioremediation of toxic substances during the first decade of the twenty-first century, several microbes were used for pesticide breakdown. Bioremediation as a key topic of microbiology study is increasing in importance due to its growing potential to reduce the risks associated with various pollutants via biodegradation. Due to their benefits over traditional bioremediation techniques, microorganisms might well be regarded as effective tools for removing contamination from water, soil, and sediments (Demnerova *et al.*, 2005). Every bioremediation method must show that the elimination of contaminants is the primary result of biodegradation and that the rate of breakdown exceeds the rate of detoxification naturally occurring.

The ability to get results that is at par with or superior to those generated in the laboratory presents one of the obstacles in the development of bioremediation systems (Juhasz *et al.*, 2000). Some of the microorganisms used in bio-remediation are presented in table 2.1.

The main method for cleaning up contamination in the environment is degradation of organic matter, which depends on the metabolic activity of microorganisms. Nevertheless, the procedure is heavily dependent on abiotic factors and the microbial population (Vogt and Richnow, 2014).

Table 2.1: Some microbes previously employed in bio-remediation of pesticides

Pesticides- Organochlorine insecticide	Microorganisms	Reference(s)
Aldrin, lindane	<i>Bacillus sp.</i> , <i>Exiguobacterium aurantiacum</i> , <i>Pandoraea sp.</i> <i>Pseudomonas, p</i> <i>seudoalcaligenes.</i> ,	Okeke et al. (2002); Lopez et al. (2005)
DDT	<i>Serratia marcescens</i>	Bidlan and Manonmani (2002)
Endosulfan	<i>Aspergillus terreus</i> , <i>Bacillus sp.</i> , <i>Cheatosartorea stromatoides</i> , <i>Cladosporium oxysporum</i> , <i>Fusarium ventricosum</i> , <i>Klebsiella oxytoca</i> <i>Klebsiella pneumoniae</i> <i>bacterium sp.ESD</i> , <i>Pandoraea sp.</i> , <i>Pseudomonas aeruginosa</i> , <i>Pseudomonas spinosa</i> , <i>Pseudomonas</i>	Sutherland et al. (2002); Siddique et al. (2003a); Sethunathan, et al. (2004); Kwon et al., (2009), Myco- al. (2005) Mukherjee and Mittal, (2005); Hussain et al. (2007a, 2007b)

2.3.1 Factors influencing performance of microbial fuel cells

The Microbial fuel cell is influenced by the number of factors: micro-organisms population , the pesticide concentration levels, pH range, substrate/filtration media, hydraulic retention time and the external resistance

2.3.1.1 Microorganisms

Electro-active bacteria (EAB), also known as electrogens, are microorganisms that function as electrons and are essential for the functioning of MFCs. By eating organic chemicals, such bacteria are able to generate energy. By sending electrons to an acceptor in the cathodic cell, these microbes can produce electricity (Yadav et al. 2012; Guang *et al.* 2020). As per Shi *et al.* (2018) and Guang *et al.*, (2018), EABs were discovered in polluted fields, anaerobic bio-slurry, sewage treatment plant sediment, soils, as well as rivers (Guang *et al.* 2020). Among the factors that are most important in influencing the efficiency of an MFC system are EAB operations. In contrast to how the cathodic cells undergo electron loss, the anodic cells' microorganisms make use of a substrate in the degradation process. Carbon dioxide, H^+ , as well as electrons, are the byproducts of the aforementioned process (Yadav *et al.*, 2018). Mbugua *et al.*, (2018) reported that the composition of the substrate, pH, and temperature affect how successfully microorganisms decompose the substrate.

(Imwene *et al.*, 2021; Srivastava *et al.*, 2019; Guang *et al.*, 2020).

2.3.1.2 Microbial growth phases

A previous study (Manhart *et al.*, 2018) found a correlation between the rate of microbial development and voltage outputs, and segmented the growth into phases. The first phase is the lag phase, this is when microorganisms gradually adapt to their surroundings, develop quickly and metabolize the organic matter within, multiply and increase in numbers. The second phase is called the log phase or exponential phase. Here the bacteria rapidly consume any organic material accessible, and expand

enormously in a short time. The third phase is the stationary phase, where the microbial population is steady and cell growth slows down. In this phase the new cells produced are balanced out by those that are dying. The fourth phase is called death phase. Death phase is characterized by more microorganisms dying than the ones that are being reproduced. Figure 2.7 illustrates how the death stage sets in as all organic material in the environment has been consumed (Koch *et al.*, 2015) .

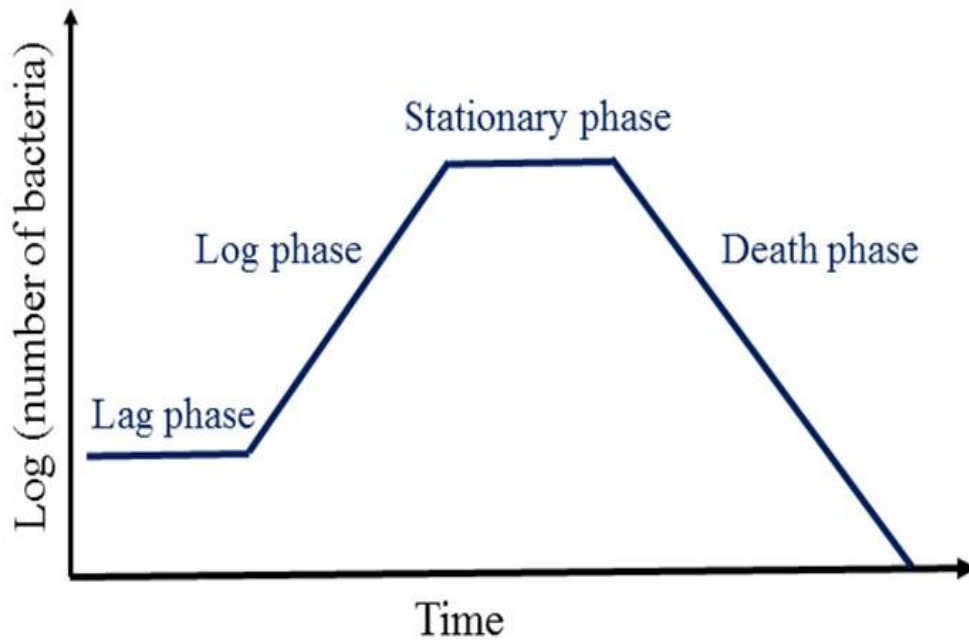


Figure 2.7: A typical bacterial growth curve (Yates, G. T., & Smotzer, 2007)

2.3.1.3 Substrate or Filtration Media

Agar or substrates, which serve as the microorganisms' nourishment, are an additional crucial part of MFCs. Filtering, trapping, adsorption, and biodegradation are only a few of the physical, chemical, as well as biological processes that substrates offer to get rid of pollutants (Yang *et al.* 2018a, 2018b). The substrate provides the microorganisms with nourishment and a place to live (habitat).

The effectiveness of the constructed wetland (CW)-microbial fuel cell is significantly influenced by the substrate or filtration material employed in the device. A crucial consideration while selecting the

substrate for the system is the accessibility of the food matrix (Dordio & Carvalho 2013). For instance, the size of the substrate particle affects the hydraulic properties and porosity of a substrate. Microorganisms carry out chemical and biological reactions while its permeability controls the passage of effluent through the system (Dordio & Carvalho 2013). Because it provides additional surface area for contact with the therapy and biofilm formation, a porous medium is frequently used.

2.3.1.4 Electrodes

Since electrodes serve as the primary hosts for the redox reaction in the system, they have a big impact on how well the system works as a whole. In MFC, choosing the right electrode material is essential (Shi *et al.*, 2018). Basically, the anode and cathode electrodes are submerged in the anodic and cathodic chambers, correspondingly, in any MFC system (Kalathil *et al.* 2018). According to Doherty *et al.*, (2015a, 2015b; Kalathil *et al.* 2018), the position and kind of material employed as the anode and cathode have a significant impact on the microbe-electrode contact which is required for biofilm growth, substrate oxidation, and electron transfer. The power density per electrode spacing is due to internal resistance. The highest power densities of MFCs are low because of large ohmic losses and electrode potential losses (Wang *et al.* 2017a, 2017b). As a result, it is critical for the advancement of CW-MFC to overcome large internal resistances. Therefore, it is vital to choose the correct electrode material and provide the anode and cathode electrodes with a suitable amount of space.

2.3.1.5 Hydraulic Retention Time (HRT)

This is the average duration a substrate stays in a digester. (Abdelgadir *et al.* 2014). There are many ways to express the hydraulic retention time (HRT). One of these is outlined in equation 2.1.

V

$$HRT = \frac{V}{\theta * X} \dots \dots \dots (2.1)$$

Where V is the capacity of the chamber, θ is the *amount of* substrate while X is the substrate flow rate in m³/h.

The primary factor affecting how microbes as well as the food matrix engage is HRT (Velvizhi 2019). Both the pollutant removal rate and the system's output power can be enhanced by raising the HRT, which enhances the system's power generating capability. Yang (2015) looked at the HRT efficiency of the system for periods of 6, 12, 18, 24, 36 and 48 hours. They found that optimum HRT efficiency is between 6 and 24 hours. Internal resistance and the lag phase for the MFC system reaches its steady voltage output when HRT rises (Shi *et al.* 2018).

2.3.1.6 PH

There is a direct correlation between the MFC voltage outputs and time-course pH fluctuations (anodic and cathodic). In acidic settings, damaged anodic microorganisms and biofilms may reduce the efficiency of MFC. A pH of 4 may eventually and maybe permanently harm MFC performance. Under acidic pH circumstances, lower voltage outputs (232-284 mV vs. 311-339 mV) and power generation (95-116 mW m² vs. 182-237 mW m²) were achieved, leading to quicker COD removal. In acidic settings, *Simplicispira*, *Variovorax*, *Comamonas*, and *Acinetobacter* predominated; in neutral conditions, *Chlorobi*, *Aquaspirillum*, and *Sphingomonas* thrived.

2.4 Summary of Gaps in Knowledge

Concerning the microbial fuel cell-based decomposition of malathion, lambda-cyhalothrin, as well as chlorpyrifos, there is currently no information in the scientific literature. Additionally, so far, there has been no information on the use of the breakdown of chlorpyrifos, lambda, and cyhalothrin as cosubstrates in microbial fuel cells for the production of electricity (green energy). Knowing the

biodegradation of pesticides used in greenhouses will be made much simpler with the assistance of this kind of knowledge. By breaking down the remnants of pesticides, the obtained information can help the county governments and the Ministry of Health to reduce environmental pesticide contamination

CHAPTER THREE

3.1 MATERIALS AND METHODS

The reagents, apparatus, as well as procedures used to accomplish the goals of this research are covered in this chapter.

3.2 Materials and Reagents

According to the processes, the common grade or analytical grade was applied as delivered. They fit into the following categories:

The pesticide standards were obtained from Dr. Ehrenstorfer GmbH Co. (Germany). The three insecticides chosen were those that the "Iranian National Standards Organization" had approved for use in tomato production. The compounds were produced as 1000 mg/L stock solutions in acetonitrile and kept at 18°C.

For this work, the following supplies and reagents were: The fresh rumen waste from the Dagoretti slaughterhouse served as the source of the microbes, whereas lambda cyhalothrin, malathion, and chlorpyrifos were obtained from an Agro-vet retail outlet in Nairobi. Some of the equipment that were used include: Analytical balance (Model BSA224S-CW), GC-MS (Model 310 SRI series), Flame photometer (Model FP910-5), 1.5 mm copper wire, and 1cm quartz cuvettes (model LAB4US quartz). Additional materials and reagents used were glass bottles, aluminum foil, graphite electrodes, plastic containers, HCl, masking tape, NaCl (pure pharma grade 99, AR 7647-14-5sigma- Aldrich) from Science Lab Nairobi, grade agarose, pH meters (Digital PH Model HQ4OD), thermometers (VTMT-02), mincers or blenders, and green Polyvinyl chloride pipes.

In the bacterial experiments, blood agar was used. The components of the blood agar were as follows: HM Peptone B # 10.000 g/Litre (Hi Media -HM- Culture Media Base RM669-500G.), Tryptose 10.000

g/Litre, Sodium chloride 5.000 g/Litre, and Agar 15.000 g/Litre. The pH was kept constant at 7.1 ± 0.2 at 25°C . Besides, MacConkey agar was also used in the research, along with peptones (meat and casein) of 3.000, pancreatic digest of gelatin of 17.000 g/Litre, lactose monohydrate of 10.000, bile salts of 1.500, crystal violet of 0.001 g, neutral red of 0.030 g, as well as agar of 13.500 g/Litre. Upon disinfection, the operating pH was kept at 7.1 ± 0.2 .

Analar grade hydrochloric acid, an oven, a thermometer, and Sulphuric (vi) acid (98%) were employed in the proximal analysis work. Materials used in the construction of the microbial fuel cells included 1.5-liter plastic containers, wicks, agarose, NaCl salt, graphite rods, a pH meter, Copper wire, a thermometer, polyvinyl chloride pipes, market products, as well as pesticides. The programs that were used include Microsoft Excel 2013, *Arduino* IDE. And Minitab 17, Origin 8.

3.3 Sampling Area

The rumen waste obtained from Dagoretti slaughter house near Dagoretti market was sealed using aluminium foil and placed in self-sealing bags and then taken to University of Nairobi laboratory for investigations and analysis. These samples were stored at -4°C in a freezer. Figure 3.1 (a and b) show the sampling area in Dagoretti slaughter house and Thigio area where Loam soil, cabbage and tomato were obtained from.



Figure 3.1: (a) Dagoretti slaughter house (b) Thigio area where loam soil, tomato and cabbage were sampled

3.4 Assessment of microbes

In order to conduct bacterial count experiments in rumen fluid, tomato, cabbage wastes and loam soil, were sampled and sealed in a five-liter refrigerated ISO cooler containers, and then taken to the University of Nairobi's microbiology laboratory at the College of Agriculture and Veterinary Sciences'.

3.4.1 Preparation of MacKonkey Agar

A suspension of 49.53 g of desiccated powder medium was made in 1 liter of deionized water. It was heated to a boil in order to solubilize it completely. The autoclaving was done using steam under pressure of approximately 15 pounds Which is equal to 103421.4 pa The goods were sterilized under pressure and at a temperature of 121 °C for a quarter of an hour, this was to prevent heating beyond desirable point. The system temperature was decreased to 45–50°C. The mixed culture was smeared throughout the plate (MacConkey's agar) (Holt and Krieg, 1994; Remel Microbiology Products, 2005)

3.4.2 Preparation of Blood Agar

40g of nutrient agar powder were dissolved in 1 liter of distilled or filtered water. To dissolve the medium completely, it was heated while stirring till it boiled. Sterilization was accomplished by

autoclaving for 15 minutes at 121°C and 1.02 atm. The system was chilled to 45–50 °C, and aseptically added to 5% v/v sterile de-fibrinated blood. Prior to transferring the mixture of various ingredients to sterile Petri plates, it was carefully and thoroughly mixed. (Salfinger and Tortorello, 2015; Murray et al., 2003).

3.5 Bacteria Total Count

The cumulative bacteria populations inside the rumen fluid and cow dung samples were determined using Standard Plate Count method (Murray et al., 2003). The samples were placed on agar substrate (semi solid nutrient) and incubated for 2 days at 30°C to promote bacteria growth. Colony forming units (cfu) were estimated by multiplying number of colonies with the dilution factor and then divide by amount or rather the quantity of the sample used.

3.6 Loam soil analysis

A model loam soil type consists of approximately 50% soil solids (a mixture of sand, silt and clay) and 50% of pore spaces plus water. Another name for loam soil is clayey earth.

(a) Analysis of P, K, Na, Ca, Mg and Mn.

Available nutrients elements (P, K, Na, Ca, Mg, and Mn) were analyzed using the Mehlich Double Acid Method (Tran and Simard, 1993, Mehlich 1953)

The soil samples were dried in an oven before being extracted in the ratio 1:5 (w/v) using a solution of 0.1N HCl and 0.025 N H₂SO₄ from Kobian wholesalers. Calcium and Sodium were determined using a flame photometer (Model FP910-5), whereas P, Mg, and Mn were determined using the calorimetric method (Mehlich, 1953).

(b) The Total organic carbon in the soil

Total organic carbon in the soil was measured using Calorimetric technique (Gislason and Craig, 2005).

Acidified dichromate was used to completely oxidize all soil sample organic carbon for half an hour at 150 °C. The cool digests were supplemented with barium chloride. Digests were given an overnight standing period after being completely mixed. At 600 nm, the reading was taken from the spectrophotometer.

(c) Total nitrogen

The total nitrogen was determined using Kjeldahl method (Persson et al., 2008). The soil samples were digested at a temperature of 350°C in strong sulfuric acid that also contained K, Se, and CuSO₄. This converted nitrogen into ammonium sulphate. K, Se and CuSO₄ are used as catalyst. The resulting solution was then distilled while adding sodium hydroxide to obtain ammonia. The amount of ammonia or rather nitrogen present is then determined by back titration.

(d) Soil pH

The Soil pH was determined in the ratio 1:1 (w/v), soil to water suspension using a pH meter.

(e) Trace elements

Copper, zinc, and iron were extracted using 0.1 M hydrochloric acid as follows:

The soil samples were oven-dried and extracted in a ratio 1:10 weight/volume proportion using 0.1 M hydrochloric acid. The elements were detected using an atomic absorption spectrophotometry (AAS).

(f) Cation Exchange Capacity (CEC) and Exchangeable Ca, Mg, K and Na at pH 7.0

Ammonium acetate (1N C₂H₇NO₂) was passed over the soil sample and buffered at pH 7. The dredging was analyzed for exchangeable calcium, magnesium, potassium, and sodium. The sample was subsequently leached using 1N potassium chloride, and the CEC was calculated using the leachate. A flame photometer was used to measure elements like sodium and potassium, while an atomic

absorption spectrophotometer (AAS) was used to measure calcium and magnesium. To measure the CEC ammonium is titrated by distillation and volumetric analysis or automated Spectro colorimetry. Here sodium is saturated with cation and is moved by ammonium cation. The CEC is calculated on the basis of concentration of sodium ion in extract. The resulting extract is titrated with 0.01M Hydrochloric acid (Turner and Simard *et al.*, 1966).

3.7 Assessment of tomato and cabbage waste

Tomato (*Lycopersicon lycopersicum*) and Cabbage (*Brassica oleracea capitata*) waste that had been discarded in a garbage heap in the market were obtained, sliced into tiny chunks and blended. The blended mixture was used for analyses of pesticide concentration, macro- and micro nutrient, heavy metal, and proximate analytical measurements for the discarded vegetables.

3.7.1 Analysis for pesticide concentration

Analysis of pesticide concentration was done on the blended fruit waste using the QUECHERS method, (Ukpebor and Ukpebor, 2016). This was done by extracting pesticide residues from the samples using acetonitrile, then phase separation done using primary secondary amine (PSA) and magnesium sulfate, to remove sugar fatty and other acids. The assessment of the samples for pesticide was performed using Gas Chromatography connected to a triple quadrupole mass spectrometer /analyzer (Golge and Kabak, 2015). By extracting using the Soxhlet method and scanning the samples using a GC-MS, the pesticide concentrations in the sample were determined.

3.7.2 Macro and micronutrient and heavy metals analysis

Tomato and cabbage samples were obtained from a dumpsite in the market. These were chopped and 0.5 kg of each vegetable was miniaturized in a household blender. These were, then, transferred to a larger (110-liter) container and mixed to create a homogenous mixture. . The mixture was divided into

two, with one being subjected to an analysis of its elemental composition while still fresh and the other was analyzed after three weeks after being allowed to undergo aerobic decomposition. The material was baked to dry in both configurations before being pulverized into fine dust and formed into a pellet. Elemental composition was determined using X-Ray fluorescence spectrophotometer (XRF). Khan *et al.*, (2011) and Obiajunwa *et al.*, (2013). [XRF analyzers analyze the sample by measuring the fluorescent (or secondary) X-ray emitted from a sample that has been excited by a primary X-ray source]. Some of the macro nutrients and micro nutrients in cabbage and tomatoes included potassium, sodium, iron, magnesium, calcium, cobalamin, folate etc.

3.8 Proximate analysis

The proximate properties of the samples are determined by use of the homogenized samples. The nitrogen-free extract, Energy, fat, fibre, ash, moisture content, protein, and carbons were all analyzed using the technique outlined in Association of Analytical Chemistry (AOAC) 2003 methods detailed in this section.

3.8.1 Moisture Content Analysis (M)

The water content was measured using the oven drier that is the drying over the oven technique (Carneiro *et al.*, 2018; Nielsen, 2010). A sample of 0.001 kg of the homogenized sample was measured in a dry crucible. The material was dried for 6–12 hours at 100–105 °C to a consistent weight. The sample was then kept in a desiccator for 30 minutes after which it was weighed. The moisture content, M, was determined using the formula outlined in equation 3.1 below.

$$M = \frac{W_1 - W_2}{W_s} \times 100\% \dots \dots \dots (3.1)$$

Where:

W_s is initial weight of the sample plus crucible prior to heating

W_1 is weight of crucible and sample before heating, and W_2

is weight of sample and the crucible after heating.

3.8.2 Determination of Ash

To determine the amount of ash in the sample, the sample was heated in a muffle furnace at 600°C for one hour. It was, then, cooled, and then weighed. The ash levels were calculated using equations 3.2 and 3.3.

$$Ash = \frac{W_3 - W_1}{W_s} * 100 \dots \dots \dots (3.2)$$

$$Ash(dry) = \frac{Ash(wet)}{100 - Moisture} * 100 \dots \dots \dots (3.3)$$

The weights of the blank crucible (w_1) and crucible with ash (w_3), and sample (w_s) before burning.

3.8.3 Crude Protein Assessment

The Kjeldahl technique was used to assess the amount of protein in the samples (Lynch & Barbano, 1999). The samples were first digested and then titrated. In the digestion process, about 0.75 g of dry sample was obtained and heated in a digestion mixture that contained Sulphuric acid, potassium sulphate, a selenium catalyst, and 0.1 M sodium hydroxide. The end product was ammonium sulphate. After the digestion process, ammonia was collected in a solution of 2% boric acid, and the mixture titrated against standard hydrochloric acid. The equations 3.4 and 3.5 were used to calculate the total protein.

$$Crudeprotein = 6.25 * \%N \dots \dots \dots (3.4)$$

$$\%N = \frac{(S - B) * N * 0.0014 * D}{W_s * V} \dots \dots \dots (3.5)$$

Where:

V is the volume used for distillation

S is the sample titration value

B is the blank titration reading

N is the Hydrochloric acids normality, D is the sample's dilution upon digestion, and

0.0014 is the milli equivalent wt. of nitrogen.

3.8.4 Determination of crude fat

Total crude fat in the samples was determined through the ether extract method (Moreau *et al*, 2011) . Approximately 2 g of the dried sample was placed in a fat-free thimble, covered in filter paper, and then placed into an extraction tube. The material was weighed into a receiving beaker that had been cleaned, dried, and filled with petroleum ether. The ether was expelled after 4-6 hours of siphoning, and the beaker was then detached before the final siphoning. The ether was then vaporized while the extract was moved to a clean glass dish in a water bath. The dish was desiccated after drying at 105 °C for two hours. The total crude fat was then calculated using equation 3.6. Ws is the combined weight of the crucible and the sample.

$$Crude\ fat = \frac{Weight\ of\ ether\ extract}{W_s} * 100 \dots \dots \dots (3.6)$$

3.8.5 Determination of crude fiber

Exactly 0.153 g of the dried sample was added to a porous crucible and the crucible placed into a Dosi-fiber apparatus. Foam-suppresser and 150 mL of Sulphuric acid was added drop wise to every column of the apparatus. The cooling circuit was opened and the solution was heated for 30 minutes achieve 30% heat energy. The acid was drained from the sample and rinsed with distilled water. This method was sustained using 1 M potassium hydroxide instead of the Sulphuric acid. After one hour of drying at 1500 °C, the sample was cooled and then weighed (W₁). The resulting sample was further dried for 3–4 hours at 55°C in a muffle furnace, then cooled and weighed again (W₂). The crude fiber was calculated using Equation 3.7 below.

$$crude\ fiber = \frac{W_1 - W_2}{W_s} * 100 \dots \dots \dots (3.7)$$

3.8.6 Nitrogen free Extract (NFE)

The nitrogen free extract was computed by subtracting the sum of several attributes from the dry mass as shown in equation 3.8.

$$\%NFE = DM - (CL + C.P + Ash + \%C.F) \dots \dots \dots (3.8)$$

NFE is for a nitrogen-free extract sample

D.M. stands for dry mass

C.L. stands for crude lipids

C.P. stands for crude protein

C.F. stands for crude fiber (Nielsen, 2010).

3.8.7 Energy calculation

By multiplying the crude protein, carbohydrate, as well as lipid contents by the factors 4, 9, and 4, respectively, and adding the resulting products, the energy content of the fruit and vegetable waste samples was determined (equation 3.9). After that, the findings were presented as calories per 100 grams of the sample (Nielsen, 2010).

$$\text{Energy} = C. P * 4 + C. L * 4 + C. F * 9 \dots \dots \dots (3.9)$$

3.9 Microbial Fuel Cells Construction

Two 1.5 L plastic containers were obtained and on each container a hole was drilled on the side, and the two joined by a polyvinyl chloride pipe to make an anodic and a cathodic cell. Figure 3.2 (A) below demonstrates plastics containers under construction. Each container lid also had a tiny hole drilled into it, and a copper wire passed through. Figure 3.2(B) shows containers lids with a hole for connection of the wires to the multimeter.



(A) plastic containers



(B) container lid with hole

Figure 3.2:

plastic containers representing the anodic and cathodic chambers.

3.9.1 Salt bridge

To create the salt bridge and the solution thereof, 2500 cm³ of 1M sodium chloride, lamp wicks and 3% agarose solution were used. The wicks were placed in a boiled solution of sodium chloride and agarose (3%) solution for ten minutes. Thereafter they were placed in a freezer at -4 °C to solidify. To make the chambers leak-proof, the hardened salt bridge was routed through polyvinyl chloride pipes and fastened to them using Araldite adhesive. This is shown in figure 3.3 below.



Figure 3.3: The wicks used to construct the salt bridge.

3.9.2 Electrode preparation

The electrodes for this study were made of carbon graphite rods that were joined together using a zero-resistance copper wire (figure 3.4). The carbon rods were retrieved from used dry cells (batteries), scraped with sandpaper and cleaned thoroughly with deionized water. After a 24-hour immersion in concentrated sulfuric acid, they were stacking one on top of the other. The working surface area of the electrode was 0.00331 cm².

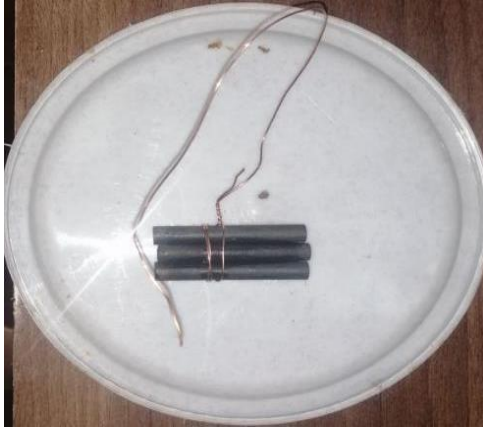


Figure 3.4: A representation of the graphite rods and copper wire that were used

3.9.3 Circuit Assembly

The dual chamber MFC was set up as shown in figure 3.5, which was previously published by Mbugua *et al* (2020).



Figure 3.5: A multi-meter equipped twin cell (MFC)

3.10 Control experiments

For the control studies the tomato and cabbage were sliced into minute pieces, which were blended using a home blender into a syrup and stored as samples weighing approximately 1kg each. A mixture of 0.750 L of rumen wastes and 0.750 L of sample was added to the cathodic chamber of a microbial fuel cell that had been constructed as depicted in figures 3.6 to 3.9



Figure 3.6: Microbial fuel cell control experiment setup with rumen in the anodic chamber



Figure 3.7: Microbial fuel cell control experiment setup with cabbage in the anodic chamber



Figure 3.8: microbial fuel cell control experiment setup with tomato in the anodic chamber



Figure 3.9: Microbial fuel cell control experiment setup with Loam soil in the anodic chamber

After completely mixing the waste with 750 cm^3 of deionized water in the anodic chamber, the prepared electrodes were added. The cathodic chamber was flushed with carbon dioxide prior to getting sealed airtight. 1500 milliliters of deionized water were placed into the anodic chamber.

Voltage and current readings generated from the cell were recorded every day using a multimeter.

The set up was allowed to run until maximum voltage was realized.

3.11 Voltage and current measurements

V and I (current) measurements were made using two different techniques, namely the digital multimeter and the Arduino-based micro-controllers.

3.11.1 Multimeter voltage and current measuring method

In this technique, the multi-meter's anode was connected to one terminal, and the cathode to the other.

The readings appearing as voltage and current were observed on the multi-meter's liquid crystal display (LCD) screen, as shown in figure 3.10.



Figure 3.10: A multimeter displayed voltage reading

3.11.2 Arduino based voltage and current sensor method

Two chambers with a capacity of 1500 cm³ were constructed using plastic containers. Five carbon rods were stacked together and when combined they gave a surface area of 0.00666 m² and were placed in each chamber connected to a copper wire as depicted in figure 3.10 (Mbugua *et al.*, (2020)). The experiment used an external resistor with 1000 ohms. The compartments were separated by a NaCl salt bridge. The anode chamber was inoculated with cow dung waste and tomato waste, whilst the cathodic area was filled with deionized water. The analyte and catholyte's starting potential of hydrogen pH in the procedure was 7.01 ± 0.31 .

Every 60 seconds, a digital multimeter (DT9205A) and an Arduino UNO were used to measure the cell voltage. and the second method involved use of Arduino UNO in measuring the cell voltage .

The Arduino UNO pins were wired up with the I and V sensors as shown in figures 3.11 and 3.12. Using Dip Trace v3.3.4, the component connections to the Arduino were made, as shown by the schematics (figure 3.11). Figure 3.11 represents the block diagram that illustrates the connection of the

components to the Arduino board. According to Figure 3.11, the analog pins A0 and A3 are linked to the current and voltage sensors respectively.

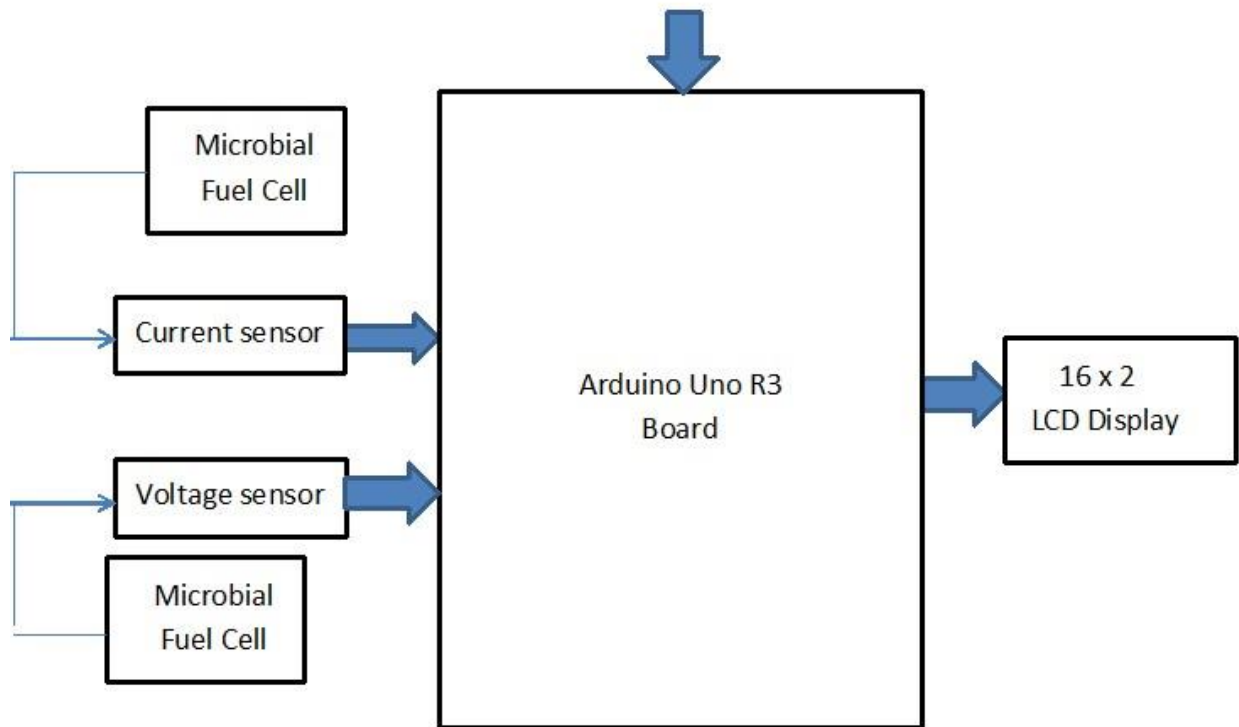


Figure 3.11: A block diagram for connecting potential difference and current sensors to the Arduino board.

The output signal, typically displayed as V and I, is shown on a liquid display crystal (LCD) screen connected to the Arduino board's analog pins SDA and SCL and powered by a 5V pin while grounded (GND). Since the Arduino board had one 5V pin and three GND pins, all the parts were linked using a solderless breadboard, as shown in Figure 3.12 below.

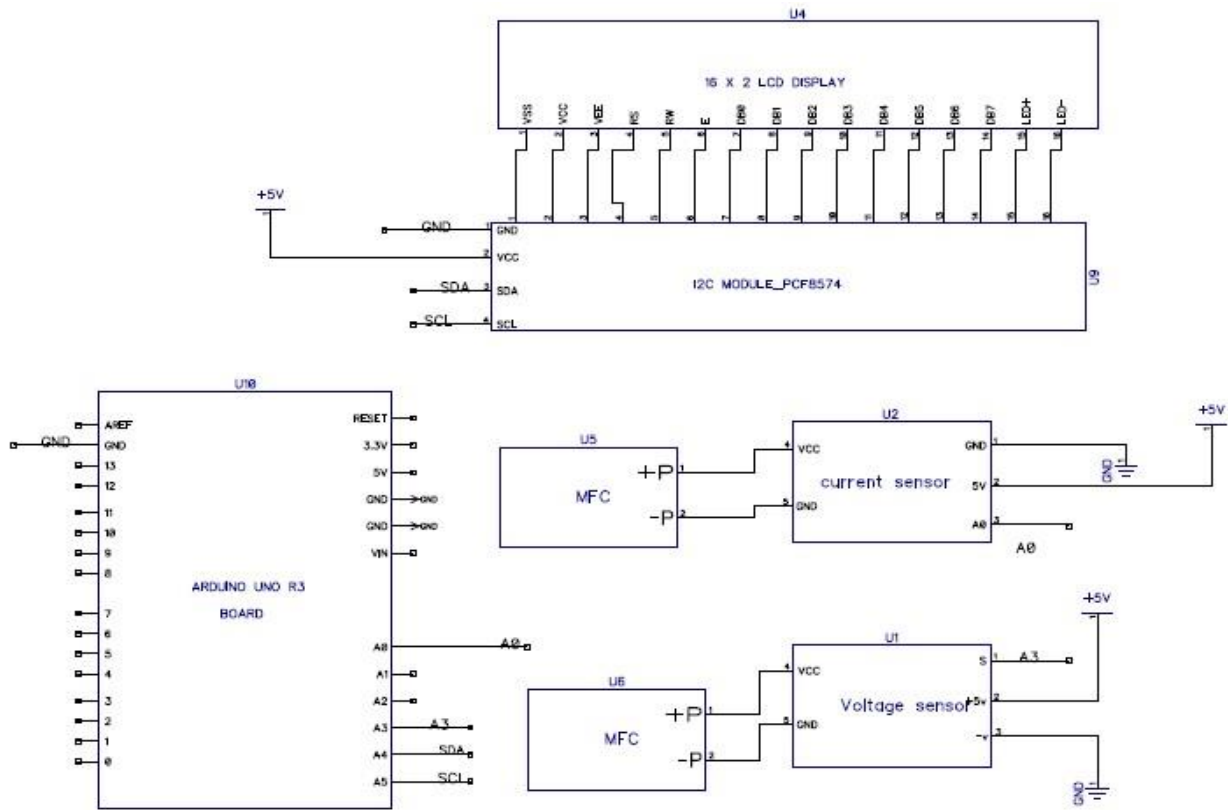


Figure 3.12: Diagram showing connections between the Arduino boards, sensors and LCD connections.

The figure 3.13 below illustrates how the MFC, multimeter, Arduino-based voltage and current monitors device were connected.



Figure 3.13: Arduino potential difference and current MFC monitoring gadget

The configuration, which is depicted in appendix A, was configured to aggregate I and V data every 60 seconds and stored in Excel program using the PLX-DAQ interface. Equations 3.10 and 3.11 were then used to determine the absolute and relative errors respectively:

$$Abserror = |E_{Arduino} - E_{Multimeter}| \dots \dots \dots (3.10)$$

$$Relativeerror(\%) = \frac{|E_{Arduino} - E_{Multimeter}| * 100}{E_{Multimeter}} \dots \dots \dots (3.11)$$

Where: $E_{Multi-meter}$ is the multimeter voltage measurement at any given moment, and E-Arduino is the Arduino UNO's simultaneous potential reading.

Calculations were made to determine the power, current density, and power density for the setup.

3.12 Data collection and observation

At intervals of a day for the specified number of days, the generated V and I were recorded using the digital multi-meter. Using equations 3.12 to 3.14, power, current, and power density calculations were performed using the voltage and current average values.

$$P = VI \text{ or } IR^2 \dots \dots \dots (3.12)$$

$$CurrentDensity = \frac{current}{A_{area}} \dots \dots \dots (3.13)$$

$$PowerDensity = \frac{Power}{A_{area}} \dots \dots \dots (3.14)$$

Where A_{area} represent electrode surface area.

P represents power,

V represents volt

I represent current while

R represents resistant

3.13 Pesticide solutions

The pesticides were diluted to various concentrations as required to prepare standard stock solution and working stock solutions used in various experiments as demonstrated below.

3.13.1 Preparation of Standard Stock Solution

The pesticide standards for lambda cyhalothrin, malathion, and chlorpyrifos were utilized as received. To create a stock solution of 10 ppm, 98% acetone was used to solubilize each insecticide. The calibration curves were prepared using the standard solution.

3.13.2 Preparation of working Stock Solution

Pesticides primarily composed of cyhalothrin lambda, malathion, and chlorpyrifos, were purchased from nearby agrochemical stores and then diluted in water to create a 10-ppm solution before being employed in a serial dilution procedure to create the functioning pesticide solutions.

3.13.3 Investigation of the potential of cabbages, tomato, loam soil and rumen wastes

About 0.750 kg of tomato and cabbage wastes were separately diced, minced using a meat mincer, and combined in a kitchen blender. 0.750 L of rumen waste was then added, and everything was properly homogenized before being transferred to the anodic chamber of the H-shaped MFC. 1500 cm³ of distilled water were used to fill the cathodic chamber. The same procedure for placing top loam soil in chambers was repeated where 0.75 kg of soil and water were combined to form a homogeneous mixture, which was then loaded into the cathodic chamber along with 750 mL of rumen waste. 0.75kg of the rumen waste and 750mL deionized water was placed in the cathodic chamber create a second set for investigation. V and I were recorded while being monitored for a 24 Hydraulic Retention Time (HRT).

3.13.4 Microbial Fuel Cell Parameter Optimization

The tomato, cabbage and loam soils were used in the optimization trials, along with varied of electrode surface area, pH, microbe concentration, external resistance, and pesticide concentration.

These procedures are laid out in the subsequent sections.

3.13.4.1 Analyzing the impact of microbe concentration

To assess the impact of microbial concentration, 0.750 kg of tomato was added to the anodic cell along with 0.25 L rumen wastes that were spiked with a 0.010 L mixed solution of lambda cyhalothrin, malathion, and chlorpyrifos. Above procedure was repeated for 0.5L of rumen spiked with 0.01 of each of the pesticide. Then same procedure was repeated with 0.75L and 1L volumes for rumen wastes spiked with 0.01L of each of the pesticides. Daily records of the voltage and current produced by various microbe concentration ranges were kept. Same procedure was repeated for cabbage and loam soil. The residues of the substrate were then obtained and analyzed using the QuEChERS extraction procedure and taken to GC-MS to determine the quantity of pesticides within the residue.

3.13.4.2 The impact of pH on the production of electricity

In microbial fuel cells, pH is a crucial variable that may have an impact on energy output. To investigate the effect of pH on the MFC setup, anodic reactor was loaded with 0.750 kg of tomato loaded with 750 mL of rumen wastes spiked with 10 mL of a mixed solution of lambda cyhalothrin, malathion, and chlorpyrifos in order to achieve the ideal potential of hydrogen. The above procedure was repeated for cabbage and soil. Investigated pH ranges included pH-2, pH-7, and pH-11, while values for other variables, such as the temperature of operation, inoculate level, electrode materials, electrode coverage, were held constant. The current and voltage output for each of the pH ranges were measured on a daily basis.

3.13.4.3 Investigation of the effect of External Resistance

To determine the impact of external resistance, the anodic chamber was fed with 0.750 kg of tomato and cathode loaded with 0.750 L of rumen waste spiked with 0.010 L of a 10-ppm mixed solution of lambda cyhalothrin, malathion, and chlorpyrifos. Both Copper wire terminals were connected to 1k Ω resistor. Another set was repeated with 2k Ω , and lastly another set with 45 k Ω resistors. V and I were monitored across each resistor and recorded. Other set ups for cabbage, and soil were prepared and same procedure repeated for substrate. V and I were monitored and recorded daily for 90 days.

3.13.4.4 Investigation of the effect of concentration of pesticides

Three different anodic cells were fed with 0.75 kg of tomato, 0.75kg cabbage, and 0.75kg soil loaded with 0.75 L of rumen wastes spiked with 10 mL of 10 ppm mixed solutions of lambda cyhalothrin, malathion, and Chlorpyrifos. Daily records of V and I were kept. Same procedure for 50 ppm, 100 ppm, and 1000 ppm mixed solutions of lambda cyhalothrin, malathion, and Chlorpyrifos were repeated for all the three substrates .and effects of various pesticide and every day voltage and current produced by the various concentrations were reported and recorded.

3.14 Bio-remediation studies

The objective of the research was to determine the extent to which the MFCs degraded the three pesticide residues. Three different set ups of MFC anodic chambers were loaded with each 0.75 kg of tomato, 0.75kg cabbage and 0.75kg loam soil. Their cathode chambers were loaded with 0.750L of rumen wastes spiked with 10 ml of 10 ppm lambda cyhalothrin. The pesticide concentration was monitored every 5 days for 3months. Daily records of V and I were monitored and recorded. The degradation levels were established after extraction with a GC-MS machine. The other set ups for 10ml of 10ppm malathion, and 10 ml of 10 ppm Chlorpyrifos as well as 10ml of 10ppm mixed solution of the three pesticides were also set for each of the substrate being investigated . V and I were monitored and recorded for 90 days. Each pesticide concentration was monitored every five days for 90 days as well. Each of the pesticides Degradation levels were established after extraction using a GC-MS and documented.

3.15 Fitting, modeling and simulation of degradation data

The (voltage data produced by the bio-remediation of malathion, Chlorpyrifos, as well as lambdacyhalothrin was integrated into a variety of models, including linear, exponential, and Gompertz models.

3.15.1 Microbial Growth Simulation

Energy production and substrate utilization, is directly related to the kinetics of anode respiration bacteria (ARB). Due to the anode biofilm's involvement in the computation of the kinetic constants of ARB, several models have been developed (Lee *et al.*, 2010). The matrix levels and the cellular potential difference are two aspects to take into account when choosing kinetic parameters (Liu, & Logan, 2005). Prior research primarily used the Monod model (Equation 3.15), which states that a mono substrate restricts the development of bacteria (Liu & Logan, 2005). Haldane Andrew's kinetics

model, which incorporates the substrate inhibitory effect, was developed to address this setback (Equation 3.17). The Han-Levenspiel model (Equation 3.17), which accounted for competitive, uncompetitive, as well as noncompetitive inhibition, was employed to describe how microbial growth completely stopped when a threshold inhibitor concentration (S_m) was reached (Benoit and Christophe, 2019). According to Imwene *et al* (2020)'s description, the study of the voltage data's fitness to these models was carried out.

Monod Model:

$$r = r_{max} * \frac{S}{K_s + S} \dots \dots \dots (3.15)$$

Andrew's Kinetic Model:

$$r = r_{max} * \frac{S}{\left(K_s + S + \frac{S^2}{K_{IH}}\right)} \dots \dots \dots (3.16)$$

Han-Levenspiel Model:

$$r = r_{max} * \frac{S \left(1 - \frac{S}{S_m}\right)}{S + K_s \left(1 - \frac{S}{S_m}\right)} \dots \dots \dots (3.17)$$

Where: \mathbf{r} is maximum potential difference (mV), peak power density (mW/m²), or output current density (mA/m²) at every substrate concentration.

\mathbf{r}_{\max} signifies the highest range of substrate level in terms of output current density (mA/m²), power density (mW/m²), or voltage (mV).

\mathbf{S} (mgL⁻¹) is the substrate levels

\mathbf{K}_s (mgL⁻¹) signifies the half-saturation factor.

\mathbf{K}_{IH} (mgL⁻¹) denotes the self-inhibition coefficient.

\mathbf{S}_m in mg/L is the critical inhibitory concentration over which growth ceases.

\mathbf{n} and \mathbf{m} are the empirical constants used to account for various kinds of inhibition.

3.15.2 Microbial Fuel Cells Kinetic Study

Anaerobic digestion kinetic studies can be used to estimate how well any microbial anaerobic degradation process will operate. The kinetic studies can also be used to identify the limiting factors. First-order kinetic models were used to examine how well the anaerobic digestion (AD) process performed (Liu *et al* 2018; Mata-Alvarez *et al.*, 1993).

3.15.2.1 Linear kinetic model

According to equation 3.18, the model suggests that cathodic chamber of the MFC CO₂ production increases with hydraulic retention time (HRT) (Ghatak and Mahanta, 2014).

$$V_1 = a_1 + b_1 t \dots \dots \dots (3.18)$$

In which V_1 is the voltage generation rate (V kg₁d₁) which equivalent to carbon (IV) gas generation rate, t is time duration in days or is duration for digestion in days, a_1 is the line intercept

b_1 is the slope of the graph obtained from the intercept and the slope of graph V_1 verses t .

When b_1 is positive the limb is rising and its negative for a falling limb.

The acquired data was fitted to a linear kinetic model, and various statistical characteristics, including the coefficient of determination R^2 , were noted and recorded.

3.15.2.2 Gaussian Kinetic Model

The Gaussian equation, shown in equation 3.21 (Aritra and Mondal, 2015), was employed to anticipate voltage recovery rates, including ascending and descending limbs, under the assumption that microbial kinetic growth and voltage generation rates, as well as its decays follow the normal distribution curve throughout the breakdown time frame.

$$V_1 = a_1 \exp(-0.5(t - t_0/b)^2) \dots \dots \dots (3.19)$$

Where V_1 is gas production rate or voltage generation rate (V kg₁d₁) or

May refer to microbial kinetic growth rate, t is the hydraulic retention time in days ,

t_0 denotes time in days at which maximum biogas production rate or voltage generation took place/occurred

a and **b** denote constant in days in (mL g⁻¹) and (d⁻¹) respectively.

Statistical Mini-tab 17-19 program and/or QtiPlot program were employed to create the growth normal distribution curves.

3.16 Bio-remediation Decay Kinetics

The 1st order, 2nd, and 3rd order decay curves were fitted onto the experimental data and were used to replicate the bio-remediation decay plots. Equations 3.20, 3.21, and 3.22 illustrate the first, second, and third order curves respectively.

$$C_s = C_{s0} \exp(-k_1 t) \dots \dots \dots (3.20)$$

$$K_s \ln \left(\frac{C_s}{C_{s0}} \right) + C_s - C_{s0} = -k_2 t \dots \dots \dots (3.21)$$

$$Y = -k_{3,1} - \left(- \frac{k_{3,1}}{2} \right) = \frac{1}{t} \ln(C_{s0} - p + K_0) / C_{s0} \dots (3.22)$$

Where **t**₁ represents the 1st decay time,

t₂ is the second decay time, **t**₃

is the third decay time, and

C_{s0} is the beginning pesticide dosage.

As per Mbugua *et al.* (2022b) and Kinyua *et al.* (2022), the fitness of the decaying order was evaluated using the

QtiPlot software program 0.9.8.6 in addition to other statistical studies.

Note: QtiPlot software program 0.9.8.6 is a cross-platform scientific application for data analysis and visualization

CHAPTER FOUR

4.1 RESULTS AND DISCUSSION

The results of the investigation are given, examined, clarified, and discussed in this section. All calculations were done using the mean and standard deviation, unless otherwise specified.

4.2 The food Wastage situation in Kenya

When the food waste was assessed in this study, it was realized that food waste pattern in the country varied across different seasons due to some individual characteristics of foods such as vegetables and fruits. For example, some vegetables, such as cabbages, are generally abundant during rainy seasons and prone to surplus supply, which led to increase in amount of waste, unlike during dry the season. The other observation that was made was that, in most cases, tomato and cabbage wastage could be attributed to improper handling of the food commodities whereby these products are availed to the markets with the intention of consumption but end up being waste due to excess supply as shown in figure 4.1 below. It was also established that foodstuffs such as tomatoes offered in the market had white spots, which could be a result of pesticides applied on such crops, a situation that may lead to health complications if the crops are consumed without proper washing.



Figure 4.1: (a) Image of tomatoes that had been sprayed (b) sorted as waste/ unsuitable for use (c) tomatoes being sorted.

The nutrient composition of these foodstuffs was analyzed to determine an approximate nutrients alignment and values.

4.3 Cabbage and tomato analysis

The QuEChERS extraction procedure was used to identify the pesticide levels in cabbage and in tomato samples. This involved dispersive solid phase (d-SPE) which is a sample preparation technique ideal for multi-residual analysis for pesticides. The GC-MS was used to measure the pesticide concentrations, and the chromatograms attained are shown in figure 4.2 below.

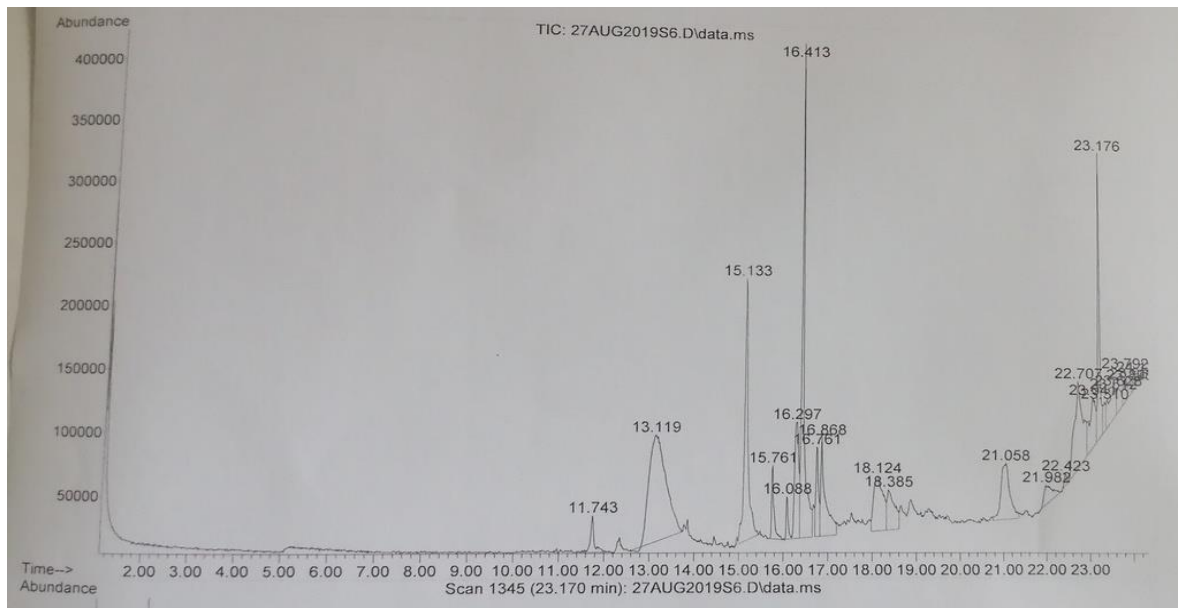


Figure 4.2: GC-MS chromatogram for mixed tomato and cabbage samples

From the above image, it can be concluded that although some tomatoes had white spot supposed to be pesticides, the results showed that there were no Pesticide/insecticide residues in the food samples investigated. This means the levels were too low to be detected by the GC-MS machine used. The peaks in the chromatography pertain to secondary metabolites found in plant waste. The pesticide present in the waste products used for anaerobic digestion has a significant impact on the microbe's behavior.

4.3.2 Proximate analysis

Table 4.1 and 4.2 presents results from the proximate properties analyses on the dry and wet samples. The term nitrogen-free extract (NFE) stands for sugars and starch and is attained by connecting it to the other strictures equation 3.8 ($\%NFE = DM - (CL + CP + Ash + \% CF)$) instead of measurement. NFE refers to soluble carbohydrates, while crude fiber represented insoluble carbohydrates (Analytical Techniques in Aquaculture Study, 2009). From table 1, the NFE in this research ranged from $55.42 \pm 4.23\%$ to $57.71 \pm 3.90\%$ in dry tomato and cabbage respectively. In fresh samples NFE ranged from $15.08 \pm 1.11\%$ to $3.22 \pm 0.89\%$. The ranges in dry tomatoes and cabbages samples were 55.36 ± 4.23 and $57.71 \pm 5.55\%$, respectively. The observed proximate properties on fresh weight were found to be higher than proximate properties on the dried samples. This was most probably due to the dilution characteristics of the in-height dampness levels in the fresh samples. On the other hand, the energy ranks for fresh samples wastes ranged between 2.93 ± 0.05 Kcal/100g in tomatoes and 16.64 ± 4.01 Kcal/100g in cabbage. The ash levels in dry waste samples ranged from 9.53% in tomatoes to 9.70% in cabbage samples.

Table 4.1: Analyzed dry weight on fruit and vegetable wastes

Dry Samples	%Moisture	% Protein	% Fat	% Ash	% Fiber	% Carb.	% NFE	E(Kcal/100g)energy
Tomato	4.84±1.76	11.89±2.90	2.57±0.23	9.53±1.11	15.75±2.00	55.42±4.23	55.36±4.23	292.37±13.23
Cabbage	5.13±0.11	16.12±3.90	0.96±0.03	9.70±1.99	10.38±1.77	57.71±5.55	57.71±3.90	303.96±13.00

From the table above, the proximate quantities of carbohydrates were more than that of proteins and fats. This is because sugar is a vital component block in tissues. Moreover, this accounts for higher energy/100g of individual waste. The table 4.2 below shows the values obtained from individual dry samples. As expected, the moisture levels in dried samples were significantly lower than those in the wet waste. Adubo *et al.* (2012) identified ash amounts of 2.89 – 7.33% in tomato waste.

Table 4.2: Proximate analyzed fresh weight of fruit and vegetable waste

Wet samples	% Moisture	% Protein	% Fat	% Ash	% Fiber	% Carb.	% NFE	Energy (Kcal/100g)
Tomato	95.16±4.00	0.57±0.01	0.12±0.01	0.46±0.01	0.76±0.01	2.93±0.09	15.08±1.11	2.93±0.05
Cabbage	94.87±2.56	0.83±0.07	0.05±0.01	0.49±0.02	0.54±0.06	3.22±0.92	3.22±0.89	16.64±4.01

4.3.3 Elemental composition of the samples

The elemental composition analysis is the ultimate composition analysis that involves the identification of sulphur, carbon, oxygen, nitrogen, and hydrogen components in the dried waste samples. These components are vital since they form the samples' carbohydrates, proteins, and lipid components. It was established that carbon amounts were among the highest in quantity, recording 47.18 % in

tomatoes, while cabbages had 47.45 %. Overall, samples with high amounts of lipids have complex C-H chains. The higher ultimate matter composition leads to a high voltage potential, which hinders microbial activities, ensuring flotation of sludge (Neve *et al.*, 2010; Dave & Monil, 2015).

Table 4.3: The elemental composition cabbage and tomato samples

SAMPLE	%C	%H	%O	%N
Tomato	47.18±6.80	6.61±0.66	43.47±4.43	2.73±0.87
Cabbage	47.45±7.23	6.48±1.88	42.97±9.91	3.11±0.08

To establish the percentage of oxygen, nitrogen, carbon and hydrogen, the individual percentages were divided by the total percentage from the other components, and then subtracted from 100%. It was presumed that these were the only components of the samples of tomato and cabbage. It was established that 43.47±9.91%, was the resultant oxygen percentage in cabbage while tomato was with 43.47±4.43. Generally, these values of the two samples are almost similar.

The physical-chemical results for the analyzed samples are highlighted in table 4.4. To obtain the percentage of total solids, the percent moisture was subtracted from 100%. The fresh tomatoes sample gave moisture level of 95.16% while that of the dry samples gave 4.69% . Eressa *et al.* (2016) obtained moisture percentage levels of 83.12%, while Hammed *et al.* (2017) obtained moisture levels of 90.74% from their previous research study.

In tomatoes and cabbage, the aggregates moisture level from the wet samples was 95.16% and 94.87%, respectively. However, total wet solid of tomato was 4.83% compared to 5.23% in cabbage. Tomatoes and cabbage had 4.37% and 4.69% of the volatile matter (VM) present. This volatile matter served as a vital source of food for the bacteria responsible for growth and development. The mineral matter (MM) for both cabbage and tomato were almost similar (0.539 and 0.506%).

Table 4.4: The physical characteristics of different market wastes

Sample	% Moisture		Total Solids		% Ash		%MM		%Vm		% Fs	
	Wet	Dry	Wet	Dry	Wet	Dry	Wet	Dry	Wet	Dry	Wet	Dry
Tomato	95.1	4.69	4.83	95.16	0.46	9.43	0.506	10.473	4.37	85.63	3.92	75.9
Cabbage	84.87	5.12	5.23	94.67	0.49	9.71	0.539	10.67	4.64	85.27	4.15	75.47

Moisture amounts obtained in fresh cabbages were at 84.87%, while dry cabbage was found to contain 5.12%. The volatile levels obtained were 4.64% for the fresh samples, unlike in the dry samples, which were at 85.27%. These figures correspond to those obtained by Kamau *et al.* (2020) on both sets of vegetable samples obtained from Kenyan markets, and they also concluded cabbages had more carbohydrate when compared to tomatoes.

4.3.4 Inoculum analysis

The outcome obtained for the bacteria amounts obtained from samples of the cow dung rumen samples, soil, cabbages, and tomatoes are represented in table 4.5 below.

Table 4.5: Total microbial population from dung and rumen fluid samples

Sample	Unit	Count
Cow dung	cfu/g	$1.50 \pm 0.02 * 10^{10}$
Rumen waste	cfu/ml	$3.15 \pm 0.01 * 10^{10}$
Tomato	cfu/g	$1.31 \pm 0.06 * 10^6$
Cabbage	cfu/g	$1.011 \pm 0.03 * 10^5$
Loam soil	cfu/g	$3.01 \pm 0.02 * 10^9$

From the table, the bacteria concentrations were $1.31 \pm 0.05 * 10^6$ CFU/ml in rumen fluid, $1.01 \pm 0.03 * 10^5$ cfu/g in cabbage, $3.01 \pm 0.02 * 10^9$ cfu/g in loam soil, and $3.15 \pm 0.01 * 10^6$ cfu/g in tomatoes. $5.15 \pm 0.01 * 10^{10}$ CFU/ml were found in rumen waste by Obayram *et al.* (2018) and Liu *et al.* (2016). It was found that rumen waste possessed highest quantities of microbes than those in loam soil, cabbage and tomatoes.

Determining Bacteria population in a sample

Bacteria population was determined by calculating the number of bacteria (CFU) per milliliter or gram of sample by dividing the number of colonies by the dilution factor multiplied by the amount of specimen added to liquefied agar. This is the standard plate count (SPC). The determination of bacterial cell numbers was achieved by culture turbidity method as shown in figure 4.3 and figure 4.4 below.

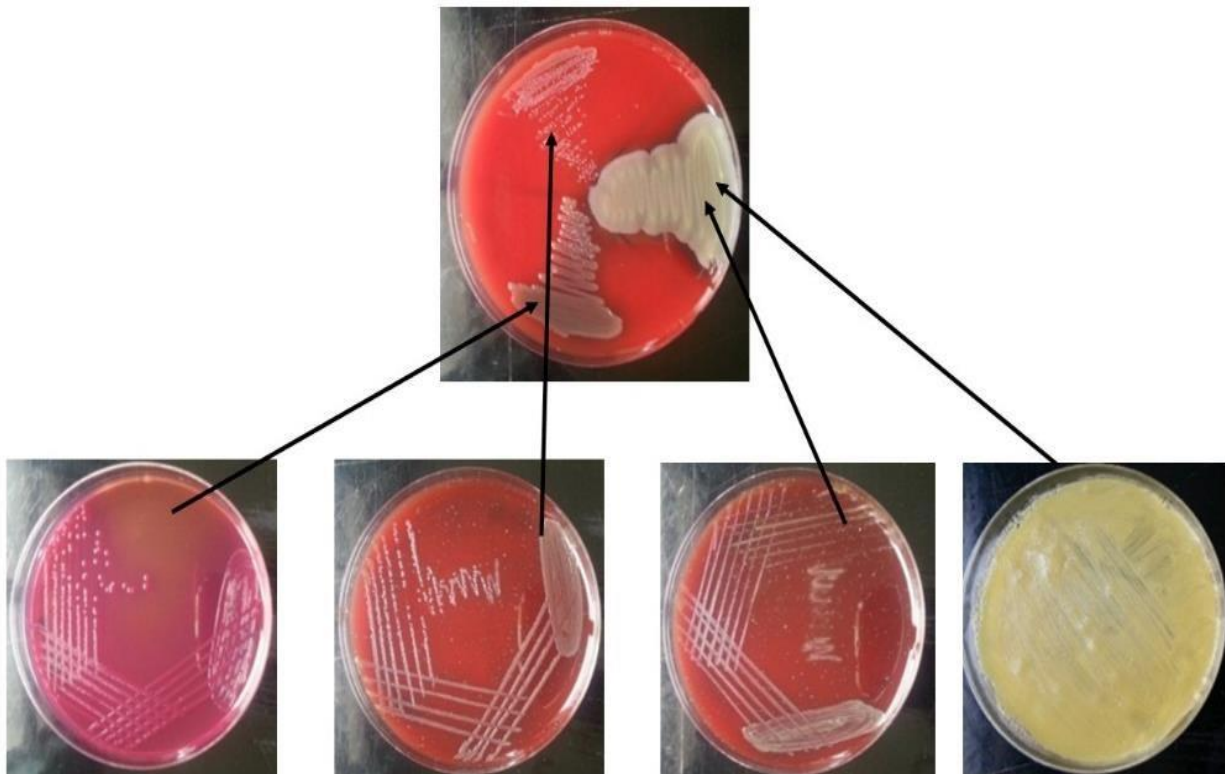


Figure 4.3: The cultured and isolated bacteria from Rumen fluid

The microbial concentration is determined by counting the colonies on a part of the petri dish where they are easily countable and dividing this count by the appropriate volume. Approximately one inoculation determines microbial densities between 500 and 500,000 microorganisms/ml.

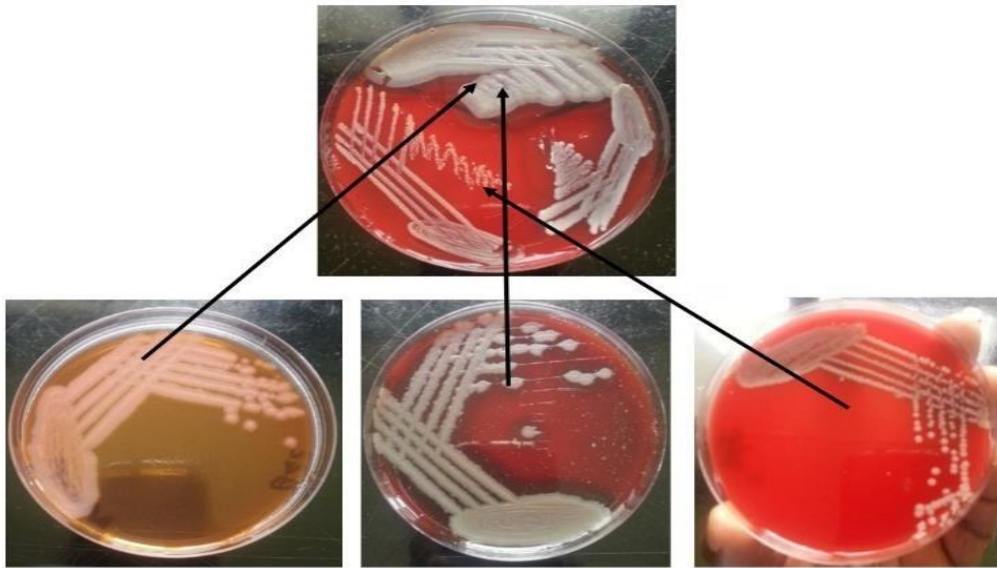


Figure 4.4: The cultured and isolated bacteria from cow dung

The bacteria count is an indication of the rate at which the substrate is decomposed or the pollutants are bio-remediated. The speed at which the substrate is degraded could be attributed to the number of bacteria present in the sample. Abele & Aquilla (2014) concluded that higher bacterial activity led to higher rates of bio-degradation while time duration from sampling has no significance on the same. It is also notable that for rumen usage in testing bio-degradation, the time duration should not exceed 4 days (Mwaniki, 2016). Due to varying bacterial load and diversity levels, Inoculum sources affect the substrate's ability to degrade (Moreno-Andrade and Buitr'on (2004); Tabatabaei *et al* (2010).

4.3.5 Features of loam soil

The properties of the loam soil employed in this experiment are listed in Table 4.6. The soil's pH was determined to be 6.60. When compared to data from Mbugua *et al.* (2015) on Limuru loam soil, it was found to be comparable to the loam soil used in this experiment; the soil moisture content was at 43.36 percent, which is similar to that found in this study.

Table 4.6: Characteristics of the loam soil used.

Profile	Properties	Profile	Properties
Soil depth cm	Top	Calcium milli-equivalent%	44.4±2.11
Soil pH-H ₂ O (1:2.5)	6.5±0.51	Magnesium me%	3.1±0.09
Elect. Cond. ms/cm	0.3±0.01	Potassium me%	1.5±0.66
Carbon %	2.7±0.32	Sodium me%	3.6±1.11
Sand %	40±3.56	Sum me%	52.6±3.44
Silt %	40±4.55	Base %	100+
Clay %	20±2.88	ESP	14.4±6.74
Texture Class	Loam	Total nitrogen %	0.25±0.08
Cat. Exch. Capacity. me%	24.8±2.67	Phosphorus ppm	44±5.00
Zinc ppm	62.9±10.22	Iron ppm	96.2±12.90
Copper ppm	1.22±0.11	me is milli-equivalent	

The above type of soil was the most suitable for the study and was collected not deeper than 2cm from the surface after the organic filtrate had been collected and used for the same research. The soil pH was determined to be 6.6±0.5 and the carbon percentages were at 2.69±0.31 %. The counts of macro and micro-organics are as indicated in table 4.7 below

Table 4.7: Macro and micro-organic matter in loam soil.

Macro organic matter	Counts in %ppm	Micro organic matter	Counts in % ppm
Carbon	2.7 ±0.32	Zinc	62.9±10.22
Nitrogen	0.25±0.08	Copper	1.22±0.11
Potassium	1.5±0.66	Sodium	3.6±1.11
Calcium	44.4±2.11	Iron	96.2±12.90
Magnesium	3.1±0.09	Chloride	0.5±0.01
Phosphorus	44.0 ±5.00	Manganese	0.002±0.30

4.4 Microbial Fuel Cells

Microbial fuel cells (MFCs) are the newest bio-electrochemical technique that works with the objective to generate electricity by use of electrons derived from biochemical reactions.

4.4.1 The voltage and current of the MFC

This section examines the voltage and current production in individual experiments shown and analyzed in this section. Afterwards, average voltage and currents were used to obtain curves/plots for modeling purposes.

4.4.2 Voltage and Current Measurements

A comparison of the voltage and current data was carried on from both the Arduino sensors and multi-meter for a fortnight and the average readings recorded. Figure 4.5 displays the electricity readings obtained from both tomato and rumen samples.

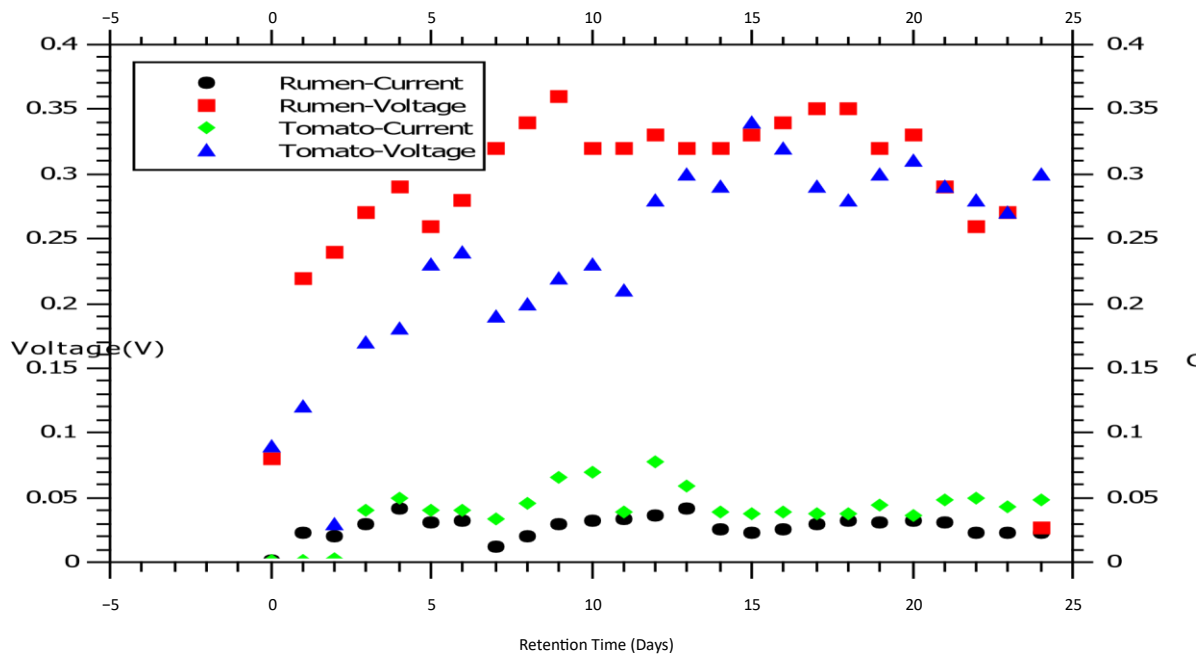


Figure 4.5: Plot of multi-meter voltage and current interpretations from tomato and rumen

Data obtained from both samples over the fortnight is recorded in Figure 4.6. It was observed that daily voltage ranged between 0.05V and 0.35V, and the current readings were 0.0022 and 0.071 mA.

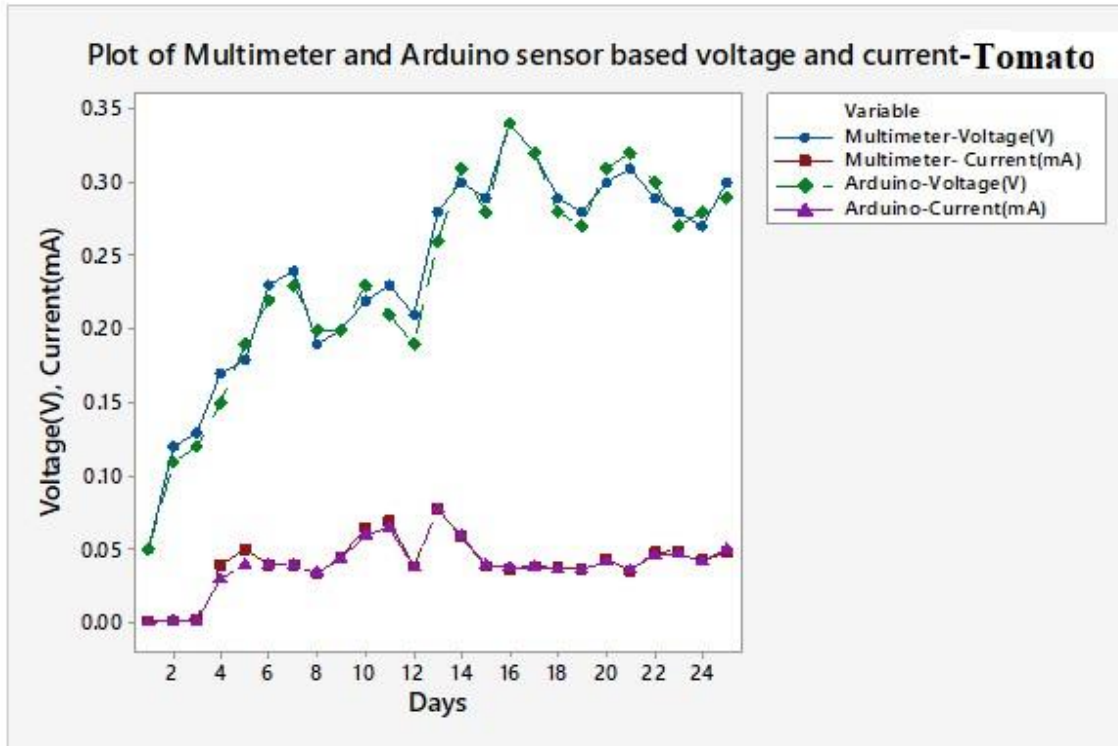


Figure 4.6: A plot of multimeter and Arduino sensor-based voltage and current readings from tomato samples.

It can be seen that the readings derived from both sets of machines were quite similar and that there was due correspondence between the two systems. Voltage averages of 0.2391 ± 0.071 V and 0.237 ± 0.072 V were obtained from both the multi-meter and Arduino sensors, respectively, at current values of 0.0391 ± 0.018 mA and 0.041 ± 0.017 mA. The results from both machines were used to draw up the curves displayed in figure 4.7 shown below.

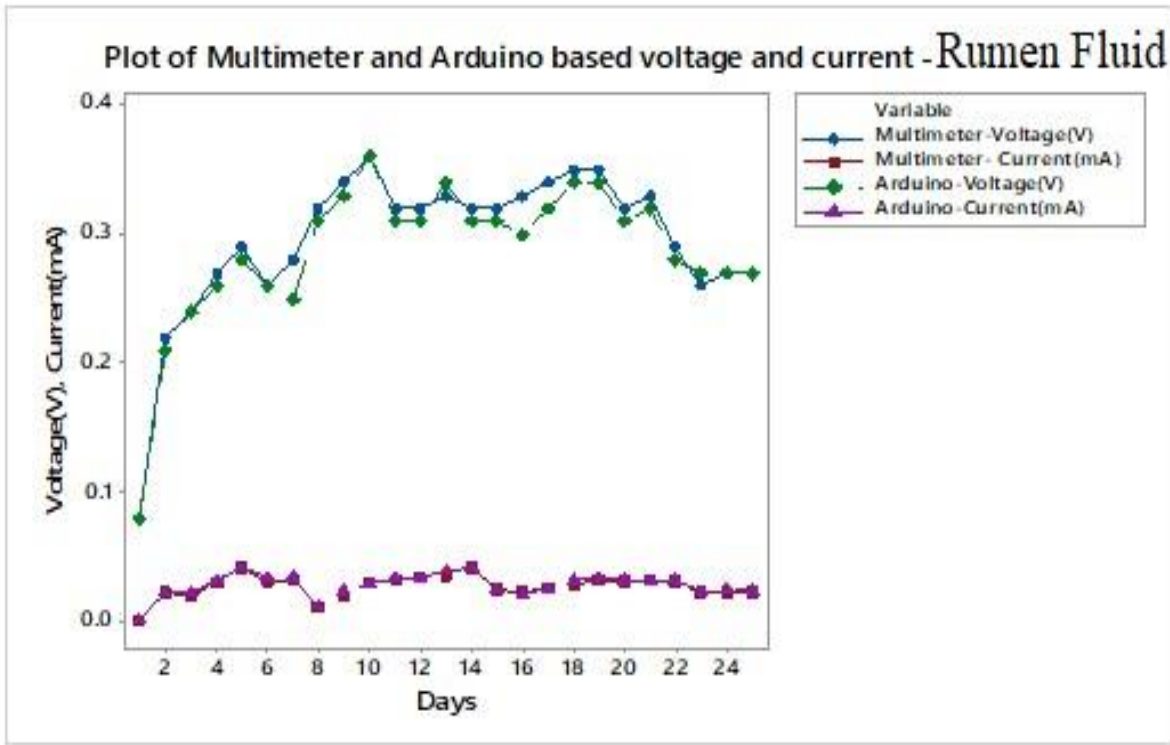


Figure 4.7: A plot of voltage and current from rumen on the Arduino-UNO and the multi-meter.

According to Motahhir *et al.* (2015), the Arduino UNO is an integrated embedded inbuilt board which insignificantly less expensive than the multi-meter used in potential measurement in MFC. It also significantly reduces voltage and current errors and saves time.

The curves were drawn using the mean voltage and current values produced by the rumen fluid, tomato, cabbage, and loam soil in the current investigation.

4.5 Control Experiment

The anodic chamber of the MFC was filled with untreated loam soil, cabbage, and tomatoes for the control tests, and daily voltage was measured using a multimeter. Figure 4.8 shows the voltage that was obtained from the setup. From the original set up through day 30, was 0.568 V, and the rumen fluid voltage showed an upward tendency and thereafter, a decrease trend was observed. The voltage in the

tomato sample peaked on day 26 at 0.579 V, while the voltage in cabbage fruits peaked on day 30 at 0.474 V.

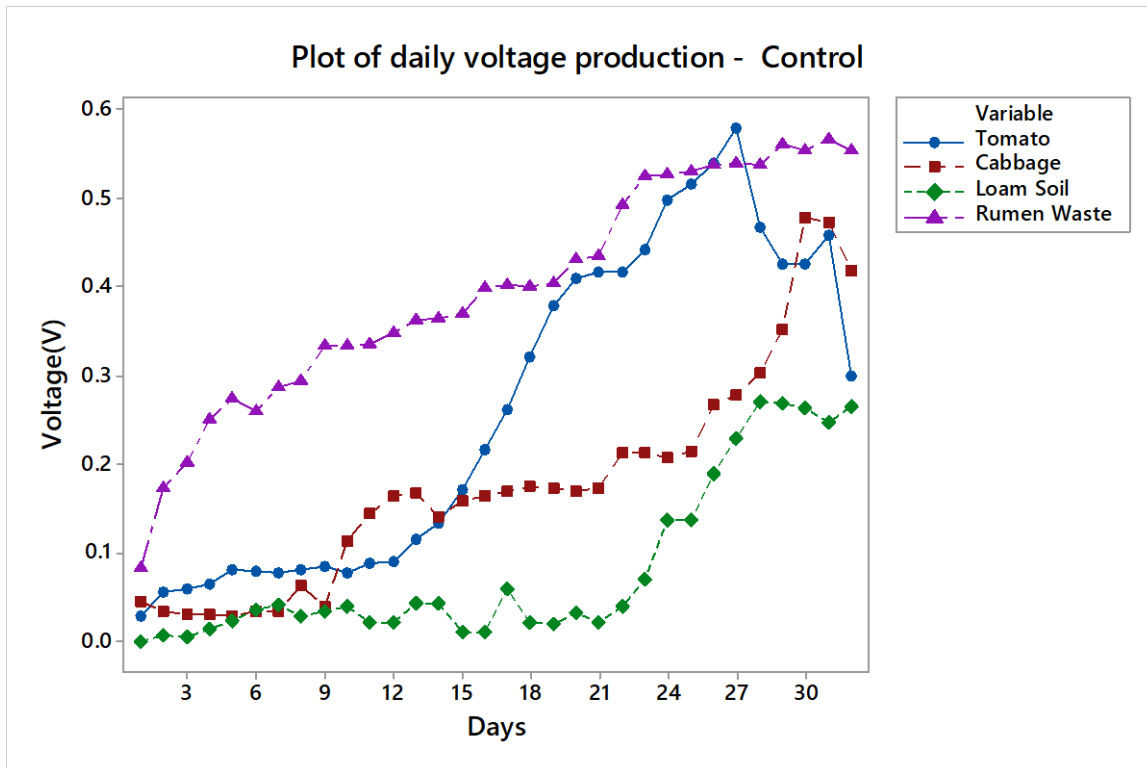


Figure 4.8: Daily voltage readings from tomato, cabbage, loam soil, and rumen samples.

In comparison to the other four matrices, the voltage pattern in loam soil was the weakest, with the peak voltage value being obtained at 0.272 V. This was most probably due to the soil's low carbon content as depicted in figure 4.9 below . The voltage generation in rumen fluid could be attributed to the strong bacterial diversity.

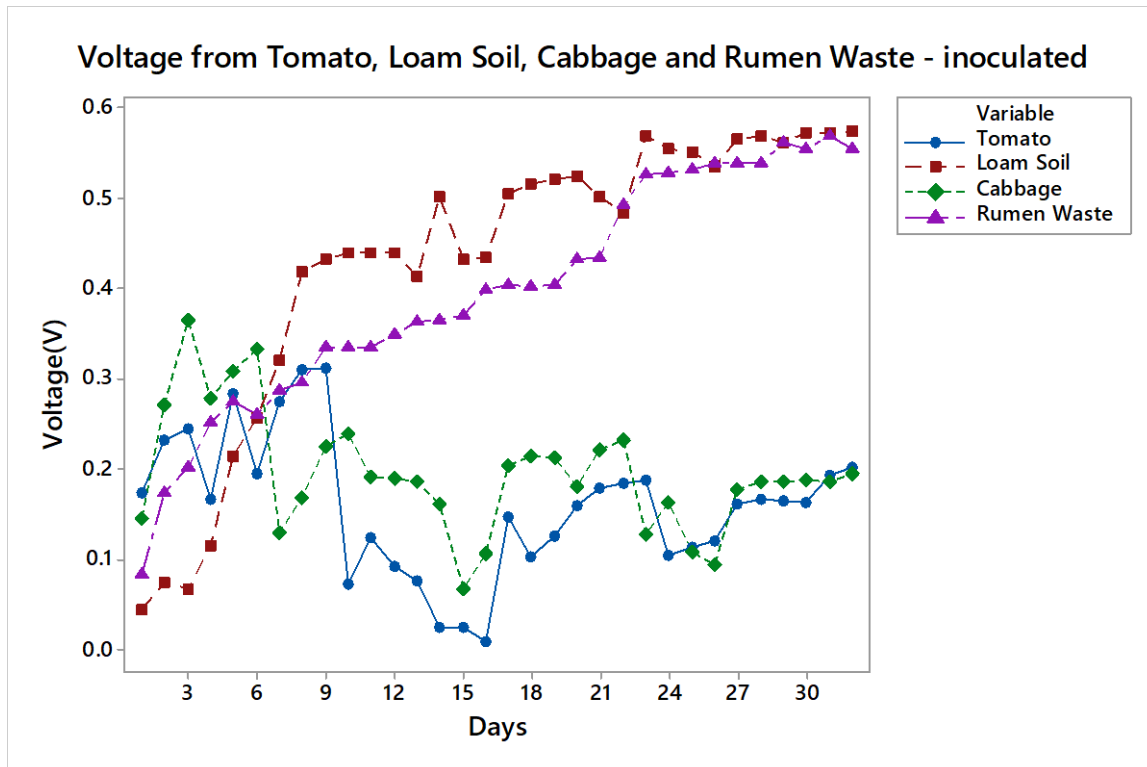


Figure 4.9: Daily voltage generated from tomato, cabbage, loam soil, and rumen waste

Following the induction of the microorganisms, the voltage from the soil increased by a great margin. For instance, on the sixth day, the voltage readings in the inoculated setup were 0.0421 V, whereas those for the rumen-loaded MFC measurements were 0.324 V, which translated to a sevenfold increase. In the untreated control experiment, the maximum voltage from loam soil recorded was 0.271 V on day 27, while it was 0.571 V on day 30. The voltage trend in the tomato and the cabbage was similar (figure 4.7). For the first three days, an increasing tendency was seen, but after that, a rigid production pattern was observed. This could have been caused by the rapid change in pH after the microbes degraded the organic materials. The microbial processes result in the production of acid, which decreases the operation.

4.5.1 Pesticide Voltage study

Figure 4.8 shows Voltage Studies produced by the four matrices doped with pesticide mixtures containing malathion, lambda-cyhalothrin, and chlorpyrifos abbreviated as (CLM). On day 26, a highest voltage of 0.576 V was recorded in the rumen fluid matrix, while on days 27, 30, and 26, voltages of 0.483 V, 0.479 V, and 0.587 V were recorded in loam soil, cabbage and tomato respectively.

The influence of microbial community, pH, retention time and proximate properties of the substrate is displayed in figure 4.10 below.

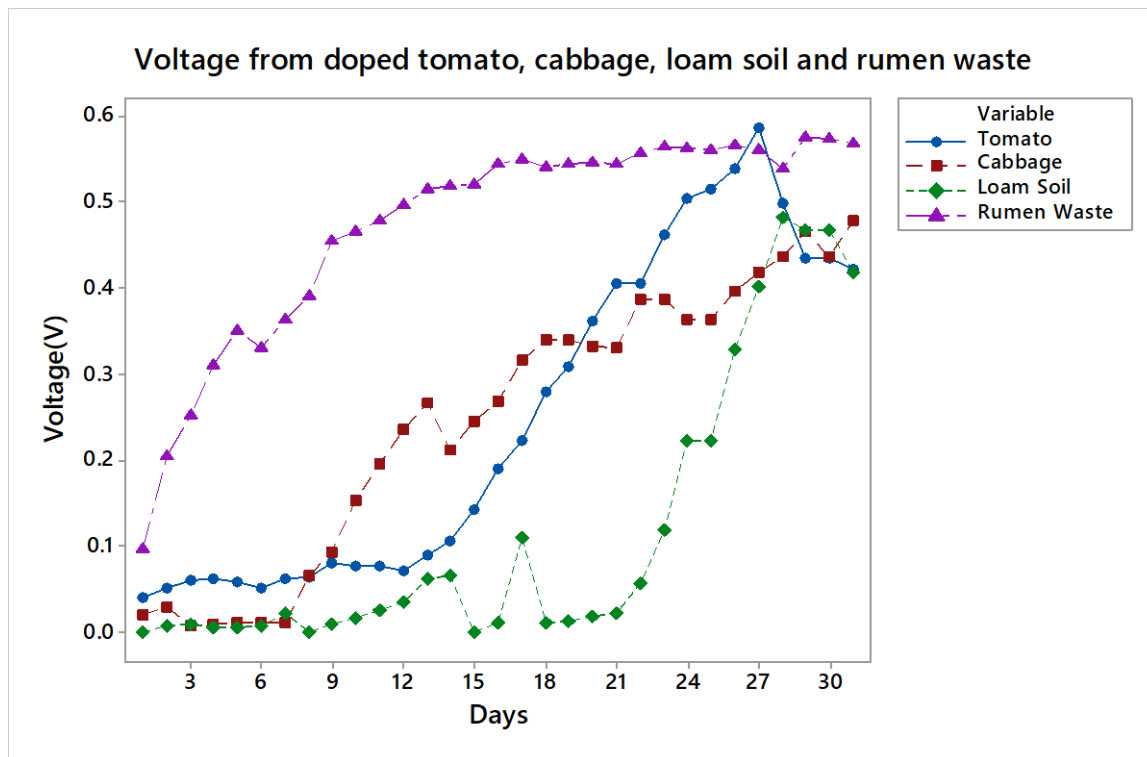


Figure 4.10: Daily voltage readings from pesticide doped un-inoculated samples.

The rumen fluid demonstrated the maximum voltage output most probably due to the high microbial community. The voltage production in the tomato and cabbage setups began at a slower pace than in the control studies, with a dramatic increase occurring in the cabbage setup on day seven, the tomato

setup on day 14, and the loam soil setup on day 22. The introduction of the pesticide molecules caused the total voltage in all matrices to rise.

4.5.2 Voltage from Bio-remediation studies

In this section, the voltage generated from lambda cyhalothrin, chlorpyrifos and malathion doped with loam soil, rumen, tomato and cabbage matrices is represented and discussed. In figure 4.11, voltage generated from rumen fluid doped with CLM is shown.

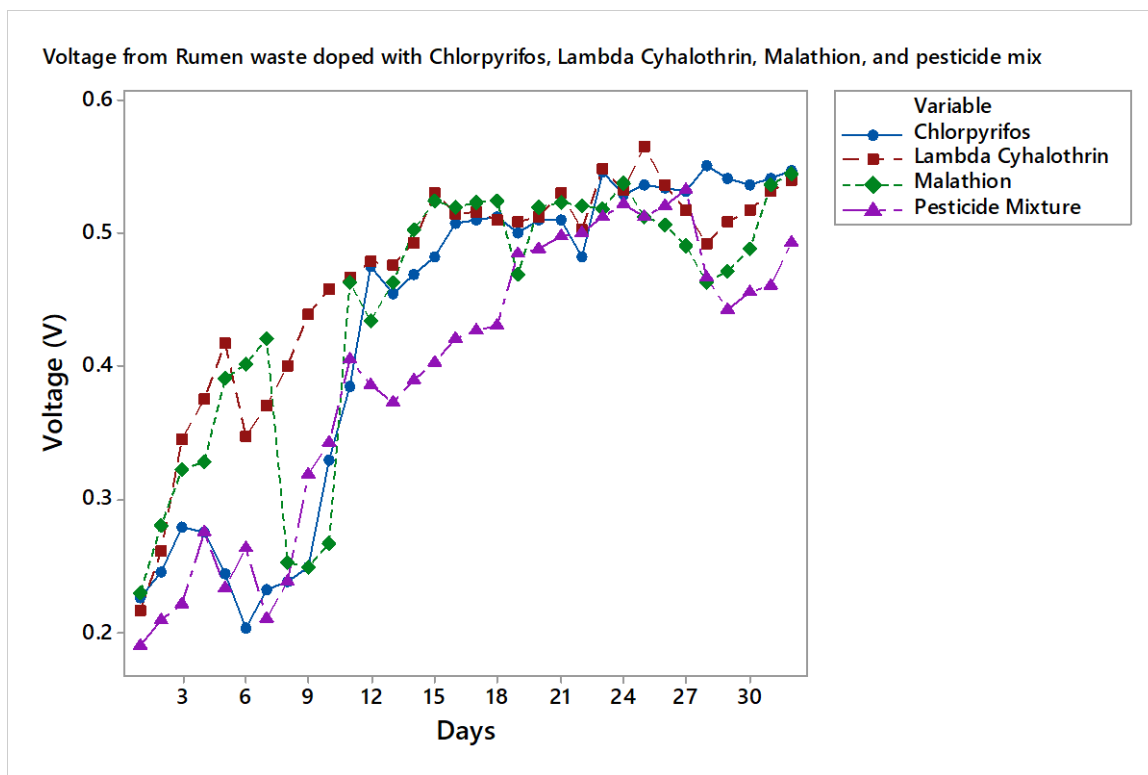


Figure 4.11: Daily voltage generated from the three samples loaded with pesticide

The measured voltage had an ascending tendency from the first to the 5th day, after which there was a brief decrease then an ascending trend up to day fourteen, when the generation of voltage stabilized. In pesticide-treated loam soil, there was an over-all upsurge in voltage for the initial 13 days. Then, it steadied until the 24th day when it started to decline, thereby displaying a Gaussian trend. According

to figure 4.12 shown below, the highest voltages for lambda-cyhalothrin, chlorpyrifos, malathion, and pesticide mixture were 0.524 V, 0.567 V, 0.560 V, and 0.485 V, respectively.

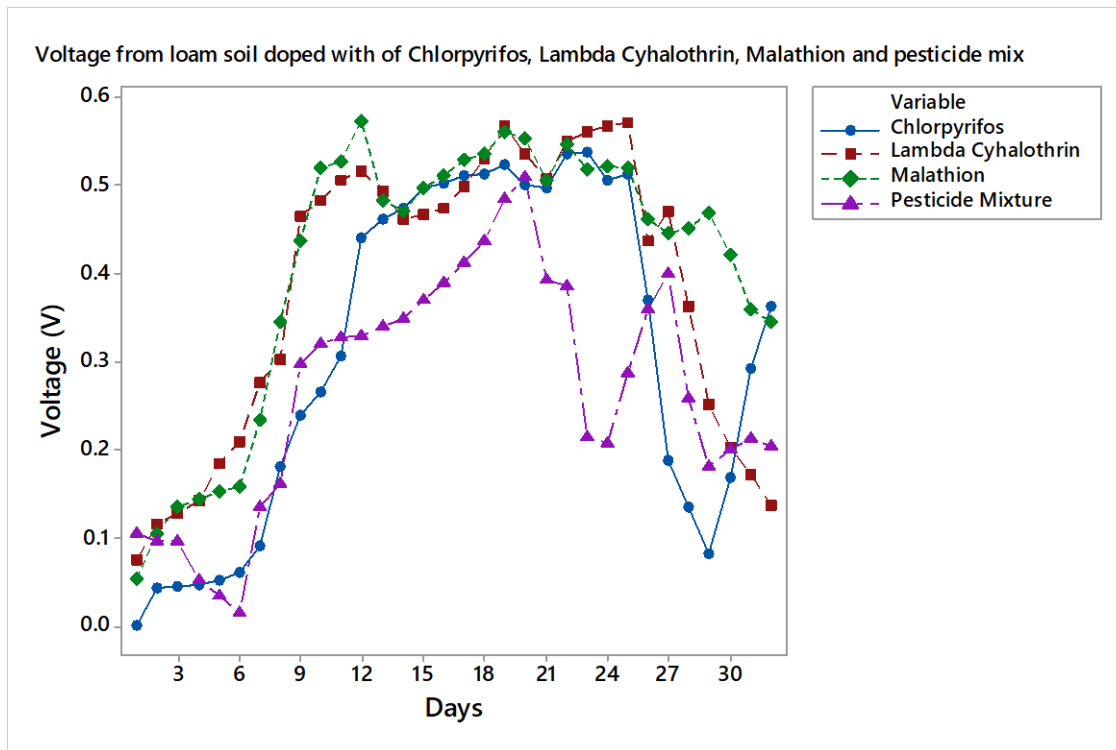


Figure 4.12: The daily voltage produced by loam soil doped with the pesticide mixture chlorpyrifos, lambda cyhalothrin, and malathion.

The voltage generation from the pesticide mixture showed a decrease trend for the 1st 6 days, then an ascending trend with fluctuations till day 30 when it became unstable showing a declining tendency .

The voltage generation trend for all the pesticides, with the exception of the pesticide mixture, showed a steep rise from day 0 to day five, as shown in Figure 4.12. The voltage then began to rise up to day 30 after which it began to trend downwards for three days. In lambda-cyhalothrin, the greatest voltage created was 0.363V, in chlorpyrifos, was 0.509V, malathion 0.582V and lambda cyhalothrin 0.363V.

The plot of voltage trend observed between tomatoes doped with pesticide increased from day 0 to day 5 for all pesticides including pesticide mixture just as was the case with tomato (figure 4.13)

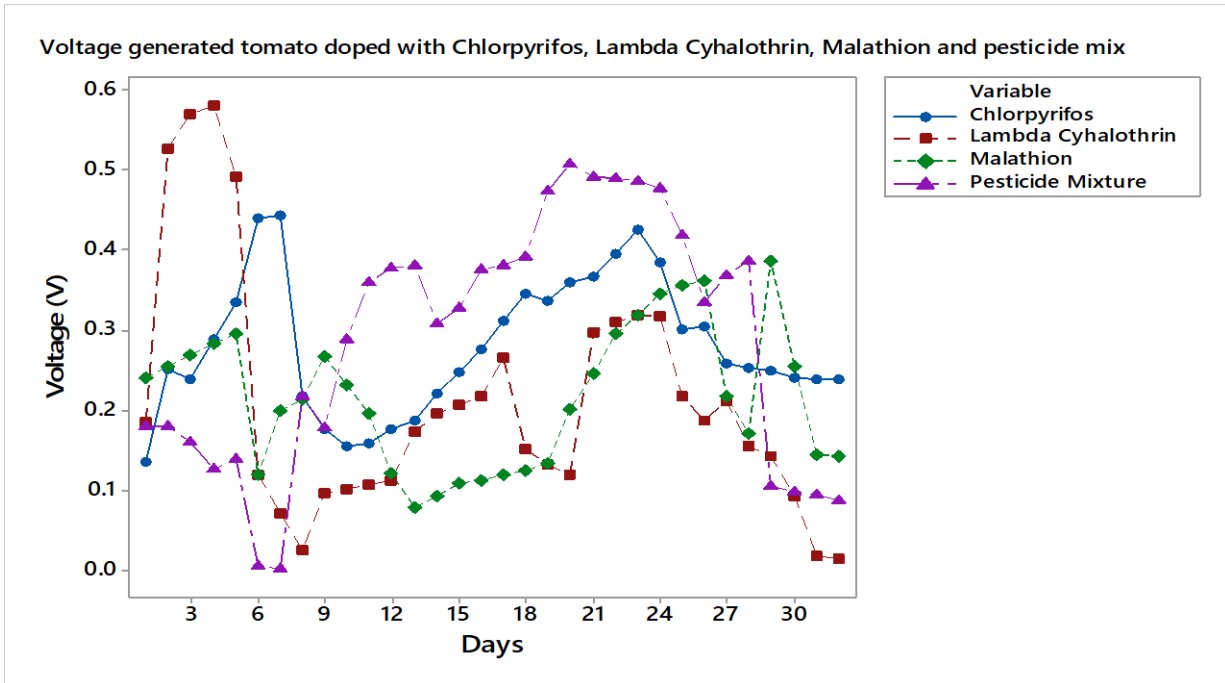


Figure 4.13: A plot of daily voltage readings for the pesticide mixture, malathion, and tomato waste that has been injected with CLM.

For cabbage doped with CLM ,and pesticide mixture, they all produced higher voltage from day 0 to day five in the dual cabbage chamber MFC. It is notable that the voltage trend rose resembling that of pesticide-loaded tomatoes as depicted in figure 4.14 below.

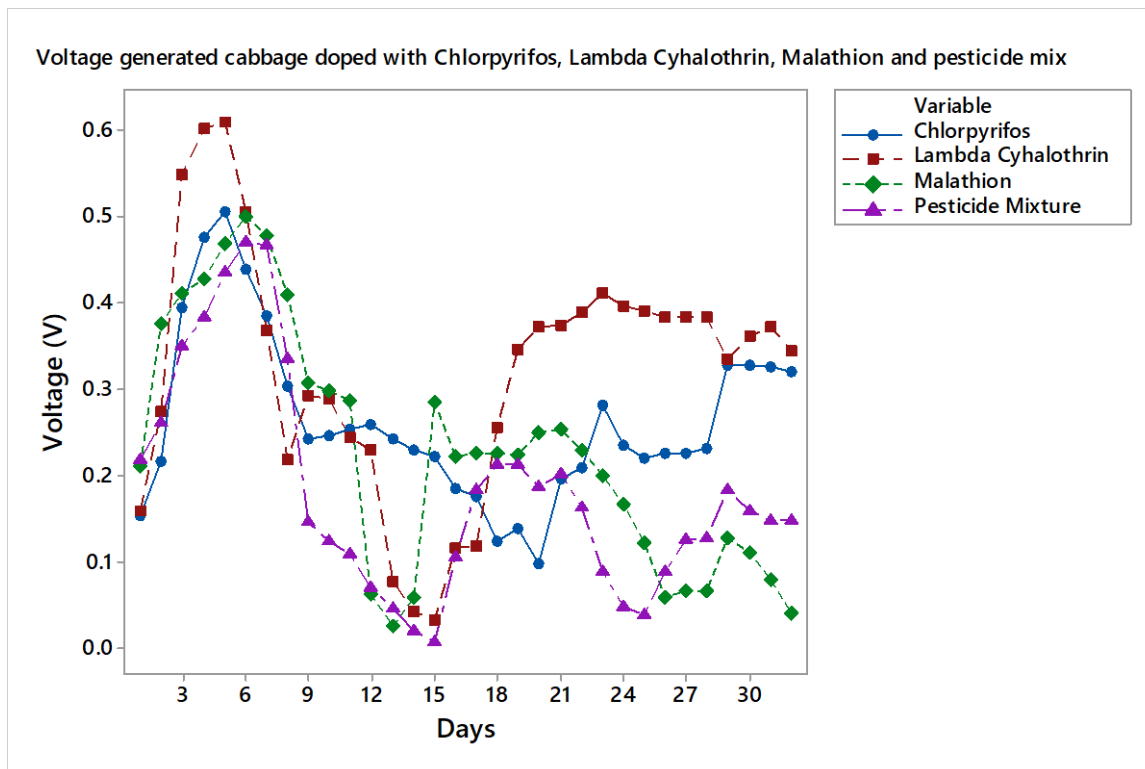


Figure 4.14: A plot of daily voltage readings for the pesticide mixture, individual pesticides for cabbage waste.

4.6 Optimization of Microbial Fuel Cell Parameters

A number of variables, including pH, temperature, substrate proximity, external resistance (Kamau *et al.*, 2017), microbial community, and pesticide concentration, have an impact on pesticide bioremediation and voltage yields, and needed to be optimized (Kamau *et al.*, 2019),(Dyson, 2002).

4.6.1 Examining the impact of the concentration of microbes.

The voltage produced was periodically recorded using a multimeter. Figure 4.15 presents the findings. When rumen fluid was introduced into the setup, high voltage was realized. This is due to numerable microbes present in the rumen fluid which degrade substrates and generate electricity as a result (Mbugua *et al.*, 2018). There were three distinct ratios of tomato to rumen matter used: 750 g of tomato

in 750 mL of rumen matter (R 1:1), 750 g in 375 mL of rumen matter (R 1:0.5), and 750 g in 1500 mL of rumen matter (R 1:0.5). (R 1:0.5). (R 1:2)

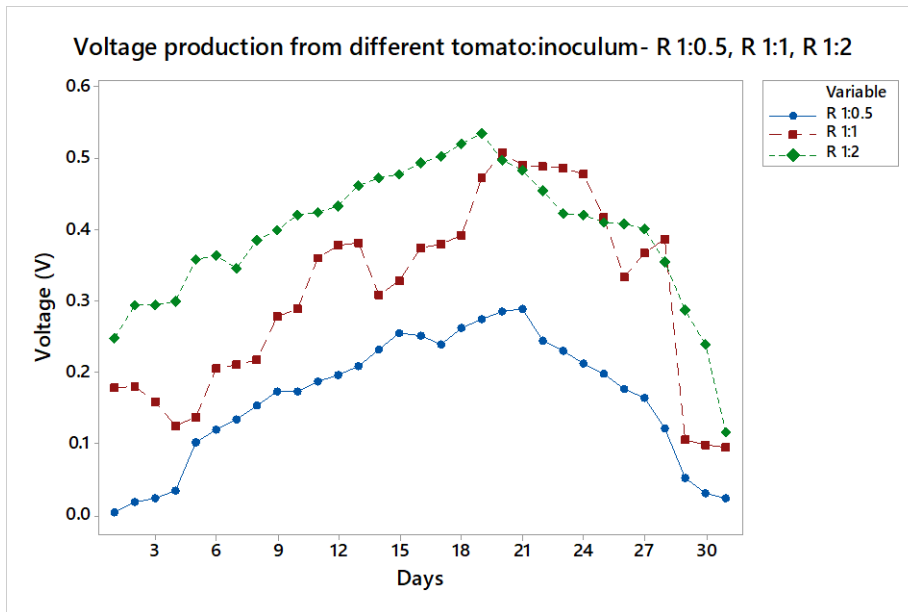


Figure 4.15: Daily voltage readings for various tomato: inoculum ratios

There were three different ratios: 750 g of cabbage in 750 mL of rumen matter (R 1:1), 750 g in 375 mL of rumen matter (R 1:0.5), and 750 g in 1500 mL of rumen matter (R 1:2). The results for cabbage ratio 1:1, 1:0.5 and 1:2 is as shown in figure 4.16 below.

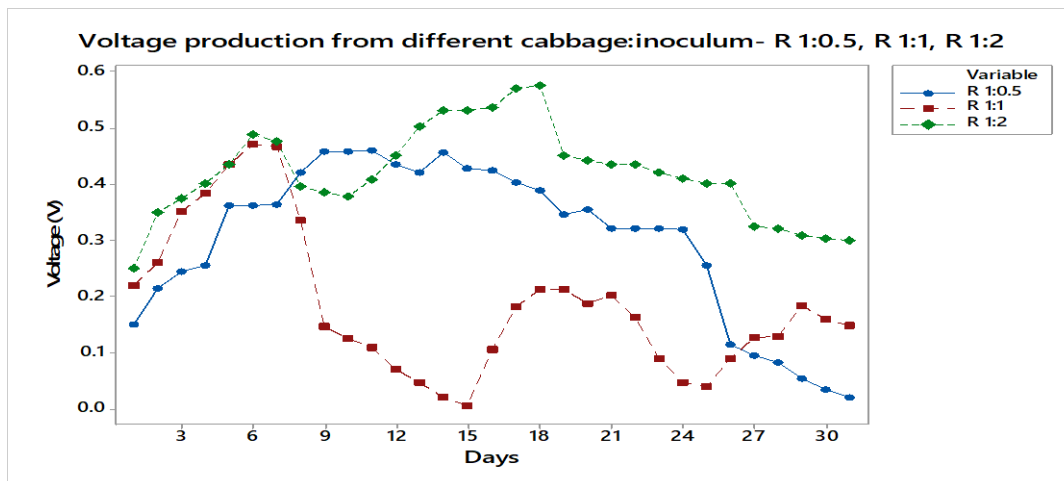


Figure 4.16: Shows the voltage produced by various cabbage-to-Inoculum ratios.

The ratios for rumen matter in loam soil were 750 g of loam soil in 750 mL rumen matter (R 1:1), 750 g of loam soil in 375 mL rumen tissue (R 1:0.5), and 750 g of loam soil in 1500 mL rumen matter (R 1:2).

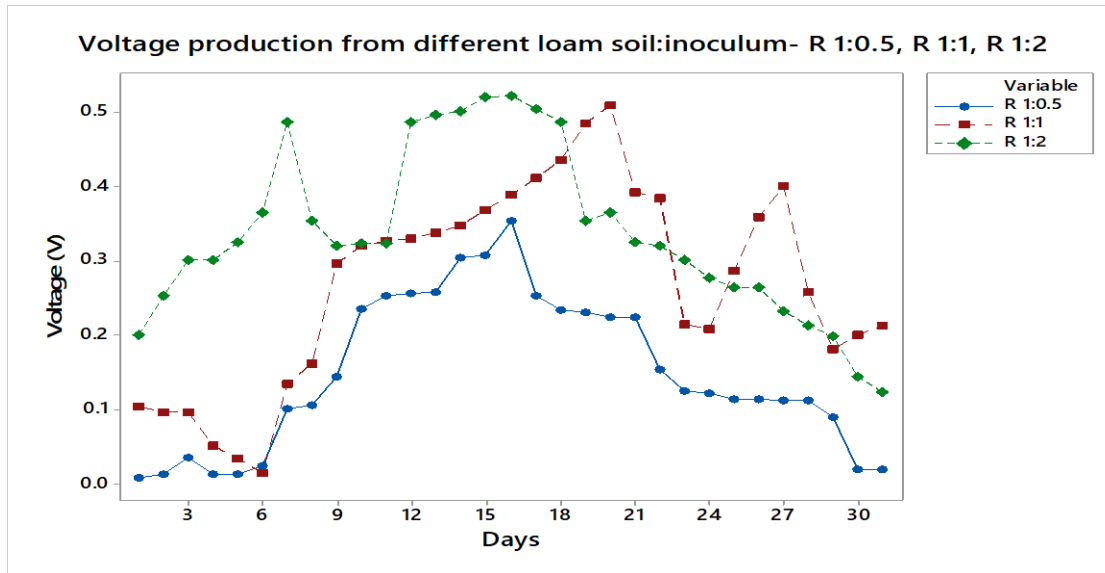


Figure 4.17: Daily Voltage produced by various loam soil inoculation ratios

In figure 4.17, the current produced by the loam soil is depicted. The rumen fluid inoculation configuration had the largest current, which was explained by a larger microbial population causing a faster rate of substrate breakdown (Kamau *et al.*, 2018a). It was noted that the voltage was highest at the set up that had 350 mL of rumen fluid.

This might be because the bacteria got virtually enough nourishment during the experiment. The maximum voltage was obtained by 500ml of rumen fluid after the first 24 hours. This might be the case because the competition among bacteria for the substrate encourages rapid electron generation. The 250ml of rumen fluid continued to produce energy continuously throughout the experiment. This is because there wasn't much competition for the food, and the microbes were able to sustain the biodegradation. This was also reported by Kamau *et al.*, (2018b) who noted that substrate utility and

voltage generation was strongly dependent on the substrate's concentration and high population of microorganisms. The proximate properties and ultimate composition matter were other factor that enhanced how well the microorganisms survived in their habitat.

4.6.2 Impact of pH on electricity generation

The condition of the fermentation process can be estimated using the pH. The optimal pH range for any anaerobic degradation process is expected to be between 6.5 and 7.5. (Pratima & Bhakta, 2015 Lazor *et al.*, 2010). Some of the substrates have a tendency to lower the pH in the chamber of the MFC. Figure 4.18 shows how the pH of the various samples changed on a daily basis. For all wastes, the pH of the four units that had been blended and anaerobically incubated dropped over the course of the incubation process. For instance, the pH of tomato dropped from 5.86 to 3.04 and that of cabbage from 6.62 to 3.14. While in loam soil, minor pH shifts from 7.32 to 7.08 were seen. It is probable that soil may contain calcium hydrogen carbonate molecules that act as a system buffer, preventing significant pH swings and thereby maintaining high voltage generation within the system.

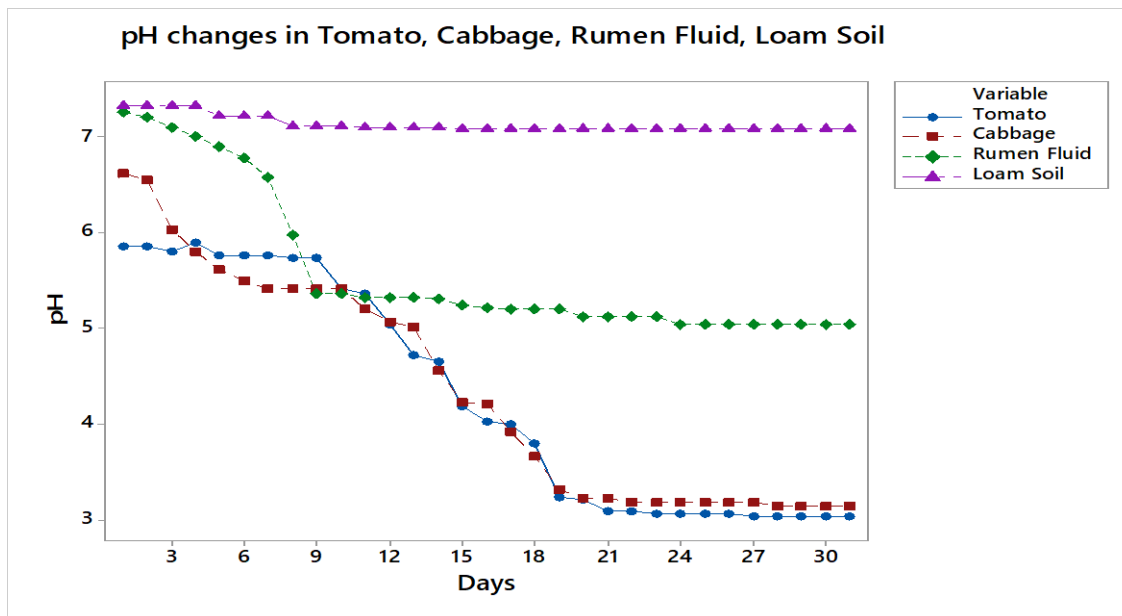


Figure 4.18: Daily pH changes per substrate waste.

There was no discernible difference between the voltage produced at pH 11 and pH 7 in the rumen fluid set up (figure 4.19). The initial pH 11 arrangement produced the highest voltage, especially from day 0 to day 21, whereas the initial pH 7 setup produced a relatively high voltage from day 0 to day 27. The arrangement with an initial pH of 2 produced low voltage, as seen in figure 4.19.

Anaerobes are especially susceptible to pH changes and do not function effectively at low pH levels (Mbugua et al. 2021), leading to lower production of electricity. .

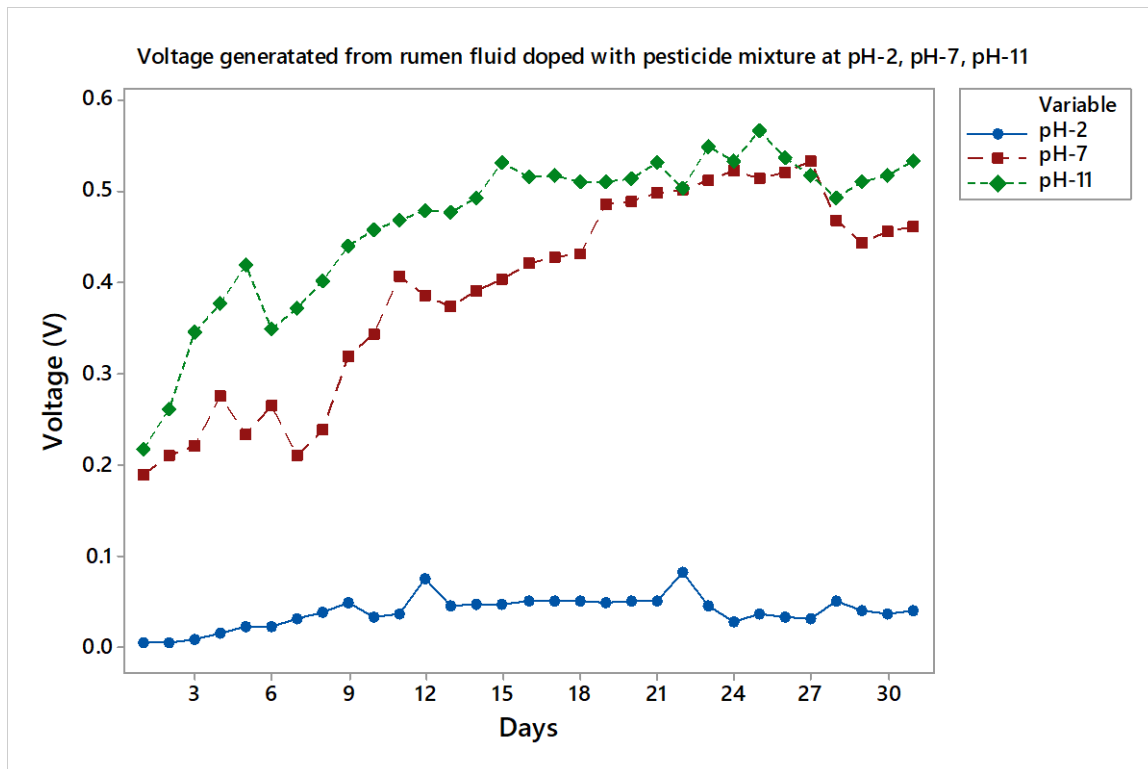


Figure 4.19: Voltage produced by rumen fluid doped with pesticides at various pH levels

Figure 4.20 represents the variation of initial pH with voltage in pesticide-doped tomatoes inoculated with rumen fluid up till day 30. The lowest voltage was observed with the pH 2 setup. In the pH 7 setup the pH was observed to increase in a manner similar to that observed in the rumen fluid setting. For the initial pH 11 setup, voltage peaked at 0.562 V in the first few days before trending downward.

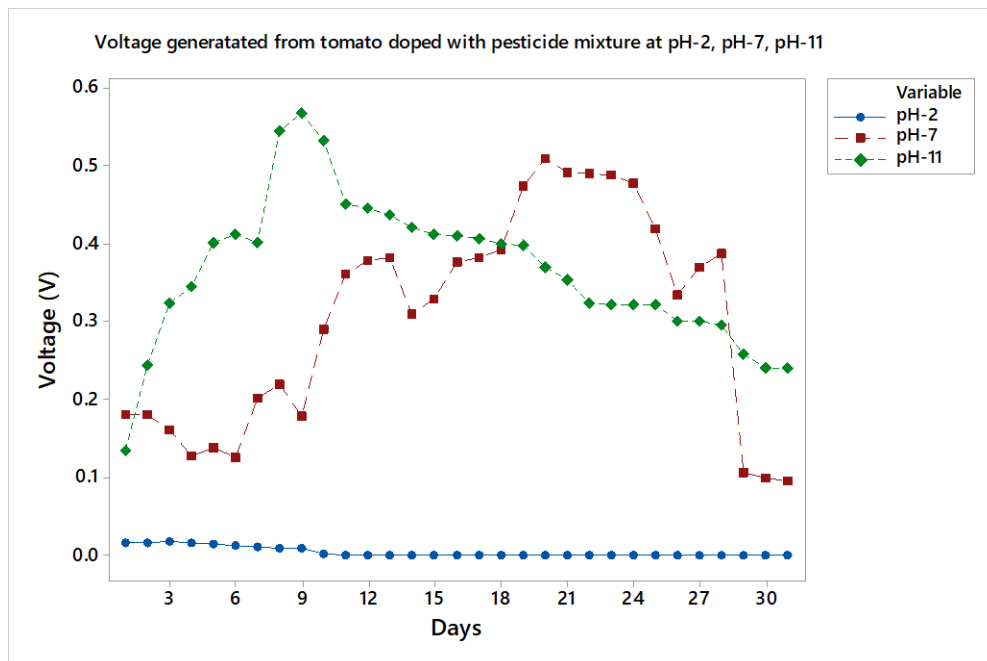


Figure 4.20: Voltage produced from doped tomato at different pH levels

The observations in the effect of initial pH on voltage production in cabbage are illustrated in figure 4.21. As observed with the other setups, the initial pH 2 setup had the lowest voltage, due to the fact that anaerobic bacteria do not operate optimally at low pH levels. The initial pH 7 setup had an initial increase in pH up till day 6, after which the voltage dropped significantly. This may be because the mixture became more acidic and with the drop in pH the microbial activity, and the corresponding voltage declined. A similar pattern was shown in the initial pH 11 setup with the decline taking place after day 10. This is shown in the figure 4.21 below.

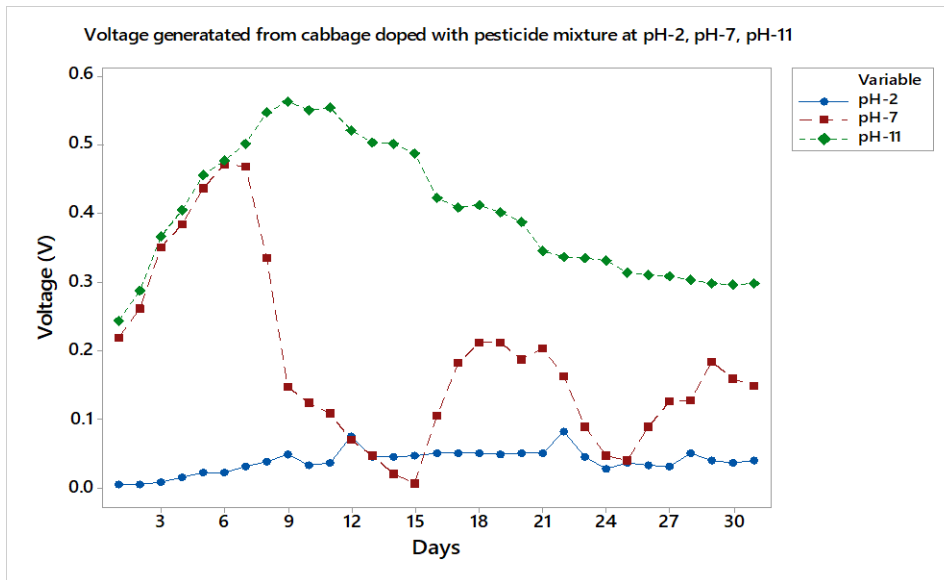


Figure 4.21: Voltage produced from doped cabbage at different pH

In samples of loam soil with initial pH values of 7 and 11, a small initial voltage was observed up till day 9 when the voltage had a steep increase, especially with initial pH 11 setup (figure 4.22). The voltage peaked on day 24 after which it dropped. As stated earlier, it is possible that the soil had traces of hydrogen carbonate that buffered any change of pH and therefore the microbial activity was maintained. As with the other setups, lower voltage was observed at a pH of 2.

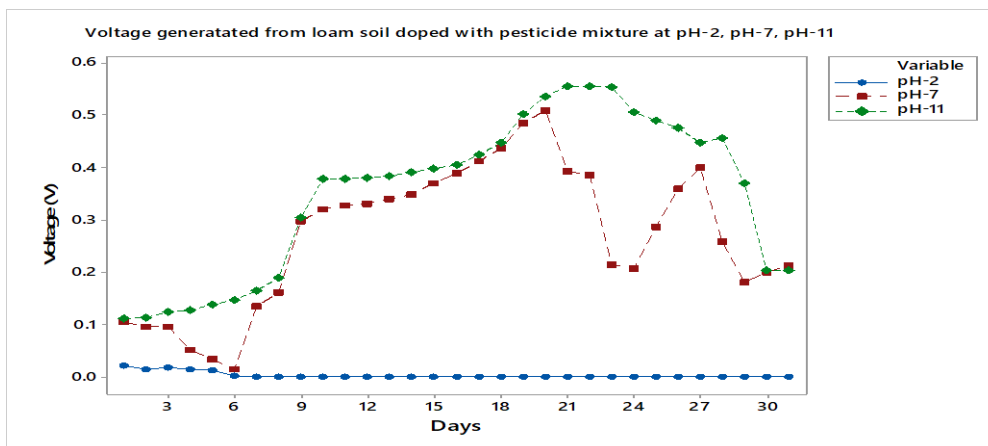


Figure 4.22: Voltage produced by doped loam soil at various pH levels

Moderate pH (6–8) is ideal for MFC efficiency and microbial metabolic activity in both anode and cathode chambers (Shukla and Kumar, 2018, Puig *et al.*, 2010). It is known that proton creation during photosynthesis results in the lowering of the pH in the anode compartment, which becomes acidic (Elshobary *et al.*, 2020). Proton buildup causes a pH gradient resistance, which over time impacts current density and electrode potential (Zhang *et al.*, 2013; Timmers *et al.*, 2010). In the cathodic chamber, on the other hand, water is produced through reduction of oxygen. The pH gradient shifts when the amounts of oxygen, protons, or electrons are altered, resulting in the lowering of the amount of power produced. The ideal cathode potential at pH 7.0 is 0.81 V (Zhang *et al.*, 2013), however actual values are almost invariably lower due to the mixed potential of contaminating species. In order to counteract the negative impacts of pH changes on the performance of MFCs, Oliveira *et al.* (2013) used a range of buffers. However, they noted that this process may raise net production costs (Nam *et al.*, 2010).

Oliveira *et al.* (2013) realized that pH 8 produced the highest production (in terms of voltage, current density, and power density) under the current testing conditions. The voltage values in the present investigation were marginally greater than those previously noted in the literature. With river water serving as the electrolyte and graphite rods and PbO₂ graphite as the electrodes for MFC operation, Dhiraj *et al.* (2020) were able to achieve maximum voltages, currents, and power densities of 937mV, 382 J, and 86 Wcm², respectively. Additionally, Musi River water was employed as the electrolyte in a hybrid electrode by Behera *et al.* (2010), who realized a maximum current density of 62.23 A/m² and a power density of 15.56 W/m³ (Behera *et al.*, 2010). Gil *et al.* in 2003 found that a neutral pH was excellent for microbial activity and that an operating pH of more than 10 was undesirable for bio-electricity gathering .

Abdul-Halim and Yong in 2018 reported that after fifteen days of operation, COD elimination was 88, 90, 94, 91, and 89 percent for initial electrolyte pH of 6, 7, 8, 9, and 10. The coulomb efficiencies were

found to be 32.85 percent, 36.6 percent, 41.7 percent, 37.4 percent, and 35.7 percent for electrolytes with pH values of 6, 7, 8, 9, and 10. They concluded that, MFCs were appropriate for producing bio-electricity and micro-treating wastewater (Abdul-Halim and Yong, 2018).

4.6.3 Study of the effect of External Resistance

Pesticide doping of tomato, loam soil, cabbage, and rumen fluid as well as measurements of the voltage across various resistors revealed similar voltage patterns, with the voltage readings increasing with increasing external resistance. It was found that the open circuit voltage (OCV) was the greatest in all of the settings, as illustrated in figures 4.23 to 4.25. Figure 4.23 also depicts the voltage that was generated across various resistors. The OCV is highest because in this setup, all resistance from the cathode, anode, and electrolyte materials is overcome internally.

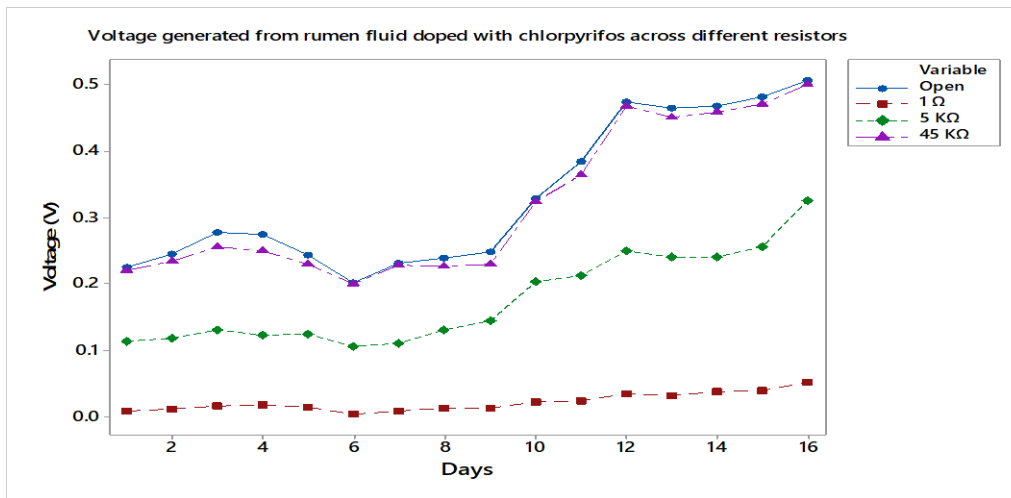


Figure 4.23: Plot showing the voltage produced across different external resistors by rumen fluid containing chlorpyrifos.

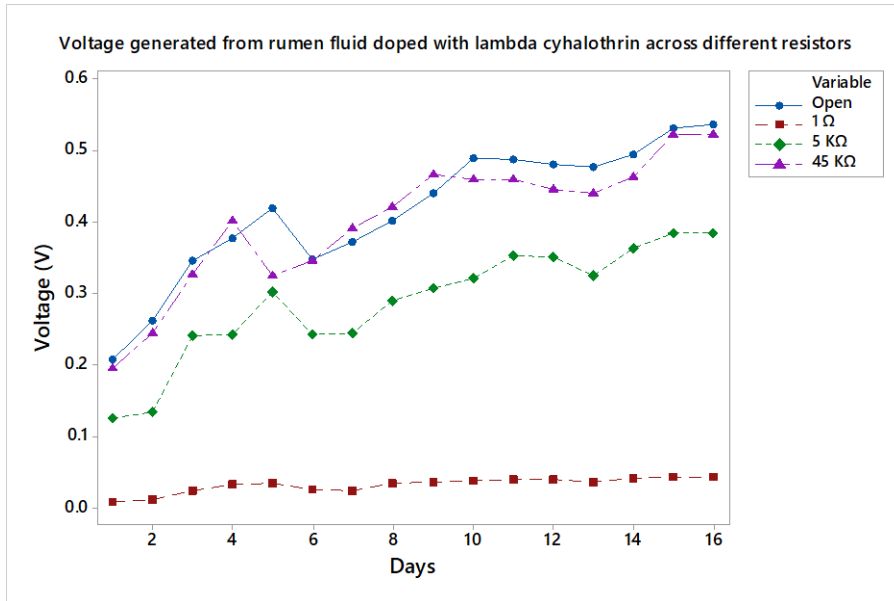


Figure 4.24: Voltage generated from lambda cyhalothrin-doped rumen fluid across different external resistors

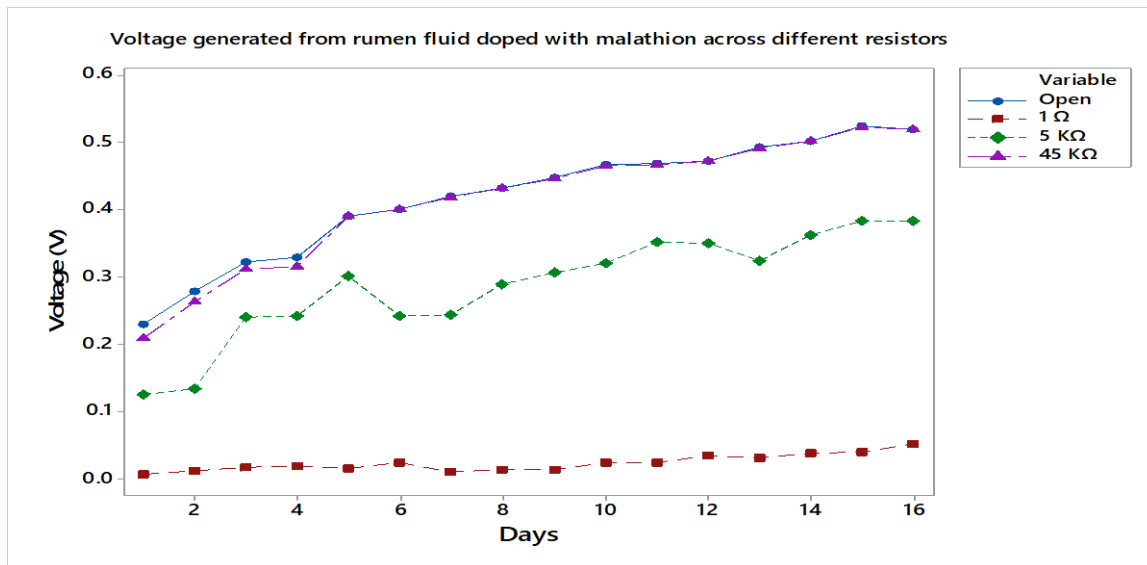


Figure 4.25: Voltage generated from malathion doped rumen across various external resistors

A 45Ω resistor generated the highest voltage when compared to the other resistors. This was observed by Kamau *et al.* in 2017. The outcome is in line with Ohm's law, which states that voltage is directly proportional to current and resistance i.e.($V= IR$). Using a range of 6 to 0.125Ω, Menicucci *et al.* (2011) observed that the cell voltage decreased as the external resistance increased. According to

Ghangrekar *et al.* (2012), a voltage of 358 mV was obtained across an external resistance of 4,000 Ω . Power values rose as external resistance increased from 0 to 4,000. Similar cathode potentials were found by Rismani-Yazdi *et al.* (2011) at varied external resistances. On the other hand, the anode potential varied according to the external conditions employed. In MFCs with lower external resistances, anode potentials were lower as per Ohms law. Song *et al.* (2013), which utilized a sediment microbial fuel cell, had similar observations.

4.6.4 Examining the impact of pesticide concentration

Figures 4.26 to 4.29 show the findings on the impact of pesticide concentration on voltage generation in the MFCs. 20 ppm of pesticide solution had the highest voltage, which was followed by 10 ppm and 1 ppm solutions. The addition of glucose-doped fluid in this instance had no significant effect on voltage. For instance, in tomato, the voltage generated from the 20ppm doped solution was high for the first 8 days (figure 4.26) possibly because there was more carbon available as a food supply for the bacteria. The voltage generation rate subsequently declined up until day 30. The voltage for 10 ppm increased and peaked on the 28th day then after which it declined. In the 1 ppm setup, the same was observed on day 15. Similar results had been observed by Imwene *et al.*, (2020) and Mbugua *et al.*, (2018).

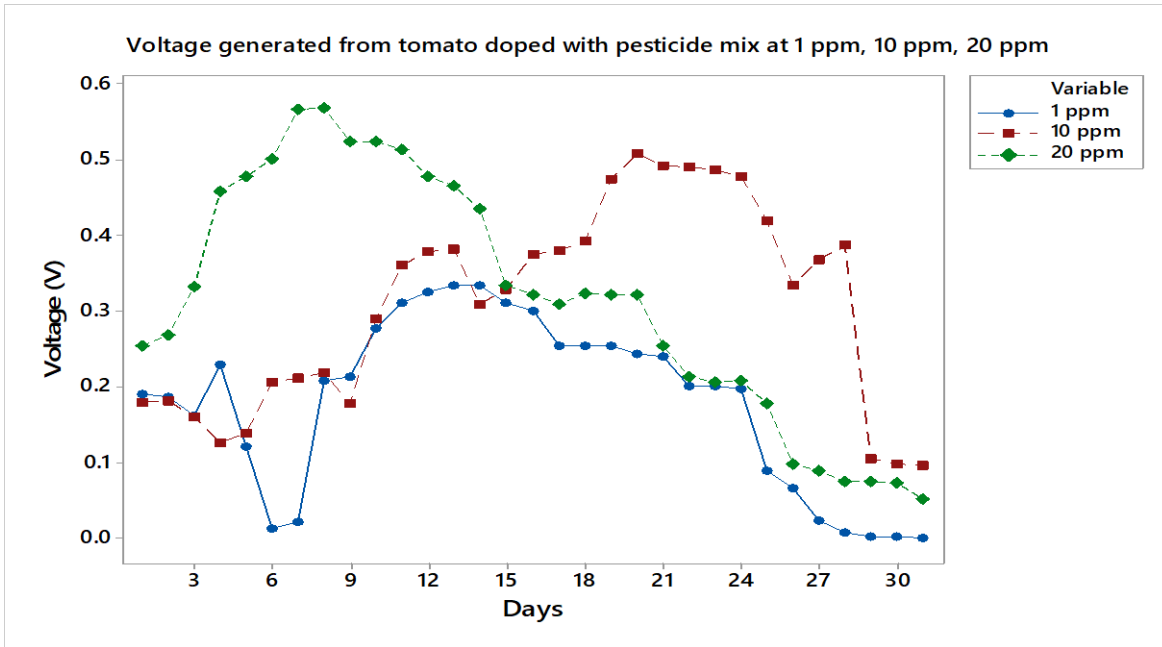


Figure 4.26: Voltage produced by pesticide-contaminated tomato waste

From day 0, the voltage production in the cabbage setup rose in all pesticide concentrations (figure 4.27) with a sudden drop in voltage production on day 6 up till day 15 where an upward trend was, again, observed. On day 11, the voltage at 20 ppm began to rise gradually and did so until day 30, whereas the voltage at the other concentrations fell.

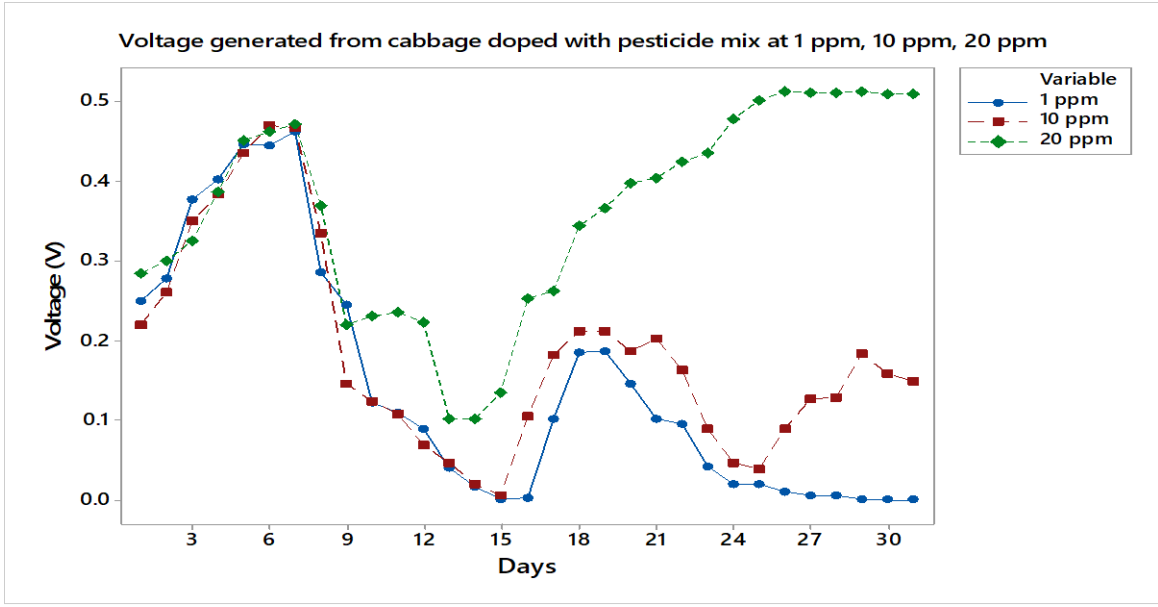


Figure 4.27: the voltage produced by pesticide-doped cabbage.

Figure 4.28 displays the voltage produced by doped rumen fluid at various degrees of doping. In comparison to the 20ppm solution, lower voltage was seen in the 1 ppm and 10 ppm solutions. The voltage generation rate was generally highest with the rumen-doped mixture in the 20ppm setting, which peaked and began to decline on day 14. Except for 10 ppm solution which rose up to day 27.

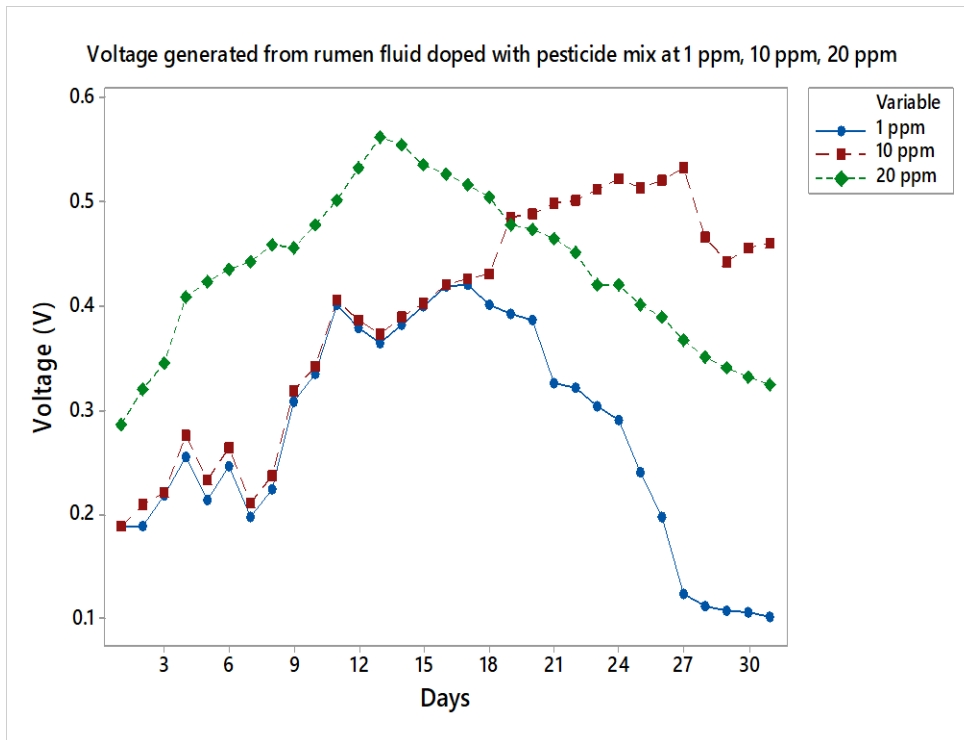


Figure 4.28: Voltage produced by rumen fluid containing varying pesticide combination

In the loam soil doped setup, a steady trend of slowly rising voltage over time was seen. With a minimal carbon source, a 20 ppm arrangement produced the highest voltage, followed by the 10-ppm setup, and finally the 1 ppm setup. For the first 24 days, the 20ppm trend indicated an increasing trend, followed by 24 days of continuous output (figure 4.29). This means the 20-ppm solution provided the most carbon for the microbes, which served as food, translating to higher voltage generation than the other solutions. Mbugua *et al.*, (2020) observed that proximate matter dictated by carbon composition influenced voltage recovery from a substrate. Imwene *et al.*, (2020) also showed that a carbon source is a key parameter in optimization of MFC performance.

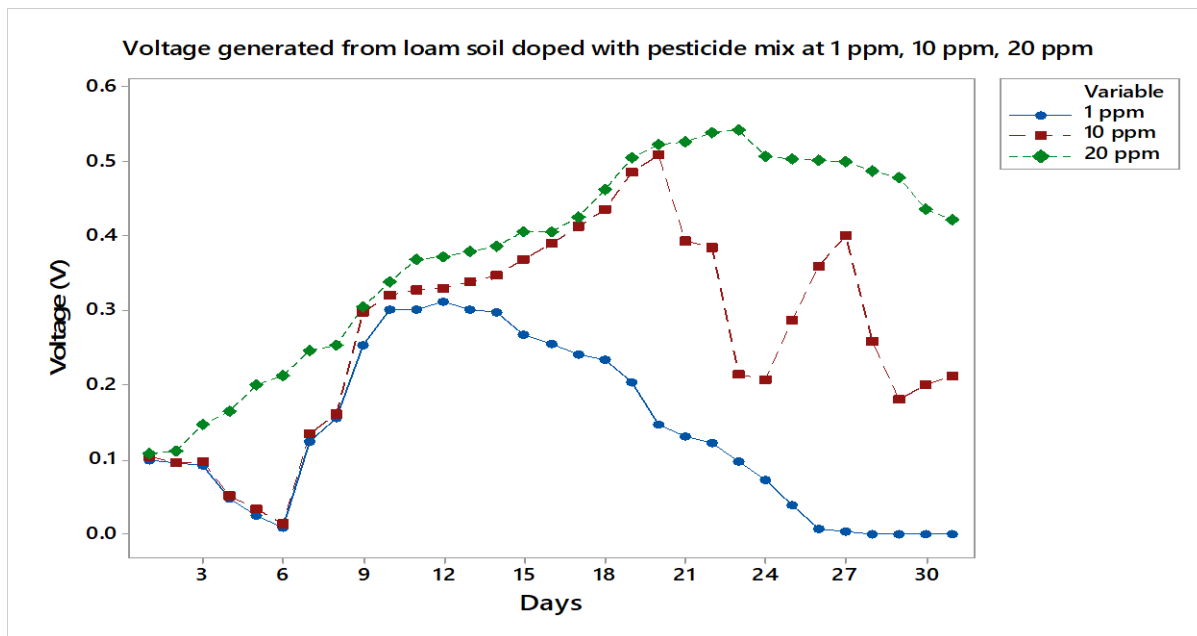


Figure 4.29: Voltage produced by pesticide-infused loam soil

4.7 Bioremediation Studies

This section discusses the three pesticides that were utilized in this study's microbial breakdown in loam soil, cabbage, tomatoes, and rumen matter. To do this, materials were doped with a specified quantity of pesticide, voltage and current generation from setups were observed, and the residual pesticides were examined after a predetermined retention period.

4.7.1 Concentration studies

Concentration experiments entailed utilizing GC-MS to scan various pesticide concentrations and measure the peak area so as to investigate the leftover insecticide sample after a specified retention time. The calibration graphs were drawn from figure 4.28, which represents a GC-MS chromatogram for standard pesticides

The prepared concentrations were separated into two sets, high (greater than 1 ppm) and low (less than 0.5 ppm), in order to observe whether or not they complied with Beer's Law. Figures 4.30-4.33 for malathion,

lambda-cyhalothrin, and chlorpyrifos, respectively, illustrate the resulting calibration curves which were henceforth used for concentration studies in various setups.

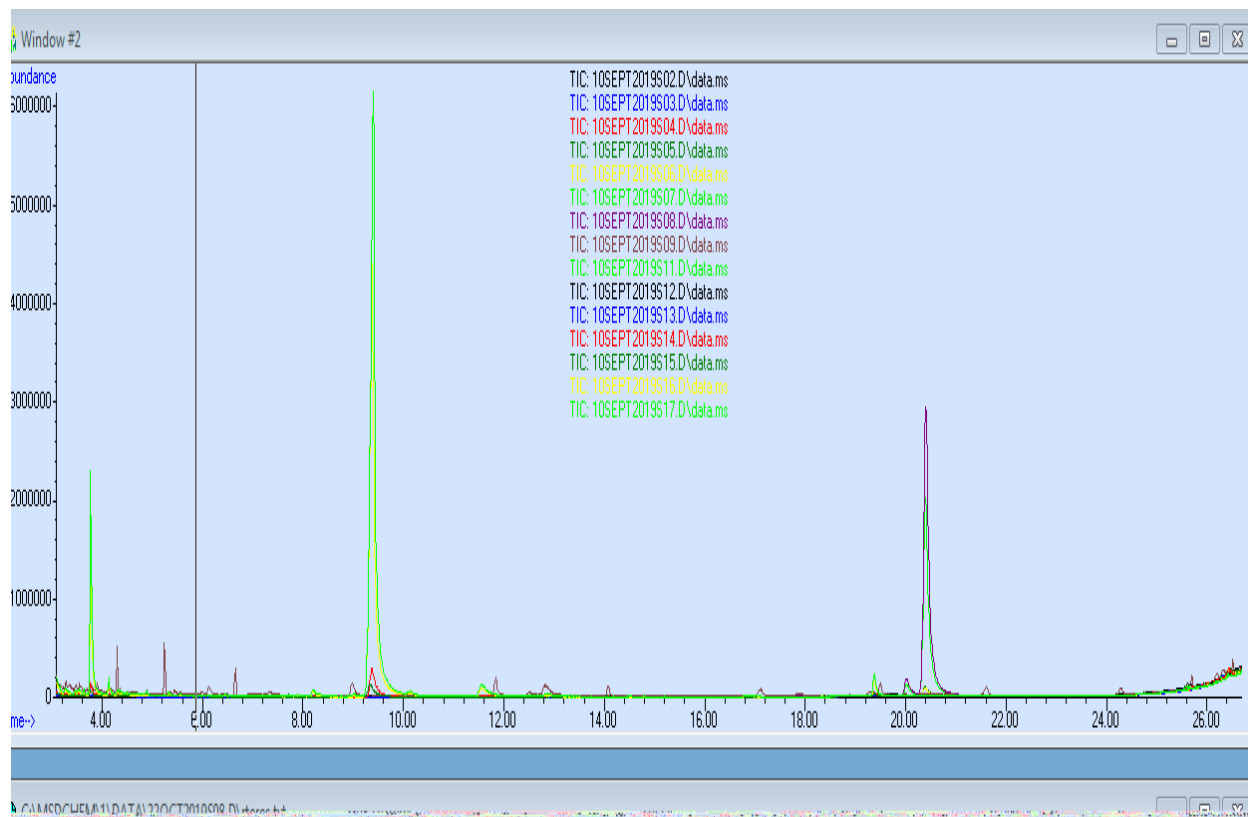


Figure 4.30: A GC-MS chromatogram for standard pesticides.

The resulting calibration curves are as shown in figures 4.31, 4.32 and 4.33 below for malathion lambda cyhalothrin and chlorpyrifos respectively.

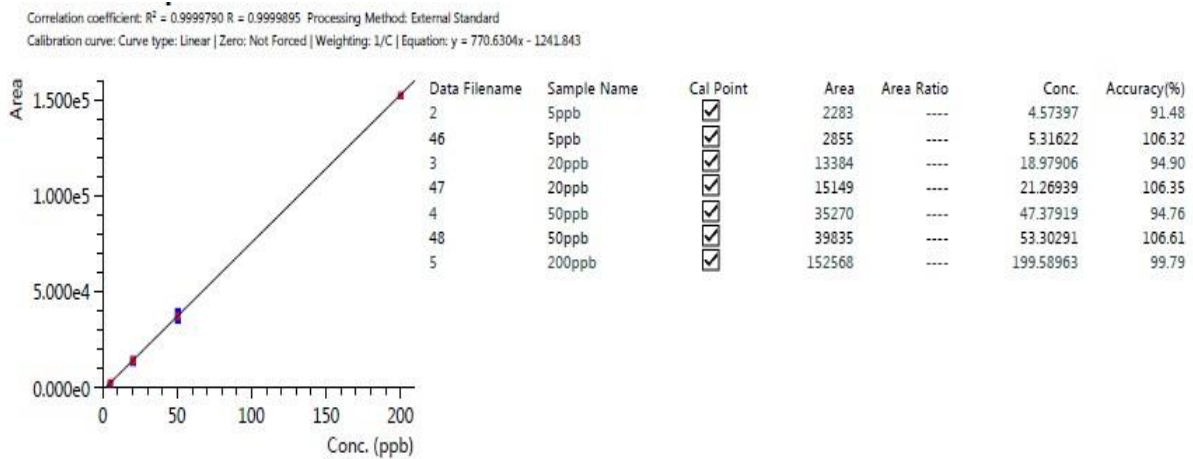


Figure 4.31: Malathion calibration curve

ID49: **lambda-Cyhalothrin**

Correlation coefficient: $R^2 = 0.9999112$ $R = 0.9999556$ Processing Method: External Standard
 Calibration curve: Curve type: Linear | Zero: Not Forced | Weighting: 1/C | Equation: $y = 1647.827x - 1302.635$

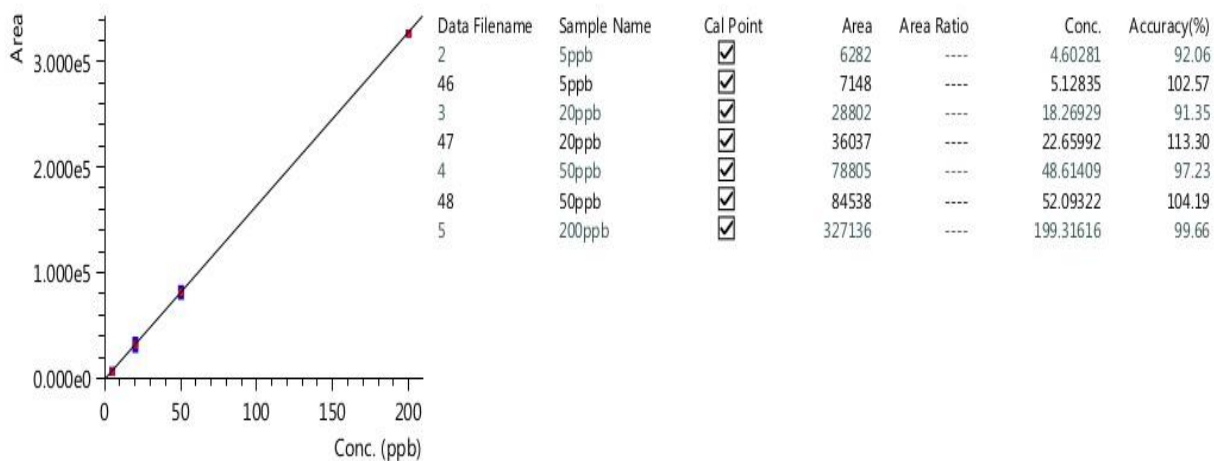


Figure 4.32: Lambda cyhalothrin calibration curve

ID61: Chlorpyrifos-methyl

Correlation coefficient: $R^2 = 0.9998935$ $R = 0.9999468$ Processing Method: External Standard

Calibration curve: Curve type: Linear | Zero: Not Forced | Weighting: 1/C | Equation: $y = 756.7909x - 1766.377$

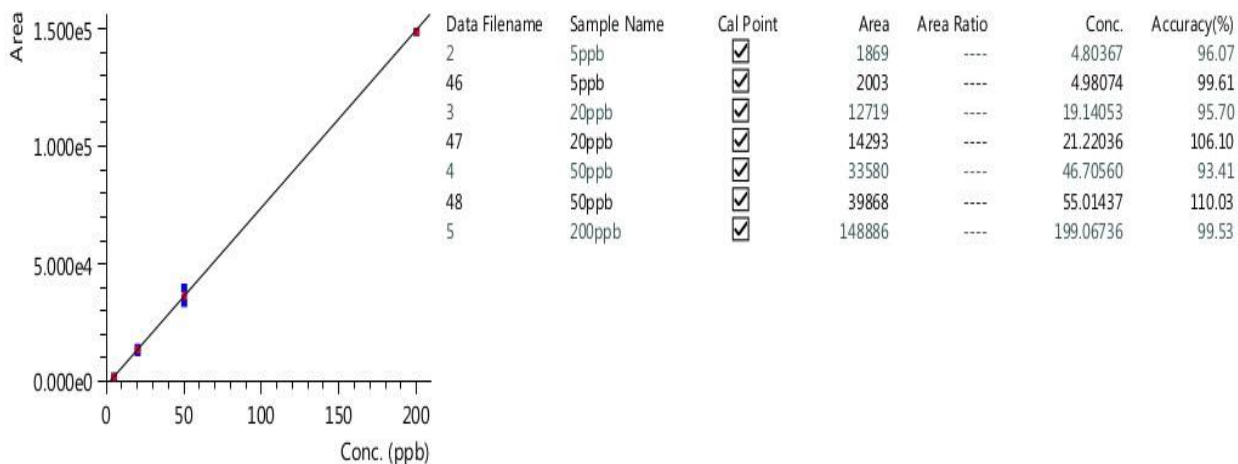


Figure 4.33: Chlorpyrifos calibration curve

Appendices 2, 3, and 4 provide the calibration curves at high concentrations that were utilized to obtain the bioremediation levels in this work. The pesticides elution time and concentration are two examples of the data that were used to plot the calibration curve in the appendix. The concentration of fenpropathrin, which was found in lambda-cyhalothrin in trace amounts, is displayed in the appendix 5.

In the appendix 6, a few chromatograms from the initial works are also included.

4.7.2 Bio-remediation on different matrices

The daily voltage generated and breakdown levels are described for pesticide stock solution treatments on cabbages, tomatoes, loam soil, and rumen fluid. The highest voltage values that could be achieved via doping the rumen fluid were, in descending order, 0.551 V for chlorpyrifos, 0.545 V for lambda-cyhalothrin, 0.538 V for malathion, and 0.533 V for pesticide mix (CLM). From day 0 to day 17, the voltage generated increased steadily until day 31, when the rate slowed and low voltage readings were observed (figure 4.34). The bio-degradation rates of malathion and chlorpyrifos were observed to be

73.40% and 87.70%, respectively, on day 90 of this experiment, whereas lambda cyhalothrin was not detected. This is well displayed in figure 4.35.

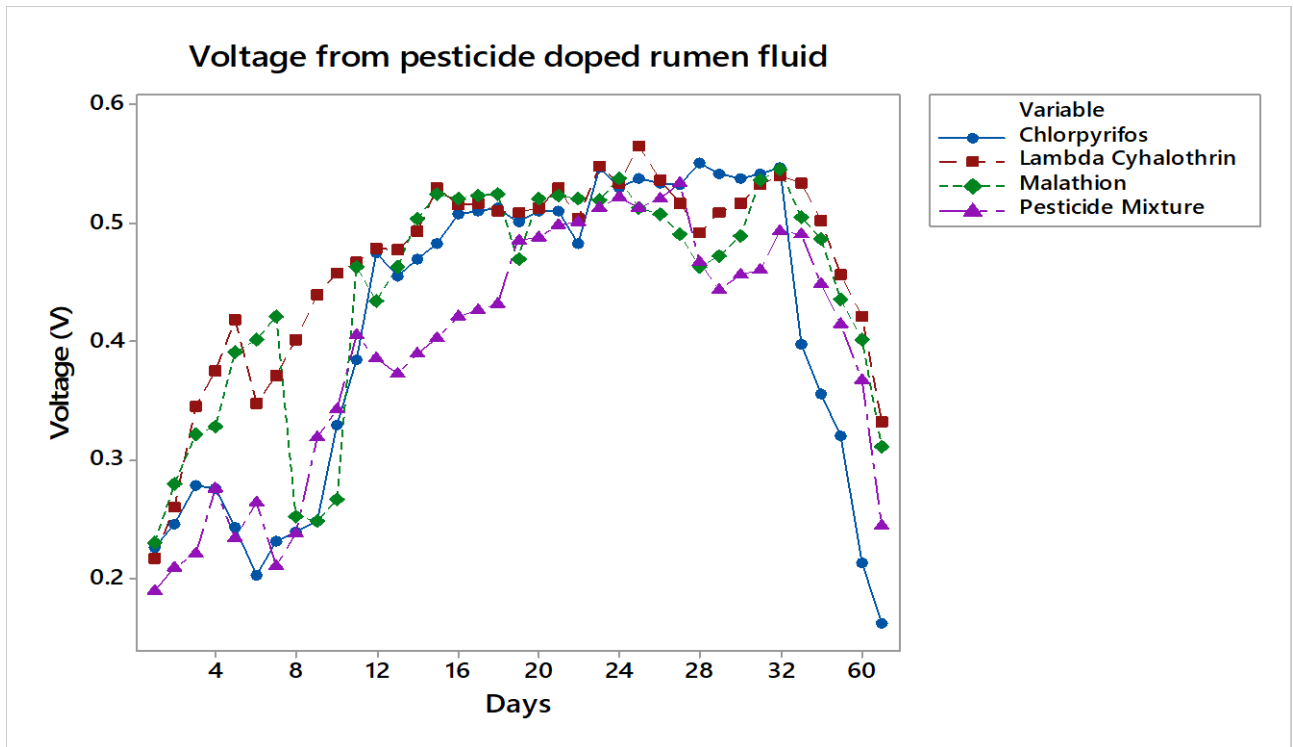


Figure 4.34: Daily voltage produced for cabbage treated with a pesticide mixture, malathion, and chlorpyrifos

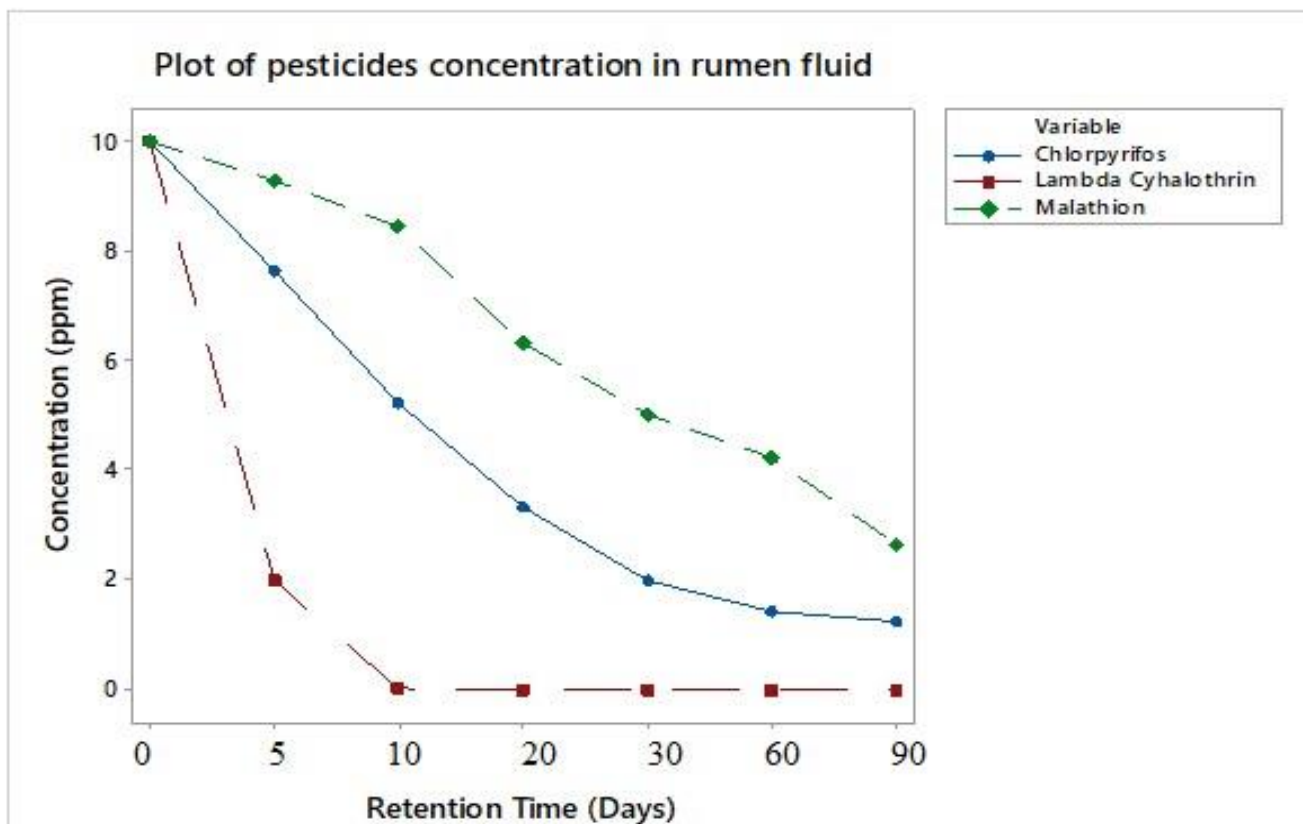


Figure 4.35: The levels of pesticide degradation in rumen fluid.

A convenient way of illustrating the relationship between pesticide concentration's influence on voltage production and retention time in rumen fluid is with 3D graphs. Voltage rises with retention time as shown in Figures 4.36, 4.37, and 4.38, whereas pesticide concentration falls with retention duration.

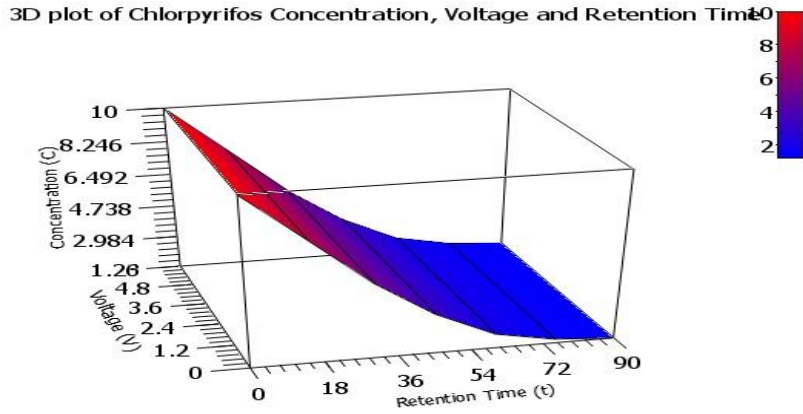


Figure 4.36: A 3D plot of the rumen fluid's chlorpyrifos concentration, voltage, and retention time.

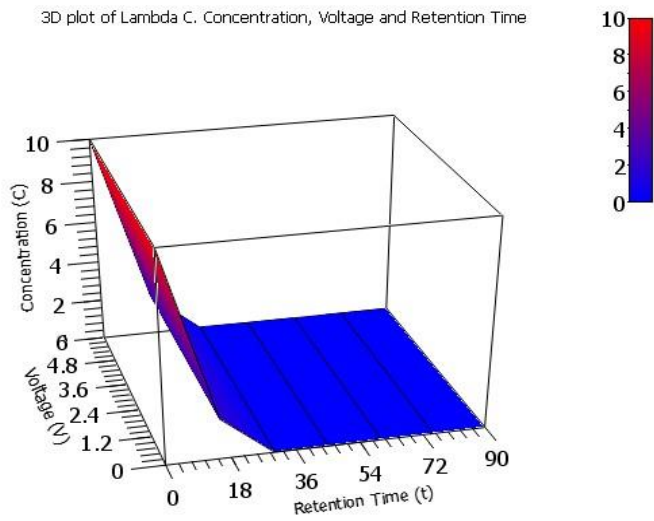


Figure 4.37: A 3D plot of the concentration, voltage, and retention time of lambda-cyhalothrin in rumen fluid

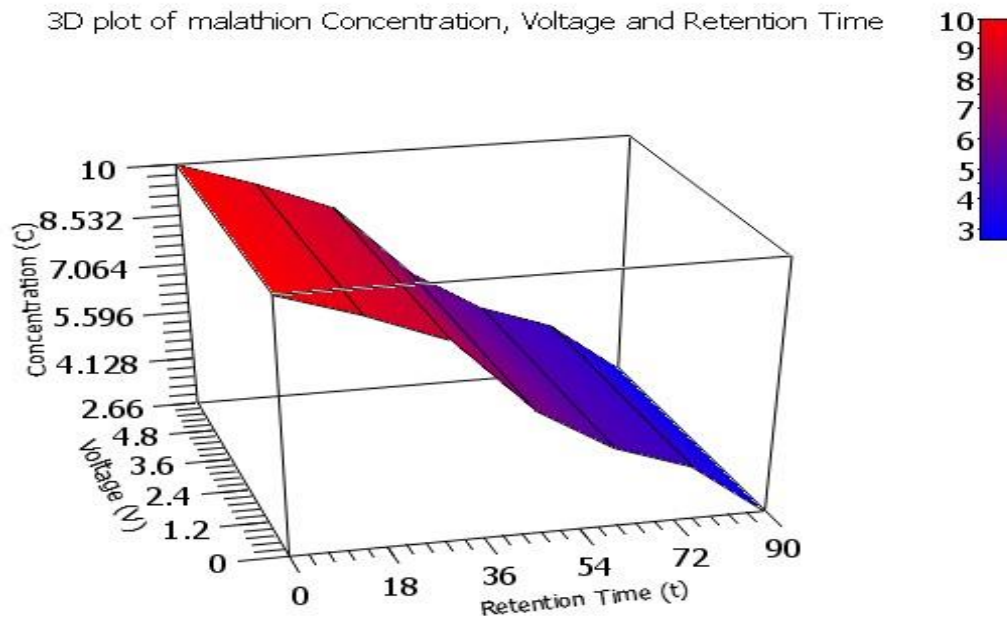


Figure 4.38: 3-D plot of Malathion concentration, voltage, and retention time in rumen fluid.

According to Figure 4.39, all pesticides excluding the pesticide mixture caused an increase in voltage generation from treated tomato fruits from day 0 to day 5. After three days of a decreasing trend, there was a rise in voltage that persisted up to day 31. The highest voltage produced in the degradation of the pesticides is as follows: for chlorpyrifos, 0.582 V for lambda-cyhalothrin, 0.336 V for malathion, and 0.509 V for pesticide mixture. As indicated in figure 4.39, the observed degradation levels at the time were 75.60% and 80.10% for malathion and chlorpyrifos, correspondingly, with extremely low levels for lambda-cyhalothrin.

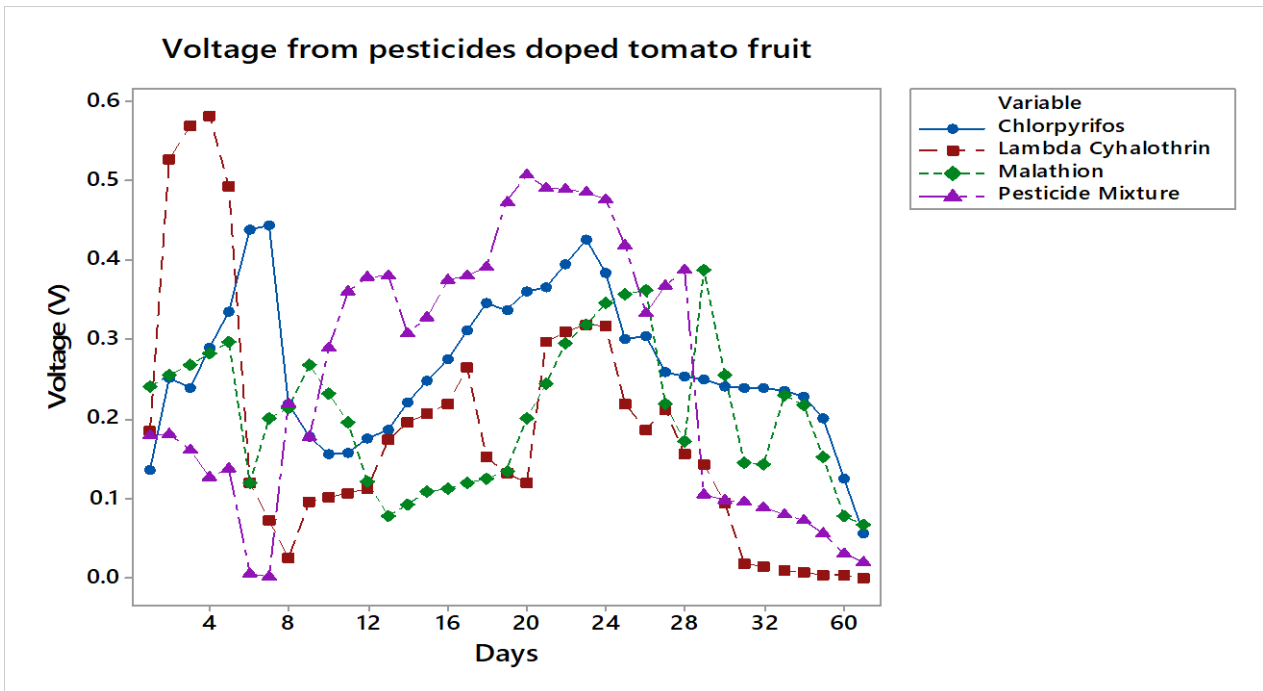


Figure 4.39: Pesticide mixture, chlorpyrifos, lambda cyhalothrin, and daily voltage-generated tomato

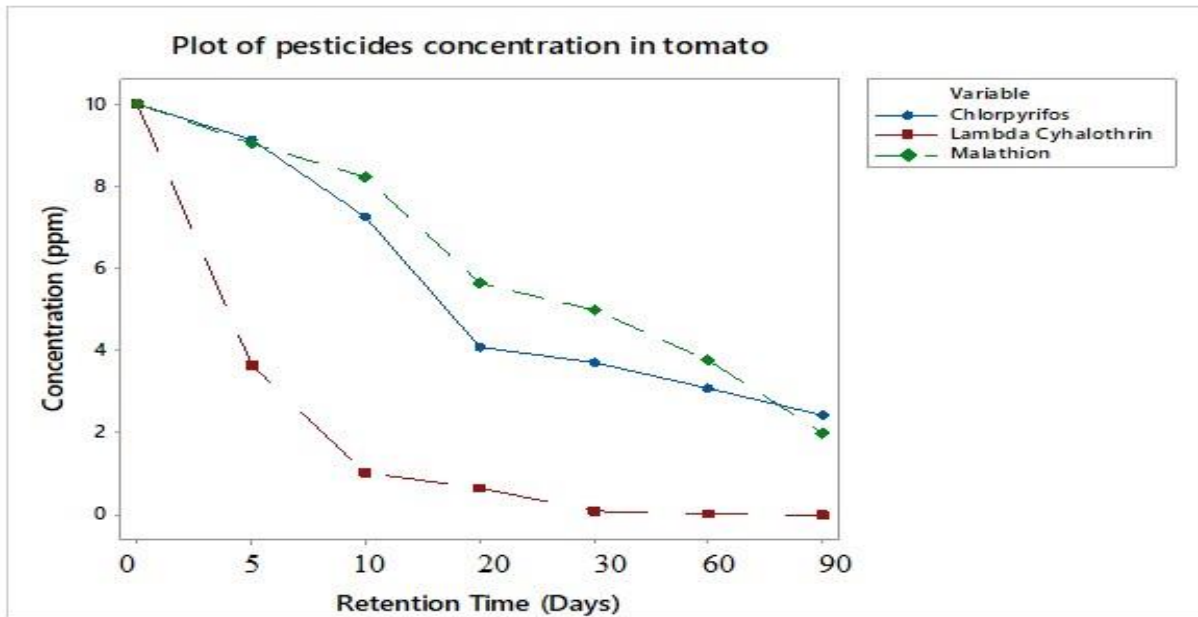


Figure 4.40: The degradation levels from pesticide-treated tomato fruits.

Figures 4.41–4.43 display the 3D plot of pesticide concentration and voltage with retention time in tomatoes.

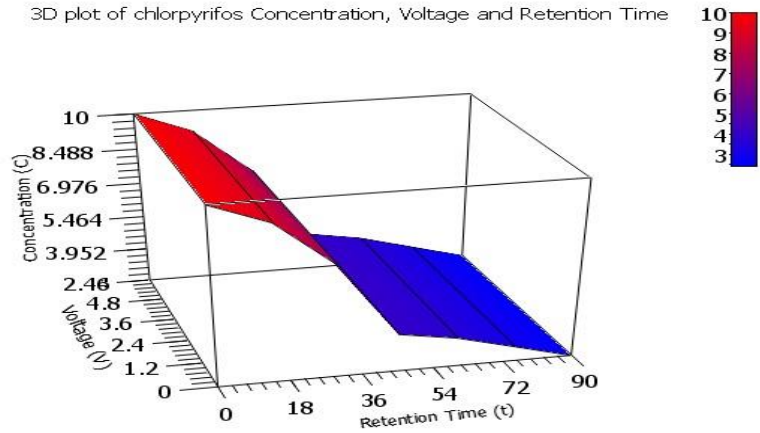


Figure 4.41: Displays a 3D plot of the concentration, voltage, and retention time of chlorpyrifos in tomato.

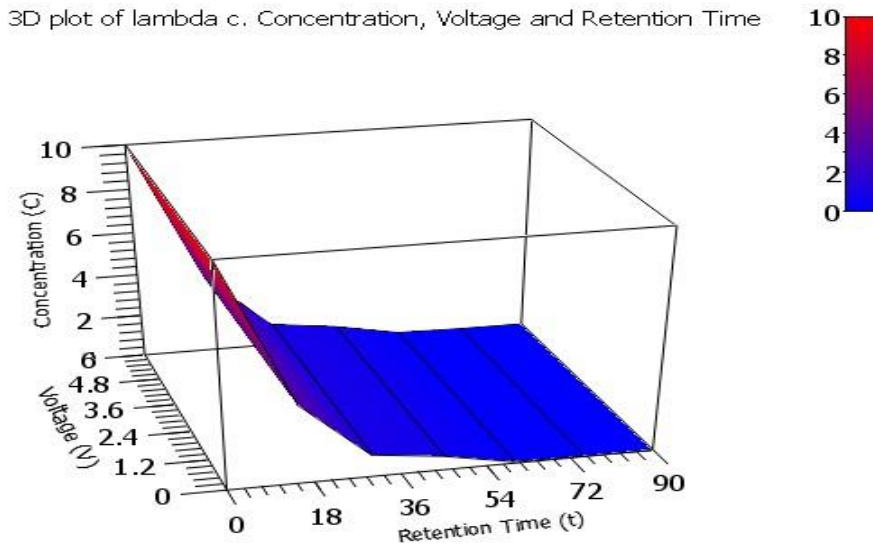


Figure 4.42: shows the concentration, voltage, and retention time of lambda-cyhalothrin in a tomato in a 3D plot

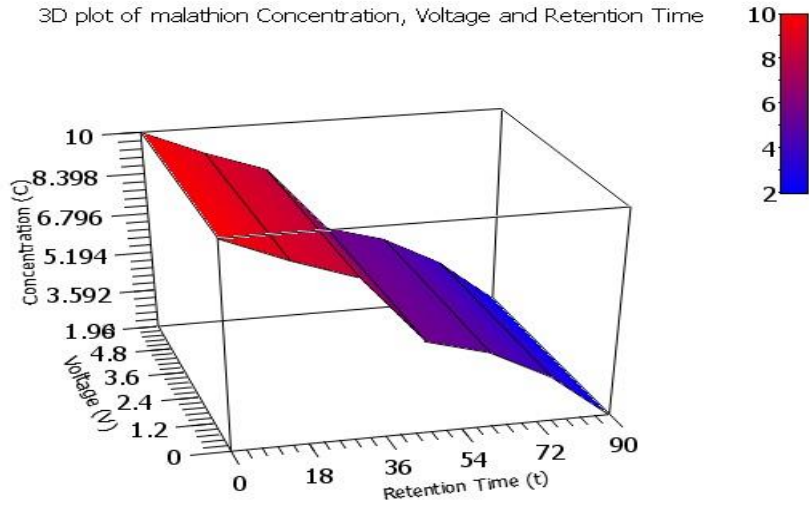


Figure 4.43: shows the concentration, voltage, and retention time of malathion in a tomato in a 3D plot.

The voltage produced from the dual chamber MFC (figure 4.44) increased from day 0 to day 5 for all the pesticides, including the pesticide mixture, when tomato was contaminated with the pesticide residues. From that point forward, a falling trend persisted up to day 15, after which an upward tendency persisted for five days before a constant voltage was noticed.

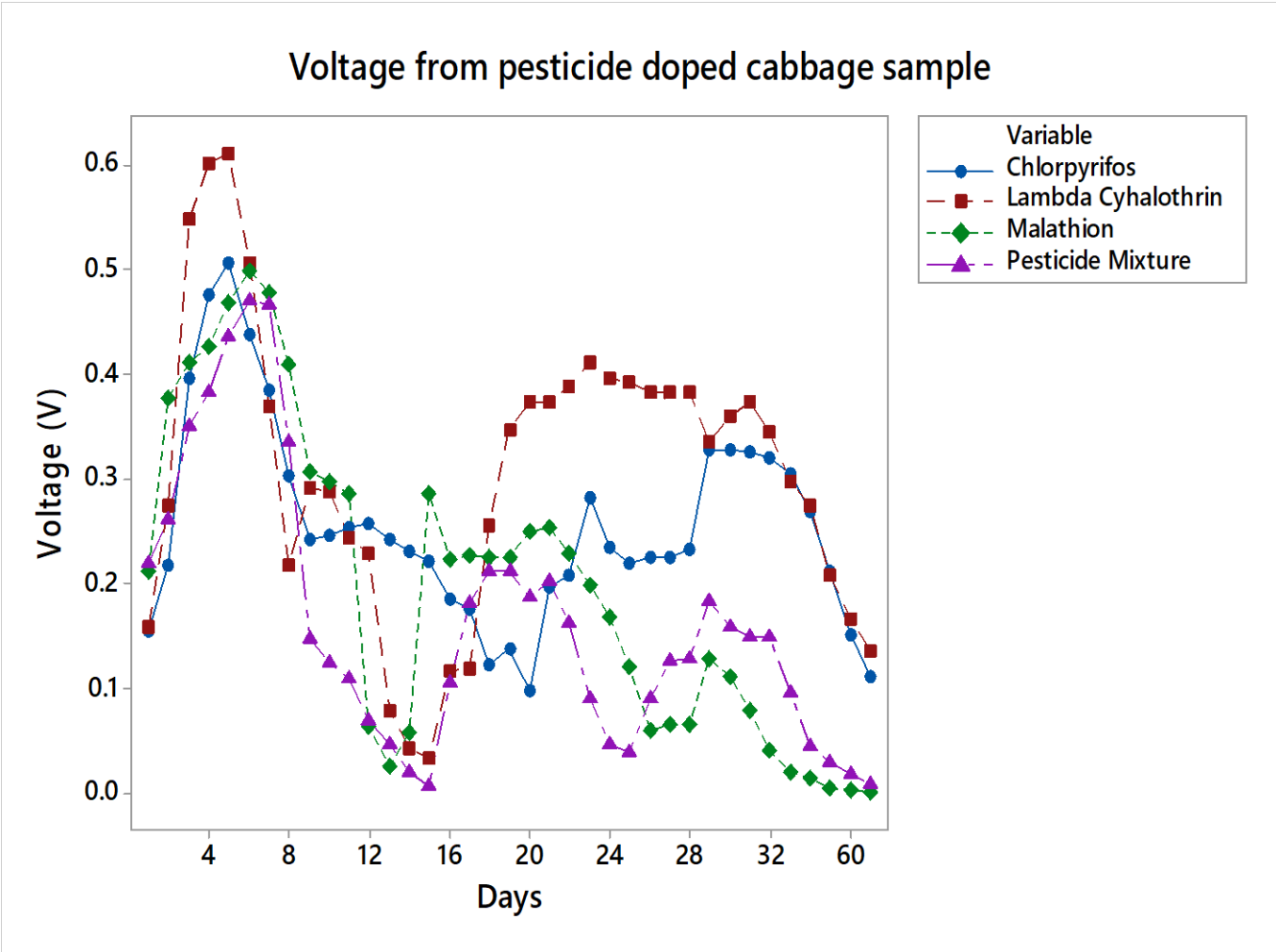


Figure 4.44: A daily voltage-generated of pesticide mixture -doped cabbage

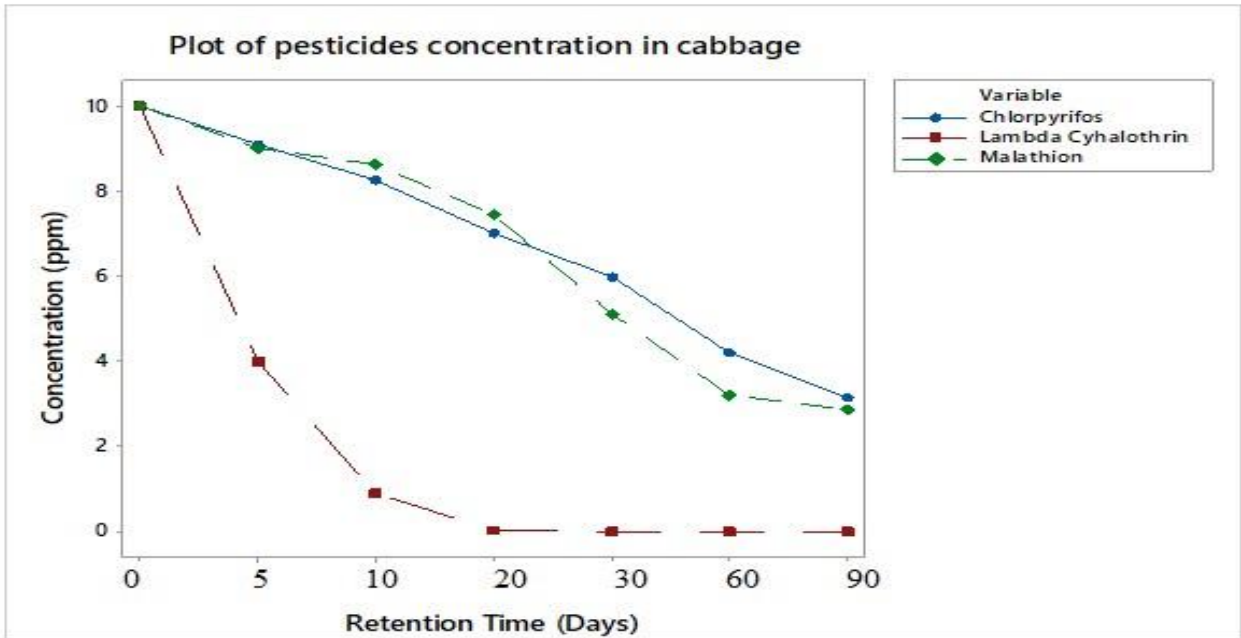


Figure 4.45: Pesticide-infused cabbage daily voltage and degradation levels

Figures 4.46-4.48 display the 3D plot of the concentration, voltage, and retention duration of pesticides in cabbage.

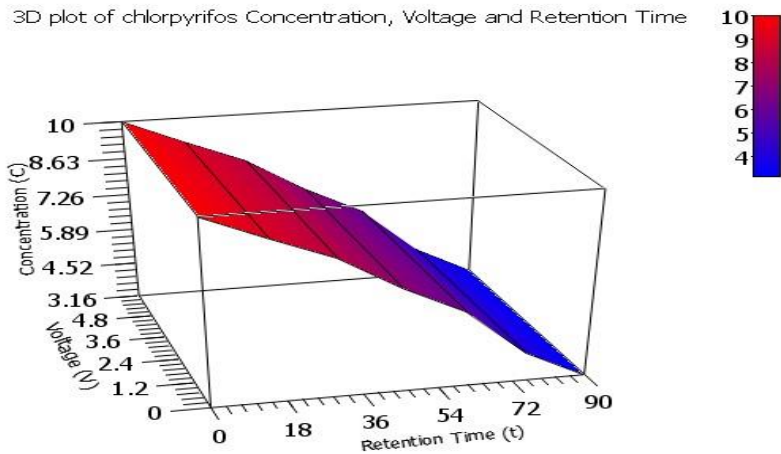


Figure 4.46: shows a 3D plot of the voltage, retention time, and Chlorpyrifos concentration in cabbage.

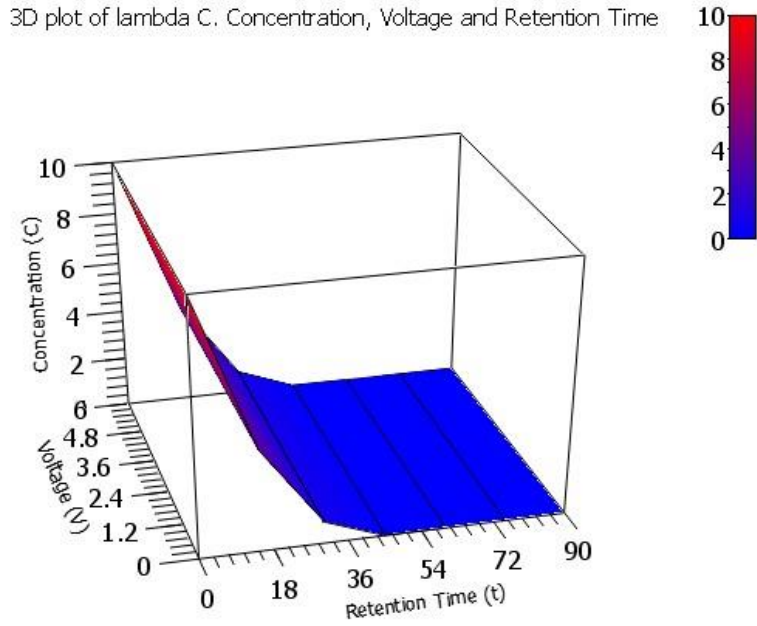


Figure 4.47: shows a 3D plot of the concentration, voltage, and retention time of lambda-cyhalothrin in cabbage

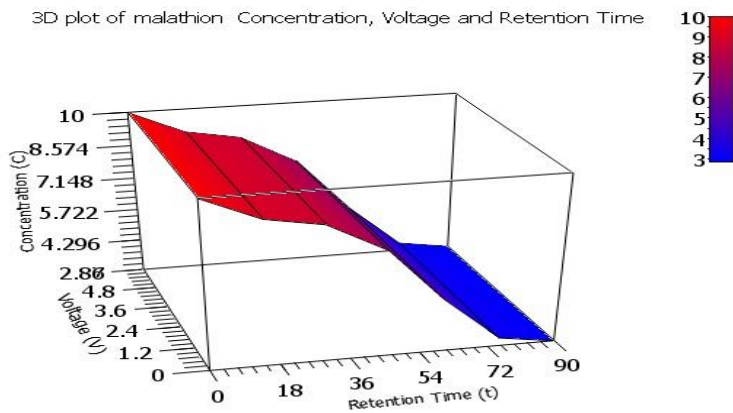


Figure 4.48: Malathion concentration, voltage, and retention time in cabbage are depicted in a 3D plot Malathion and chlorpyrifos had bio-remediation levels of 65.80% and 71.32%, respectively, and there was no detectable lambda-cyhalothrin after day 60 of the investigation (figure 4.49). From day 0 to day 15 for lambda-cyhalothrin

and malathion and from day 0 to day 20 for the chlorpyrifos lambda cyhalothrin and malathion mixture, the voltage produced by the herbicide loam soil increased over time. Thereafter, constant values were noted for three days with subsequent steep declines. The greatest voltages created by lambda-cyhalothrin, malathion, chlorpyrifos, and MCL were 0.537 V, 0.571 V, 0.572 V, and 0.509 V, respectively.

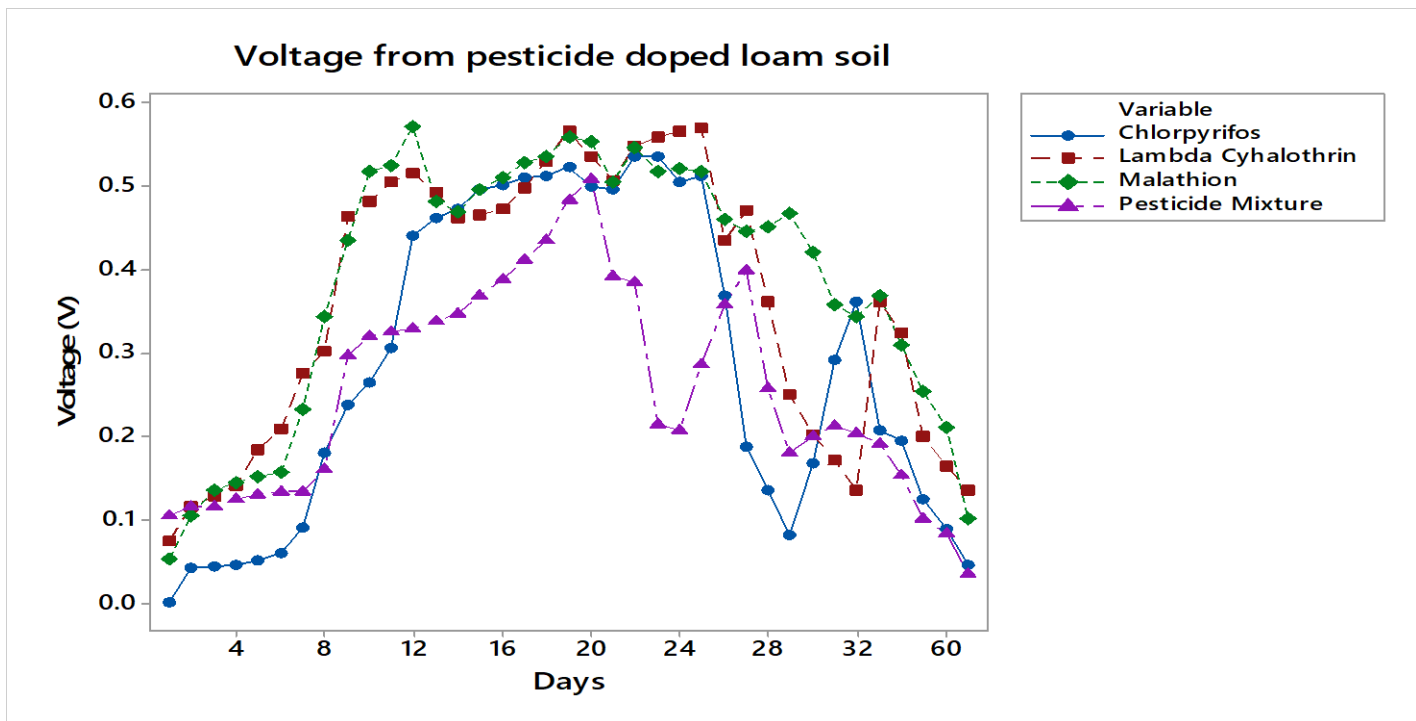


Figure 4.49: A pesticide mixture, chlorpyrifos, lambda cyhalothrin, and daily voltage-generated cabbage

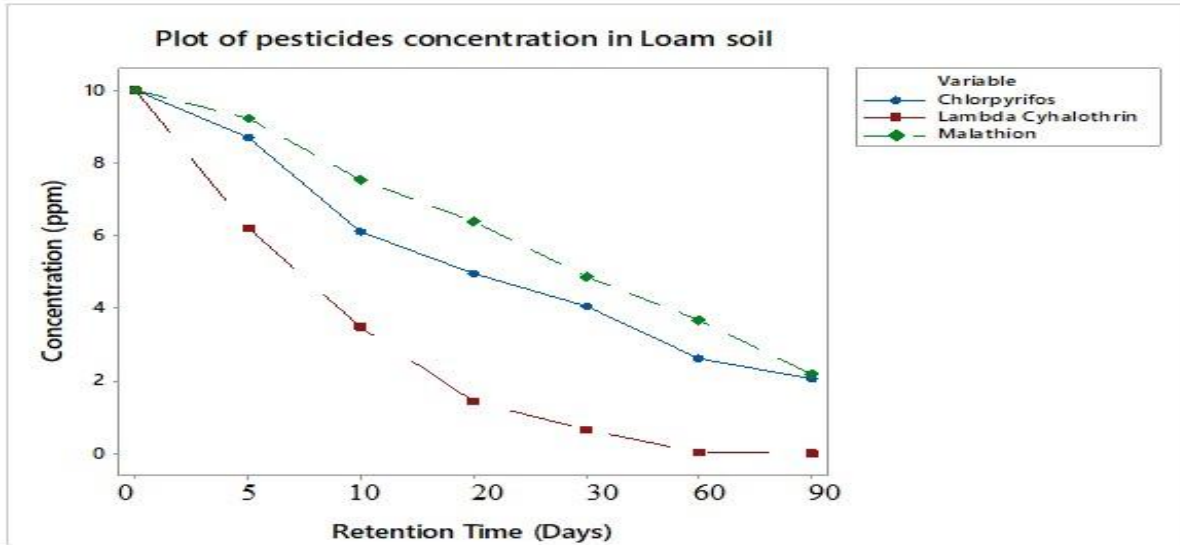


Figure 4.50: Pesticide-infused loam soil daily voltage and degradation levels

The measured degradation rates for malathion, lambda-cyhalothrin, and chlorpyrifos were 79.32%, 99.90%, and 78.20%, respectively, as shown in Figure 4.50. The 3D plot of pesticide content, voltage, and residence time in loam soil is shown in Figures 4.51 to 4.53.

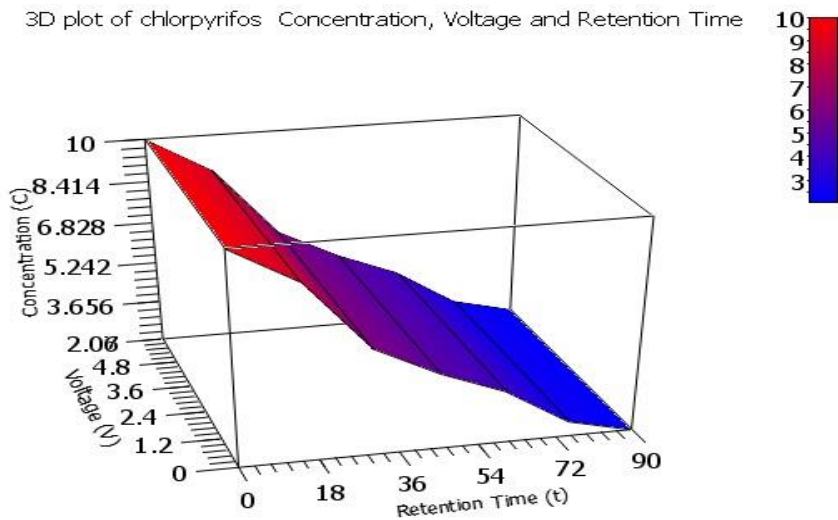


Figure 4.51: A 3D plot of the concentration, voltage, and retention time of chlorpyrifos in a loam soil.

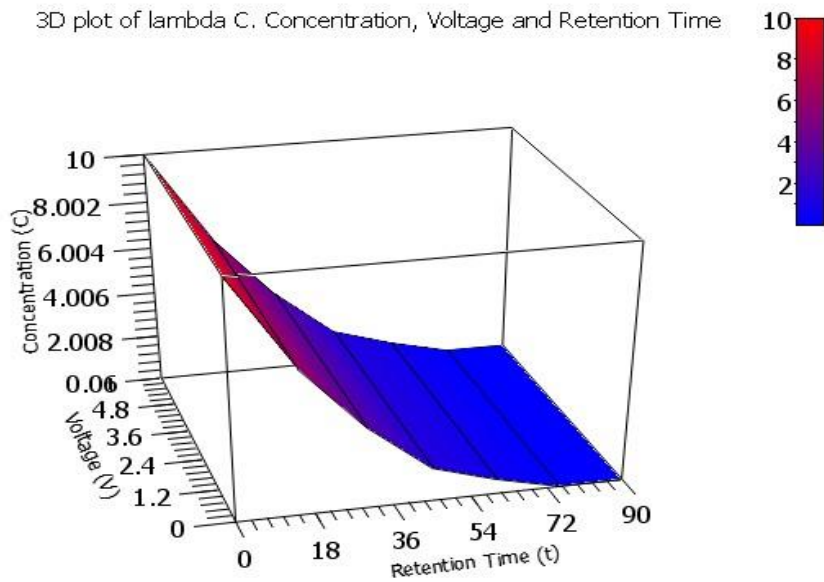


Figure 4.52: A 3D plot of the concentration, voltage, and retention time of lambda-cyhalothrin in loam soil.

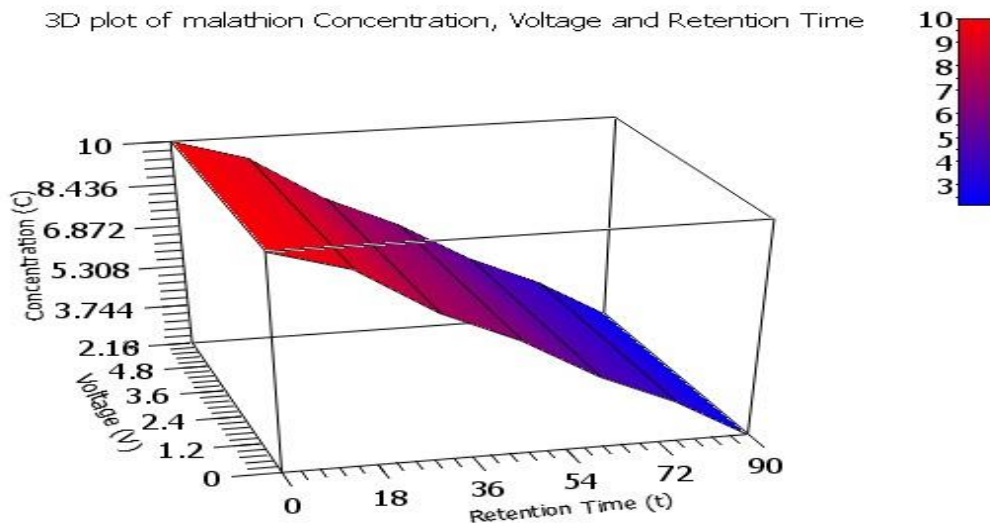


Figure 4.53: A 3D plot of concentration, voltage, and retention time for malathion-doped loam soil.

4.8 Discussion on Degradation Data

In an investigation of voltage generation from market wastes, Mbugua *et al.* (2020) reported that the highest voltage from tomato waste was 0.702 V on day 20 and 0.396 V from cabbage wastes inoculated with rumen fluid. These findings are consistent with the voltage range of 0.354 to 0.769 V attained in this study. Mbugua *et al.* (2020) reported that the proximal characteristics of substrates had an impact on how current and voltage are generated in a microbial fuel cell (Mbugua et al., 2020). In Figure 4.54, the pathway of chlorpyrifos degradation is shown.

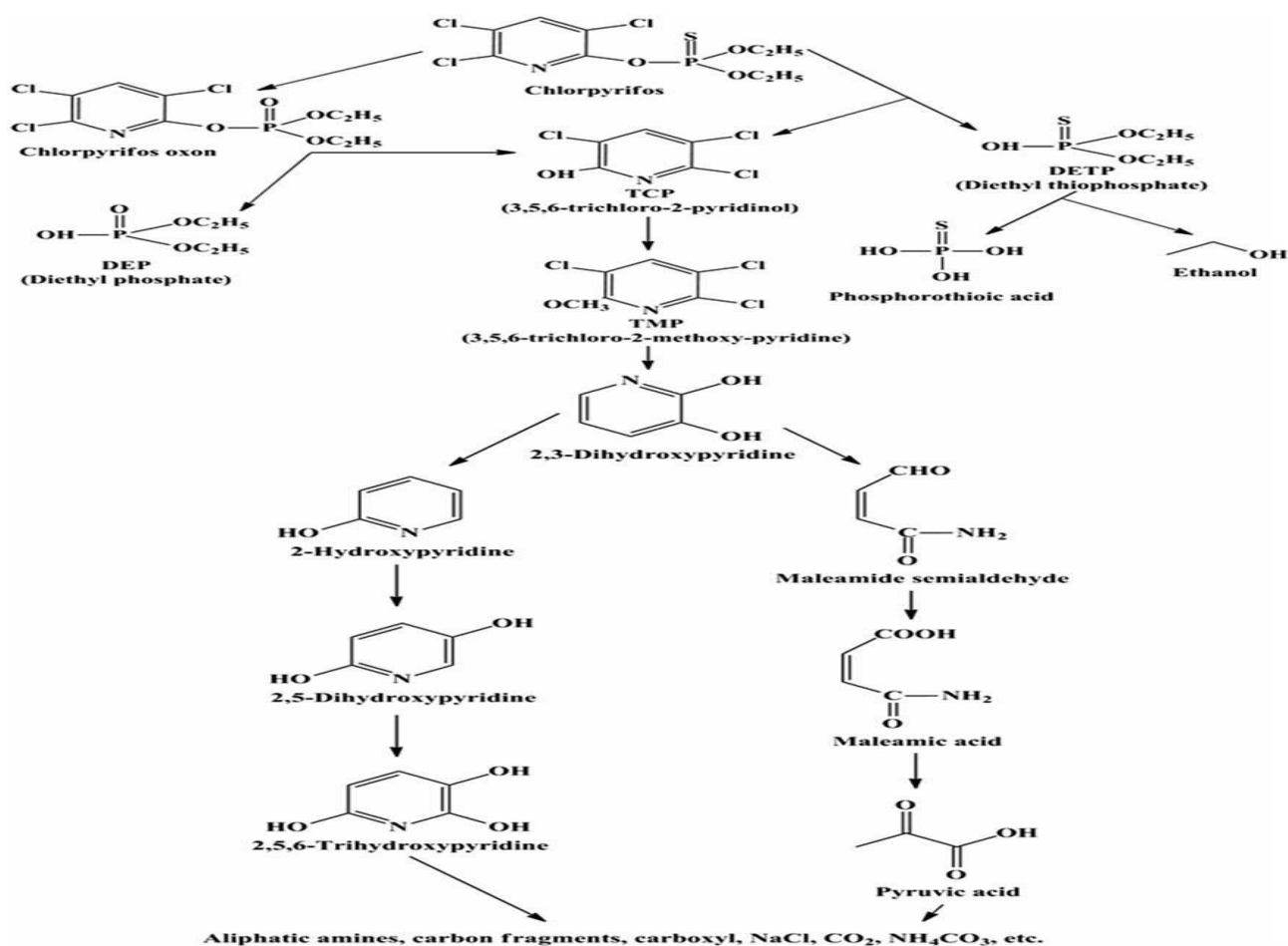


Figure 4.54: The general Chlorpyrifos breakdown mechanism (Singh, 2009; Singh & Walker, 2006; Reddy et al., 2013).

The proposed degradation pathway for malathion is illustrated in figure 4.55 below.

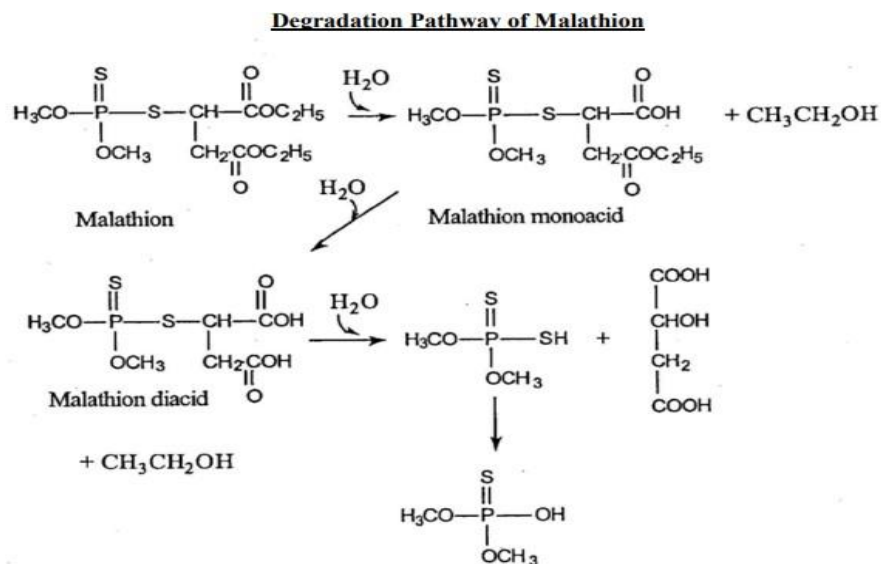


Figure 4.55: Malathion (2-(dimethoxyphosphinothioylthio) decomposition pathway (Mulla et al. 1981)

Lambda cyhalothrin is a pyrethroid and its decomposition pathway is proposed in figure 4.56 below.

The end product from its decomposition is proposed to be phenol.

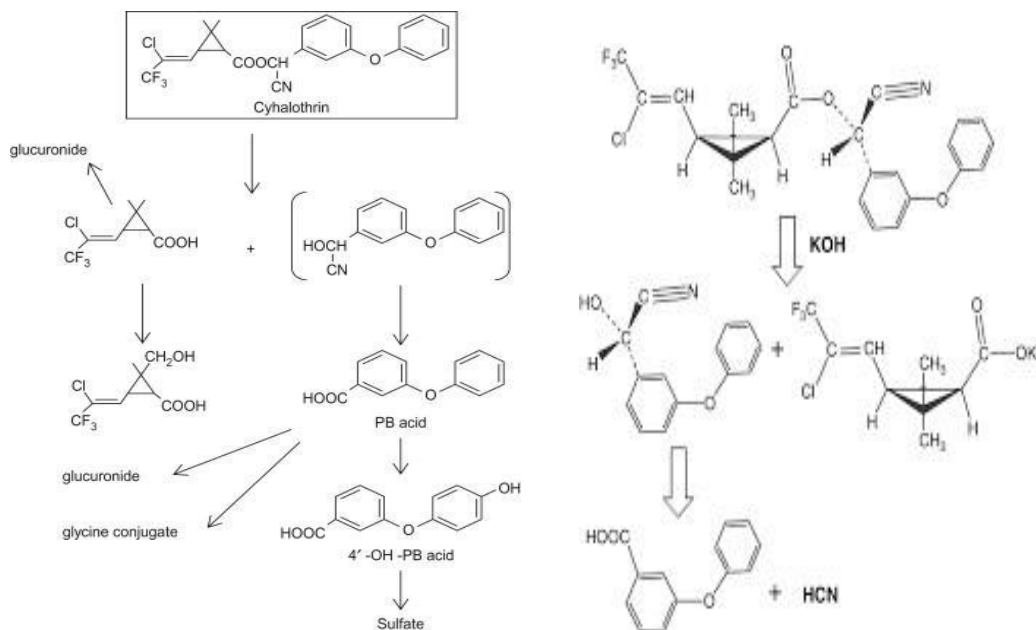


Figure 4.56: Lambda cyhalothrin degradation pathway. (Zining Ci *et al.* 1980)

It's worth noting that independent research by Istiqomah *et al.* (2021) found four isolates in a different study that could tolerate the highest exposure to pesticides (90 ppm) in the 10⁵-colony forming unit (Cfu) level Bacterial adaptability to pesticides that leads to pesticide resistance. Possible explanations include the development of biofilms, induced mutations, horizontal or vertical genetic transformation via plasmids or transposons, and increased production of certain hydrolytic enzymes (Alav *et al.*, 2018).

4.9 Modeling kinetics of voltage

Monod, Haldane Andrew's Kinetic and Han-Lavenspiel Models were used to explain and demonstrate the how microorganism's growth rate is related to voltage and current production .

4.9.1 Anode respiration Kinetic parameter estimation

Here the existing inhibitory growth models and bio-kinetic parameters are used to model microorganisms' growth

4.9.1.1 Bacterial development

Since the unstructured and unsegregated phenomenon in the cell is explained by the Monod model (Equation 4.0), the model was utilized to establish the kinetic parameters for bacterial growth in the batch MFC. The growth rate coefficient μ , half-saturation coefficient (K_s), and maximum growth rate (μ_{max}) of bacteria in the various fruit waste-fed MFC were assessed after 408 hours (17 days) of microbial activity (4.0 to 4.3 as per chapter 3 procedures).

Monod Classical:

$$r = \frac{r_{max} * S}{K_s + S} \dots \dots \dots 4.0$$

$$(K_s + S)$$

Taking the reciprocal of Monod Equation: ($y = MX + c$)

$$\frac{1}{S \mu_{max}} = \frac{K_s + S}{\mu_{max} S} = \left(\frac{K_s}{\mu_{max} S}\right) + \left(\frac{1}{\mu_{max}}\right) \dots \dots \dots 4.1 \mu_{max} * S \mu_{max}$$

$$\mu = \frac{\text{amount of biomass produced}}{\text{time taken}} \dots \dots \dots 4.2$$

$$\mu_{max} = \frac{\text{amount of biomass produced}}{\text{initial biomass} \times \text{time taken}} \dots \dots \dots 4.3$$

Taking an example of tomato fruit, the maximum voltage produced = 456 mV, and time taken = 504 hours (21 days)

$\mu = 0.001$ obtained from manual calculation using equations 4.0 to 4.3.

Specific growth rate (μ) = $0.001 h^{-1}$ $\mu_{max} = 0.000003 h^{-1}$

Optimal growth rate ($\mu|_{max}$) = $0.003 h^{-1}$ Using Monod equation: (K_s)-half-saturation coefficient for tomato fruit was calculated:

$$\frac{1}{\mu_{max} S} = \frac{K_s + S}{\mu_{max} S} = \left(\frac{K_s}{\mu_{max} S}\right) + \left(\frac{1}{\mu_{max}}\right) \dots \dots \dots 4.4 \mu_{max} * S$$

$$K_s = 366.90 \pm 0.03 \text{ mgL}^{-1}$$

The same equations (4.0 - 4.3) above were used to compute and summarize the half-saturation coefficient (K_s), growth yield coefficient (μ) and maximum growth rate (μ_{max}) findings for the substrate samples used in this experiment (Table 4.7).

Values for the maximum growth rate, growth yield coefficient, and half-saturation coefficient for MFCs fed with vegetable waste are shown in Figure 4.39.

Monod Model

Table 4.8: Maximum growth rate, growth yield coefficient, and half-saturation coefficient

No	Sample	μ	μ_{max}	K_s
1	SOIL	0.00111h ⁻¹	0.000003h ⁻¹	330.0 gL ⁻¹
2	CABBAGE	0.001h ⁻¹	0.000003h ⁻¹	366.7 gL ⁻¹
3	TOMATO	0.011h ⁻¹	0.000003h ⁻¹	366.9 gL ⁻¹
4	RUMEN	0.001h ⁻¹	0.000003h ⁻¹	353.6 gL ⁻¹

The results of this investigation show that tomato fruit had the highest growth yield of 0.011h⁻¹ and the highest half-saturation coefficient of 366.9.660±.03 mgL⁻¹. This is because tomato samples had more readily available carbon sources than the other samples. The loam soil sample produced the lowest growth yield coefficient of 0.001 h⁻¹, both of which can be attributed to competitive reactions among the substrates that slowed the degradation of the substrate. Nasrollahzadeh *et al.* (2010) found that at high substrate concentrations, the harmful effects of other vegetables prevented the degradation process from occurring. Restricting the bioavailability of a residue will therefore increase the pattern of degradation by decreasing microbial substrate's access or slow down degradation by reducing the cytotoxic effects of contaminants on microorganisms. According to Chai *et al.* (2021), the

physiological responses of bacteria to substrate concentration levels are the main focus of the kinetics of a self-inhibitive residue. This study has theoretically examined the function and links between self-inhibition and mass transfer limitations using numerical solutions, yielding a straightforward model that may be helpful in reality. For example, small changes in the concentration level of a substrate in the vicinity of a microbial cell can trigger the physiological response of the cell in form of changes in its metabolic activity, such as specific growth rate, consumption rate, respiration rate or chemo taxis. It is assumed that the increasing of substrate concentration would promote biodegradation activity, two additional mechanisms may intervene this is the inhibitory effect of substrate at high concentrations and the substrate bioavailability. Some environmental factors can limit the physical accessibility of substrate to the cells and thus directly influence the biodegradation kinetics. Such mass-transfer limitations of substrate access to the microbial cells are generally known as bioavailability limitations and are well-known type and have obvious importance for the metabolic activities of microbes.

Mehdi Gharasoo (2014) did state that, Self-inhibition and mass transfer when considered individually have detrimental effects on decomposition. However, when they are combined, they accelerate the overall degradation dynamics and reduce the effects of pollutant toxicity on microorganisms, which in turn boosts the rate of deterioration over a concentration gradient.

The Monod model does not account for the impact of self-inhibition; it simply explains microbial proliferation and activity. In order to track substrate consumption, measure bacterial growth, and calculate the kinetic parameters of substrate degradation, this study used additional models, namely the Haldane Andrew's Kinetic and Han-Lavenspiel Models.

4.9.1.2 Substrate self-inhibitory effect

The kinetic model of Haldane Andrew (Equation 3.4) was used to determine the substrate's selfinhibitory effect coefficient (K_{IH}). Applying Equation 4.5 to 4.8 and 3.4 to 3.5, it was realized that substrate self-inhibitory effect was $50.180 \pm 0.04 \text{mgL}^{-1}$ after 408 hours (21 days) of microbial activity, indicating that the inhibitory impact was modest since the K_{IH} value was high.

Haldane Andrew's Kinetic Model

$$r = \frac{\mu_{max} S}{\left(K_S + S + \frac{S^2}{K_{IH}}\right)} \dots \dots \dots (4.5)$$

Taking the reciprocal of Haldane Andrew's Kinetic Equation: we obtain equation 4.6 which is of the form $y = Mx + c$.

S²

$$\frac{1}{r} = \frac{K_S + \mu_{max} K_{IH} + S}{\mu_{max} S} \dots \dots \dots (4.6)$$

Where S is matrix capacity and μ is the microbe growth coefficient. The ideal growth rate (optimal) is maximum (μ_{max}) and K_S is a half-saturation coefficient.

Given: $\mu = 0.82 \text{h}^{-1}$; $\mu_{max} = 0.003 \text{h}^{-1}$; $S = 100 \text{mgL}^{-1}$; $K_S = 99.63 \text{mgL}^{-1}$

The (K_{IH}) - inhibitory effect coefficient for the tomato sample was determined using Haldane Andrew's equation 4.5:

$$K_{IH} = 333.1 \pm 0.04 \text{gL}^{-1}$$

The self-inhibitory effect coefficient (K_{IH}) results for the tomato, loam soil, rumen and cabbage samples were calculated and are reported in table 4.8 below using the same equations (4.5 - 4.8) above.

Table 4.9: Self-inhibitory effect coefficient for all the samples

NUMBER	SAMPLE	(K_{IH})
1	SOIL	333.3 gL ⁻¹
2	CABBAGE	373.7 gL ⁻¹
3	TOMATO	333.1 gL ⁻¹
4	RUMEN	350 gL ⁻¹

In this investigation, the inhibitor coefficient output of the matrices was 333.3gL⁻¹, 373.7 gL⁻¹, 333.1 gL⁻¹ and 350.0 gL⁻¹ in loam soil, cabbage, tomato and rumen matter, respectively. As per the Monod model suggestion, the substrate composition in the different matrices was enough to sustain microbial activity for 21 days retention time.

4.9.1.3 Severe inhibitor concentration

The critical inhibitor concentration factor (S_m) for the substrates was determined using the HanLavenspiel model (Equation 4.6 above). Equations 4.0 to 4.9 were used to calculate the amount of substrate that the microbes were able to break down after 408 hours (17 days) of microbial activity.

This data suggests that after consuming the 100 mgL⁻¹ substrate and the 0.75 mgL⁻¹ substrate that was initially present in the rumen fluid, the chemical reaction completely ceased, production of electrons and protons stopped indicating the death of the microbes and the end of a chemical reaction.

Han-Lavenspiel Model:

$$r = \frac{r_{max} * S}{S + K_S * (1 - S_m)} \dots \dots \dots 4.9$$

Given: $\mu = 0.82h^{-1}$, $\mu_{max} = 0.003h^{-1}$, $S = 100mgL^{-1}$, $K_S = 99.63mgL^{-1}$

The (S_m) - substrate concentration for tomato fruit waste was determined using the Han-Levenspiel equation

$$4.9: S_m = 346.70 \pm 3.67mgL^{-1}$$

Using the same equation (4.9 above, the critical inhibitor concentration coefficient) was calculated from the four matrices as shown in table 4.10 below

Table 4.10: Critical inhibitor concentration coefficient for all the samples

No.	Sample	S _m
1	SOIL	346.8 gL ⁻¹

2	CABBAGE	349.9 gL ⁻¹
3	TOMATO	346.7 gL ⁻¹
4	RUMEN	349.4 gL ⁻¹

It is clear from this study that all the experimental samples in this study were altered at various levels of bio-degradation, that is at a respective unique sample critical inhibitor concentration coefficient. For instance, tomato fruit waste was completely broken down by the bacteria up to a substrate concentration of 346.7 g/L, whereas the initial substrate concentration in the rumen fluid was 349.4 g/L, meaning that the chemical process ceased 5 hours after reaching its peak at 504 hours (21 days). This behavior suggested a competitive inhibition model in which an inhibitor that resembled a substrate bound to the active site of the enzyme had prevented the substrate from binding. When an inhibitor only binds to the enzyme-substrate complex and not the free enzyme, uncompetitive inhibition takes place. As a result, microbial growth slows down, which helps a chemical reaction in an MFC to come to a conclusion. Research by Wang and Wan, (2008) was altered on getting to the critical inhibitor (S_m) and they accounted for different inhibitions using the Han-Lavenspiel model (Chai *et al.*, 2021).

Wu *et al.* (2018) researched on co-metabolic degradation kinetics, microbial growth kinetics and electricity generation capacity in a bacteria strain via MFC. The results show that Haldane and Aiba models suit the growth kinetics of a single substrate MFC with 0.995 correlation coefficient. Moreover, the Haldane model was appropriate to describe the growth kinetics of a single substrate MFC with 0.986 correlation coefficient. The growth kinetics of a mixed substrate MFC can be explained well by

the SKIP model with correlation coefficient 0.995. Second order and three-half order models were found to suitably describe the cyanide degradation process (Wu *et al.*, 2018). The rate of bio-degradation in soil depends on four variables are as follows: (i) Availability of pesticide or metabolite to the microorganisms (ii) Physiological status of the microorganisms (iii) Survival and/or proliferation of pesticide degrading microorganisms at contaminated site (iv) Sustainable population of these microorganisms (Singh, 2008).

4.9.2 Modeling, simulating, and fitting decaying data

The voltage data produced during the bio-remediation of lambda-cyhalothrin, malathion, and chlorpyrifos were modeled using a variety of linear and non-linear plots, including Boltzmann, Gaussian, and Lorentz equations, which are represented by equations 3.18 and 3.19 in chapter 3.

Figure 4.57 displays the voltage generated against time in days series plot.

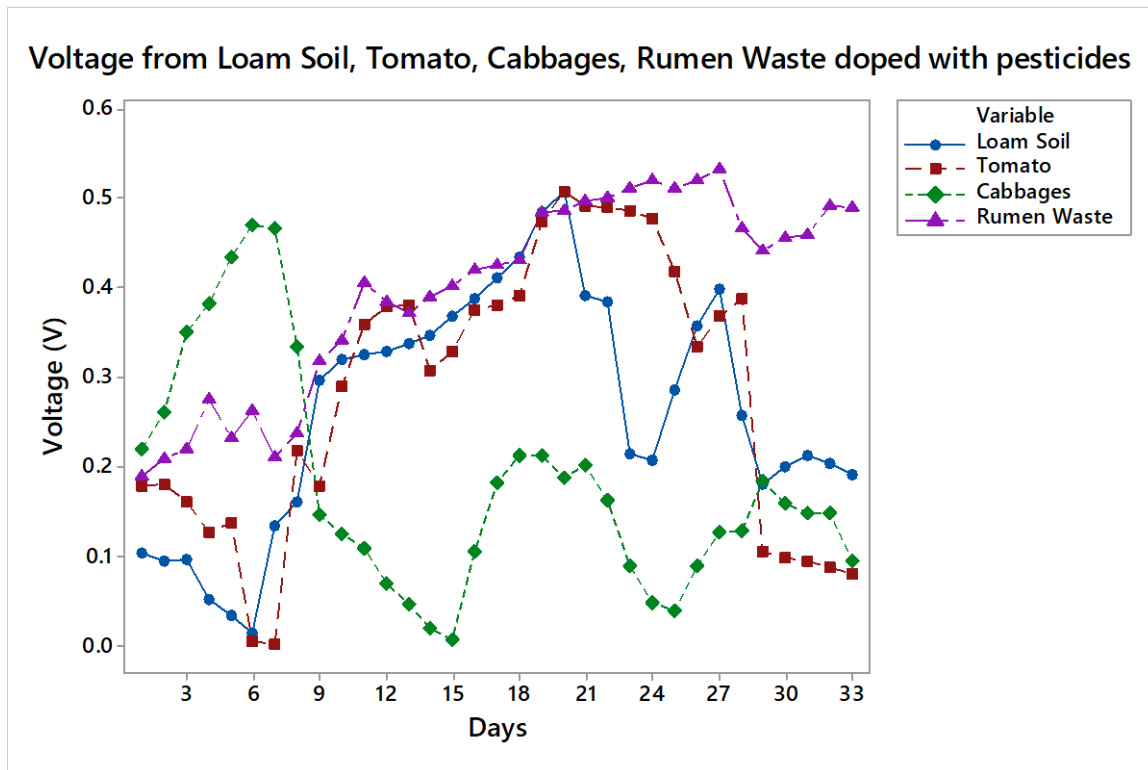


Figure 4.57: Voltage produced by rumen, tomatoes, cabbages, and loam soil solutions doped with pesticides.

Modeling the output of MFC enables to forecast their efficiency. The kinetic studies can also be used to identify the limiting factors. First-order kinetic models were used to investigate the MFC process' performance (Mata-Alvarez et al., 2014). The fitness indicates whether a model can be employed to explain the voltage data of a particular substrate. High regression values suggest that the model can be updated or modified to fit data from other fruits. . The shortfall of the outcome can be explained by the kinetic studies. The MFC performance was studied and first kinetic model was found fit to explain the resulting outcome.

4.9.2.1 Linear plots

Voltage data was fitted to linear plots and the scatter plot was plotted as shown in figure 4.58 below and fitness regression tabulated in table 4.11. The regression values suggest mixed order kinetics dictated by the matrix properties.

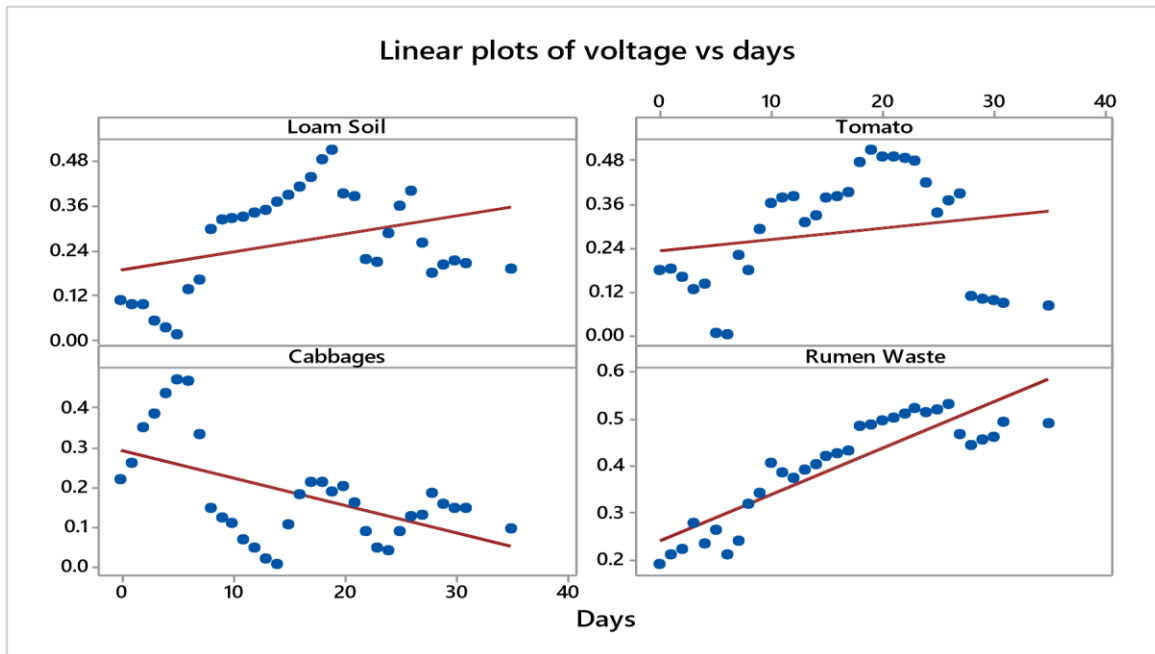


Figure 4.58: Linear plot of voltage against time in days.

Table 4.11: Table of linear plot equation and regression values

Matrix	Equation	R ² (%)	Remarks
Loam soil	Y=0.1877+0.004823x	12.70	Unfit
Cabbage	Y=0.2323+0.003091x	3.80	Unfit
Tomato	Y=0.2928-0.006931x	29.40	Unfit
Rumen Waste	Y=0.2392+0.009854x	77.40	Moderately fit

From figure 4.58 and table 4.11, the statistical analysis suggests that linear plots cannot be used to explain the voltage data from these four-substrate due to the low R² values.

By fitting the mean voltage data to the Boltzmann, Gaussian, and Lorentz equations, the voltage output data from the bio-remediation of pesticide mixture containing lambda-cyhalothrin, Malathion, and chlorpyrifos were modeled. Equations 4.10 to 4.12, , display the equations

$$y = A_1 \frac{e^{\frac{-A_2}{(x-x_0)^2}}}{1 + \frac{A_2}{(x-x_0)^2}} + A_2 \dots \dots \dots (4.10)$$

A₁ is the low Y limit, A₂ is the high Y limit, x₀ is the inflection (half amplitude) point, and dx is the width of the plotted graph.

$$y = y_0 + A \exp \left[-\frac{A}{w^2(x-x_c)^2} \right] \dots \dots \dots (4.11)$$

where A is the height, w is the width of the plotted graph, xc is the center, and y₀ is the Y-values offset.

$$y = y_0 + \frac{A}{1 + \frac{4}{w^2}(X - X_c)^2} \dots \dots \dots (4.12)$$

Where A represents the area, w is the width of the plotted graph curve, x_c is the center, and y_0 is the Y-values offset.

Bacteriological growth and activity are best represented by a non-linear equation and model, which depicts their exponential development, continual growth, and eventual demise. By analyzing degrading byproducts like biogas and voltage produced during substrate breakdown, their activities can be identified. Figure 4.59 below shows the fitted plots from the voltage produced by pesticide mixture-doped loam soil. The results are from the statistical analysis provided in the table provided in appendix 7.

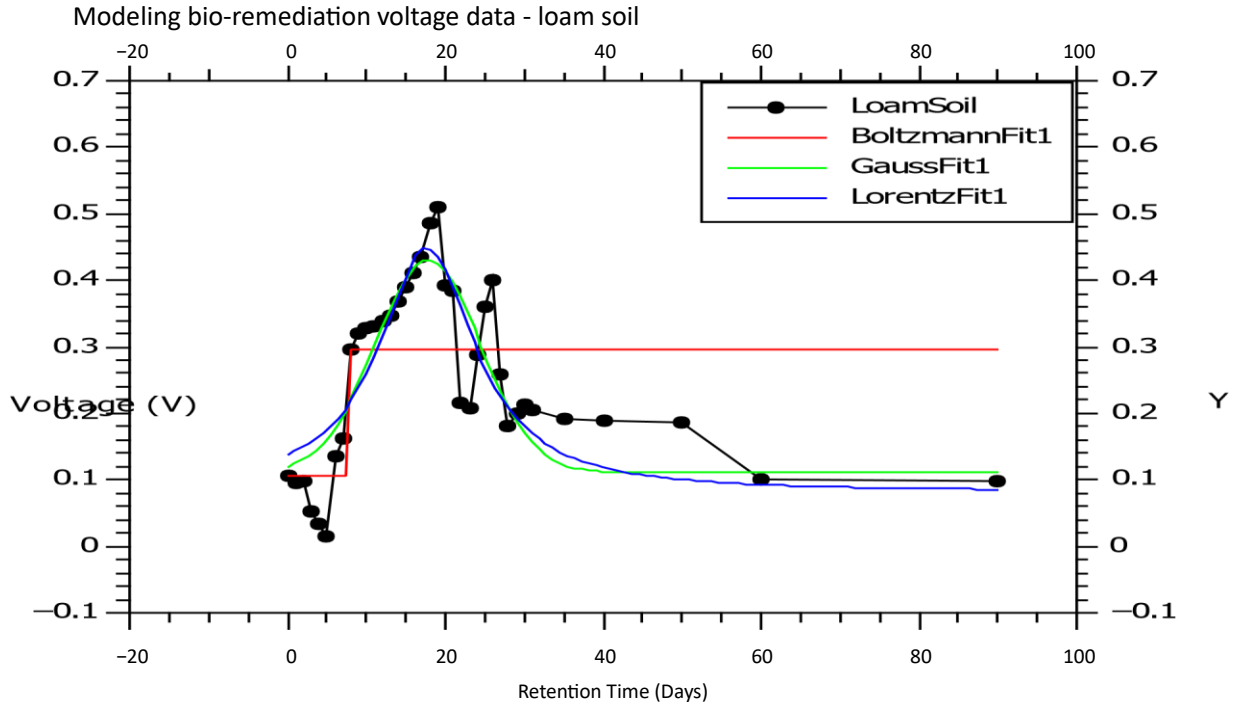


Figure 4.59: Modeling of voltage bio-remediation of pesticide mix in loam soil

The plots created by the pesticide mixture and tomato is shown in Figure 4.60, and has a table of the statistical parameters in appendix section , Appendix 8.

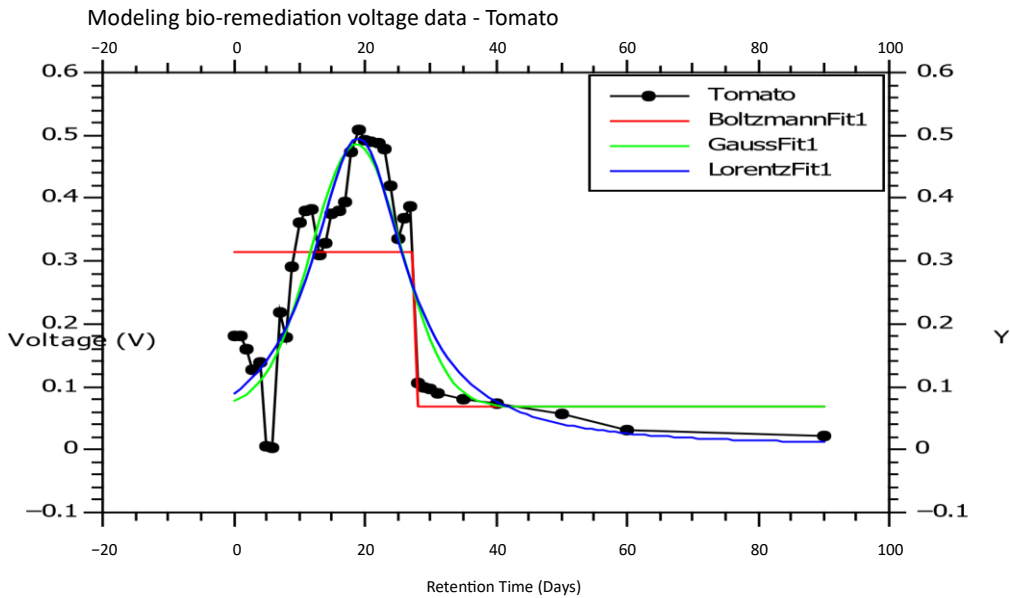


Figure 4.60: Modeling of voltage bio-remediation of pesticide mix in tomato

Figure 4.61 shows , the cabbage doped with the pesticide mixture, and the resultant plots, while the statistical parameters are tabulated in Appendix 9

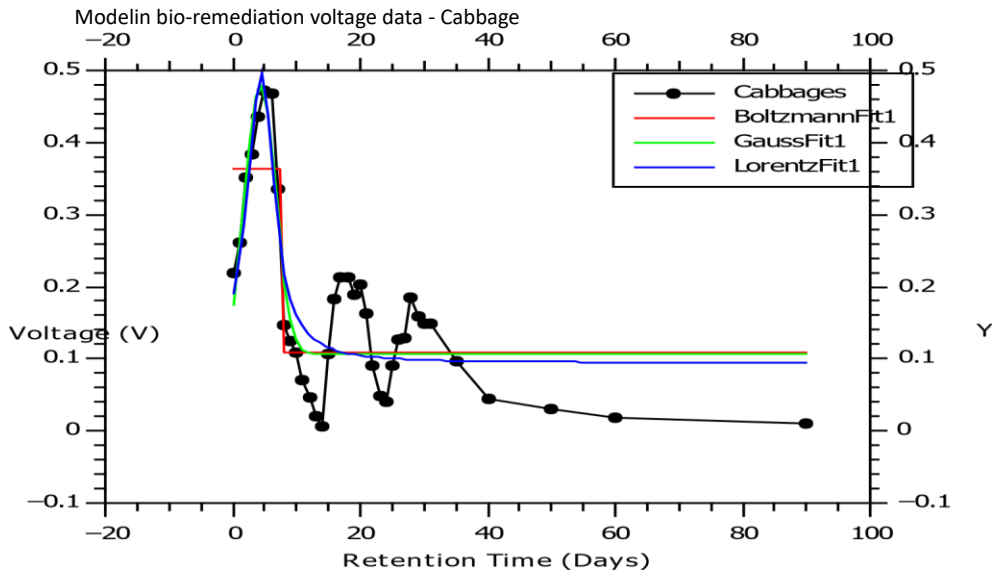
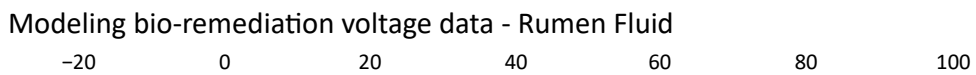


Figure 4.61: Modeling of voltage bio-remediation of pesticide mix in cabbage.

Figure 4.62 below shows the plots created when rumen fluid was infused with the pesticide mixture and its resultant plot. The statistical parameter is tabulated in Appendix 10.



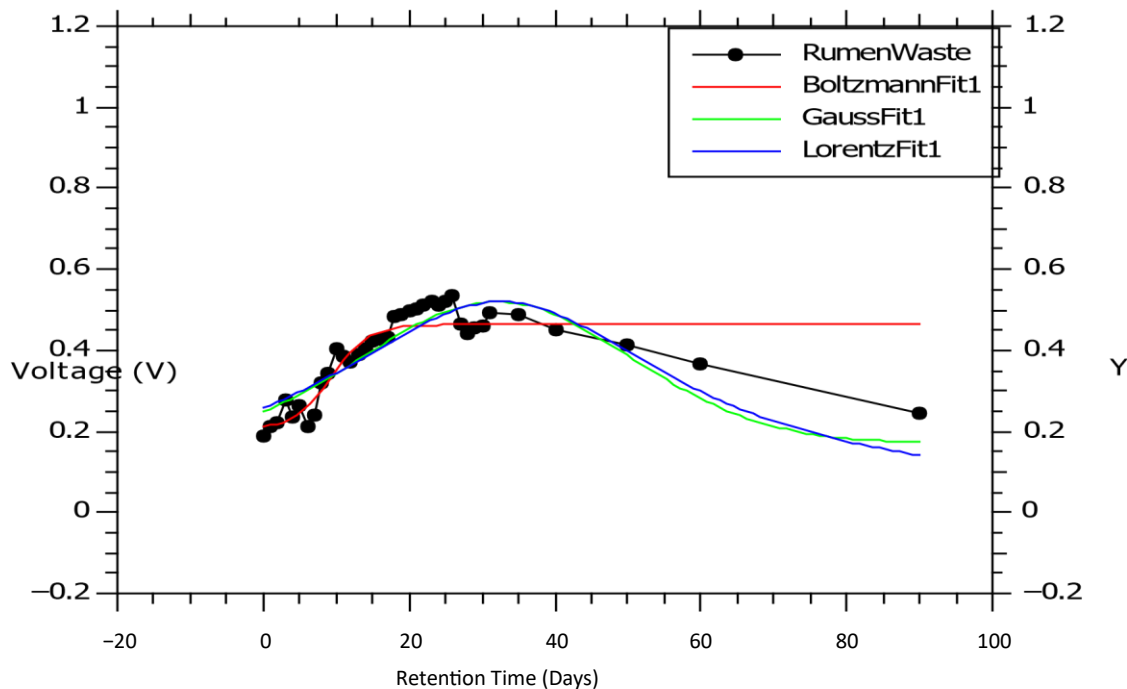


Figure 4.62: Modeling of voltage bio-remediation of pesticide mix in rumen fluid.

From the different voltage fit data into the respective models, the voltage from the bio-remediation studies shows that in rumen fluid, the voltage generation follows a normal distribution curve. That is, the generated voltage increases for the first 20 days, stabilize for 3 days and then production start dropping. This suggests normal growth curve of microbes. In the other three matrices, loam soil and tomato, the initial voltage drops for the first 5 days after which an upward trend is observed for the next 15 days then stable voltage generation was observed. In cabbage, the trend increased sharply up to day 20 before stable voltage generation was observed. Therefore, the Boltzmann, Gauss and the Lorentz equation were generally appropriate in modeling voltage data from the experimental matrices and therefore can be applied in future simulation works in MFC.

4.9.3 Bio-remediation Decay orders

In addition to the , growth kinetics of substrate inhibition, the degradation of lambda cyhalothrin, chlorpyrifos and malathion in co-metabolism MFC was modelled using zero order, pseudo-first, pseudo-second and three-half order equations (Costa and Tavares, 2012; Singh and Balomajumder, 2016) the equations of these models are given in equation 4.13 - 4.15. The first, second, and third order decay curves fitted onto the experimental data were used to mimic the bio-remediation decay conspiracies. Equations 4.13 to 4.15, in that order, display the first, second, and third order curves.

$$Y = Y_0 + Ae^{-x/t} \dots \dots \dots (4.13)$$

$$Y = Y_0 + A_1e^{-x/t_1} + A_2e^{-x/t_2} \dots \dots \dots (4.14)$$

$$Y = Y_0 + A_1e^{-x/t_1} + A_2e^{-x/t_2} + A_3e^{-x/t_3} \dots \dots \dots (4.15)$$

Whereby Y_0 represents the original insecticide concentration, t_1 , t_2 and t_3 are 1st, 2nd, and 3rd decay periods, correspondingly. All the other parameters can be determined from the respective plots which were made using QtiPlot 0.9.9. The fitness of the degradation data to the decay order was determined by the regression value which are shown in tables 4.11 to 4.23.

The close-fitting plots are displayed in figures 4.59 to 4.74 alongside the first, second, and third order decay curves. The resultant arithmetic study for fitness displayed values ranging from 0.9874 to 0.9907, liable to the characteristics of the pesticide, and are shown in table 4.12.

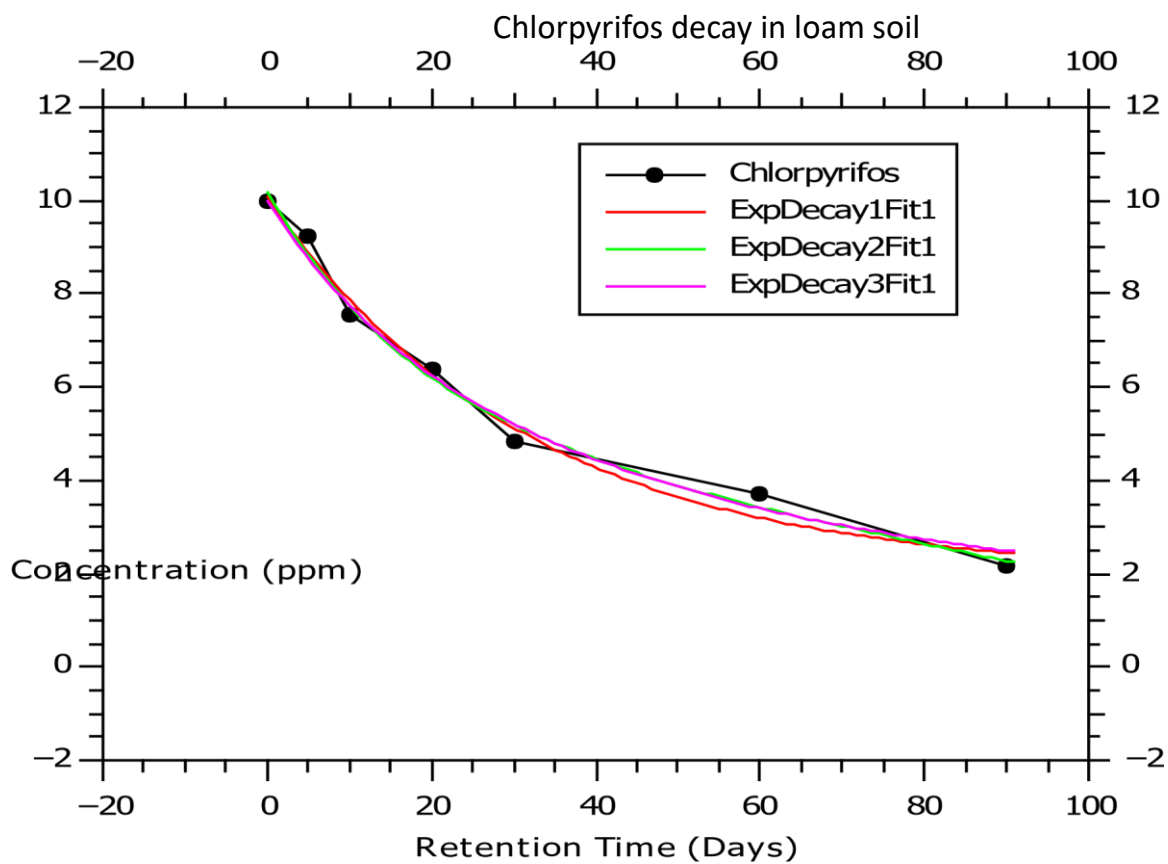


Figure 4.63:Fitted plots of chlorpyrifos degradation curves in loam soil.

Table 4.12: Arithmetic study data for chlorpyrifos decay curves in loam soil

<i>Decay order</i>	<i>Parameters</i>	<i>Chi²/doF</i>	<i>R²</i>	<i>Adjusted R²</i>	<i>RMSE</i>	<i>RSS</i>
<i>First Order</i>	$A=8.0822\pm0.54378$ $t=3.1696\pm0.59086$ $y_0=1.9833\pm0.56191$	1.5546	0.9874	0.9750	0.3943	0.6219
<i>Second Order</i>	$A_1=4.9276\pm0.46240$ $t_1=1.8083\pm0.12763$ $A_2=5.8544\pm0.4683$ $t_2=1.7470\pm0.14229$ $y_0=-5.8544\pm0.47683$	2.2818	0.9907	0.9450	0.4776	0.4563
<i>Third Order</i>	$A_1=2.844$ $t_1=1.6448$ $A_2=3.0571$ $t_2=5.73490$ $A_3=2.8441$ $t_3=5.7348$ $y_0=1.2551$		0.9883			0.5863

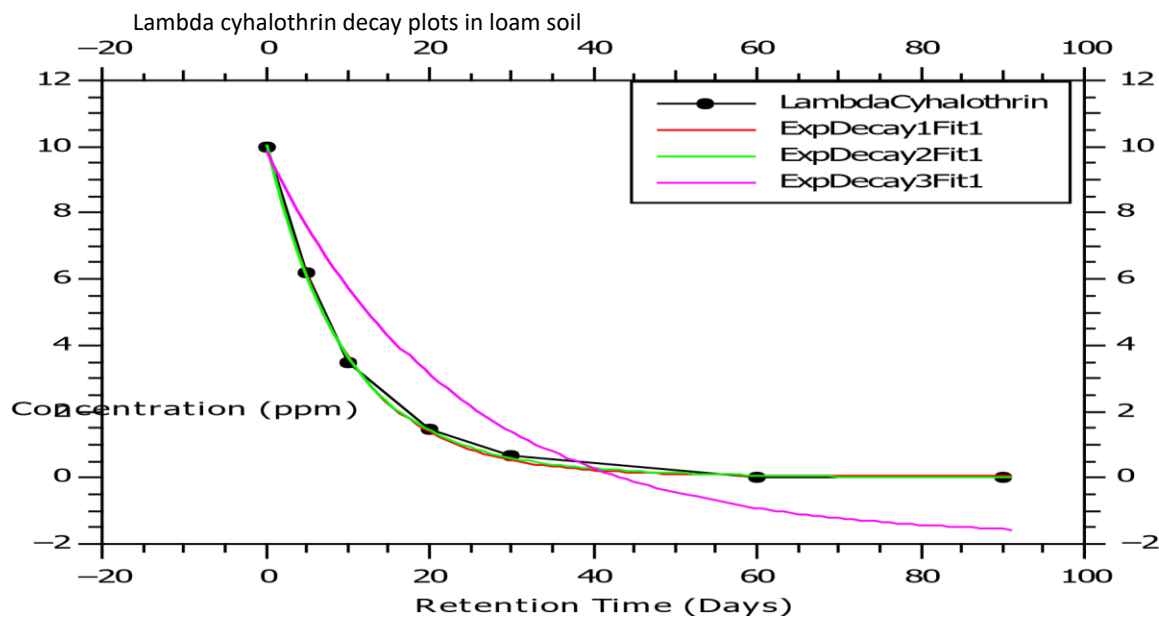


Figure 4.64 :Fitted plots of lambda-cyhalothrin decay curve in loam soil

Table 4.13: Statistical analysis data for lambda-cyhalothrin decay curves in loam soil

Decay order	Parameters	Chi ² /doF	R ²	Adjusted R ²	RMSE	RSS
First Order	A ₁ =9.9656±0.14737 T ₁ = 9.9324± 0.35318 y ₀ =5.2534±0.86697	1.8522	0.9991	0.9982	0.1361	0.0741
Second Order	A ₁ =9.4705± 0.40731 t ₁ =9.3627±0.25342 A ₂ =6.3204±0.33231 t ₂ =3.6530 ± 0.28302 y ₀ =-6.2868± 0.87473	3.1302	0.9993	0.9956	0.17691	0.0626
Third	A ₁ =3.8729		0.83876			13.7174

Order	$t_1=2.3208$ $A_2=3.8729$ $t_2=2.3208$ $A_3=3.729$ $t_3=2.3208$ $y_0=-1.7887$					
-------	---	--	--	--	--	--

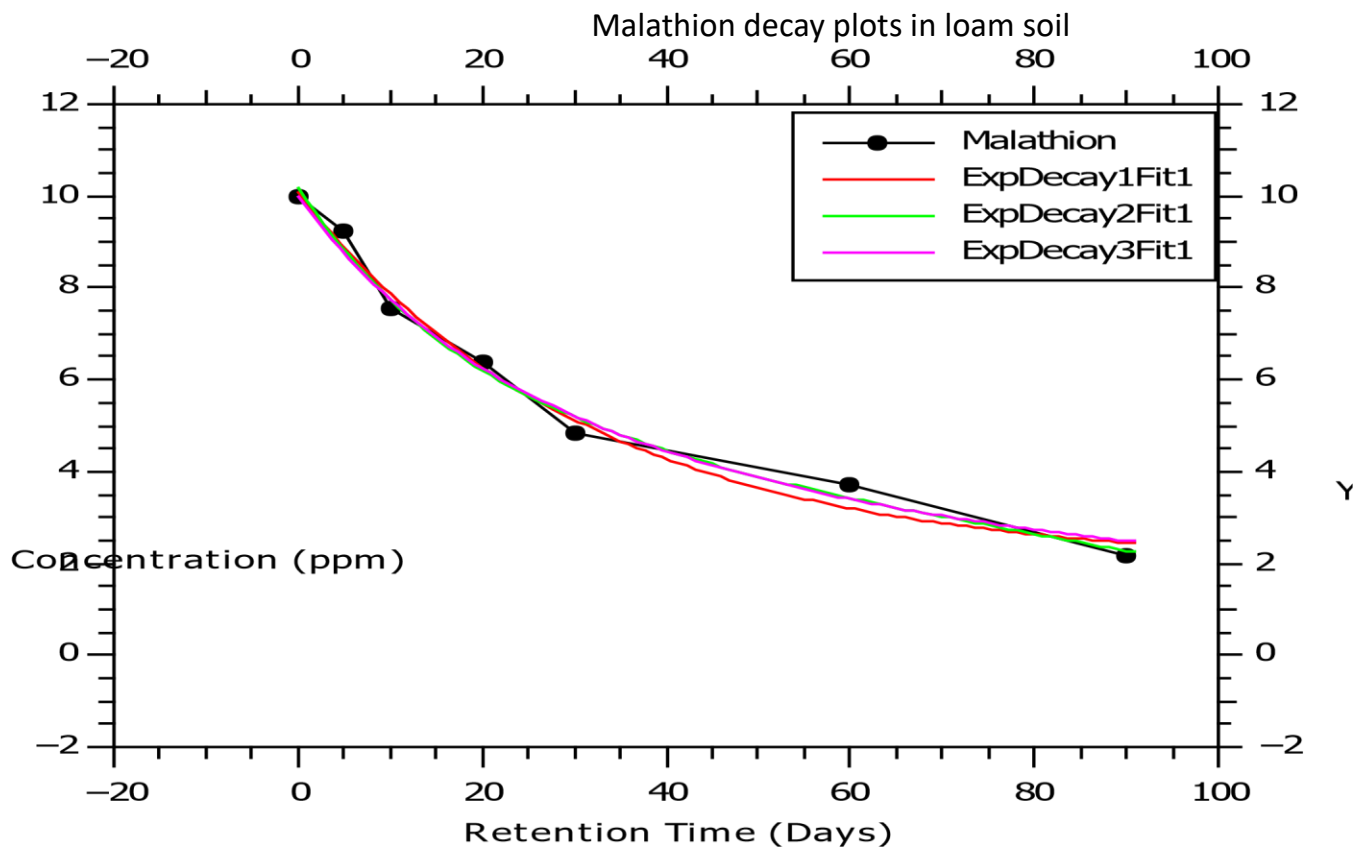


Figure 4.65: Fitted plots of malathion degradation curves in loam soil .

Table 4.14: Statistical data of the decay curves of malathion in loam soil

Decay order	Parameters	Chi ² /doF	R ²	Adjusted R ²	RMSE	RSS	
First Order	A=8.0822± 0.54378 t ₁ =3.1700± 0.59086 y ₀ =1.9833±0.56191	1.5547	0.9875	0.9750	0.3943	0.6219	
Second Order	A ₁ =4.9276±0.46240 t ₁ =1.8083± 0.12763 A ₂ =5.8544±0.47683 t ₂ =1.7469± 0.14229 y ₀ =5.8544±0.47683	2.2817	0.9908	0.9449	0.4777	0.4564	
Third Order	A ₁ =2.8440 t ₁ =1.6449 A ₂ =3.0569 t ₂ =5.7349 A ₃ =2.844 t ₃ =5.7349 y ₀ =-1.2549		0.9882			0.5864	

The consequent plots for the three pesticides in rumen waste are displayed in figures 4.66 to 4.68, and the statistical data from the plots is shown in tables 4.15 to 4.16.

Chlorpyrifos decay plot in Rumen Fluid

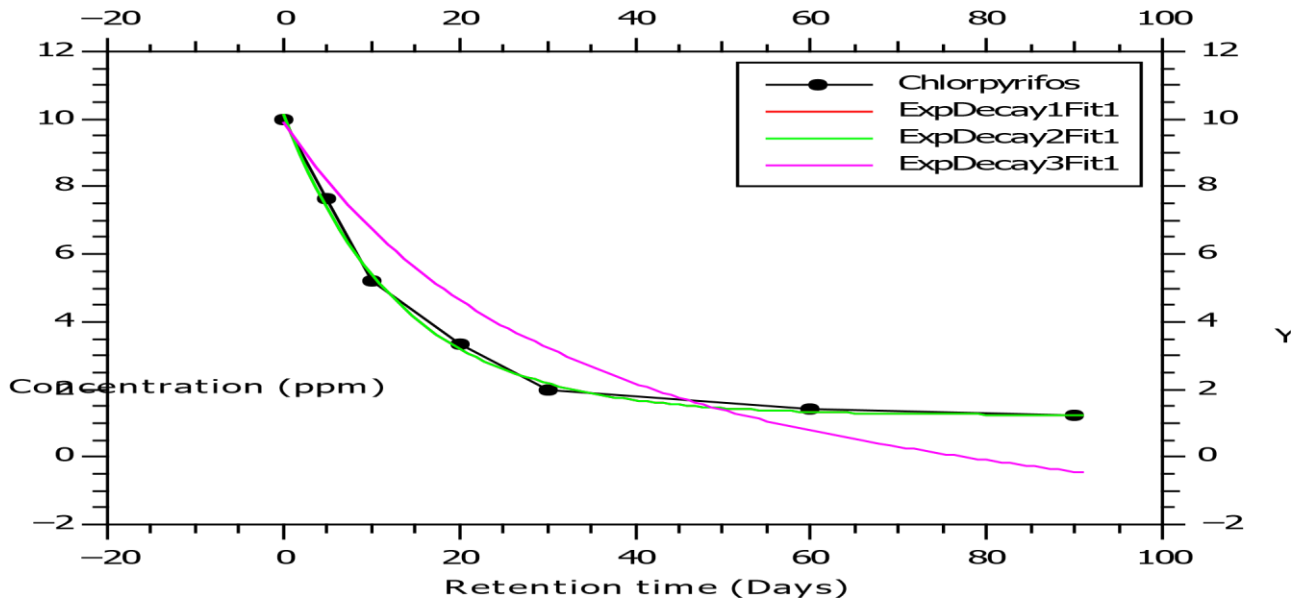


Figure 4.66: Fitted plots of chlorpyrifos degradation curves in rumen fluid Table

4.15: Statistical data for the rumen fluid's chlorpyrifos decay curves.

Decay order	Parameters	Chi ² /doF	R ²	Adjusted R ²	RMSE	RSS
First Order	A ₁ =8.8782±0.23781 T ₁ =1.3380±0.88260 y ₀ =1.2301± 0.15809	4.8826	0.9971	0.9943	0.22096	0.19530
Second Order	A ₁ =4.4072±0.37675 t ₁ =1.3381± 0.61158 A ₂ =4.4709±0.37675 t ₂ =1.3381± 0.61230 y ₀ =1.2302±	9.7652	0.9977	0.9828	0.3124	0.1953

	0.39033					
Third Order	$A_1=4.95985$ $t_1=1.7916$ $A_2=2.3427$ $t_2=6.6612$ $A_3=4.9598$ $t_3=6.6612$ $y_0=-2.3583$		0.8563			9.1927

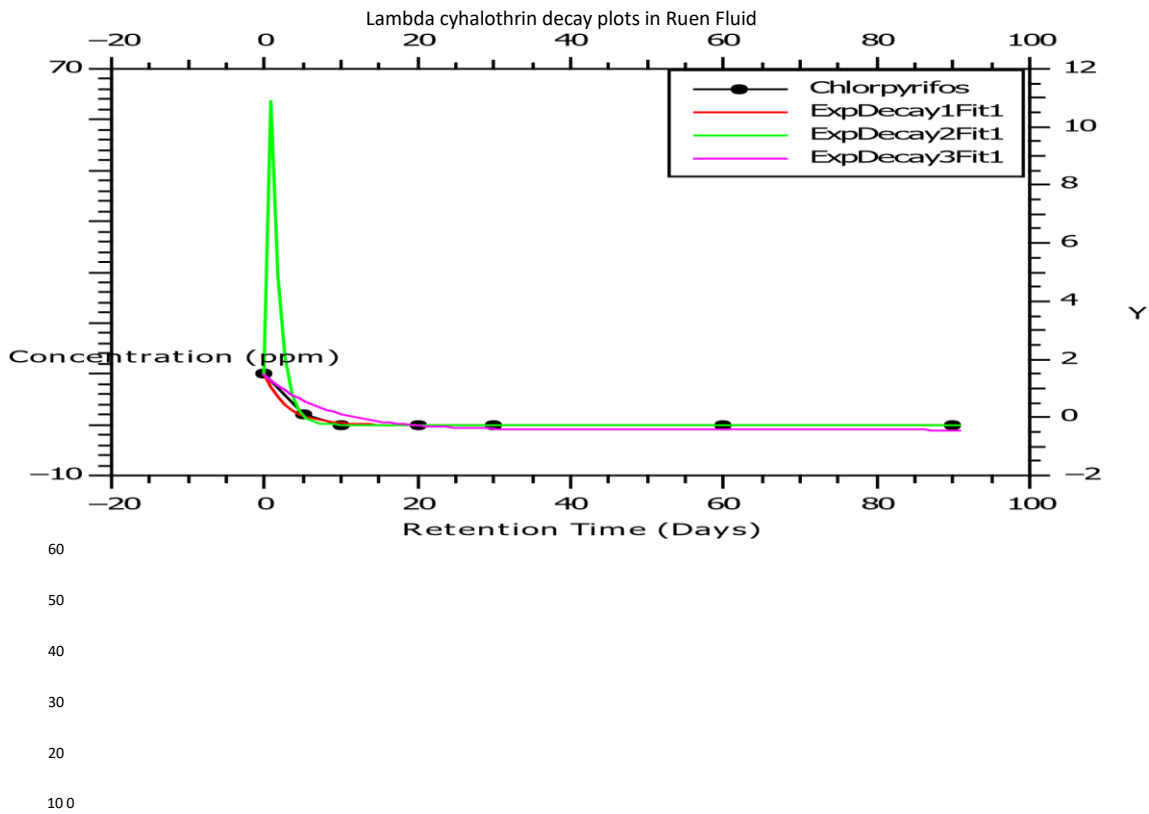


Figure 4.67: Fitted plots of the lambda-cyhalothrin decay curves in rumen fluid

Table 4.16: Statistical study of lambda-cyhalothrin decay curves in rumen fluid

Decay order	Parameters	Chi ² /doF	R ²	Adjusted R ²	RMSE	RSS
First Order	A ₁ =1.0061±0.18132 t ₁ =3.03641±0.16831 y ₀ =5.0384±0.79138	2.6958	0.9987	0.9974	0.1642	0.10784
Second Order	A ₁ =1.2893±0.082427 t ₁ =3.5933±0.32134 A ₂ =1.3893±0.082427 t ₂ =1.1788± 0.082455 y ₀ =1.2476±0.17659	9.3527	0.9999	0.9999	0.0031	1.8705

Third	$A_1=4.2285$ $t_1=8.05125$					
Order	$A_2=2.4922$ $t_2=8.0513$ $A_3=4.2285$ $t_3=8.05125$ $y_0=-1.0370$		0.8169			15.2539

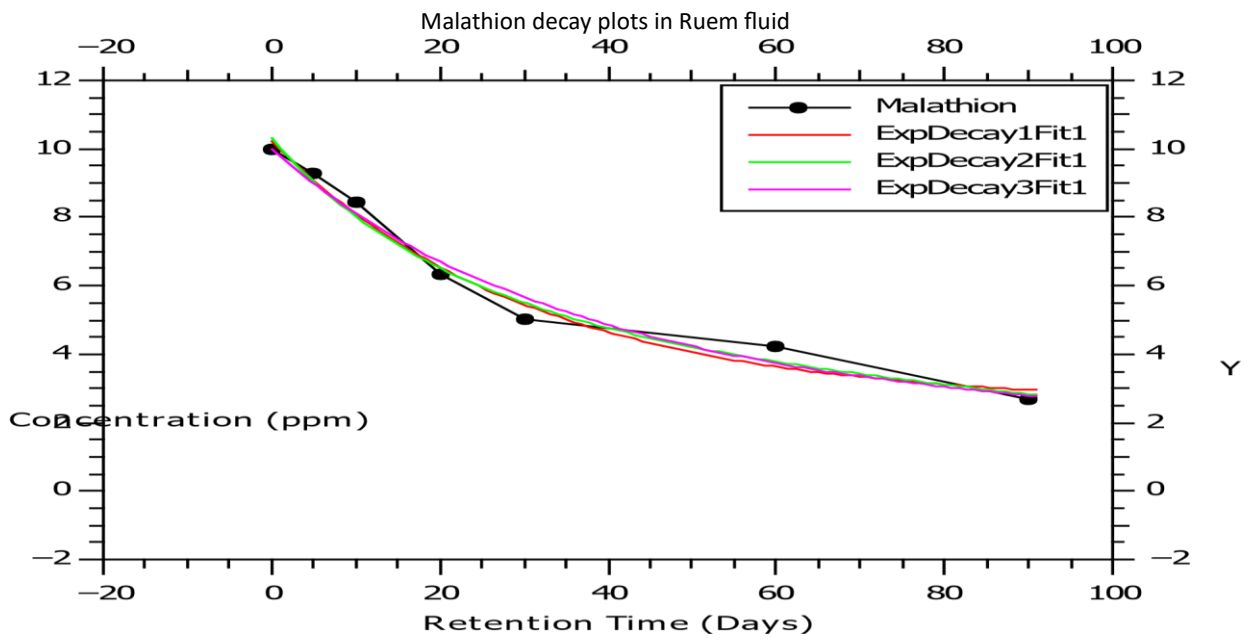


Figure 4.68: Fitted plots of malathion decay curves in rumen fluid

Table 4.17: Arithmetic study data for malathion decay curves in rumen fluid

Decay order	Parameters	Chi ² /doF	R ²	Adjusted R ²	RMSE	RSS
First Order	A ₁ =7.6936±0.64654 T ₁ =3.0898±0.72111 y ₀ =2.53462±0.661459	2.3003	0.9799	0.9598	0.4796	0.92011
Second Order	A ₁ =5.4093±0.45514 T ₁ =2.1347±0.23392 A ₂ =7.6199±0.89514 t ₂ =3.2094±0.37702	4.1895	0.9817	0.89043	0.6473	0.8379
Third Order	A ₁ =2.87676 t ₁ =2.36075 A ₂ =3.1635 t ₂ =5.6736 A ₃ =2.36099 t ₃ =5.67364 y ₀ =1.59866		0.97719			1.04612

Figures 4.69 display the fitted decay plots for the three pesticides in the chlorpyrifos, and tables 4.17 display the statistical information from the plots.

Chlorpyrifos decay plots in tomato

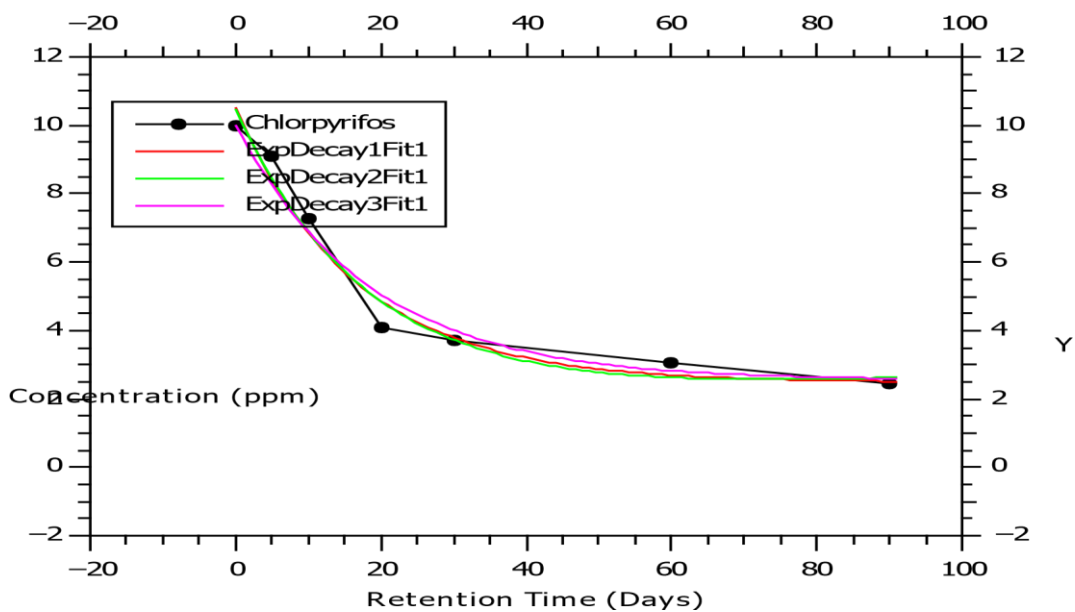


Figure 4.69: Fitted plots of chlorpyrifos decay curves in tomato

Table 4.18: Statistical analysis data for chlorpyrifos decay curves in tomato

Decay order	Parameters	Chi ² /doF	R ²	Adjusted R ²	RMSE	RSS
First Order	A=8.010±0.704298 t=1.65994± 0.370087 y0=2.48008±0.51766	4.2372	0.97016	0.9403	0.6509	1.6948
Second Order	A ₁ =8.7047±0.89006 T ₁ =1.8362±0.26123 A ₂ =1.1124±0.23292 T ₂ =-1.3440±0.26253 y ₀ =-1.1924± 0.23292	8.3125	0.97072	0.8243	0.91173	1.6625

Third Order	$A_1 = -6.2415$ $t_1 = 1.5946$ $A_2 = 1.2483$ $t_2 = 1.5946$ $A_3 = -6.2415$ $t_3 = 1.5946$ $y_0 = 2.5523$		0.9638			2.0529
-------------	--	--	--------	--	--	--------

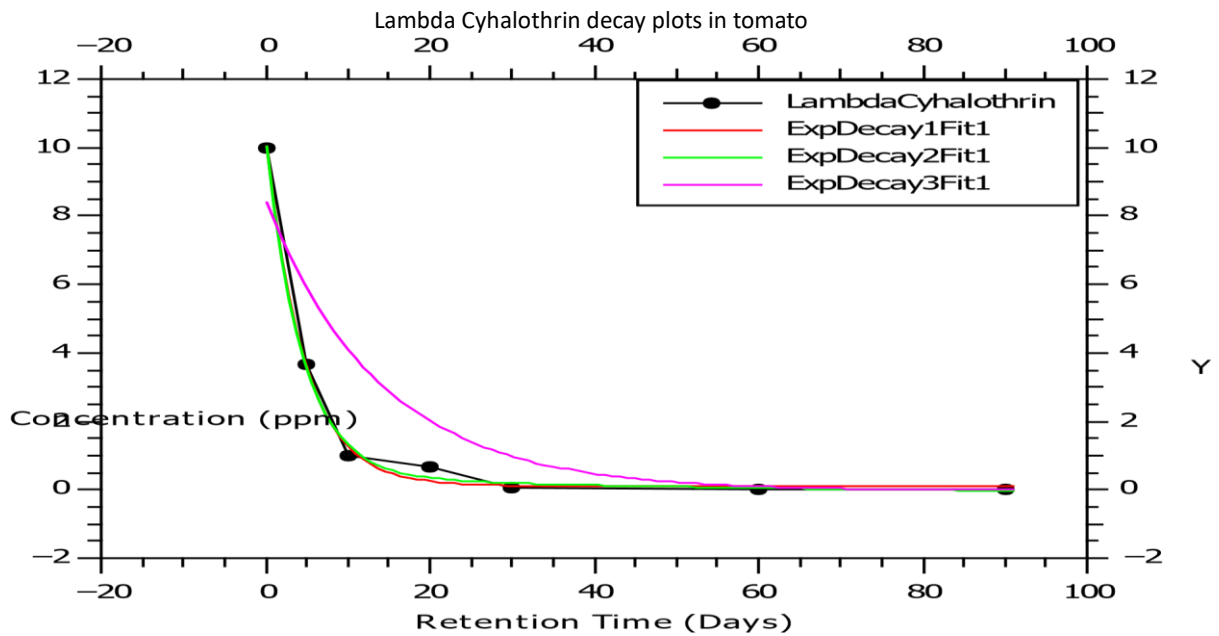
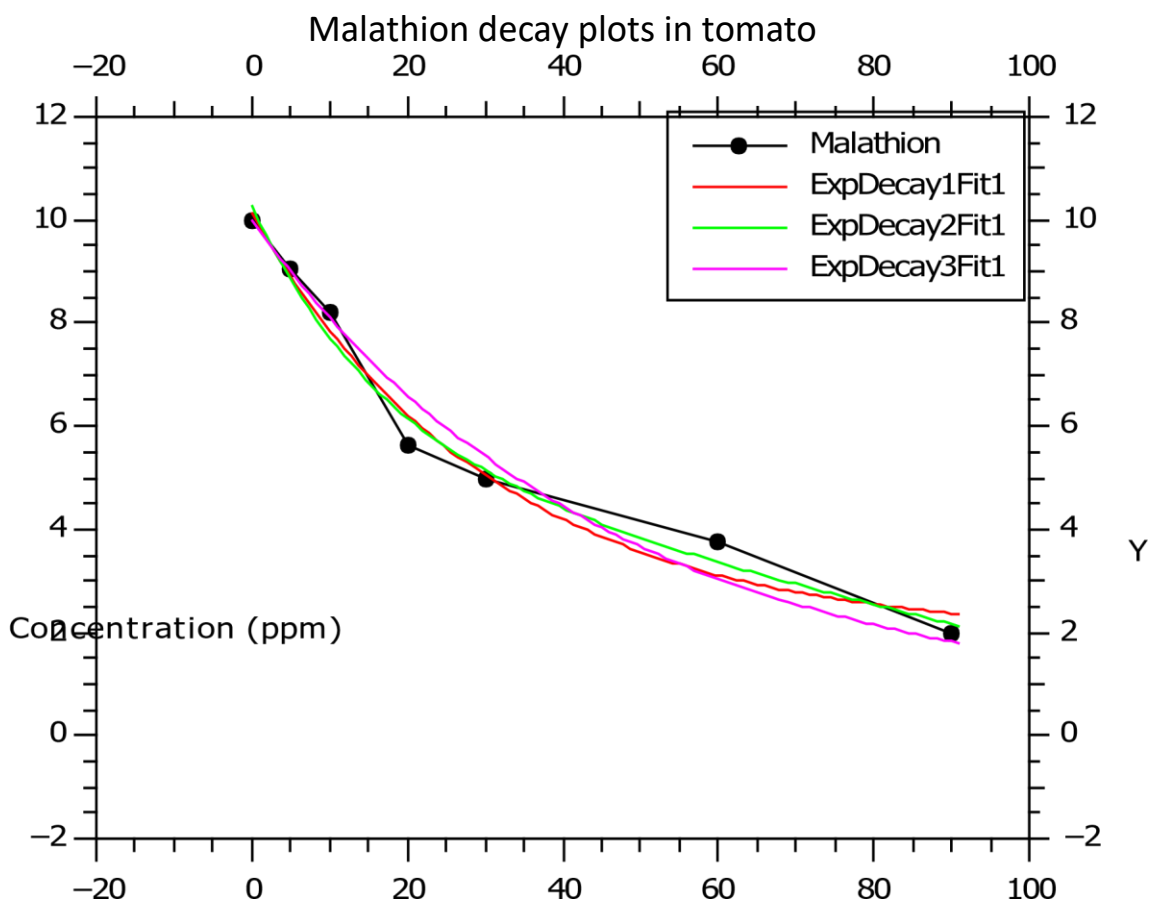


Figure 4.70:Fitted plots of decay curves in tomato

Table 4.18: Statistical analysis data for lambda-cyhalothrin decay curves in tomato

Decay order	Parameters	Chi ² /doF	R ²	Adjusted R ²	RMSE	RSS

First Order	$A_1=9.9081 \pm 0.28684$ $T_1=4.70297 \pm 0.33632$ $y_0=1.07196 \pm 0.13389$	6.7431	0.9967	0.9933	0.2597	0.2697
Second Order	$A_1=9.6181 \pm 0.15693$ $T_1=14.4480 \pm 0.10287$ $A_2=5.3048 \pm 0.11654$ $T_2= 5.0996 \pm 0.61143$ $y_0=1.2484 \pm 0.22413$	1.1483	0.9971	0.9829	0.3389	0.2296
Third Order	$A_1=2.8119$ $T_1=1.4076$ $A_2=2.8120$ $t_2= 1.4076$ $A_3=2.8120$ $t_3=1.4079$ $y_0=-2.1240$		0.7543			19.8615



Retention Time (Days)

Figure 4.71: Fitted plots of decay curves in tomato

Table 4.20: Statistical analysis data for malathion decay curves in tomato

Decay order	Parameters	Chi ² /doF	R ²	Adjusted R ²	RMSE	RSS
First Order	A ₁ =8.2003±0.72146 T ₁ =3.1205±0.76185 y ₀ =1.9141± 0.74103	2.8151	0.9784	0.9567	0.5305	1.1260
Second Order	A ₁ =4.8691±0.38420 t ₁ =1.7134± 0.28950 A ₂ =1.6924±0.12221 t ₂ =4.6981± 0.33928 y ₀ =-1.6924± 0.12222	4.3664	0.9832	0.8992	0.6607	0.8732

Third	$A_1=8.4529$		0.9667			1.7309
Order	$T_1=4.5307$					
	$A_2=1.7852$					
	$T_2=4.5307$					
	$A_3=-8.4529$					
	$T_3=4.5307$					

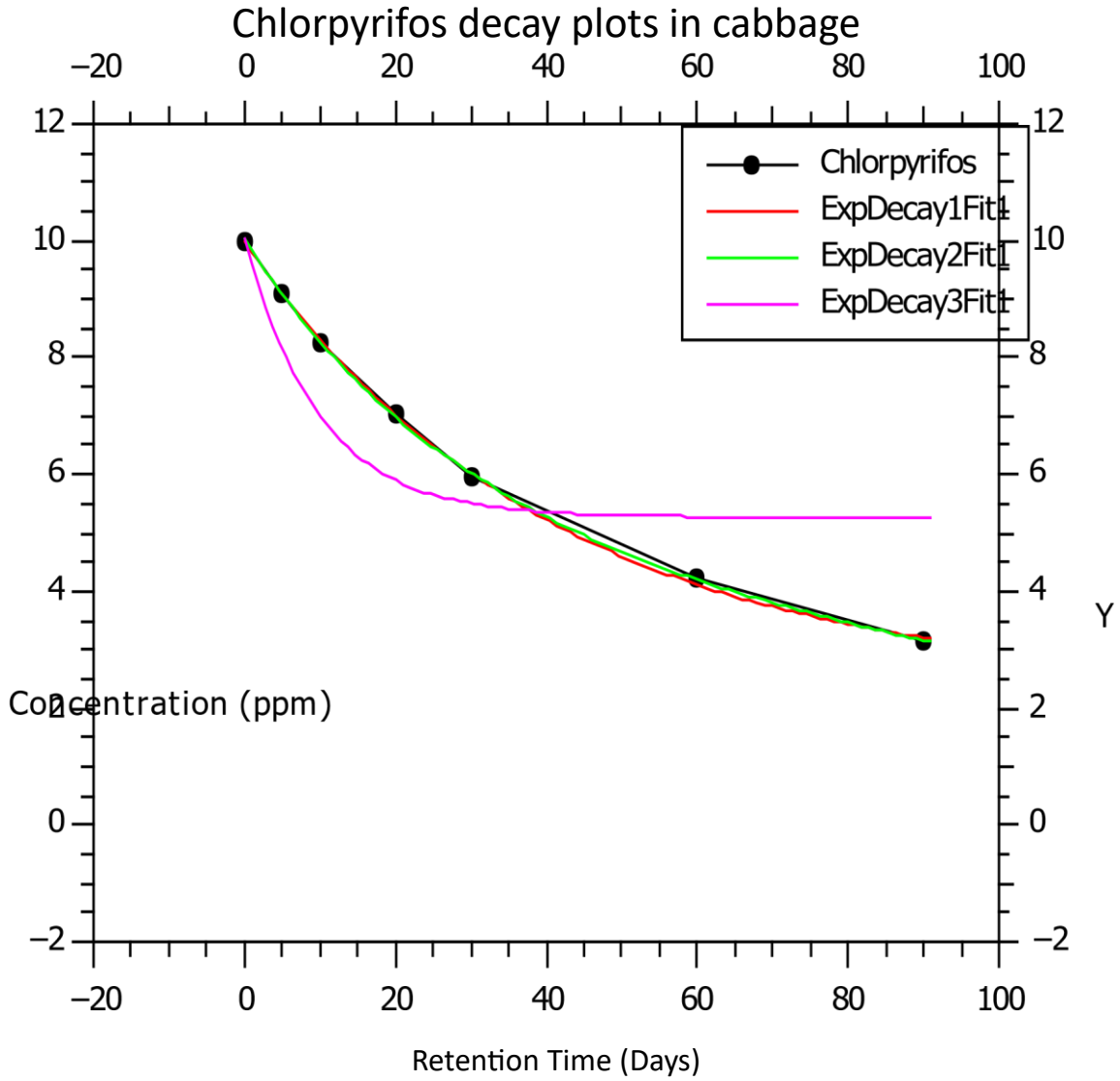


Figure 4.72: Close-fitting subversions of chlorpyrifos decay curves in cabbage

Table 4.21: Statistical analysis data for chlorpyrifos decay curves in cabbage

Decay order	Parameters	Chi ² /doF	R ²	Adjusted R ²	RMSE	RSS
First Order	A ₁ =7.599±0.12737 t=4.0735±0.17609 y ₀ =2.34742±0.13964	4.646	0.9996	0.9990	0.0682	0.0185
Second Order	A ₁ =2.0131 0.35547 t ₁ =9.7952±0.17296 A ₂ =5.2467±0.22392 t ₂ =2.9038±0.068900 y ₀ =2.0131±0.35547	1.9193	0.99999	0.9995	0.0437	0.00382
Third Order	A ₁ =1.5831 t ₁ =9.9810 A ₂ =1.5831 t ₂ = 9.9810 A ₃ =1.5831 t ₃ =9.98104 y ₀ =5.2670		0.7505			9.5883

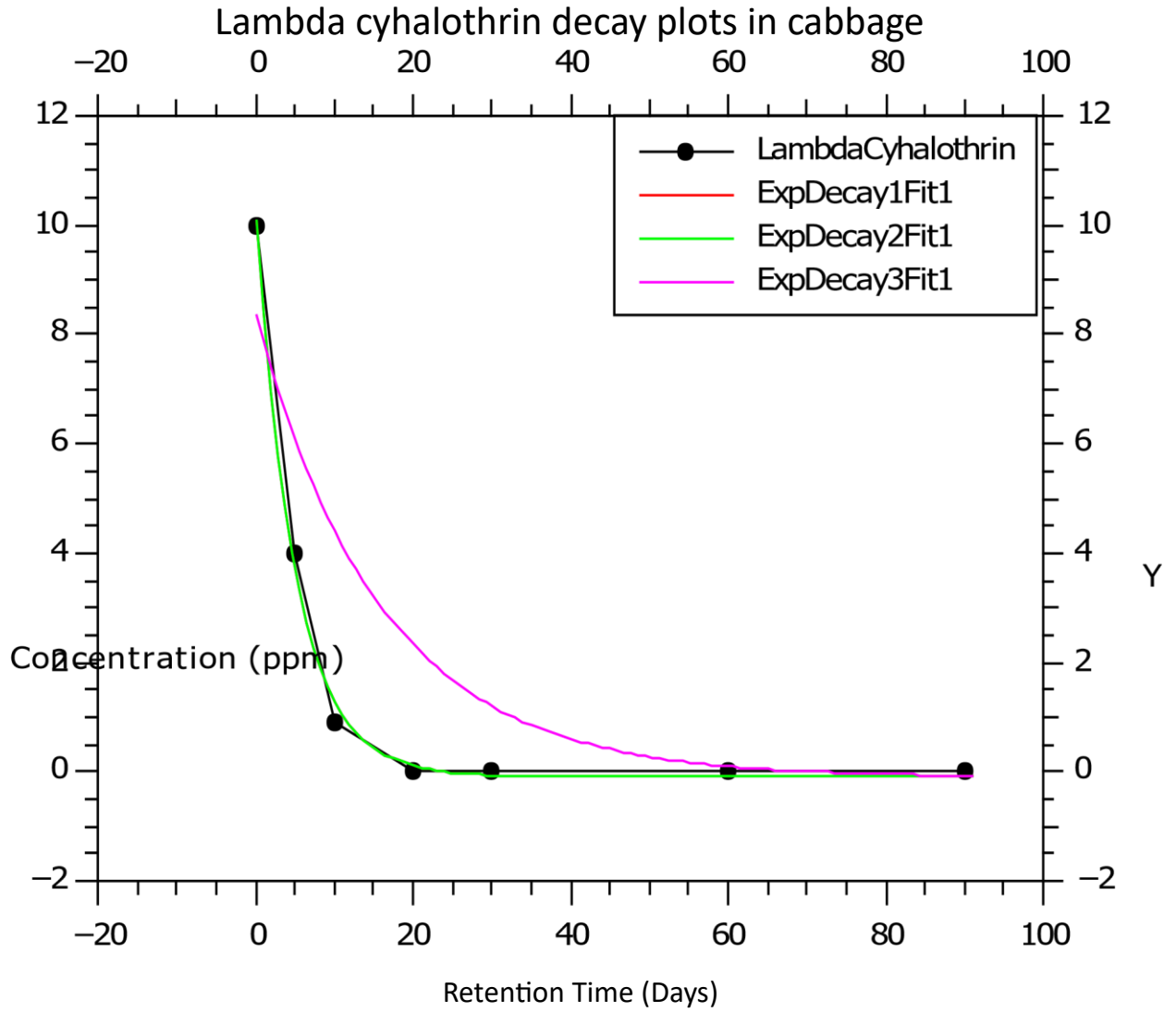


Figure 4.73:Fitted plots of decay curves in cabbage

Table 4.22: Statistical data for lambda-cyhalothrin decay curves in cabbage

Decay order	Parameters	Chi ² /doF	R ²	Adjusted R ²	RMSE	RSS
First Order	A=1.0148±0.303019 T ₁ =5.0462±0.36612 y ₀ =-8.779±0.14457	7.5359	0.9965	0.9929	0.2745	0.3014
Second Order	A ₁ =5.1547 ±0.55799 t ₁ =5.0462±0.25219 A ₂ =4.9938±0.55799 t ₂ =5.04621± 0.26031 y ₀ =- 8.7798±0.30717	1.5072	0.9964	0.9787	0.3882	0.3014
Third Order	A ₁ =2.8119 t ₁ =1.60803 A ₂ =2.8119 T ₂ =1.6080 A ₃ =2.3119 t ₃ =1.60804 y ₀ =- 1.0214		0.69013			26.3418

Malathion decay plots in cabbage

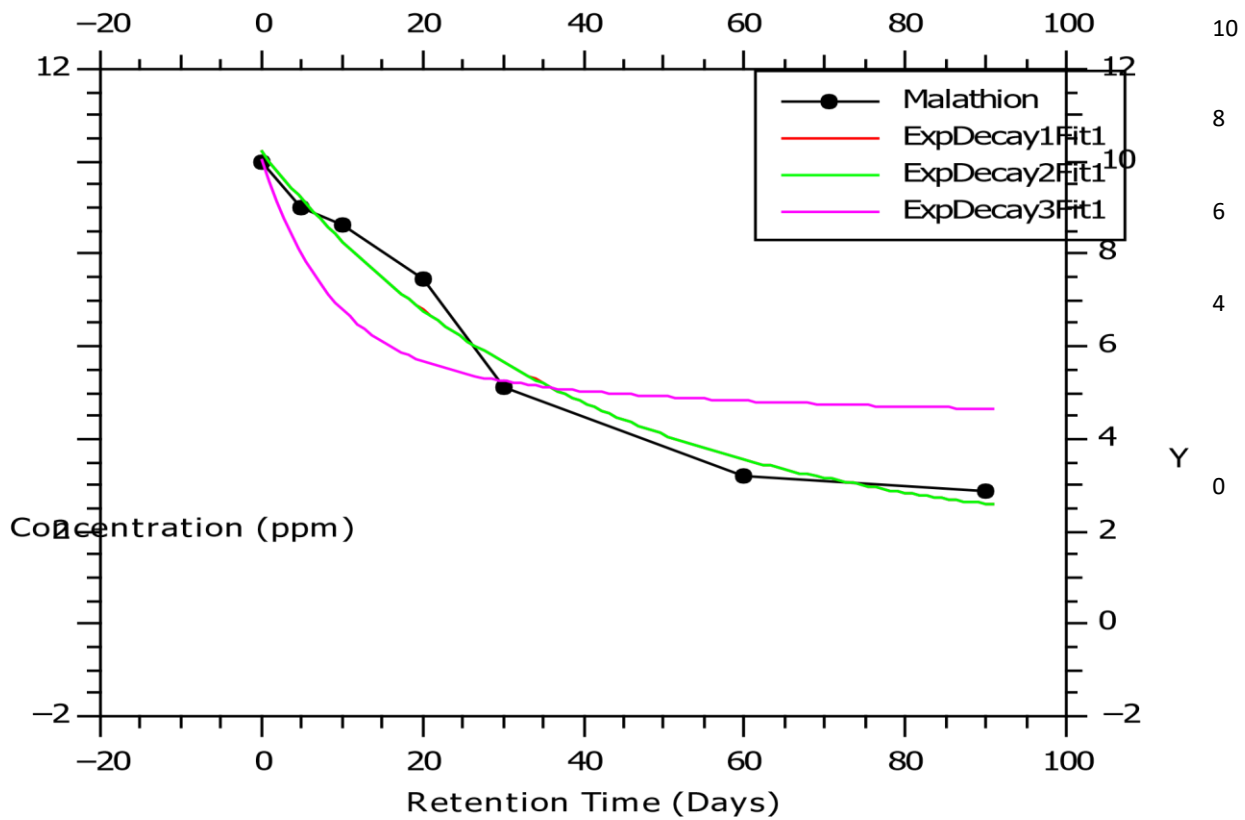


Figure 4.74 Fitted plots of malathion degradation curves in cabbage

Table 4.23: Statistical data analysis for malathion decay curves in cabbage

Decay order	Parameters	Chi ² /doF	Chi ² /doF	R ²	Adjusted R ²	RMSE
First order	A ₁ =8.443±0.9095 T ₁ =38.8545±11.0109 y ₀ =1.7589±0.9914	0.27127i	0.9782	0.9564	0.5208	1.0851
Second order	A ₁ =4.1905 t ₁ =3.8852 A ₂ =4.2525 t ₂ =3.8851 y ₀ = 1.7592	5.4255	0.9782	0.8692	0.7365	1.0851
THIRD ORDER	A ₁ = 4.4191 t ₁ = 8.7219 A ₂ = -7.449 t ₂ = 5.4504 A ₃ = 1.9245 t ₃ =5.4505 y ₀ =4.4216		0.7350			13.1929

The kinetics of the bio-remediation process can be assessed by fitting the pesticide concentration degradation levels at any given time (t) against the initial concentration. This gives the degradation rates (k) which can further be employed to calculate the pesticide half-life in a given matrix. In the current study, the first, second and third order kinetics equations were employed to fit the degradation data and their fitness to each equation assessed using the regression values. The observed general trend of the degradation kinetics in this study was that the first and second order models fitted the three pesticides degradation data in the four matrices perfectly with regression values greater than 0.9900 compared to the third decay order whose regression values were in the range of 0.760 - 0.967 for the three pesticides in the matrices under study.

This study is key in understanding kinetics dynamics based on model parameter listed in tables 4.124.22. The second order model was found to be most fitting for the three pesticides bio-degradation studies , as the data had a high correlation coefficient (>0.99).

The first order and second order models have the shortcoming that they do not consider the factors of bacterial growth. To overcome this limitation, Brunner and Fotcht (1984) proposed a three-half order model integrating the microbial growth and substrate degradation. The correlation coefficient (0.760 – 0.990) of the three-half order model was slightly lower than the second order model, but it could also be used as a suitable model for prediction of the influence of substrates in co-metabolism research studies.

CHAPTER FIVE

CONCLUSION AND RECOMMENDATIONS

5.1 CONCLUSION

In this study, the quantity of the voltage, current, power and power density derived from bioremediation of lambda cyhalothrin, chlorpyrifos and malathion on loam soil, tomato and cabbage wastes and rumen waste was assessed.

The maximum voltage derived from tomatoes, cabbages, rumen fluid and loam soil were 0.479 V, 0.587 V, 0.568 V, and 0.483 V, respectively. The current generated in these matrices was in the range of 0.003 – 0.223mA.

On determining the effects of pH, microbe concentration, concentration of pesticides and external resistance on degradation of the pesticides using MFCs on the four-substrates used in this study, it was observed that the optimal pH range was 6.93 – 7.40, 1:2 substrate to inoculum/rumen matter was the optimal microbe concentration and the Open Circuit Voltage (OCV) was the optimal external resistance

In assessing the efficacy of anaerobic-air cathode microbial degradation of the pesticides in the MFC on loam soil, tomato and cabbage wastes and rumen waste, it was observed degradation levels achieved were 73.40% and 87.70% for malathion and chlorpyrifos respectively while no lambda cyhalothrin was detected on the 90th day of this study. The maximum generated voltage from tomato matrix was in the range of 0.363 - 0.582 V in the four matrices.

The bio remediation levels for chlorpyrifos and malathion were 65.80 % and 71.32 %, respectively while no detectable, lambda cyhalothrin was observed after day 60 of the study in cabbage.

In the loam soil, the observed degradation levels were 79.32 %, 99.90 % and 78.20 % in chlorpyrifos, lambda cyhalothrin and malathion, respectively.

Finally, on fitting the mineralization voltage data to various models, the results showed that the linear models were unfit to describe the performance of the microbial fuel cell bio-remediation processes; this is based on lower regression coefficient of (3.254 to 77.89). Kinetics studies revealed that first order seemed to be obey/fit while second and third order did not seem to fit. Lastly Non-linear equations were widely used to fit the data with higher fit coefficients.

5.2 Recommendations

The suggested recommendations are as follows;

Assessment of bio-remediation of other hydrocarbon pollutants like greasy/oily soil using MFCs

That the bio-remediation studies to be performed on other pesticides used in crop production Bio-remediation particles and mechanism could be monitored simultaneously as the voltage is monitored to thoroughly understand the working principles of MFC.

That policy to be put in place to prevent high pesticide pollution as it results to high pesticide concentrations which are toxic and the rate of degradation low.

The non-linear models could be employed in microbial related degradation based on high regression coefficient values.

5.3 Recommendations for further works

Further studies suggested from this study include

Investigation of bio-remediation of pesticides in other plants, since this study only targeted tomato and cabbage.

Assessment of the bio-remediation pathways of lambda cyhalothrin, chlorpyrifos and malathion to understand the degradation mechanism

To investigate other non-linear models employable in analyzing the power obtained from bioremediation of lambda cyhalothrin, chlorpyrifos and malathion in the environment.

REFERENCES

Abdul Halim K. and Yong E.L. (2018). Integrating two-stage up-flow anaerobic sludge blanket with a single-stage aerobic packed-bed reactor for raw palm oil mill effluent treatment, *Malaysian Journal of Sustainable Agriculture (MJSA)*, 2(1): 15-18.

Adebule A.P., Aderiye B.I. and Adebayo A.A. (2018). Improving Bio-electricity Generation of Microbial Fuel Cell (MFC) With Mediators Using Kitchen Waste as Substrate. *Ann Appl Microbiol Biotechnol J*, **2**(1), 1008

Adubofuor, J., Amankwah, E.A., Arthur, B., & Appiah, F. (2010). Comparative study related to physico-chemical properties and sensory qualities of tomato juice and cocktail juice produced from oranges, tomatoes and carrots. *African Journal of Food Science*, **4**, 427-433.

Aislabie J.M., Richards N.K., Boul H.L. (1997). Microbial degradation of DDT and its residues, A review, New Zealand. *Journal of Agricultural Research*, **40**: 269-282.

Alav, I., Sutton, J. M., & Rahman, K. M. (2018). Role of bacterial efflux pumps in biofilm formation. *The Journal of antimicrobial chemotherapy*, **73**(8), 2003–2020

Alexander Robert T., Terry. (1964). Chemical degradation, choliambic (1) stable to hydrolytic degradation. *Non sterile soil*. **10**. (6) 20-27

Amirahmadi M., Yazdanpanah H., Shoeibi S.H., Pirali Hamedani M., OstadGholami M., Mohseninia M.F., Kobarfard F. (2013). Simultaneous Determination of 17 Pesticide Residues in Rice by GC/MS using a Direct Sample Introduction Procedure and Spiked Calibration Curves. *Iran J PHarm Res*, **2**: 295-302.

Analytical Techniques in Aquaculture Research.(2009. Retrieved from <https://aquaculture.ugent.be/Education/coursematerial/online%20courses/ATA/analysis/NFE.htm> on May 26th, 2022

Anastassiades M., Lehotay S.J., Stajnbaher D., Schenck F.J. (2003). Fast and easy multi residue method employing acetonitrile extraction/partitioning and “dispersive solid phase extraction” for the determination of pesticide residues in products. *J. AOAC Int*, **86**: 412-431.

Aritra D. and Mondal C. (2015). Comparative Kinetic Study of Anaerobic Treatment of

Azubuike, C. C., Chikere, C. B., & Okpokwasili, G. C. (2016). Bio-remediation techniques classification based on site of application: principles, advantages, limitations and prospects. *World journal of microbiology & biotechnology*, 32(11), 180.

Barupal T., Chittora D., and Meena M. (2019a). Solid waste: characterization, assessment, monitoring, and remediation, in *Advances in Waste-to-Energy Technologies*, eds R. P. Singh, V.

Prasad, and B. Vaish (Boca Raton; London; New York, NY: Taylor & Francis; CRC Press), 1–19.

Barupal T., Meena, M., and Sharma K. (2019b). Inhibitory effects of leaf extract of *Lawsonia inermis* on *Curvularia lunata* and characterization of novel inhibitory compounds by GC–MS analysis. *Biotechnol. Rep.* 23: e00335.

Behera M., Jana P.S., More T. and Ghangrekar M.M., (2010) Rice mill wastewater treatment in microbial fuel cells fabricated using proton exchange membrane and earthen pot at different pH, *Bio electrochemistry*, **79**(2). 228–233

Benoit C and Christophe V. (2019). Modeling and simulation of Bio-hydrogen production Process, *Bio-Hydrogen-Second Edition*.: 445-483

Benyahia F. and Embaby A.S. (2016). Bio-remediation of crude oil contaminated desert soil: Effect of bio-stimulation, bio augmentation and bio-availability in biopile treatment systems. *Int J Environ Res Public Health*. **13**: 219.

Blanco J., Minero, C., Pelizetti, E., Malato S. (1996). Large solar plant photo catalytic water decontamination degradation of atrazine. *Solar Energy*. **56**(5), 411-419.

bovine manure compost on the degradation of chlorothalonil in soil. *Soil Sediment Contam.* **18**: 195 - 204.

Brunner, W., & Focht, D. D. (1984). Deterministic three-half-order kinetic model for microbial degradation of added carbon substrates in soil. *Applied and environmental microbiology*, **47**(1), 167–172.

Carneiro J.S, Nogueira R.M, Martins M.A, Valladão M, Pires E.M. (2018). The Oven-Chai, A., Wong, Y. S., Ong, S. A., Lutpi, N. A., Sam, S. T., Kee, W. C., & Ng, H. H. Haldane Andrews (2021). substrate inhibition kinetics for pilot-scale thermophilic anaerobic degradation of sugarcane vinasse. *Bioresource Technology*, 125319.

Chaturvedi and Verma. (2016). Microbial fuel cell: a green approach for the utilization of waste and generation of bio-electricity. *Bioresour. Bioprocess.* **3**(38): 1-23.

Chen, S., Deng, Y., Chang, C (2015). Pathway and kinetics of cyhalothrin bio-degradation by *Bacillus thuringiensis* strain ZS-19. *Sci Rep*, **5**, 8784

Chen, S., Deng, Y., Chang, C. (2015). Pathway and kinetics of cyhalothrin bio-degradation by *Bacillus thuringiensis* strain ZS-19. *Sci Rep.* **5**: 8784

Chowdhury, A., Pradhan, S., Saha, M., & Sanyal, N. (2008). Impact of pesticides on soil microbiological parameters and possible bio-remediation strategies. *Indian journal of microbiology*, **48**(1), 114–127.

Composition During Dry Grind Ethanol Processing of Corn. *J. Am. Oil Chem. Soc.*, **3**,

Costa, F., Quintelas, C., & Tavares, T. (2012). Kinetics of biodegradation of diethylketone by *Arthrobacter viscosus*. *Bio degradation*, **23**(1), 81–92.

Das, S. and Dash, H. R. (2014). Microbial bio-remediation: A potential tool for restoration of contaminated areas. *Microbial bio-degradation and bio-remediation*. Elsevier.

Deressa, L., Libsu, S., Chavan, R. B., Manaye, D., & Dabassa, A. (2015). Production of biogas from fruit and vegetable wastes mixed with different wastes. *Environment and Ecology Research*, **3**(3). 65-71

Dhiraj C.J., Vijay K. D., Harish, and Datta K. (2020). Influence of microbial fuel cell employed with porous anode on the voltage generation, COD, chloride content and total dissolved solids. *Water Science and Technology*, **82**(7). 1285–1295.

Doolotkeldieva T., Konurbaeva M., Bobusheva S. (2018). Microbial communities in pesticidecontaminated soils in Kyrgyzstan and bio-remediation possibilities. *Environ. Sci. Pollut.* **25**, 31848– 31862.

Dyson J.S, Beulke S, Brown C.D, Lane M.C.G. (2002). Adsorption and degradation of the weak acid mesotrione in soil and environmental fate implications. *Organic compounds in the environment. J Environ Qual*, **31**:613–618

Dyson J.S., Beulke, S., Brown C.D., Lane M.C.G. (2002). Adsorption and degradation of the weak acid mesotrione in soil and environmental fate implications. *J. Environ. Qual.*, **31** (2), 613–618.

Ecobichon D. J. (2001). Pesticides use in developing countries. *Toxicology*.**160**(1-3):27-33 Effect of external resistance on bacterial diversity and metabolism in cellulose-fed.

El Hammoumi A, Motahhir S, Chalh A, El Ghzizal A, Derouich A. (2018). Low-cost virtual instrumentation of PV panel characteristics using Excel and Arduino in comparison with traditional instrumentation. *Renew Wind Water Sol* **5**(1):3

El-Bestawy E., Mansy AH., Attia AM., Zahran H. (2014). Bio-degradation of persistent chlorinated hydrocarbons using selected freshwater bacteria. *J Bioremed Biodeg* **5**: 1-6.

Elshobary, M.E., Zabed, H.M., Yun, J., Zhang, G., Qi, X. (2021). Recent insights into microalgae-assisted microbial fuel cells for generating sustainable bio-electricity. *Int. J. Hydrogen Energy*. **46**: 3135–3159, *Environ Sci Technol*, **40**, 1062–1068

Erguven, G.O. (2018). Comparison of Some Soil Fungi in Bio-remediation of Herbicide Acetochlor Under Agitated Culture Media. *Bull. Environ. Contam. Toxicol.*, **100**, 570–575.

Fan Y, Liu H., Hu H., Environ. (2007). Sustainable power Generation in Microbial fuel cell using bicarbonates. *Sci. Technol.*, **41**: 8154–8158.

Fang H, Xiang YQ., Hao YJ, Chu XQ., Pan XD., Yu JQ., Yu YL. (2008). Fungal degradation of chlorpyrifos by *Verticillium* sp. DSP in pure cultures and its use in bio-remediation of contaminated soil and pakchoi. *Int Biodeterior Biodegrad*, **61**:294–303.

Fang, H., Yu, Y., Chu, X., Wang, X., Yang, X., and Yu, J. (2009). Degradation of chlorpyrifos in laboratory soil and its impact on soil microbial functional diversity. *J. Environ. Sci.* **21**, 380–386.

FAOSTAT. (2021). Available online: <http://www.fao.org/faostat/en/?#data/EP/visualize> (accessed on 8 April 2021).

Farhan, M., Ahmad, M., Kanwal, A. (2021). Bio-degradation of chlorpyrifos using isolates from contaminated agricultural soil, its kinetic studies. *Sci Rep* **11**, 10320

Farhan, M., Ahmad, M., Kanwal, A. (2021). Bio-degradation of chlorpyrifos using isolates from contaminated agricultural soil, its kinetic studies. *Sci Rep* **11**, 10320

Fenner, K., Canonica, S., Wackett, L. P., Elsner, M. (2013). Evaluating Pesticide Degradation in the Environment: Blind Spots and Emerging Opportunities. *Science*, **341**, 752–758.

Foster, J.R., Kwan, B.H., & Vancov, T. (2004). *Microbial degradation of the organophosphate pesticide, Ethion L.*

Geed, S.R.; Kureel, M.K.; Shukla, A.K., Singh, R.S. and Rai, B.N. (2016). Biodegradation of malathion and evaluation of kinetic parameters using three bacterial species. *Resource-Efficient Technologies*. **2**: S3 - S11.

Ghangrekar M.M and Shinde V.B. (2007). Performance of membrane-less microbial fuel cell

Gharasoo, M., Centler, F., Van Cappellen, P., Wick, L. Y., & Thullner, M. (2015). Kinetics of substrate biodegradation under the cumulative effects of bioavailability and self-inhibition.

Environmental science & technology, **49**(9), 5529-5537.

Ghatak M. D. and Mahanta P. (2014). Comparison of kinetic models for biogas

Ghoreyshi A.A., Jafary T., Najafpour G.D. and Haghparast F. (2011). Effect of Type and Concentration of Substrate on Power Generation in a Dual Chambered Microbial Fuel Cell. *World Renewable Energy Congress*, 1174-1181.

Gil G.C., Chang I.-S., Kim B. H. (2003). Operational parameters affecting the performance of a mediator-less microbial fuel cell,” *Biosensors and Bioelectronics*,**18**(4). 327–334.

Gilden. (2010). Monitoring pesticides residues in food science and pesticide Degradation Patterns: 1-17.

Gislason, E.A. and Craig, N.C. (2005). Cementing the foundations of thermodynamics: comparison of system-based and surroundings-based definitions of work and heat, *J. Chem. Thermodynamics*. **37**, 954-966.

Golge, O. and Kabak B., (2015). Determination of 115 pesticide residues in oranges by highperformance liquid chromatography–triple-quadrupole mass spectrometry in combination with QuEChERS method. *Journal of Food Composition and Analysis*. 41: 86-97.

Hamadache M., Benkortbi O., Hanini S., Amrane A., Khaouane L., Si Moussa C. A. (2016). Quantitative Structure Activity Relationship for acute oral toxicity of pesticides on rats: Validation, domain of application and prediction. *J. Hazard. Mater.* **303**, 28–40.

Head I. M., Singleton I., and Milner M. G. (2003). *Bio remediation: A Critical Review*. Wymondham: Horizon Scientific Press.

Heard M.S., Baas J., Dorne J.L., Lahive E., Robinson A.G., Rortais A., Spurgeon D.J., Svendsen C., Hesketh H. (2017). Comparative toxicity of pesticides and environmental contaminants in bees: Are honey bees a useful proxy for wild bee species? *Sci. Total Environ.* **578**, 357–365.

Helbling D.E. (2015). Bioremediation of pesticide-contaminated water resources: the challenge of low concentrations, *Current Opinion in Biotechnology*, **33**: 142-148

Hollinger C. and Schraa G. (1994). Physiological meaning and potential for application of reductive dichlorination by anaerobic bacteria. *FEMS Microbiol Rev* **15**: 297-305.

Holt, J.G. and Krieg, N.R. (1994). "Chapter 8. Enrichment and Isolation." In (Eds.) Gerhardt, P., R.G.E. Murray, W.A. Wood and N.R. Krieg. *Methods for General and Molecular Bacteriology*. ASM Press, Washington, D.C. pg.205

http://www.who.int/ipcs/publications/pesticides_hazard_2009.pdf.

Huang K., Chen C., Shen Q, Rosen B.P., Zhao F.J. (2015) Genetically engineering *Bacillus subtilis* with a heat-resistant arsenite arsenate methyltransferase for bio remediation of arsenic-contaminated organic waste. *Appl Environ Microbiol.* **81**: 6718-6724.

Imwene K. O, Mbui D. N, Mbugua J.K, Kinyua A. P, Kairigo P. K, Onyatta J. O. (2021). Kinetic Modelling of Microbial Fuel Cell Voltage Data from Market Fruit Wastes in Nairobi, Kenya. *International Journal of Scientific Research in Chemistry (IJSRCH)*, **6**(5), 25-37.
in Lalitpur Sub-Metropolitan City, Proceedings of IOE Graduate Conference. 143–149.

Istiqomah D, Irwandhi, H R Subandrio, H I Rakhman¹, I F S Nugroho¹, Hendra¹ and A Islamite. (2021). Degradation ability of indigenous bacteria from pesticide-contaminated water and soil in Brebes Regency, Indonesia, *J. Phys.: Conf. Ser.* 1960 012012

Jahanmard E., Ansari F., Feizi M. (2016) Evaluation of QUECHERS Sample Preparation and GC Mass Spectrometry Method for the Determination of 15 Pesticide Residues in Tomatoes Used in Salad Production Plants, *Iran J Public Health.* **45**(2). 230-238

Jiang, Y. B., Zhong, W. H., Han, C., & Deng, H. (2016). Characterization of Electricity Generated by Soil in Microbial Fuel Cells and the Isolation of Soil Source Exoelectrogenic Bacteria. *Frontiers in microbiology*, *7*, 1776.

Kamau J.M, Mbui D. N, Mwaniki J.M, Mwaura F. B, Kamau G.N. (2017). Microbial Fuel Cells: Influence of External Resistors on Power, Current and Power Density. *J Thermodyn Catal*, **8**: 182:113

Kamau J.M., Mbui D.N., Mwaniki J.M., Mwaura F.B. (2018a). Characterization of Voltage from Food Market Waste: Microbial Fuel Cells. *Int J Biotech & Bioeng.* **4**:3, 37-43

Kamau J.M., Mbui D.N., Mwaniki J.M, Mwaura F.B.(2018a). Characterization of voltage from food market waste: microbial fuel cells. *Int J Biotech & Bioeng.* **4**:3

Kamau J.M., Mbui D.N., Mwaniki J.M. (2018b). Utilization of rumen fluid in production of bio-energy from market waste using microbial fuel cells technology. *J Appl Bioethanol Bioeng.*;5(4):227–231.

Kamau, J. M., Mbui, D. N., Mwaniki J. M., & Mwaura, F. B. (2020). Proximate analysis of fruits and vegetables wastes from Nairobi County, Kenya. *Research Journal of Food Science and Nutrition*, **5**(1):9-15

Khan K.Y., Khan M.A., Niamat R., Munir M., Fazal H., Mazari P., Seema N., Bashir T., Kanwal A., Ahmed S.N., (2011). Element content analysis of plants of genus *Ficus* using atomic absorption spectrometer. *Afr J Pharm Pharmacol* **5** (3):317-321.

Kim J. R., Jung S. H., Regan J. M., & Logan B. E. (2007). Electricity generation and microbial community analysis of alcohol powered microbial fuel cells. *Bioresource Technology*, **98**(13), 2568–2577.

Kim K.H.; Kabir E.; Jahan S.A. (2017). Exposure to pesticides and the associated human health effects. *Sci. Total Environ* **575**, 525–535.

Kinyua A., Mbugua J. K., Mbui D. N., Kithure J., Michira I, Wandiga S. O.(2022a). Bio-Remediation of Lambda Cyhalothrin, Malathion and Chlorpyrifos Using Microbial Fuel Cells. *International Journal of Scientific Research in Chemistry (IJSRCH)*, **7**(2), 22-32

Kinyua A., Mbugua J. K., Mbui D. N., Kithure J., Michira I, Wandiga S.O.(2022b). Voltage Recovery from Pesticides Doped Tomatoes, Cabbages and Loam Soil Inoculated with Rumen Waste: Microbial Fuel Cells. *International Journal of Scientific Research in Science, Engineering and Technology (IJSRSET)*, **9**(2), 172-180.

Konradsen, F., Van der Hoek, W., Cole, D.C., Hutchinson, G., Daisley, H., Singh, S., Eddleston, M. (2003). Reducing acute poisoning in developing countries-options for restricting the availability of pesticides. *Toxicology*, **192**: 249-261

Konstantinou I.K., Zarkadis., A.T., Albanis T.A. (2001). Photo-degradation of selected herbicides in various natural waters and soils under environmental conditions. *J. Environ. Qual.* **30** (1), 121-130.

Kuo W.S. (2002). Photo-catalytic oxidation of pesticide rinsate. *J. Environ. Sci. Health, Part B: Pesticides, Food Contam. Agric. Wastes*, **37** (1), 65–74.

Lazor M, Hutnan M, Sedlacek S, Koles N, and Spalkova V. (2010). Anaerobic codigestion

Lee D.W., Santos W., Seo J.W., Leon Felix L., Bustamante D.A. (2010); The structure of graphite oxide: Investigation of its surface chemical groups. *J. Chem.* **114**: 572375728.

Li L., He Q., Zhao X. F., Wu D., Wang X. M., Peng X. Y. (2018). Anaerobic digestion of food waste: correlation of kinetic parameters with operational conditions and process performance. *Biochem. Eng. J.* **130**, 1–9

Liu H., Cheng S.A., Logan B.E. (2005). Power generation in fed-batch microbial fuel cells as function of ionic strength, temperature, and reactor configuration. *EnvironSciTechnol.* **39**:5488–5493.

Lloyd J.R. (2002). Bioremediation of metals; the application of micro-organisms that make and break minerals. *Microbiol Today* **29**: 67-69.

Logan, B. E., Murano, C., Scott, K., Gray, N. D., & Head, I. M. (2005). Electricity generation from cysteine in a microbial fuel cell. *Water Research*, **39**(5), 942–952.

Logan, B.E. (2008) *Microbial Fuel Cells*. John Wiley & Sons, Inc., New York.

Lorenz E.S., (2009). Potential Health effect of pesticides. Scaling up microbial fuel cells and other bio-electrochemical systems. *Appl. Microbial Bioethanol.* **85**:1665–1671.

Lovley D. R. (2003). Cleaning up with genomics: applying molecular biology to bioremediation. *Nat. Rev. Microbiol.* **1**, 35–44.

Lynch, J. M., & Barbano, D. M. (1999). Kjeldahl nitrogen analysis as a reference method for protein determination in dairy products. *Journal of AOAC International*, **82**(6), 1389–1398.

Marcella C., Ulrich S, Karl V., Kordesch, Julio C T, Patrik S. (2007). Principals, functions and classification of fuels, **10**:1002.

Mata-Alvarez J., Dosta J., Romero-Güiza M.So., Fonoll X., Peces M., Astals S. (2014). A critical review on anaerobic co-digestion achievements between 2010 and 2013. *Renewable and Sustainable Energy Reviews*, 36, 412–427.

Mata-Alvarez J., Kurniawan T. A., Llabrés-Lueng P., Cecchi F. (1993). Kinetic and performance study of a batch two-phase anaerobic digestion of fruit and vegetable wastes. *Biomass Bioenergy* 5, 481–488

Mbugua J.K, Kinyua A, Kithure JGN, Waswa GA. (2022). Effect of Incandescent and Fluorescence Bulb on Pentachlorophenol and Di-methoate on Spinach Leaf Surface. *J Membrane Sci Techno.* 12:263

Mbugua J.K, Kinyua A., Waswa A.G, Mbui D.N, Kithure J, Michira I and Wandiga S.O. (2022). BioRemediation of Lambda Cyhalothrin, Malathion and Chlorpyrifos Using Anaerobic Digestion BioSlurry Microbes. *Medicon Agriculture & Environmental Sciences*, 2(5), 03-12.

Mbugua J.K., Mbui D., Kamau G. (2015); Adsorption and Photo-degradation of Pesticide Residues in Selected Plants Grown in Organic Container Garden Food Security Phenomenon.

Mbugua J.K., Mbui D.N., Mwaniki J., Mwaura F. and Sheriff S. (2020). Influence of Substrate Proximate Properties on Voltage Production in Microbial Fuel Cells. *Journal of Sustainable Bioenergy Systems.* 10: 43-51.

Mehlich, A. (1953). Determination of P, Ca, Mg, K, Na, and NH₄. North Carolina Soil Test Division (Mimeo 1953), 23-89.

Mendel J.L. and Walton M.S. (1966). Conversion of p,p' -DDT to p,p' -DDD by intestinal flora of the rat. *Science* 151: 1527-1528.

Menicucci J, Beyenal H, Marsili E, Veluchamy RA, Demir G, Lewandowski Z. (2011). microbial fuel cells. *Bioresour Technol*, 102, 278–283

Miller J.N. and Miller J.C. (2005). Statistics and chemometrics for analytical chemistry, 5th ed., Pearson Education Limited, England.

Mirsal I.A. (2008). Soil Pollution Origin, Monitoring & Remediation, 2nd ed.; Springer-Verlag: Berlin/Heidelberg, Germany, 2008; ISBN 9783540707752

Mohammed, S. M., Abdurrahman, A. A., & Attahiru, M. (2017). Proximate analysis and total lycopene content of some tomato cultivars obtained from Kano State, Nigeria. *ChemSearch Journal*, **8**(1), 64-69

Mondal S.K. and Das N. (2018). Application of microbial fuel cells for bioremediation of environmental pollutants: An overview. *J. Microbiol. Biotechnol. Food Sci.*, **7**, 437–444.

Moreau, R. A., Liu, K. S., Winkler-Moser, J. K., and Singh, V. (2011). Changes in Lipid

Moreno-Andrade I & Buitrón G (2004) Variation of the microorganism's activity during the acclimation phase of a SBR system degrading 4-chlorophenol. *Water Sci Technol* **50**(10): 251–258

Mota R., Rossi F., Andrenelli L., Pereira S.B, De Philippis R. (2016). Released polysaccharides (RPS) from *Cyanotheca* sp. CCY 0110 as bio sorbent for heavy metals bioremediation: interactions between metals and RPS binding sites. *Appl Microbiol Bioethanol* in Press.

Motahhir, S, El Hammoumi, A., Chalh, A. (2018). Low-cost virtual instrumentation of PV panel characteristics using Excel and Arduino in comparison with traditional instrumentation. *Renewables* **5**(3): 2-16

Mulder G, Ridder F. D, Coenen P, Weyen D, Martens A. (2008). Evaluation of an on-site cell voltage monitor for fuel cell systems, *International Journal of Hydrogen Energy*, **30**(20): 5728-5737

Murray P. R., Baron J. H., Jorgensen J. H., Pfaller M. A., Tenover F. C., Tenover F. C., (Eds.), 8th Ed., 2003, Manual of Clinical Microbiology, ASM, Washington, D.C.

Mwaniki J. M., Kali A.M., Mbugua J.K., Kamau G.N. (2016); A New Variant of the Hydraulic Stirring Mechanism for Pilot Scale Wet Thermophilic Anaerobic Digester: *Journal of Kenya Chemical Society*,**9**: 135-150.

Nadeau L.J., Menn F.M., Breen A., Sayler G.S. (1994). Aerobic degradation of 1-trichloro-,2-bis(4chlorophenyl) ethane (DDT) by *Alcaligenes eutrophus* A5. *Appl Environ Microbiol.* **60**: 51-55.

Nam J-Y, Kim H-W, Lim K-H, Shin H-S, Logan B.E. (2010) Variation of power generation at different buffer types and conductivities in single chamber microbial fuel cells. *Biosens Bioelectron*; **25**:1155-9.

Nasrollahzadeh, H. S., Najafpour, G. D., Pazouki, M., Younesi, H., Zinatizadeh, A. A., & Mohammadi, M. (2010). Biodegradation of phenanthrene in an anaerobic batch reactor: Growth kinetics. *Chemical Industry and Chemical Engineering Quarterly/CICEQ*, **16**(2), 157-165.

Nastro, R.A.; Gambino, E.; Toscanesi, M.; Arienzo, M.; Ferrara, L.; Trifuoggi, M. (2019). Microbial Fuel Cells (MFCs) Remediation Activity of Marine Sediments Sampled at a Dismissed Industrial Site: What Opportunities? *J. Clean. Prod.*, **235**, 1559–1566.

Neves, C. A., Santos, W. B. R. dos, Santos, G. T. D., Silva, D. C. da ; Jobim, C. C. ; Santos, F. S. ; Visentainer, J. V. ; Petit, H. V. (2009). Production performance and milk composition of dairy cows fed extruded canola seeds treated with or without lignosulfonate. *Anim. Feed Sci. Tech.*, **154** (1/2): 83-92

Nielsen, S.S. (2010). Food analysis. In S. Suzanne Nielsen (Ed.), (4th ed.). New York

Obiajunwa EI, Adebajo AC, Omobuwajo OR (2002). Essential and trace element contents of some Nigerian medicinal plants. *J Radioanal Nucl Chem.* **252**:473–476.

Oliveira V.B.B., Simoes M., Melo L.F.F., Pinto A. (2013). Overview on the developments of microbial fuel cells. *Biochem Eng J.* **73**:53-64.

Ozbayram E.G, Orhan I, Bahar I, Hauke H and Sabine K. (2018). Comparison of Rumen waste and Manure Micro-biome and Implications for the Inoculation of Anaerobic Digesters

Pal R., Chakrabarti K., Chakraborty A., Chowdhury A. (2006). Degradation and effects of pesticides on soil microbiological parameters-A review. *Int. J. Agric.***1**(33):240-258.

PCPB. (2008). Annual Report, July 2007/June 2008. Pest Control Products Board, Nairobi, Kenya: 10-13.

PCPB. (2012). Annual Report, July 2011/June 2012, © 2010 Pest Control Products Board, Nairobi, Kenya: 9-10

Peixoto R.S., Vermelho A.B., Rosado A.S. (2011). Petroleum-degrading enzymes: Bioremediation and new prospects. *Enzyme Res* 2011: 475193.

Penuela G.A. and Barceló, D. (1998). Application of C 18 disks followed by gas chromatography techniques to degradation kinetics, stability and monitoring of endosulfan in water. *J. Chromatogram. A*, **795**(1), 93-104.

Persson J., Wennerholm W., O'Halloran S. (2008). Handbook for Kjeldahl Digestion, 11- 42

Pratima K. C. and Bhakta B. A. (2015). Production of Biogas from Slaughterhouse Waste

Prevot A.B. and Pramauro, E. (1999). Analytical monitoring of photocatalytic treatments.

Degradation of 2,3,6-trichlorobenzoic acid in aqueous TiO₂ dispersions. *Talanta*, **48**(4), 847-857.

Puig S., Serra M., Coma M., Cabre M., Balaguer M.D., Colprim J. (2010). Procedure for determining maximum sustainable power generated by microbial fuel cell, production rate from sawdust. *International Journal of Research in Engineering and Effect of pH on nutrient dynamics and electricity production using microbial fuel cells. Bioresour Technol*, **101**: 9594-9.

Rabaey K., Boon N., Siciliano S.D., Verhaege M., Verstraete W. (2004). Biofuel cells select for Microbial consortia that self-mediate electron transfer. *Appl Environ Microbiol.* **70**(9):5373–5382

Rabaey K., Lissens G., Siciliano S. D., & Verstraete W. (2003). A MFC capable of converting glucose to electricity at high rate and efficiency.pdf. *Biotechnology Letter*, **25**, 1531– 1535.

Rabaey, K., Boon, N., Siciliano, S.D., Verhaege, M., Verstraete, W., 2004. Biofuel cells select for microbial consortia that self-mediate electron transfer. *Appl. Environ. Microbiol.* **70**, 5373-5382.

Raffa, C. M., & Chiampo, F. (2021). Bioremediation of Agricultural Soils Polluted with Pesticides: A Review. *Bioengineering (Basel, Switzerland)*. **8**(7): 92.

Rafqah S. Wong-Wah-Chung P., Aamili, A., Sarakha M. (2005). Degradation of metsulfuron methyl by heterogeneous photocatalysis on TiO₂ in aqueous suspensions Kinetic and analytical studies. *J. Mol. Catal. A: Chem.*, **237**(1-2), 50-59.

Rajmohan, K. S., Chandrasekaran, R., & Varjani, S. (2020). A Review on Occurrence of Pesticides in Environment and Current Technologies for Their Remediation and Management. *Indian journal of microbiology*, **60**(2), 125–138.

Remel Microbiology Products (2005). Instructions for Use of MacConkey Agar. Accessed June 2005, <http://www.remelinc.com/IFUs/IFU1550.pdf>

Rismani-Yazdi H, Christy A, Carver S.M, Yu Z, Dehority B.A, Tuovinen O.H. (2011).

Salfinger Y. and Tortorello M.L. (2015) Compendium of Methods for the Microbiological Examination of Foods, 5th Ed., American Public Health Association, Washington, D.C.

Saratale, G. D., Saratale, R. G., Shahid, M. K., Zhen, G., Kumar, G., Shin, H.-S., et al. (2017). A

Comprehensive Overview on Electro-Active Biofilms, Role of Exo-Electrogens and Their Microbial Niches in Microbial Fuel Cells (MFCs). *Chemosphere* **178**, 534–547

Sardar D, Kole RK. (2005). Metabolism of chlorpyrifos in relation to its effect on the availability of some plant nutrients in soil. *Chemosphere*, **61**, 1273–80.

Sarkar S., Bernardes G. J, Keeley J, Möhring N, Jansen K.(2021) The use of pesticides in developing countries and their impact on health and the right to food. Policy Department for External Relations Directorate General for External Policies of the Union, PE 653.622 - January 2021

Seluy, L.G. and Isla, M.A. (2014). A process to treat high-strength brewery wastewater via ethanol recovery and vinasse fermentation. *Ind. Eng. Chem. Res.* **53** (44), 17043–17050.

Senko O., Maslova O., Efremenko E. (2017). Optimization of the Use of His 6-OPH-Based Enzymatic Biocatalysts for the Destruction of Chlorpyrifos in Soil. *Int. J. Environ. Res. Public Health*, **14**, 1438.

Shankar M.V., Anandan S., Venkatachalam N., Arabindoo B., Murugesan V. (2004). Novel thin-film reactor for photocatalytic degradation of pesticides in aqueous Solutions. *J. Chem. Technol. Biotechnol.*, **79**(11), 1279–1285.

Shukla M and Kumar S. (2018). Algal growth in photosynthetic algal microbial fuel cell and its subsequent utilization for biofuels. *Renew Sustain Energy Rev*, **82**:402-14

Singh B. K. (2009). Organophosphorus-degrading bacteria: ecology and industrial applications. *Nature Rev Microbiol* **7**, 156–163

Singh B. K. and Walker A. (2006). Microbial degradation of organophosphorus compounds. *FEMS Microbiol Rev.* **30**: 428–471.

Singh D.K. (2008). Biodegradation and bioremediation of pesticide in soil: concept, method and recent developments. *Indian J. Microbiol.* **48**:35–40

Singh N. and Balomajumder C. (2016).Batch growth kinetic studies for elimination of phenol and cyanide using mixed microbial culture. *Journal of Water Process Engineering.***11**:130–137

Soliman, M. M. (2012). Effects of UV-light, temperature and storage on the stability and biological effectiveness of some insecticides. *Journal of Plant Protection Research*, *52*(2), 275-280

Song, H, Fang, Z., L., Cang, N. & Li, X.-N. 2013 Performance of microbial fuel cell coupled constructed wetland system for decolorization of azo dye and bioelectricity generation. *Bioresource Technology* **144**, 165–171.

Srivastava J. Naraiyan R, Kalra S.J.S., Chandra H. (2014). Advances in microbial bioremediation and the factors influencing the process. *Int J Environ Sci Technol.* **11**: 1787-1800.

SSCHE May, 24–28.

Stockholm Convention. (2021). Available online: <https://www.unido.org/our-focus-safeguardingenvironment-implementationmultilateral-environmental-agreements/stockholm-convention> (accessed on 8 April 2021).

Tabatabaei M, Marashi N. F and Mekarizade A, (2010). Transferable plasmid mediating multiantibiotic resistance in non-pathogenic Escherichia coli isolates from chicken flocks. *Global Veterinaria*, **5**: 371-375. *Technology*, **3**(7), 248–254. Thermally Pretreated Source-Sorted Organic Market Refuse, *Journal of Engineering*, 1-15

Timmers R.A., Strik D.P., Hamelers H.V.M., Buisman C.J.N. (2010) Long-term performance of a plant microbial fuel cell with *Spartina anglica*. *Appl Microbiol Biotechnol*; **86**:973-81.

Tiwari MK, Guha S. (2014). Kinetics of biotransformation of chlorpyrifos in aqueous and soil slurry environments. *Water Res*, **51**, 73–85.

Torres C.I, Brown R.K., Parameswaran P., Marcus A.K., Wanger G., Gorby Y.A., Rittman B.E. (2009) *Selecting anode-respiring bacteria based on anode potential: phylogenetic, electrochemical, and microscopic characterization. EnvironSciTechnol.* **43**:9519–9524.

Tran, T. S. & Simard R. R. (1993). Mehlich III-Extractable Elements. In: M. R. Carter, Ed. *Soil treating wastewater and effect of electrode distance and area on electricity production.*

Tudi, M., Daniel Ruan, H., Wang, L., Lyu, J., Sadler, R., Connell, D., Chu, C., & Phung, D. T.

(2021). Agriculture Development, Pesticide Application and Its Impact on the Environment.

International journal of environmental research and public health, *18*(3), 1112.

Tudi, M., Daniel Ruan, H., Wang, L., Lyu, J., Sadler, R., Connell, D., Chu, C., & Phung, D. T.

(2021). Agriculture Development, Pesticide Application and Its Impact on the Environment.

International Journal of Environmental Research and Public Health, **18**(3), 1112

Turner, R.C. & Clark J.S. (1966). Lime potential in acid clay and soil suspensions. Trans. Comm. II & IV Int. Soc. *Soil Science*, 208-215.

Ukpebor, J.E., & Ukpebor, E.E. (2016). Application of QUECHERS method for multi-residue pesticides determination in lettuce and apple using gas chromatography-mass spectrometry.

Nigerian Journal of Technology, **35**, 544-549.

Uygun U. (1997). Degradation of clofenvinphos in carrots during storage. *Food Chemistry*, **60**(4), 479-487.

Vargas J.M. (1975). Pesticide degradation. *Journal of Arboriculture*, **1**:332-333

Vicente A. and Yolanda P., (2004) Determination of pesticides and their degradation Products in soil: critical review and comparison of methods, *Trace Trends in Analytical Chemistry*, Volume **23**, Issues 10–11, and P. 772 -789.

Vijay, A., Chhabra, M., & Vincent, T. (2019). Microbial community modulates electrochemical performance and denitrification rate in a biocathodic autotrophic and heterotrophic denitrifying microbial fuel cell. *Bioresource technology*, **272**, 217-225.

Wang H., Xu S., Hu J., Wang X., (2009). Effect of potassium dihydrogen phosphate and bovine manure compost on the degradation of chlorothalonil in soil, *Soil & Sediment Contamination (30)*, 94—97.

Wang J and W. Wan. (2008). The effect of substrate concentration on bio-hydrogen production by using kinetic models, *Science in China B*, **51**(11), 1110–1117.

Wang Q. and Lemley A. T. (2001). Kinetic Model and Optimization of 2,4-D degradation by anodic Fenton Treatment. *Environ. Sci. Technol.* **35**(22), 4509-4514.

Webb D and Møller-Holst S. (2001). Measuring individual cell voltages in fuel cell stacks. *Journal of Power Sources*.;1:54–60.

WHO. (2007). Pesticide residue in food; toxicology and environment protection? P 86/2 In Chem. 1988 No. 756-770.

WHO. (2009). The WHO Recommended Classification of Pesticides by Hazard and Guidelines to Classification. WHO, Geneva.

Wrighton K. C., Viridis, B., Clauwaert P., Read S. T., Daly R. A., Boon N., Piceno Y., Andersen G. L., Coates J. D., & Rabaey K. (2010). Bacterial community structure corresponds to performance during cathodic nitrate reduction. *ISME Journal*, **4**(11), 1443–1455.

Wu, H., Feng, Y. L., Li, H. R., Wang, H. J., & Wang, J. J. (2018). Co-metabolism kinetics and electrogenesis change during cyanide degradation in a microbial fuel cell. *RSC advances*, **8**(70), 40407–40416.

Yadav M, Srivastva N, Shukla AK (2014). Efficacy of *Aspergillus* sp. for degradation of chlorpyrifos in batch and continuous aerated packed bed bioreactors. *Appl Biochem Biotechnol*, **175**, 16–24.

Zhai Y., Li, K., Song, J., Shi, Y. & Yan, Y. (2012). Molecular cloning, purification and biochemical characterization of a novel pyrethroid-hydrolyzing carboxylesterase gene from *Urobacterium anthropic* YZ-1. *J Hazard Mater*. 221–222, 206–212

Zhang E.R., Liu L., Cui Y.Y., (2013). Effect of PH on the performance of the anode in microbial fuel cells. *In Adv. Mater. Res.* **608**: 884-8.

Zhang Jiqiang., Ping Zhang., Meng Zhang., Hiu Chen., Tingting Chen., Zuofu Xie., Jing Cai, and Ghulam Abbs. (2013). Kinetics of substrate degradation and electricity generation in anodic denitrification microbial fuel cell (AD-MFC). *Bioresource Technology*, 149: 44-50

Zhang, Y.F., Min, B., Huang, L.P., Angelidaki, I., (2011). Electricity generation and microbial community response to substrate changes in microbial fuel cell. *Bioresour. Technol.* 102, 1166-1173.

Zhi, W., Ge, Z., He, Z., and Zhang, H. (2014). Methods for understanding microbial community structures and functions in microbial fuel cells: a review. *Bioresour. Technol.* 171, 461–468.

Zhi, W., Ge, Z., He, Z., and Zhang, H. (2014). Methods for understanding microbial community structures and functions in microbial fuel cells: a review. *Bioresour. Technol.* 171, 461–468.

APPENDICES

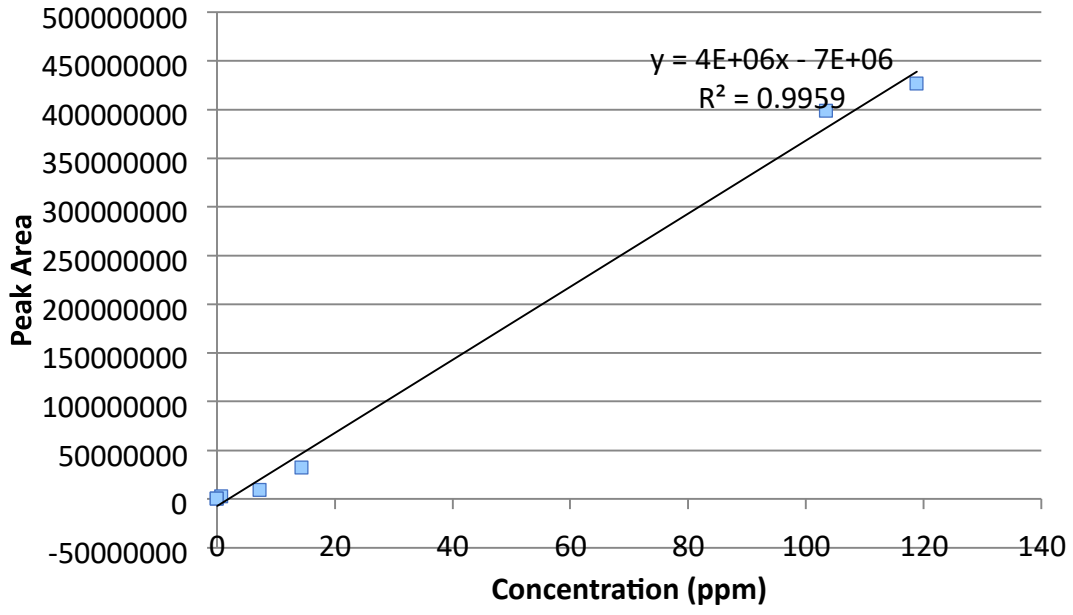
Appendix 1: Arduino Based Voltage and Current MFC Code

```

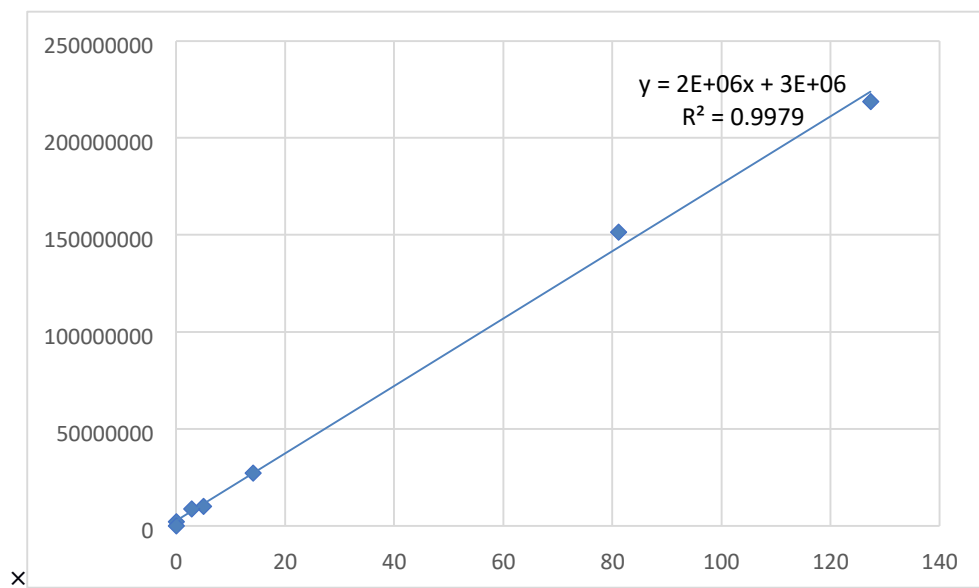
#include "Wire.h"
#include "LiquidCrystal_I2C.h"
LiquidCrystal_I2C lcd(0x27,16,2);
const int SensorPin = A3; // Voltage sensor pin
const int SensorPin1 = A0; // Current sensor pin
float vIn; // measured voltage (3.3V = max. 16.5V, 5V = max 25V)
float voltage;
float SensorVal; // value on pin A3 (0 - 1023)
const float factor = 5.128; // reduction factor of the Voltage Sensor shield
const float vCC = 5.00; // Arduino input voltage
void setup() {
  // put your setup code here, to run once:
  Serial.begin(9600);
  Serial.println("CLEARDATA");
  Serial.println("LABEL,Date,Time,Voltage (V)");
  Serial.println("LABEL,Date,Time,Current (I)");
  lcd.begin(16,2); // initialize the LCD1602
  lcd.backlight(); // turn the backlight ON for the LCD
  lcd.print("MFC");
  lcd.setCursor(0,1);
  lcd.print("MFC Voltage ");
  lcd.setCursor(0,2);
  lcd.print("MFC current");
  delay(2000);
  lcd.clear();
}
void loop() {
  // put your main code here, to run repeatedly:
  lcd.clear(); // clear previous values from screen
  float current = 0;
  for(int i = 0; i < 1000; i++)
  {
    current = current + (.0264 * analogRead(A0) -13.51) / 1000;
    delay(1);
  }
  Serial.println(current);
  SensorVal = analogRead(SensorPin); // read the current sensor value (0 - 1023)
  voltage = (SensorVal / 1024) * vCC; // convert the value to the real voltage on the analog pin
  vIn = voltage * factor; // convert the voltage on the source by multiplying with the factor
  Serial.print(vIn);
  Serial.println();
  lcd.setCursor(0,1);
  lcd.print("voltage=");
  lcd.print(voltage);
  lcd.setCursor(0,2);
  lcd.print("current=");
  lcd.print(current);
  delay(1000);
}

```

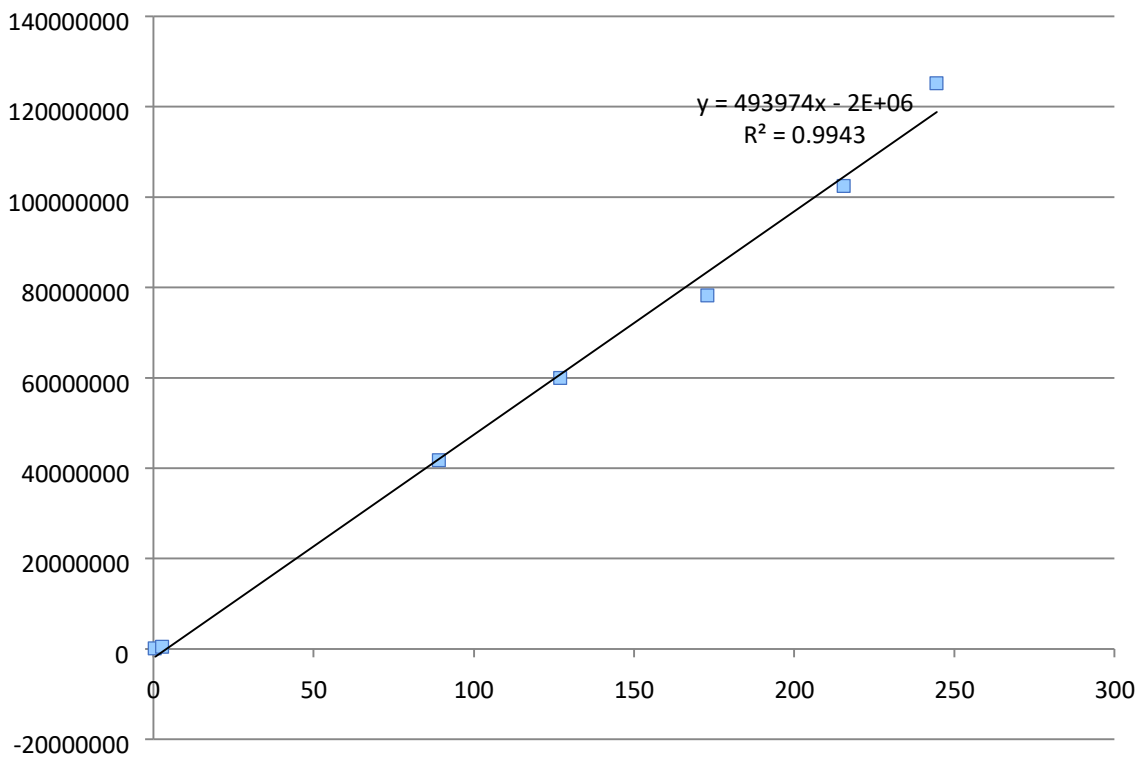
Appendix 2: Malathion calibration curve



Appendix 3: Lambda Cyhalothrin Calibration Curve



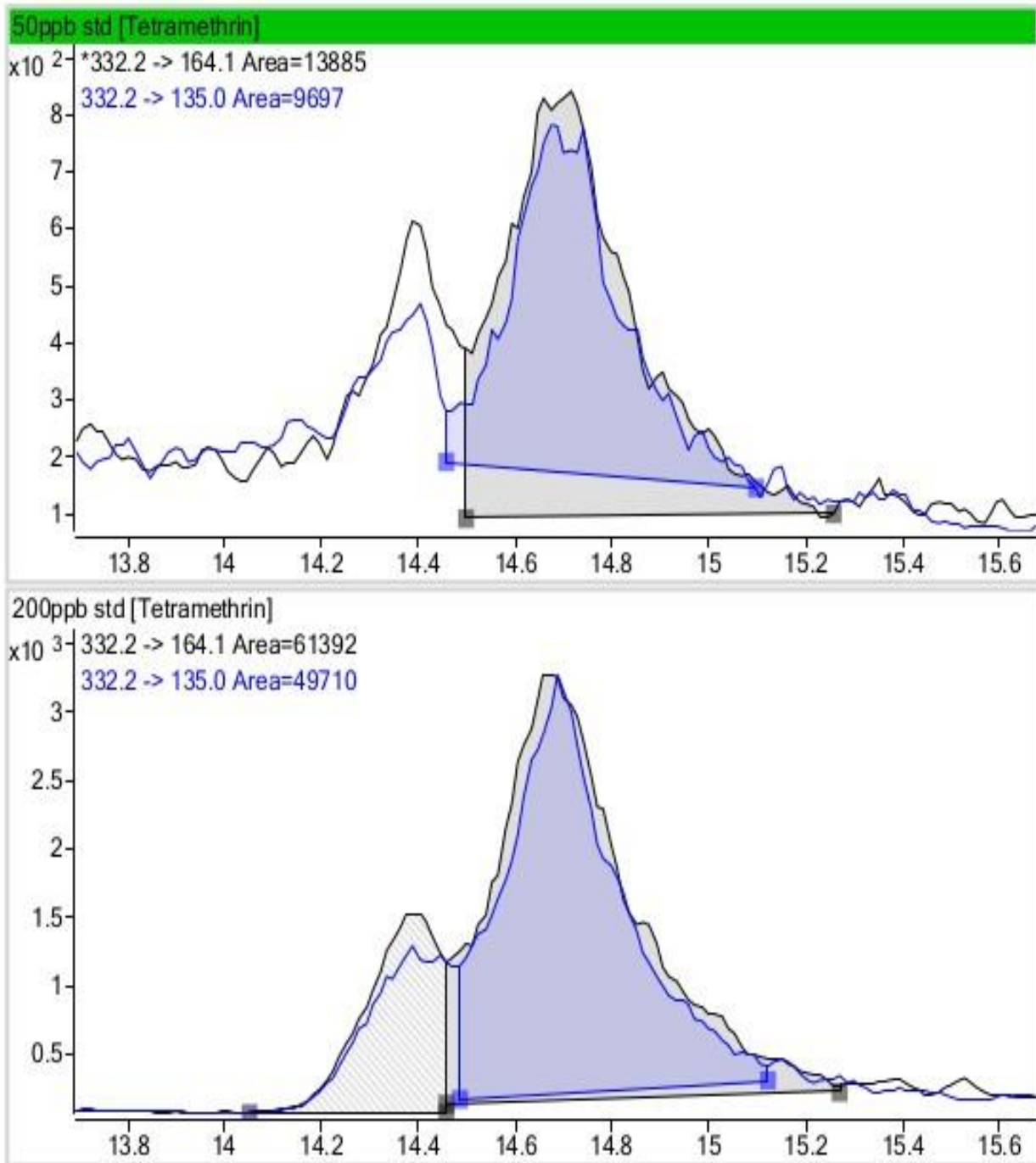
Appendix 4: Calibration of Chlorpyrifos



Appendix 5: Table Shows Pesticide Recovered after Spiking the Substrates

	Compounds				
Samples	Lambda cyhalothrin	Chlorpyrifos	Fenpropathrin(commonest) pesticide	Malathion	
Tomatoes	<LOQ	2.28 ppm	2.75 ppm	2.06 ppm	
Rumen	<LOQ	1.42 ppm	1.68 ppm	0.45 ppm	
Soil	0.01 ppm	1.5 ppm	1.68 ppm	1.1 ppm	
Cabbage	0.01 ppm	1.41 ppm	1.72 ppm	0.78 ppm	
±Compound	Method	Retention Time(Mins)	Precursor Ion	Product Ions	Recoveries
Chlorpyrifos	LC-MS/MS	18.25	352	200	86.31%
				198	
Malathion	LC-MS/MS	13.85	331	126.9	82.16%
				99	
Lambda Cyhalothrin	GC-MS/MS	12.046	197	141	74%
				161	
Fenpropathrin	LC-MS/MS	18.24	350.2	97.1	84.12%
				125.1	

Appendix 6: Tetramethrin (C19H25NO4) Curve



Appendix 7 : Table of statistical parameters for Modeling of voltage bio-remediation .

Model Equation	Parameters	Chi²/doF	R²	Adjusted R²	RMSE	RSS
Boltzmann (Sigmoidal) Fit	A1(initial value)=1.0478± nan A2(final value)=2.9705± nan X0(center)=7.7519± nan Dx(time constant)=9.8018± nan	1.0679	0.4389	0.3688	0.1033	0.3524
Gauss Fit	A (area)=5.3247± 1.0183 Xc(center)=1.7791± 6.1648 W(width)=1.3333± 1.8777 Y0(offset)=1.1119± 2.7710	5.0229	0.7361	0.7031	0.07087	0.16575
Lorentz Fit	A (area)=8.5982+/-2.1746 Xc(center)=1.7681± 6.2641 W(width)=1.4920± 3.1423 Y0(offset)=8.1727±0.5326	5.4022	0.7161	0.6807	0.0735	0.1782

Appendix 8 : Table of statistical parameters for Modeling of voltage bio-remediation of pesticide mix on Tomato

Model Equation	Parameters	Chi²/doF	R²	Adjusted R²	RMSE	RSS
Boltzmann (Sigmoidal) Fit	A1(initial value) = 6.8249±nan A2 (final value) = 3.1554 ± nan X ₀ (center) = 2.7946 ± nan Dx(time constant)=-3.2599± nan	1.7566	0.4105	0.3369	0.1325	0.5796
Gauss Fit	A (area) = 2.086 ± 1.1038 X _c (center)=1.87067±5.06845 W(width)=1.3761± 1.5537 Y ₀ (offset)=6.7418 ±2.9237	5.5406	0.8140	0.7908	0.0744	0.1828
Lorentz Fit	A (area) = 1.3506± 2.7860 X _c (center)=1.8980±5.3660 W(width)=1.7498± 2.8673 Y ₀ (offset)=4.5081± 4.0594	5.8297	0.8043	0.7799	0.07635	0.1923

Appendix 9: Table of statistical parameters for Modeling of voltage bio-remediation of pesticide mix on Cabbage

Model Equation	Parameters	Chi²/doF	R²	Adjusted R²	RMSE	RSS
Boltzmann (Sigmoidal) Fit	A1 (initial value) =3.6322± nan A2 (final value) =1.0839+/- nan X ₀ (center)=7.6464± nan Dx(time constant)=5.8233± nan	5.4489	0.6967	0.6587	0.0738	0.1798
Gauss Fit	A (area) =2.2101±2.7742 Xc(center)=4.3385± 2.8455 W(width)=4.7226± 6.1963 Y0(offset)=1.0591±1.26323	4.1538	0.7687	0.7398	0.0644	0.13707
Lorentz Fit	A (area) = 3.1305±5.4850 Xc(center)=4.4395 ±3.0812 W(width) = 4.9595± 1.0466 Y ₀ (offset)= 9.4653± 1.5234	4.7569	0.7352	0.7021	0.06897	0.1569

Appendix 10: Table of statistical parameters for Modeling of voltage bio-remediation of pesticide mix in Rumen Fluid

Model Equation	Parameters	Chi²/doF	R²	Adjusted R²	RMSE	RSS

Boltzmann (Sigmoidal) Fit	A1(initial value)=2.0527 ± 4.0408 A2(final value)=4.6322±1.3132 X ₀ (center)=9.2805±1.3979 Dx(time constant)=2.5352±1.14003	2.9493	0.7641	0.7345	0.0543	0.0973
Gauss Fit	A (area) = 1.6202 ±4.1044 X _c (center)=3.1973±1.4472 W(width)=3.7039 ±5.1598 Y ₀ (offset)=1.7075±4.5685	2.2161	0.8227	0.8006	0.04708	0.07313
Lorentz Fit	A (area) = 4.5080±1.8355 X _c (center)=3.2548±1.6909 W(width)=5.9656 ±1.3411 Y ₀ (offset)=3.9215±9.6492	2.5939	0.7924	0.7666	0.0509	0.0856